



The role of *DA1* in organ size control in *Arabidopsis thaliana*

Rachel Emily Prior

A thesis submitted to the University of East Anglia in fulfilment of the Degree of Doctor of Philosophy

John Innes Centre, Norwich

December 2017

© This copy of the thesis has been supplied on condition that anyone who consults it is understood to recognise that its copyright rests with the author and that use of any information derived there from must be in accordance with current UK Copyright Law. In addition, any quotation or extract must include full attribution.

This thesis is dedicated to my grandfathers, Bill Oliver and Peter Prior.

ABSTRACT

Despite the sizes of organs and organisms being a key defining feature, very little is known about how the final sizes of organs is determined. Recent progress has highlighted the important role of the DA1 peptidase as a negative regulator of organ size in *Arabidopsis thaliana*. Previous studies have proposed that DA1, and the E3 ligase BIG BROTHER (a protein known to regulate DA1 activity), work synergistically to regulate the duration of cell proliferation. In the present study, we take a multidisciplinary approach to further our understanding of the biological activities of *DA1* and *BB*.

Protoplast transient expression analyses were used to explore potential new substrates for DA1 peptidase activity, and to work towards identifying a conserved target site for DA1-mediated cleavage. Using confocal microscopy and bespoke segmentation software, I embarked on a global analysis of leaf cellular phenotypes in the *da1-1*, *bb*, and *da1-1bb* mutants throughout early development. This allowed a holistic comparison to wild type of parameters such as total cell number, and cell area, density, and circularity. In addition, scanning electron microscopy was used to examine cells in mature leaves of wild type, and *da1-1*, *bb*, and *da1-1bb* mutants, revealing novel insights into the control of final organ size in these mutants relative to wild type. Finally, innovative live cell imaging has, for the first time, allowed cell divisions to be observed in plants carrying the *da1-1*, *bb*, and *da1-1bb* mutations. My observations and interpretations establish new insights into how *DA1* and *BB* control growth by controlling the arrest of cell proliferation, and the population-level rate of cell proliferation. The approaches I have developed show the promise of quantitative cell imaging for understanding organ growth, and establish a framework for precisely comparing the effects of different mutations on organ growth.

LIST OF CONTENTS

LIST OF CONTENTS	4
LIST OF FIGURES	9
LIST OF TABLES	12
LIST OF EQUATIONS	13
LIST OF SUPPLEMENTARY FIGURES	14
ACKNOWLEDGEMENTS	15
1 GENERAL INTRODUCTION	17
1.1 Population growth and the need to increase food production	17
1.2 Control of leaf growth in plants	17
1.2.1 Initiation	17
1.2.2 Leaf polarity	18
1.2.3 Cell proliferation	20
1.2.4 Cell growth	25
1.2.5 Control of the transition from cell proliferation to cell expansion	26
1.2.6 Hormonal coordination of cell division and cell expansion throughout growth 27	
1.2.7 The compensation mechanism	28
1.2.8 Organ-level coordination of growth	29
1.2.9 Modelling organ growth	30
1.3 Organ growth and the cell cycle in plants	31
1.3.1 The endocycle	32
1.4 The role of the DA1 regulatory system in growth control	33
1.4.1 A model for growth control via the DA1 regulatory system	33
1.4.2 Structure and function in the DA1 family	34
1.4.3 The <i>da1-1</i> phenotype	37
1.5 The ubiquitin system	47
1.5.1 Ubiquitin	48

1.5.2	E1 ubiquitin activating enzymes	48
1.5.3	E2 ubiquitin conjugating enzymes	49
1.5.4	E3 ubiquitin ligase enzymes	49
1.5.5	Consequences of ubiquitination	52
1.6	Aims for this thesis.....	53
2	ANALYSING THE PEPTIDASE ACTIVITY OF DA1	54
2.1	Introduction	54
2.1.1	The biochemical function of DA1.....	54
2.1.2	Finding new substrates of the DA1 peptidase	58
2.1.3	Prediction of a conserved DA1 peptidase cleavage site	66
2.1.4	Finding the cleavage site in known substrates of DA1.....	69
2.1.5	Aims for this Chapter	70
2.2	Materials and Methods.....	72
2.2.1	RNA extraction	72
2.2.2	cDNA synthesis.....	72
2.2.3	PCR amplification of DNA.....	72
2.2.4	Gel extraction DNA purification	73
2.2.5	Subcloning.....	73
2.2.6	Bacterial transformation.....	73
2.2.7	Sequencing.....	74
2.2.8	Protoplast assays	74
2.2.9	Western blotting	75
2.2.10	Vectors and primers.....	76
2.3	Results.....	78
2.3.1	Assaying for new targets of DA1	79
2.3.2	Testing a predicted cleavage site for DA1	80
2.3.3	Finding the cleavage site in known targets.....	81
2.4	Discussion	83

2.4.1	Summary	86
3	QUANTITATIVE ANALYSES OF <i>DA1</i> AND <i>BB</i> FUNCTION IN LEAF GROWTH.....	88
3.1	Introduction	88
3.1.1	Leaf growth	89
3.1.2	The <i>DA1</i> regulatory system in the control of whole organ size	90
3.1.3	The <i>DA1</i> regulatory system in the control of cellular phenotypes	92
3.1.4	Advances in plant phenotyping.....	95
3.1.5	Aims for this Chapter	98
3.2	Materials and Methods.....	99
3.2.1	Plants used in this Chapter	99
3.2.2	Transformation of <i>Agrobacterium tumefaciens</i>	99
3.2.3	<i>Arabidopsis thaliana</i> transformation	99
3.2.4	Plant growth conditions.....	100
3.2.5	Plant imaging	101
3.2.6	Image analysis.....	102
3.3	Results.....	106
3.3.1	Whole organ phenotype	106
3.3.2	Cellular phenotype in growing leaves	117
3.3.3	Cellular phenotype in mature leaves	136
3.4	Discussion	144
3.4.1	<i>da1-1</i> , <i>bb</i> , and <i>da1-1bb</i> mutants exhibit increased leaf sizes throughout growth and at final size.....	144
3.4.2	<i>da1-1</i> , <i>bb</i> , and <i>da1-1bb</i> mutants exhibit increased rates of leaf growth.....	145
3.4.3	Increased mature leaf size in <i>da1-1</i> , <i>bb</i> , and <i>da1-1bb</i> mutants is due to increased cell number, not cell size	147
3.4.4	Mutations in <i>DA1</i> and <i>BB</i> also affect other cell characteristics throughout growth and in mature leaves	149
3.4.5	Summary	152

4	LIVE CELL IMAGING ANALYSIS OF <i>DA1</i> AND <i>BB</i> ACTIVITY	153
4.1	Introduction	153
4.1.1	Applications of live cell imaging	153
4.1.2	Modelling leaf growth through live cell imaging	154
4.1.3	Aims for this Chapter	156
4.2	Materials and Methods.....	157
4.2.1	Plants used in this Chapter	157
4.2.2	<i>Arabidopsis thaliana</i> crossing	157
4.2.3	<i>Arabidopsis thaliana</i> genotyping	157
4.2.4	Plant imaging	159
4.2.5	Image analysis.....	161
4.3	Results.....	162
4.3.1	Maintenance of the <i>da1-1</i> , <i>bb</i> , and <i>da1-1bb</i> large organ phenotypes	162
4.3.2	Competency to divide	166
4.3.3	Number of cell divisions per cell	176
4.3.4	Cell cycle time	176
4.3.5	Cell area at time of division	180
4.3.6	Cell division symmetry	186
4.3.7	Cell growth.....	189
4.3.8	Anisotropy of cell growth.....	191
4.4	Discussion	193
4.4.1	Mutations in <i>DA1</i> and <i>BB</i> promote an increased duration, and population-level rate, of cell proliferation	193
4.4.2	Mutations in <i>BB</i> and <i>DA1</i> may affect cell cycle time and cell area at division	194
4.4.3	Mutations in <i>DA1</i> and <i>BB</i> promote asymmetric cell divisions in pavement cells	196
4.4.4	The increased final organ size and shape change observed in <i>da1-1</i> , <i>bb</i> , and <i>da1-1bb</i> mutants is due to cell division dynamics rather than cell growth.....	198

4.4.5	Two possible mechanisms promoting increased final leaf size in <i>da1-1</i> , <i>bb</i> , and <i>da1-1bb</i> mutants	198
4.4.6	Modelling the effects of <i>da1-1</i> and <i>bb</i>	200
4.4.7	Summary	201
5	GENERAL DISCUSSION	202
5.1	Building our knowledge of DA1 and BB activity.....	203
5.2	DA1 and BB as factors in a quantitative framework for the control of organ size and shape	206
5.3	A new model incorporating competence to divide within a cell population?	207
	BIBLIOGRAPHY.....	210
	APPENDIX 1 - SUPPLEMENTARY FIGURES	237
	APPENDIX 2 - DONG ET AL., 2017.....	244

LIST OF FIGURES

Figure 1.1 Schematic representation of cell cycle control in plants.....	31
Figure 1.2 A proposed model for the DA1 regulatory system.....	34
Figure 1.3 Structure of DA1.....	34
Figure 1.4 The <i>DA1</i> gene family	37
Figure 1.5 The <i>TCP</i> gene family	44
Figure 2.1 Sequence upstream of <i>DA1</i>	61
Figure 2.2 Annotation of peptidase cleavage sites	66
Figure 2.3 Amino acid sequence of TCP22	69
Figure 2.4 Amino acid sequence of TCP15	70
Figure 2.5 STY1, STY2, TMK4, TMK1 and MEE14 are not cleaved by DA1.....	79
Figure 2.6 TCP3, TCP8 and TCP21 are not cleaved by DA1.....	80
Figure 2.7 Deletion of a predicted cleavage site in TCP15 does not inhibit cleavage by DA1	81
Figure 2.8 Deletion of a predicted cleavage site in TCP22 does not inhibit cleavage by DA1	82
Figure 3.1 Comparison of wild type and <i>da1-1</i> plants grown on soil and on media.....	97
Figure 3.2 Leaf Analysis Toolkit pipeline	103
Figure 3.3 Projections generated by Leaf Analysis Toolkit.....	104
Figure 3.4 Leaf dimensions.....	106
Figure 3.5 Mature leaf size in <i>da1-1</i> , <i>bb</i> , and <i>da1-1bb</i> mutants	108
Figure 3.6 Mature leaf shape in <i>da1-1</i> , <i>bb</i> , and <i>da1-1bb</i> mutants.....	109
Figure 3.7 Growth curve of wild type, <i>da1-1</i> , <i>bb</i> , and <i>da1-1bb</i> leaves	113
Figure 3.8 Natural log growth curve of wild type, <i>da1-1</i> , <i>bb</i> , and <i>da1-1bb</i> leaves	114
Figure 3.9 Linear phase growth of wild type, <i>da1-1</i> , <i>bb</i> , and <i>da1-1bb</i> leaves.....	116
Figure 3.10 Exclusion of leaf margin and midvein cells from segmentation.....	117
Figure 3.11 Total cell number of wild type, <i>da1-1</i> , <i>bb</i> , and <i>da1-1bb</i> leaves	119
Figure 3.12 Mean cell area of wild type, <i>da1-1</i> , <i>bb</i> , and <i>da1-1bb</i> leaves.....	120
Figure 3.13 Cell area distributions within wild type, <i>da1-1</i> , <i>bb</i> , and <i>da1-1bb</i> leaves	122
Figure 3.14 Frequency distributions of cell areas in wild type, <i>da1-1</i> , <i>bb</i> , and <i>da1-1bb</i> leaves	124
Figure 3.15 Mean cell density of wild type, <i>da1-1</i> , <i>bb</i> , and <i>da1-1bb</i> leaves	125
Figure 3.16 Heatmaps of relative cell density within wild type, <i>da1-1</i> , <i>bb</i> , and <i>da1-1bb</i> leaves	126

Figure 3.17 Relative cell density distributions within wild type, <i>da1-1</i> , <i>bb</i> , and <i>da1-1bb</i> leaves	128
Figure 3.18 Frequency distributions of relative cell densities in wild type, <i>da1-1</i> , <i>bb</i> , and <i>da1-1bb</i> leaves	130
Figure 3.19 Mean cell circularity of wild type, <i>da1-1</i> , <i>bb</i> , and <i>da1-1bb</i> leaves	131
Figure 3.20 Cell circularity distributions within wild type, <i>da1-1</i> , <i>bb</i> , and <i>da1-1bb</i> leaves	133
Figure 3.21 Frequency distributions of cell circularities in wild type, <i>da1-1</i> , <i>bb</i> , and <i>da1-1bb</i> leaves	135
Figure 3.22 Collection of SEM images from mature leaves	136
Figure 3.23 Cell area, perimeter, and circularity in mature leaves	138
Figure 3.24 Cell area by location in mature leaves	141
Figure 3.25 Cell perimeter by location in mature leaves	142
Figure 3.26 Cell circularity by location in mature leaves	143
Figure 3.27 Proposed model for the activity of <i>DA1</i> and <i>BB</i> in the control of final cell area	148
Figure 4.1 Model proposed by Kuchen et al. to explain observed growth rates in leaf development	155
Figure 4.2 Growth of <i>spch</i> , <i>spch da1-1</i> , <i>spch bb</i> , and <i>spch da1-1bb</i> leaves	164
Figure 4.3 Growth of <i>spch</i> , <i>spch da1-1</i> , <i>spch bb</i> , and <i>spch da1-1bb</i> leaves relative to wild type, <i>da1-1</i> , <i>bb</i> , and <i>da1-1bb</i>	165
Figure 4.4 Division competency of cells in <i>spch</i>	168
Figure 4.5 Division competency of cells in <i>spch da1-1</i>	169
Figure 4.6 Division competency of cells in <i>spch bb</i>	170
Figure 4.7 Division competency of cells in <i>spch da1-1bb</i>	171
Figure 4.8 Division competency of cells in <i>spch</i> , <i>spch da1-1</i> , <i>spch bb</i> , and <i>spch da1-1bb</i> ..	173
Figure 4.9 Cell area of cells in <i>spch</i> , <i>spch da1-1</i> , <i>spch bb</i> , and <i>spch da1-1bb</i>	175
Figure 4.10 Cell cycle time in <i>spch</i> , <i>spch da1-1</i> , <i>spch bb</i> , and <i>spch da1-1bb</i> leaves	177
Figure 4.11 Cell cycle time over time in <i>spch</i> , <i>spch da1-1</i> , <i>spch bb</i> , and <i>spch da1-1bb</i> leaves	179
Figure 4.12 Cell area at time of division in <i>spch</i> , <i>spch da1-1</i> , <i>spch bb</i> , and <i>spch da1-1bb</i> leaves	180
Figure 4.13 Cell area at time of division over time in <i>spch</i> , <i>spch da1-1</i> , <i>spch bb</i> , and <i>spch da1-1bb</i> leaves	182

Figure 4.14 Area at time of division of cells in <i>spch</i> , <i>spch da1-1</i> , <i>spch bb</i> , and <i>spch da1-1bb</i>	185
Figure 4.15 Cell division symmetry in <i>spch</i> , <i>spch da1-1</i> , <i>spch bb</i> , and <i>spch da1-1bb</i> leaves	186
Figure 4.16 Cell division symmetry over time in <i>spch</i> , <i>spch da1-1</i> , <i>spch bb</i> , and <i>spch da1-1bb</i> leaves	188
Figure 4.17 Areal growth rates of cells in <i>spch</i> , <i>spch da1-1</i> , <i>spch bb</i> , and <i>spch da1-1bb</i>	190
Figure 4.18 Anisotropic growth of cells in <i>spch</i> , <i>spch da1-1</i> , <i>spch bb</i> , and <i>spch da1-1bb</i> ...	192
Figure 4.19 Division competency at the cell population level.....	199

LIST OF TABLES

Table 2.1 List of DA1-interacting proteins identified from the first round of the yeast-2-hybrid screen.....	59
Table 2.2 List of DA1 substrates and putative cleavage sites.....	67
Table 2.3 Phusion High Fidelity PCR protocol	72
Table 2.4 Colony PCR protocol	73
Table 2.5 Vectors used in Chapter 2.....	76
Table 2.6 Primers used in Chapter 2	77
Table 3.1 Plant lines used in Chapter 3	99
Table 3.2 Logistic function parameter values for curve fitting.....	110
Table 3.3 Time at final size of wild type, <i>da1-1</i> , <i>bb</i> , and <i>da1-1bb</i> leaves.....	110
Table 3.4 Significance of difference of <i>da1-1</i> , <i>bb</i> , and <i>da1-1bb</i> from wild type through leaf growth.....	111
Table 3.5 Cell area, perimeter, and circularity in mature leaves.....	137
Table 3.6 Cell area, perimeter, and circularity across sampling positions in mature leaves	139
Table 4.1 Plant lines used in Chapter 4	157
Table 4.2 TaKaRa PCR protocol	158
Table 4.3 Primers used in Chapter 4	159
Table 5.1 Calculations for a model describing the effects of <i>da1-1</i> , <i>bb</i> and <i>da1-1bb</i> on leaf size.....	209

LIST OF EQUATIONS

Equation 3.1 The Boltzmann or Logistic function.....	110
Equation 3.2 Formula for calculating cell circularity	131
Equation 5.1 A model to quantify tissue development and deformation in <i>Drosophila melanogaster</i>	207
Equation 5.2 A model to predict final organ size based on cell size and division factors in <i>Arabidopsis thaliana</i>	208
Equation 5.3 A simplified model for describing the effects of <i>da1-1</i> , <i>bb</i> and <i>da1-1bb</i> on leaf size.....	208

LIST OF SUPPLEMENTARY FIGURES

Figure S1 Cell area distributions within wild type, <i>da1-1</i> , <i>bb</i> , and <i>da1-1bb</i> leaves.....	237
Figure S2 Maximum distal extent of zone of competency to divide in <i>spch</i> , <i>spch da1-1</i> , <i>spch bb</i> , and <i>spch da1-1bb</i> leaves.....	238
Figure S3 Vector map of modified pEarleyGate 103.....	239
Figure S4 Vector map of pw1266.....	240
Figure S6 Vector map of pENTR/D-TOPO.....	241
Figure S7 Vector map of pAtML1::mCitrine-RCI2A.....	242

ACKNOWLEDGEMENTS

Firstly, I must thank my supervisor, Professor Mike Bevan. Mike's enthusiasm for science is infectious, and without his motivation and guidance over the last four years my PhD would not have been the same fulfilling experience, or as successful. I am also thankful to my secondary supervisor, Professor Robert Sablowski, and also Sam Fox, for their comments, assistance and encouragement over the years. I would also like to thank BBSRC for providing the funding for my PhD, and the opportunity to complete an internship that was central to developing my interest in science policy.

I would like to thank everyone who has been involved in this project, in particular our collaborators Dr Stan Marée, Dr Veronica Grieneisen, and especially Dr Ross Carter, who really went above and beyond, answering my emails at all times of the day and night. I am also grateful to my students Jayden, Josie and Heppy - without you, this project could not have come so far. Marc - thanks for all the hours fixing code you didn't write, that wasn't even broken. I would also like to thank Horticultural Services, Lab Support, and BioImaging, most importantly Grant Calder - I'm sorry about the SP5 and your Sunday afternoon.

I have been incredibly lucky to be a part of the Bevan group during my PhD. Thanks to Charlotte for always being ready to talk (about science, or not science at all), Hui and Jing for all the advice and suggestions, and Benguo for the encouragement and ideas. Thanks to Fu-Hao for reminding me how to pipette at the start, Caroline for keeping me on track and always having the answers to my questions, and finally thanks to Neil, for always being ready with a thumbs up. My PhD definitely wouldn't have been the same without any of you.

I feel privileged to have made an amazing group of friends during my time in Norwich, thanks to you all for making these four years more fun than I could possibly have imagined! I can't wait to see what you all achieve in the future, and look forwards to making many more happy memories with you all. In particular, Jemima, thanks for being the best co-social sec, vice chair, co-wheelbarrower, flatmate, and friend that I could have asked for. Thanks also to all the ringers, for reminding me that life goes on outside the bubble.

Thanks to Robert, for all the stability and support over the years, always trying to fix everything, and for proofreading this whole thesis in a single day. You're a hero.

And finally, my family, who have offered unwavering support over the last four years, despite most of the time not understanding what I was doing, or why. Something to do with big saucepans? Thank you.

"I don't feel I really know the story if I don't watch the plant all the way along."

- Barbara McClintock

1 GENERAL INTRODUCTION

1.1 Population growth and the need to increase food production

Global agricultural demand is expected to double from its current state by 2050, as a result of a range of factors including population growth and increasing consumption of biofuels (Ray et al., 2013). It is estimated that, while in the past the annual increase in global agricultural land have been rapid, from now until 2050 this rate will decline, as less land is available for use in farming (Alexandratos and Bruinsma, 2012). While in the past, rates of agricultural production have been able to keep up with population increase due to innovations such as mechanisation or, more recently, the Green Revolution of the 1960s, a new shift in agricultural yield potential is required to increase yields sufficiently where simply increasing the area of arable farmland in use is not possible.

The final yields of crop plants depend on a complex and relatively poorly understood interplay between plant growth and development and the growing environment. Work in this thesis aims to elucidate one mechanism that contributes to determining the final sizes of plant organs such as leaves and seeds, an understanding of which at a genetic and cellular level promises to make important contributions to food security.

1.2 Control of leaf growth in plants

Leaf growth is a multi-phase process, characterised by initial allocation of cells to a primordium from the meristem, followed by the organisation of organ polarity, a period of cell proliferation, and finally cell growth. The coordination of these processes by a complex system of genetic and extracellular signalling results in the production of a determinate leaf size and shape.

1.2.1 Initiation

The shoot apical meristem (SAM) can be divided into several zones, in which cells perform different functions to maintain a population of stem cells while also allocating cells to new organ primordia. The central zone (CZ) at the centre of the apex of the SAM contains the stem cell population, in which cells divide slowly. The peripheral zone (PZ) surrounds the CZ, and contains fast-dividing cells from which organ primordia are initiated (Steeves and Sussex, 1989). The maintenance of the stem cell population in the SAM CZ is controlled by the expression of *WUSCHEL* (*WUS*), in an underlying cell layer known as the organising centre (OC), although not in the stem cells themselves (Mayer et al., 1998). *WUS* expression is inhibited in a negative feedback loop with *CLAVATA1* (*CLV1*), *CLAVATA2* (*CLV2*) and

CLAVATA3 (CLV3). These three genes form a receptor kinase signalling pathway that promotes the progression of cells in the CZ towards the PZ and into organ initiation (Somssich et al., 2016). *CLV3*, a small signalling peptide, is expressed in stem cells and perceived by the *CLV1* receptor (Clark et al., 1997), and another receptor heterodimer formed of *CLV2* and *RLK CORYNE (CRN)*, in the OC (Müller et al., 2008; Guo et al., 2010). The mechanism in which the *CLV* pathway causes transcriptional downregulation of *WUS* is yet unknown, but proposed mechanisms include via intermediary protein phosphatases such as *POLTERGEIST (POL)* and *POLTERGEIST-LIKE1 (PLL1)* (Song et al., 2006), and the *MAPK* cascade (Betsuyaku et al., 2011).

In addition to the *WUSCHEL-CLAVATA* pathway, the Class I *KNOX (KNOTTED1-like homeobox)* family of homeodomain transcription factors also have key roles in maintaining the pluripotent stem cell population in the CZ. The four members of this family in *Arabidopsis thaliana* are *SHOOT MERISTEMLESS (STM)*, *BREVIPEDICELLUS (BP)*, *KN1-LIKE IN ARABIDOPSIS THALIANA2 (KNAT2)* and *KNAT6*. All of these genes are expressed in the SAM, although at different stages of development (Hay and Tsiantis, 2010). The first of these, *STM*, is expressed early throughout the SAM and functions to inhibit the incorporation of cells into developing primordia and promote sustained meristem activity (Endrizzi et al., 1996), potentially via regulation of cytokinin biosynthesis and subsequently the *CYCD3* cell cycle regulator (Scofield et al., 2013). *STM* is required to maintain *WUS* expression in the OC, as well as regulating the expression of the other *KNOX* genes *BP* and *KNAT2* in the PZ (Scofield et al., 2014).

KNOX gene expression is downregulated at leaf initiation and in leaf initials by members of the *YABBY* family (Kumaran et al., 2002), *ASYMMETRIC LEAVES1 (AS1)* and *ASYMMETRIC LEAVES2 (AS2)* (Ori et al., 2000), and the *ARP* genes (Moon and Hake, 2011). In particular, auxin appears to play a role in the repression of *BP*, via a convergent pathway with *AS1* (Hay et al., 2006). Auxin is also believed to repress other *KNOX* family members via the upregulation of *AUXIN RESPONSE FACTOR6 (ARF6)* and *AUXIN RESPONSE FACTOR8 (ARF8)* (Tabata et al., 2010). Auxin has therefore emerged as an important driver of leaf initial outgrowth and regulator of phyllotaxis, and is both required for, and sufficient to, induce organogenesis from meristem tissue (Reinhardt et al., 2000; Reinhardt et al., 2003).

1.2.2 Leaf polarity

The establishment of the adaxial-abaxial, proximo-distal, and medio-lateral axes is of critical importance early in leaf growth, as cell types may be distributed differently within the leaf, according to the polarity of the tissue. For example, cells on the abaxial (ventral) side of the

blade of early leaves in *Arabidopsis* do not include trichome precursors (Telfer et al., 1997), but may include more cells that are specialised for gas exchange, compared to cells on the adaxial (dorsal) surface that may be specialised for light harvesting (Moon and Hake, 2011).

The determination of adaxial-abaxial polarity in leaves is as a result of a complex network of genes acting antagonistically. *AS1* and *AS2* upregulate the Class III homeodomain-leucine zipper (HD-ZIP III) family members *PHABULOSA (PHB)*, *PHAVOLUTA (PHV)* and *REVOLUTA (REV)* which act semi-redundantly on the adaxial side to promote adaxial tissue identity (Prigge et al., 2005; Fu et al., 2007). Members of the *KANADI* gene family, *AUXIN RESPONSE FACTOR3 (ARF3)* and *AUXIN RESPONSE FACTOR4 (ARF4)* are additionally expressed in the abaxial side of the leaf, and promote abaxial tissue specification by acting antagonistically to *AS2* and the HD-ZIP III genes, including transcriptional repression by *KANADI1* of *AS2* (Wu et al., 2008). Finally, *YABBY* family members *FILAMENTOUS FLOWER (FIL)*, *YABBY2 (YAB2)* and *YABBY3 (YAB3)* also promote abaxial cell fate in a positive feedback loop with *ARF3*, *ARF4* and *KAN1*, whereby *FIL* and *YAB3* promote *KAN1* and *ARF4* expression, and *ARF3* and *ARF4* promote the expression of all *YABBY* family members (Siegfried et al., 1999; Eshed et al., 2004; Bonaccorso et al., 2012).

miRNAs such as miR165 and miR166 also have a role in the control of adaxial-abaxial polarity. miRNAs are produced by the processing of pri-miRNA transcripts with DICERLIKE1 (DCL1), HYPONASTIC LEAVES1 (HYL1) and SERRATE (SE), creating pre-miRNA hairpin-like structures. These pre-miRNAs are subsequently processed again by DCL1, resulting in a short, single-stranded miRNA. These miRNAs are subsequently able to bind to mRNAs and specifically inhibit translation. For example, the mRNAs of the adaxial-identity genes *PHB*, *PHV* and *REV* are targeted for cleavage by mobile miR165/166 transcribed in the abaxial side (Rhoades et al., 2002; Mallory et al., 2004; Miyashima et al., 2013).

The antagonistic interactions between these groups of genes with adaxial and abaxial identity function to create the defined boundary between adaxially and abaxially specified cells required for correct leaf development (Moon and Hake, 2011; Fukushima and Hasebe, 2014).

The definition of the proximo-distal axis in simple leaves (leaves with undivided leaf blades, as opposed to compound leaves that are divided into several leaflets) is important for the determination of the petiole-lamina boundary. *KNOX* genes again play a key role in defining the petiole-lamina boundary, with the exclusion of *KNOX* expression in leaves required for correct petiole formation. In the *Arabidopsis blade on petiole (bop)* mutant, *KNOX* expression

is de-repressed in the leaf and *AS2* is upregulated, resulting in ectopic blade tissue growth on the leaf petiole in a more proximal position than in wild type (Norberg et al., 2005).

Finally, the medio-lateral axis is involved in the formation of the flat leaf blade from the initial dome-shaped primordium. This is in part controlled by the interaction of adaxial and abaxial identity promoting genes at the leaf margin, and the development of margin cells. Blade outgrowth is promoted by the *WUSCHEL-RELATED HOMEODOMAIN (WOX)* family gene, *PRESSED FLOWER (PRS)*. *PRS* is upregulated by *YABBY* family members, and is involved in promoting cell proliferation in leaf primordia margins, in conjunction with *WOX1* (Nakata et al., 2012).

1.2.3 Cell proliferation

The early proliferative stage of organ growth is of critical importance in controlling final organ size, by defining a population of cells which will later enter the cell growth phase. For this reason, changes in the rate, duration, or spatial extent of cell proliferation can have a profound impact on final organ size. The rate of cell division is defined as the number of cell division cycles that occur during any given time period - an increase in which, therefore, would result in an increased population of cells being produced within such a time period. The duration of cell proliferation is a measure of the time elapsed before the arrest of cell proliferation throughout the developing organ, a delay in which would also result in a larger population of cells entering the cell growth phase. Finally, the spatial extent, or area, of cell division, denotes the spatial distribution of cell divisions in the organ, and the overall area in which cells retain the competency to divide - the meristematic zone, or zone of competence to divide. Where this zone is larger, it contains a greater population of dividing cells and therefore results in more cell divisions, leading to a greater population of cells entering the cell growth phase.

1.2.3.1 Controlling the rate of cell proliferation

The *GROWTH-REGULATING FACTOR (GRF)* genes are a highly functionally-redundant family of transcriptional co-activators (Horiguchi et al., 2005). While it is accepted that multiple mutations in the *GRF* family result in reduced leaf areas, there is some conflict in the literature over whether this is based on a reduced cell area (Kim et al., 2003), or reduced cell proliferation (Horiguchi et al., 2005). It seems that one member of the *GRF* family, *GRF3*, has the most distinct role in the control of cell proliferation (Horiguchi et al., 2005). A further layer of regulatory complexity is added by the post-transcriptional regulation of *GRF* mRNA by miR396 (Rodriguez et al., 2010).

The *GRF-INTERACTING FACTOR (GIF)* gene family is made up of three transcription co-activators, *GIF1/ANGUSTIFOLIA3*, *GIF2* and *GIF3*. Rosette leaf area is reduced in *gif1* mutants, as a result of decreased cell numbers (Kim and Kende, 2004). While single mutations in *gif2* and *gif3* produce no obvious phenotype, the *gif1gif2gif3* triple mutant shows a very strong reduction in leaf area, with a leaf area of only around 10% of wild type. Kinematic analysis showed that both the rate and duration of cell proliferation was reduced in all mutants with the *gif1* mutation, which conferred the strongest phenotype relative to wild type (Lee et al., 2009). RT-PCR revealed that the expression of some cyclins and cyclin-dependent kinases was reduced in *gif* mutants, suggesting a role for the *GIF* family in the positive regulation of cell proliferation by the control of genes involved in the cell cycle (Lee et al., 2009). The GRF and GIF families work together as transcriptional coactivators to control cell proliferation, potentially via diverse pathways (Kim and Tsukaya, 2015).

The *SLEEPY1* gene codes for an F-Box component of an SCF E3 ubiquitin ligase complex (explored further in Section 1.5.4) (McGinnis et al., 2003), which relieves the DELLA-mediated repression of gibberellin biosynthesis (Ariizumi et al., 2011). In the knockdown *sly1* mutant, the DELLA-mediated repression of gibberellin biosynthesis is not de-repressed, resulting in a reduced leaf area due to a decreased rate of cell proliferation (Achard et al., 2009), positioning *SLEEPY1* as an indirect promoter of the rate of cell proliferation.

As well as a range of genes promoting an increased rate of cell proliferation, there are a number of genes known to inhibit the rate of cell proliferation. Contrasting with *SLY1*, other F-box proteins have also been found to affect leaf size by controlling the rate of cell proliferation, for example *FBX92*, where reduced *FBX92* expression promoted an increased rate of cell division, and a reduced cell cycle time (Baute et al., 2017). This indicates a role for *FBX92* in the repression of cell proliferation, although the mechanism by which it functions is not yet known.

INHIBITOR OF CDK1 (ICK1) was the founder member of the *ICK/KRP* family of CDK inhibitors (Wang et al., 1997), which redundantly control CDK activity by repressing the E2F pathway (explored in more detail in Section 1.3). Mutations in the *ICK/KRP* family result in increased CDK activity, and quadruple and quintuple mutants exhibit larger leaves with an increased cell number (Cheng et al., 2013). This supports a role for the *ICK/KRP* family in the repression of the rate of cell proliferation via the repression of genes involved in the promotion of the cell cycle.

The four-member *NGATHA* family of transcription factors is known to have a role in the control of organ size. The *nga1* mutant exhibits larger petals as a result of increased cell number (Alvarez et al., 2009), and *NGA* overexpressor lines show significantly reduced leaf areas, particularly in width, which is primarily as a result of a reduction in cell number - although there was also some impact on leaf area from cell growth. Kinematic analyses revealed that this reduction in cell number was due to a reduction in the cell proliferation rate in the overexpressors (Lee et al., 2015), positioning the *NGATHA* family as repressors of the rate of cell proliferation.

1.2.3.2 Controlling the duration of cell proliferation

Overexpression of the auxin-inducible gene *ARGOS* leads to an increase in leaf area of 50-120%, relative to wild type, whereas in plants where *ARGOS* expression is repressed, leaves are significantly smaller. These differences are primarily as a result of changes in cell number, rather than in cell area, and kinematic analyses indicated that there was an increased duration of cell proliferation in *ARGOS* overexpressor plants, rather than an increased rate (Hu et al., 2003). Given the similarity of the overexpressor phenotypes of *ARGOS* and *AINTEGUMENTA (ANT)* (Mizukami and Fischer, 2000), it is unsurprising that *ARGOS* appears to promote the duration of *ANT* expression (Hu et al., 2003), which is known to promote an extended duration of cell proliferation (Mizukami and Fischer, 2000). In tandem with this, the expression of the cell cycle gene *CYCD3;1* was also prolonged in *ARGOS* overexpressors (Hu et al., 2003).

The *KLUH (KLU)* gene encodes the cytochrome P450 CYP78A5. In *klu* mutants, the reduced leaf, sepal and petal size is a result of decreased cell number, and not a change in cell area. Analysis of the growth of *klu* mutants and wild type showed that the mutants increased in size at the same rate as wild type, yet stopped growing earlier. Further analysis of cell division rates revealed that there was no change in early cell division rates in the mutant (Anastasiou et al., 2007), presenting a probable role for *KLUH* in delaying the arrest of cell proliferation.

The *STRUWWELPETER* gene also appears to play an important role in defining the window of cell division by delaying the arrest of cell proliferation. Leaves in *swp* mutant plants are smaller than in wild type, and this was shown to be primarily as a result of decreased cell number, although this was partly compensated for by increased cell areas. Using confocal imaging over a 2-day time period, it was established that there is no change in the rate of cell proliferation. Further kinematic analysis concluded that cells in the *swp* mutant arrest

cell proliferation earlier than in wild type, leading to a reduced overall cell number (Autran et al., 2002).

As well as the promotion of the duration of cell proliferation, several genes have been reported as reducing the duration of cell proliferation in organ growth. Among these are *DA1*, *DA2* and *BIG BROTHER (BB)*, each of which have been reported as limiting the duration of organ growth, based on kinematic analyses of growth (Disch et al., 2006; Li et al., 2008; Xia et al., 2013), and transcriptional analysis (Vanhaeren et al., 2017). Both *DA2* and *BB* have been found to genetically interact with *DA1*, and we have recently shown that, as E3 ligases, *DA2* and *BB* are both able to ubiquitinate *DA1* (Dong et al., 2017), activating peptidase activity in *DA1* which is thought to indirectly result in growth regulation (see Section 1.4).

Mutations in *AUXIN RESPONSE FACTOR2 (ARF2)* generate larger leaves and floral organs - partially as a result of larger cells, but also as a result of an increased number of cells. In *arf2* mutants the expression of *ANT* and *CYCD3;1* was prolonged, indicating a regulatory mechanism to precisely control the timing of cell proliferation arrest (Schruff et al., 2006). The identification of *ARF2* as a positive regulator of leaf senescence (Ellis et al., 2005) suggests that it may have a wider role in controlling the progression of tissue through the life cycle, by promoting the arrest of cell proliferation and subsequent senescence.

1.2.3.3 Controlling the area of the leaf meristem

While most mutants with aberrant determination of cell number are as a result of a change in the rate or duration of proliferation, some genes are known to control the area of the leaf meristem - that is, the spatial distribution of dividing cells within the leaf. Little is known of genes that promote an increase in the area of the leaf meristem. There is some limited evidence that *GIF1/AN3* may play a role in the maintenance of proliferative activity in more distal regions, although these data are unpublished (Horiguchi et al. unpublished data, see Ichihashi et al., 2010).

By contrast, several genes are known to work to limit the spatial extent of the leaf meristem during growth. In overexpressors of the *ROTUNDIFOLIA4 (ROT4)* gene, expression of *pCYCB1;1:CYCB1;1-GUS* (a marker of cell proliferation) was more proximally restricted than in wild type (Ikeuchi et al., 2011). In the *rot4-1D* dominant gain-of-function mutant, leaves were found to be shorter and more rounded than in wild type, and be formed of fewer cells specifically in the proximo-distal axis. This indicates a role for *ROT4* in the polar control of leaf shape and size by limiting the area of the meristematic zone (Narita et al., 2004).

In addition to this, loss-of-function mutants of the *SPATULA* basic helix-loop-helix transcription factor, *spt*, exhibit larger leaves than wild type. This is due to increased cell number, as there is no difference in cell area between *spt* mutants and the wild type. While at early stages of development (3 days after sowing) *spt* mutants exhibited no significant phenotypic difference from wild type, by 5 days after sowing there was a strong difference in leaf area, which was maintained subsequently. This indicated a developmental difference between the mutant and the wild type within this 2-day window. Analysis of cell areas along the proximo-distal axis suggested that the meristematic zone was larger in the *spt* mutants, indicating that *SPT* may restrict the extent of the zone of competency to divide (Ichihashi et al., 2010). Further evidence for this has been shown in roots, where *spt* mutants have a larger quiescent centre and root apical meristem (Makkena and Lamb, 2013).

Finally, there is some limited evidence that *DA1* may also have a role in limiting the meristematic zone in leaves, as *pCYCLINB1;1::GUS* expression is distally increased in the *da1-1* dominant negative mutant at 9 days after germination, although without further investigation it is impossible to determine whether this is as a result of an increased duration of growth (as predicted by Li et al., 2008), or by a decreased restriction on the area of the leaf meristem (Li et al., 2008).

1.2.3.4 Meristemoid cell division

Meristemoid cell divisions are required for the formation of stomatal guard cells. There is some level of plasticity in the number of asymmetric cell divisions that take place to generate guard cells - in *Arabidopsis* of the Columbia ecotype (as used in this thesis), two thirds of stomata are formed after only one or two asymmetric cell divisions of meristemoid cells (Geisler et al., 2000), while in other ecotypes this ranges from zero to three (Serna, 2013). After the final asymmetric cell division, the guard mother cell undergoes a final symmetric cell division to produce the two guard cells. The non-meristemoid cells that were earlier produced during the asymmetric cell divisions become pavement cells later in development (Peterson et al., 2010). It is estimated that approximately 48% of all pavement cells in the leaf epidermis are formed in this manner (Geisler et al., 2000; Bergmann and Sack, 2007), meaning that aberrations in meristemoid cell divisions may have a significant effect on organ size.

This is illustrated by loss-of-function mutations in the transcriptional regulators *PEAPOD1* (*PPD1*) and *PEAPOD2* (*PPD2*), where leaf area is increased as a result of increases in both leaf width and length. *ppd* mutants also exhibit an increased leaf curvature relative to wild type,

indicating increased growth of the leaf lamina without a concurrent increase in the leaf margin. There were observed to be increased numbers of meristemoid cells in the *ppd* mutant, indicating aberrant meristemoid divisions, leading to the observed increase in leaf area and curvature. These divisions were found to continue for a longer duration than in wild type, indicating a tissue-specific extension of the duration of proliferation, in part controlled by the *PPD* locus (White, 2006). This is supported by more recent findings describing *PPD2* as a repressor of the expression of many genes involved in the cell cycle, for example *CYCD3;2* and *CYCD3;3* (Gonzalez et al., 2015).

1.2.4 Cell growth

Cell growth may be divided into two processes that, together, result in an increase in cell volume. The first of these processes is cytoplasmic growth due to synthesis of macromolecules such as proteins, starch and lipids. The TOR (Target Of Rapamycin) pathway is central to the regulation of this mode of growth. TOR is a serine/threonine kinase from the Phosphatidylinositol-3-Kinase-related Kinase (PIKK) family, with a role in the signalling of metabolic stress. As a central regulator of macromolecular synthesis, TOR primarily controls ribosome biogenesis – a prerequisite for other biosynthetic activities required for cytoplasmic growth (Sablowski and Carnier Dornelas, 2014). TOR signalling may also be an overall limiting factor in organ growth, as higher and lower expression levels result in larger and smaller organs, respectively, as a result of changes in cell area (Deprost et al., 2007).

The second factor in cell growth is turgor-driven cell expansion – that is, yielding of the cell walls to increased turgor pressure within the cell, and their relaxation to accommodate an expanded cytoplasm. Plant cell walls are composed of a matrix of pectin and proteins, with cellulose and hemicellulose fibrils embedded within it. Acidification of the apoplast promotes the activity of *EXPANSIN* proteins to break the hydrogen bonds between these polymers and allow the cellulose microfibrils to slip past each other, which, together with pectin matrix modification, permits the extension of the cell wall. Subsequent alkalinisation of the apoplast promotes cross-linking of cell wall components to reform the cell wall and prevent further expansion, which is then finally strengthened with the secretion of more cell wall material (Wolf et al., 2012; Sablowski, 2016).

1.2.4.1 Endoreduplication-mediated cell growth

Endoreduplication is strongly correlated with cell growth in many tissues of *Arabidopsis*, including leaf epidermal cells and the hypocotyl (Melaragno et al., 1993; Gendreau et al., 1997), although the link is not so clear in root tissue (Beemster et al., 2002). One theory

surrounding the endocycle is that the volume of cytoplasm that a cell can produce and maintain is proportional to the amount of DNA in its nucleus - this is known as the “karyoplasmic ratio” (Sugimoto-Shirasu and Roberts, 2003).

Increased DNA content in the cell may result in cytoplasmic growth through ribosome biogenesis - this mechanism has been observed in yeast and *Drosophila*, in which S6 kinase phosphorylates S6, a key ribosomal assembly protein (Montagne et al., 1999). However, there is little direct evidence for ribosome biogenesis in plants as a result of increased ploidy. An alternative mechanism could be that increased ploidy results in increased gene expression, and therefore total protein synthesis - promoting macromolecular synthesis as described above in cytoplasmic growth. However, work in Arabidopsis lines with varied ploidy levels and cell sizes has shown that this variation in ploidy resulted in only a small proportion of genes being differentially expressed relative to overall gene expression levels (Lee and Chen, 2001). Therefore, the precise mechanism through which increased amounts of DNA results in an increased cell size remains unclear.

1.2.5 Control of the transition from cell proliferation to cell expansion

The arrest front that marks the transition from cell proliferation to cell expansion has been quite well described (Kazama et al., 2010; Andriankaja et al., 2012). It is seen as a wave of arrest of cell proliferation that moves from the tip of the leaf to the base, but pauses a certain distance from the base of the leaf and is then subsequently abolished rapidly. There is also a subsequent secondary arrest front that arrests the proliferation of stomatal and vascular precursors (White, 2006), but in this section I will focus on the control of the progression of the primary arrest front.

A number of antagonistic interactions are thought to control the progression of the arrest front, and hence the timing of the arrest of cell proliferation. For example, *DA1*, *BB* and *DA2* are believed to promote the arrest of cell proliferation by affecting the timing of the movement of the arrest front (Disch et al., 2006; Li et al., 2008; Xia et al., 2013). Conversely, *KLU* and *CYCD3* may delay the movement of the arrest front, therefore negatively regulating the onset of cell expansion (Anastasiou et al., 2007; Dewitte et al., 2007; Kazama et al., 2010). *KLU* has been proposed as a mobile growth factor (MGF) which could control the progression of the arrest front from a restricted expression domain in the base of the leaf, positioning it as a potential component of a morphogen gradient controlling cell division and growth within the developing leaf (Anastasiou et al., 2007; Kazama et al., 2010). The TCP family genes are known to be key regulators of cell proliferation and expansion, and so the balance of

expression of antagonistic class I and class II TCP transcription factors could also be involved in the regulation of the progression of the arrest front (Li et al., 2005). As described in Section 1.2.3.3, *SPT* and *ROT4* may be involved in limiting the size of the leaf meristem, and therefore regulation of the spatial dynamics of the arrest front by changing the distance from the petiole-lamina boundary at which the arrest front pauses before being rapidly abolished (Narita et al., 2004; Ichihashi et al., 2010).

In addition to these genetic factors, Andriankaja et al., 2012 observed that the onset of photosynthesis and the appearance of stomata occurred just before the onset of cell expansion, at around 9 days after sowing, in the third leaf. This also coincided with the greening of the leaf tip, which also moved in a basipetal manner. Further transcriptional analysis found that chloroplast differentiation and retrograde signalling could be a trigger for the arrest of cell proliferation (Andriankaja et al., 2012). The factors that may be involved are unknown.

1.2.6 Hormonal coordination of cell division and cell expansion throughout growth

Phytohormones such as auxin, brassinosteroids, cytokinins and gibberellic acid are key regulators of organ development. As small signalling molecules, they are able to mediate long-distance signalling throughout the leaf and therefore have potentially wide-reaching impacts on both growth and development (Johnson and Lenhard, 2011).

Auxin has extensive roles in the regulation of organ morphogenesis (Perrot-Rechenmann, 2010), as well as organ initiation and outgrowth (Reinhardt et al., 2000; Reinhardt et al., 2003). For example, cells in culture may cease to divide in the absence of auxin, and when auxin is re-introduced into the system, cell division is restored - indicating that auxin is required for cell division in cultured cells (Tréhin et al., 1998; Stals and Inzé, 2001; Inzé and De Veylder, 2006). Auxin is known to regulate many aspects of the cell cycle (see Section 1.3), for example by inducing the expression of *CDKA1;1* and *CYCD3;1* (Ferreira et al., 1994; Dewitte and Murray, 2003), and by inhibiting expression of the CDK inhibitors *KRP1* and *KRP2* (Richard et al., 2001; Himanen et al., 2002). The auxin-inducible gene *ARGOS* promotes an increased duration of proliferation, potentially by functioning upstream of *ANT* and *CYCD3* and prolonging their expression (Hu et al., 2003). This positions *ARGOS* as an intermediate in the mechanism for auxin-mediated regulation of cell proliferation.

As well as cell proliferation, auxin also has a role in the regulation of cell growth, as it has been shown to be sufficient to induce rapid cell expansion in stem and hypocotyl segments

- known as the Acid Growth Theory of auxin-mediated cell elongation due to activation of a proton pump at the plasma membrane, resulting in extracellular acidification and the activation of EXPANSINS (Rayle and Cleland, 1992).

Brassinosteroids upregulate *ARGOS-LIKE (ARL)*, which shares some sequence homology with *ARGOS*. However, *ARL* is involved in the promotion of growth by enhancing cell growth, rather than stimulating cell proliferation as in the case of *ARGOS*. Brassinosteroid-mediated upregulation of *ARL* is inhibited in mutants of the *BRI1* brassinosteroid receptor, indicating that *ARL* functions downstream of *BRI1* to mediate brassinosteroid-induced cell expansion (Hu et al., 2006). In addition, brassinosteroids have also been shown to promote epidermal growth and, when expressed in the epidermis only, be sufficient to promote growth and normal vascular development in the vascular tissue layer within the organ - positioning brassinosteroids as important signalling molecules within organs to promote growth (Savaldi-Goldstein et al., 2007).

In plants deficient in cytokinin biosynthesis or signalling, the size of the SAM is repressed, indicating that cytokinins are critical for the proper maintenance of stem cell populations (Werner et al., 2001). The *ahk2ahk3ahk4* triple mutant lacks three key cytokinin receptors, and exhibits a reduced leaf area as a result of fewer cells, rather than a reduction in cell area (Higuchi et al., 2004; Nishimura et al., 2004).

The role of gibberellic acid in the regulation of cell division has been elucidated by the discovery of DELLA proteins, which repress the growth-promoting activity of gibberellins (Hauvermale et al., 2012; Davière and Achard, 2013). In quadruple-DELLA mutants, the activity of gibberellins is de-repressed, resulting in significantly larger leaves due to an increase in cell numbers - indicating that gibberellins promote larger organ sizes through an increase in the rate of cell proliferation (Achard et al., 2009).

1.2.7 The compensation mechanism

Many of the genes discussed in this section that affect cell proliferation and leaf area were also found to exhibit small changes in cell area. This may represent, at some level, the so-called “compensation” effect, whereby aberrations in cell proliferation promote a concomitant change in cell area, resulting in a final organ size similar to that of wild type.

This phenomenon is well-described in the development of *Drosophila melanogaster* wings – a similar determinate, flat, multicellular organ to leaves in *Arabidopsis*. In *Drosophila*, it is thought that the final size of an organ is actively controlled by a “total mass checkpoint”,

whereby the control of final organ size as a whole is separable from, and supersedes, the control of cell proliferation. This results in cell area reductions where cell proliferation is genetically increased, and defects in cell proliferation result in increased cell area to account for the reducing in cell number – in both cases, the wing develops to the correct final size (Potter and Xu, 2001).

That the mutants described earlier in this section exhibit defects in cell proliferation and the changes in cell area are not sufficient to return the overall organ size to that of wild type indicates that leaf size is not regulated by a similar “total mass checkpoint” to that of *Drosophila* wings. However, this does not discount the possibility of partial compensation mechanisms that have been observed in a number of mutants affecting Arabidopsis leaf growth.

Kinematic analyses of growth indicate that there could be three classes of compensation. In Class I mutants, such as *an3*, *fugu2/fas1* and *er* mutants, the rate of cell expansion is increased in the post-mitotic phase relative to wild type, but the period of cell expansion is not affected. In Class II mutants such as *fugu5*, there is an increase in the duration of cell proliferation relative to wild type. Finally, Class III is only exhibited in the *KRP2* over-expressor, whereby cells are already larger than wild type during the mitotic phase, in addition to an increased rate of cell expansion in the post-mitotic phase, in a dosage-dependent manner (Ferjani et al., 2007; Hisanaga et al., 2015).

1.2.8 Organ-level coordination of growth

The possibility described above of compensation mechanisms regulating overall organ size suggests that there could be a mechanism that allows cells to control their own growth according to cues derived from their neighbours or across the whole growing organ that “set” the correct final organ size. There are two potential models that have been suggested to regulate this - the cell-autonomous system, and the non-cell-autonomous system.

The cell-autonomous system suggests that, in the initial organ primordium, each cell is allocated a fixed amount of a factor that promotes cell growth and division, which is subsequently split between cells as they divide, so as to eventually reduce the cellular concentration of the growth promoting factor. A well-described example of this is found in *Drosophila*, in which the promoter of nuclear proliferation CYCLIN B is allocated to nuclei and degraded at each nuclear division, resulting in a fixed number of divisions per nucleus (Edgar et al., 1994). There is no direct evidence to date for a mechanism of this type in plants, although regulation of the cell cycle at this level remains entirely plausible.

By contrast, the non-cell-autonomous model involves a field of a signalling molecule(s) that provides spatial information to cells in that region, and that may promote cell division and growth. A potential mechanism for this could be the production of a division-promoting morphogen in the base of the leaf, which would diffuse throughout the leaf but promote cell division only in basal regions, as recognition by cells would be threshold-dependent (Lenhard, 2012). The activities of auxin and brassinosteroid as mobile signals within tissues and organs (see Section 1.2.6) position them as potential candidates for such a diffusible morphogen. In addition, a number of genes have been shown to control cell division both in their own expression domain and outside, for example AN3 is expressed in the mesophyll yet is able to move to the epidermis to promote cell proliferation (Kawade et al., 2013).

1.2.9 Modelling organ growth

Mathematical modelling has been applied to organ growth in *Arabidopsis* in several studies (Mündermann et al., 2005; Dochain and MacLean, 2016; Kuylén et al., 2017). One model in particular uses named “factors” to mediate tissue growth, cell growth and cell division (Kuchen et al., 2012; Fox et al., under review). In the model proposed by Kuchen and Fox, there are a number of factors which are expressed differentially within the leaf, and have different effects on tissue and cell behaviour. For example, PGRAD is a modelled growth promoting factor that is expressed in a linear gradient from the base to the tip, in a similar manner to the growth promoting factor proposed in the non-cell-autonomous model of growth described above. LATE is expressed uniformly throughout the tissue, but at later stages is able to repress the growth promoted by PGRAD. A number of other factors regulate the identity of the midvein and lamina, cell polarity, the size of the leaf meristematic zone (termed the “zone of competency to divide”) and the ability of cells to divide (Kuchen et al., 2012; Fox et al., under review). This model is described in more detail in Chapter 4.

By modulating the levels and timings of many of these factors in their models, Kuchen et al. and Fox et al. present a range of simulated phenotypes at both the cellular and whole organ level. By matching these simulated phenotypes to those of known mutants, and by matching known activity of genes or phytohormones to the proposed activities of factors in the model, it will be possible in the future to use these models and factors to test quantitatively different candidate genes and molecules in order to create a more precise and integrated model of organ development.

1.3 Organ growth and the cell cycle in plants

Control of the cell cycle is critical for the correct formation of all organs in the plant. Aberrations in the rate of progression through the cell cycle affect the rate of cell division, while changes in the regulation of the endocycle may result in changes in cell area. Either of these changes are likely to strongly impact final organ size, and it has been shown that many genes known to influence organ size via either affecting the cell number or cell area differentially regulate some components of the cell cycle (see Section 1.2).

The cell cycle is a cyclical, unidirectional process through which cells pass in order to complete mitotic cell divisions. The four phases, G1, S, G2 and M represent two gap phases separating the replication of DNA (S phase), and the cell division by cytokinesis, completing the mitotic cycle (M). Following mitosis, cells pass through the first gap phase, G1, followed by DNA replication in the S phase, a second gap phase, G2, and finally undergo mitosis again (M). At each boundary, but primarily the G1/S and G2/M boundaries, there are unidirectional checkpoints, through which the cell cycle can be controlled. Progression through these checkpoints is controlled by a series of cyclin-dependent kinases (CDKs) and their cyclin subunits (Dewitte and Murray, 2003).

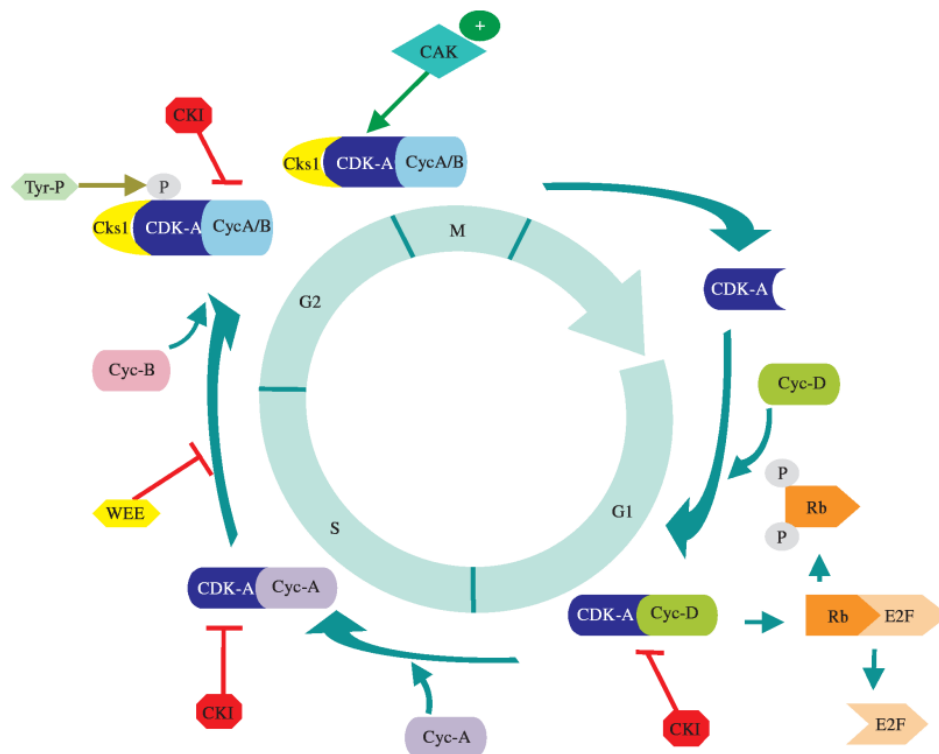


Figure 1.1 Schematic representation of cell cycle control in plants

From (Andrietta et al., 2001). Reproduced under a Creative Commons License.

There are seven classes of CDK, A-G, of which As, Bs, Ds and Fs have a known role in the regulation of the cell cycle. In plants, there are also seven classes of cyclin - A, B, C, D, H, P and (T), although primarily A, B and D cyclins are involved in the control of the cell cycle. Although there are some exceptions, in general cyclins are grouped according to the checkpoint that they regulate - A-type cyclins regulate the S phase, B-type control G2 progression and the G2/M transition, and D-type the G1/S (Dewitte and Murray, 2003; Francis, 2007).

The regulation of cyclin levels during the cell cycle is important for correct progression. There are two mechanisms by which cyclin levels are regulated - at the transcriptional level, and also by protein-turnover mechanisms. Both A-type and B-type cyclins are regulated by the identification of their "destruction box" which results in removal by the anaphase-promoting complex (APC) at the entry to the M phase. D-type cyclins are targeted for degradation in the proteasome via ubiquitination by an SCF complex (Dewitte and Murray, 2003).

CDK activity is regulated by phosphorylation by a CDK-activating kinase (CAK), of which two are known in Arabidopsis (Umeda et al., 1998; Dewitte and Murray, 2003). There are also several known repressors of CDK activity. These include *ICK/KRPs* (Cheng et al., 2013), which inhibit CDK activity by binding to the active CDK-cyclin complex (De Veylder et al., 2001), and the *WEE1* kinase (Shimotohno et al., 2006), indicating that phosphorylation has both activation and inhibition functions in the control of the cell cycle (Francis, 2007).

1.3.1 The endocycle

Entry into the endocycle is associated with an increase in cell area (see Section 1.2.4.1) and is therefore an important component of organ growth. Endoreduplication takes place when a cell completes the DNA synthesis phase, but does not undergo mitosis - resulting in a doubling of the cell DNA ploidy with every additional endocycle (Van den Heuvel, 2005). The cell cycle components *CYCA1*, *CYCA2*, *CYCBs* and *CDKB* are downregulated in cells undergoing endoreduplication, as these components are proposed to promote entry into the M phase. In addition, *CCS52*, an activator of the APC, may be responsible for targeting mitotic cyclins (such as the above) to initiate endoreduplication, although this mechanism remains unclear (Cebolla et al., 1999; Dewitte and Murray, 2003). Gibberellic acid has been observed to promote entry into the endocycle in hypocotyls and leaf trichomes via antagonistic interactions with salicylic acid (Belkhadir and Chory, 2006). *SPINDLY* represses gibberellic acid activity, and *spy* mutants exhibit over-endoreduplication phenotypes similar to wild type plants exposed to high levels of gibberellic acid (Swain et al., 2002), indicating a clear role for

gibberellic acid in the regulation of the entry to the endocycle. However, how this initiation takes place is not yet clear.

1.4 The role of the DA1 regulatory system in growth control

1.4.1 A model for growth control via the DA1 regulatory system

In Dong et al., 2017, we proposed a mechanism for DA1 activity based on a range of observed biochemical and genetic interactions. *In vitro* ubiquitination assays showed that BIG BROTHER and DA2 can multiply mono-ubiquitinate DA1 in an E1 and E2-dependent reaction (see Section 1.5), with four to five consistently ubiquitinated lysine residues in the C-terminus. Substitution of one of these four to five lysine residues to arginine does not reduce the level of ubiquitination of DA1 by DA2, while mass spectrometry analyses revealed that other lysines in DA1 are ubiquitinated in this mutant, showing that the ubiquitination mechanism in DA1 has a preference for the four to five consistently ubiquitinated lysine residues, but not a requirement (Dong et al., 2017).

Mutation of the two UIM domains (see Section 1.4.2.3) of DA1 revealed that, while a mutation in UIM1 alone did not affect the ubiquitination of DA1, in the absence of a functional UIM2, there was no ubiquitination of DA1. This indicates that the ubiquitination of DA1 is UIM-dependent (Dong et al., 2017).

Incubation of both BB and DA2 with ubiquitinated DA1 generated cleavage products of ~35kDa and ~25kDa respectively. It was found that ubiquitination mediated by either E3 ligase was sufficient to result in the cleavage of either E3 ligase. Mutation of the histidine residues in the zinc metallopeptidase domain of DA1 resulted in the DA1-pep mutant (Figure 1.3), which was able to be ubiquitinated to the same extent as DA1, but was not able to cleave BB and DA2.

Therefore, DA1 has latent metallopeptidase activity that is activated by UIM-mediated multiple mono-ubiquitination by the E3 ligases BB and DA2, and activated DA1 is able subsequently to cleave these two E3 ligases, as well as a number of other substrates (see Section 1.4.3.2), and may cleave other, unknown substrates involved in the control of organ size.

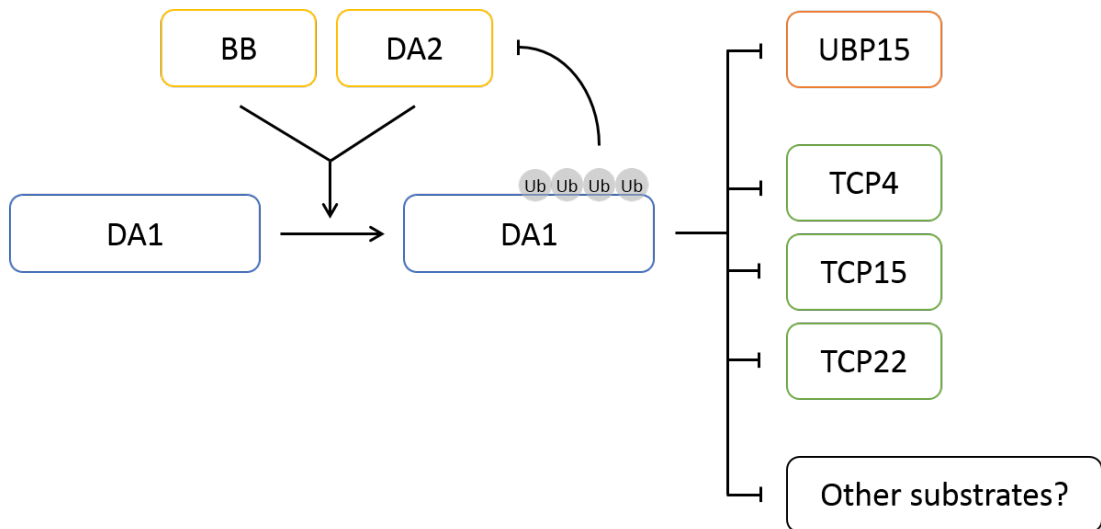


Figure 1.2 A proposed model for the DA1 regulatory system

1.4.2 Structure and function in the DA1 family

A structural analysis of DA1 was carried out by Dr Jack Dumenil (Dumenil, 2013) and is partially presented in Dong et al., 2017. DA1 was found to contain four different domains of known function: a C-terminal zinc-metallopeptidase, central LIM and LIM-like domains, and two N-terminal UIM domains. These are shown in Figure 1.3.

```

MGWFNKIFKGSNQRLRVGNKHNHNHVVYDNYPTASHDDPSAADTDADNDEPHHTQEPSTSEDNTSNDQENEDIDRAIALSLLEENQEQTSSISGKYSMPVDEDEQL
ARALQESMVVGNSPRHKSGSTYDNGNAYGAGDLYGNHMYGGGNVYANGDIYPRPITFQMDFRICAGCNMEIGHGRFLNCLNSLWHPECFRCYGCSPISEYEFS
TSGNYPFHKACYRERYHPKCDVCSHFIPNTNHAGLIEYRAHPFWVQKYCPSHEHDATPRCCSERMEPRNTRYVELNDGRKLCLELDSAVMDTMCQCPPLYLQIQNFY
EGLNMKVEQEVPLLLVERQALNEAREGEKNGHYHMPETRGGLCLSEEQTVSTVRKRKSHGTGKWAGNITEPYKLTROCEVTAAILFGLPRLTGSILAHMMHAWMRL
KGFRTLSQDVIGICQVMAHKWLDAELAAGSTNSNAASSSSSSQGLKKGPRSQYERKLGFEFFKHQIESDASPVYGDGFRAGRLAVHKYGLRKTLEHIQMTGRFPV

```

Figure 1.3 Structure of DA1

Amino acid sequence of DA1 (AT1G19270) with protein domains, ubiquitinated residues, and the *da1-1* mutation shown. Protein domains: zinc-metallopeptidase active site, red; LIM domain, cyan; LIM-like domain, dark green; UIM 1 & 2, yellow. Consistently ubiquitinated lysine (K) residues shown in orange. Key mutations shown in purple (DA1^{C274Y}, DA1^{R358K}, DA1-pep).

1.4.2.1 The zinc-metallopeptidase

The C-terminal zinc metallopeptidase domain (Pfam: PF12315) is strongly conserved among all members of the DA1 family (Figure 1.4), defining them as DA1-like (IPR022087). The DA1 peptidase domain is structurally similar to that of the human angiotensin I-converting

enzyme (ACE), a zinc metallopeptidase with a role in blood pressure homeostasis. It fulfils this role by cleaving the C-terminus of two peptides – angiotensin I and bradykinin – the first of which produces angiotensin II (a vasopressor protein), and the second of which results in the loss of bradykinin’s vasodilatory properties (Williams et al., 1994). ACE is a member of the M2 family of zinc-binding metallopeptidases, which falls within the MA clan (Pfam: CL0126) (Natesh et al., 2003). The MA clan contains 71 families and is characterised by the neutral zinc-metallopeptidase domain (PROSITE: PS00142), which has a conserved HEXXH motif (Finn et al., 2016) also found in DA1 (Figure 1.3). As well as ACE, the MA clan also includes a range of peptidases from bacteria, metazoans, fungi, archaea and plants, including soybean metalloendoprotease 1 which is expressed in mature soybean leaves and has been proposed to have a role in tissue modelling during leaf expansion (Graham et al., 1991; Sigrist et al., 2013).

The activity of metallopeptidases has been shown to be regulated by a “cysteine switch” mechanism, in which a cysteine is dissociated from the peptidase active site, promoting peptidase activity. For example, in latent human fibroblast collagenase, Cys⁷³ is localised in such a manner that it blocks the active site at the active site zinc atom. All known activation mechanisms, for example by aminophenyl mercuric acetate, have been shown to disassociate the Cys⁷³ from the zinc atom, leading to activation of the peptidase (Van Wart and Birkedal-Hansen, 1990). The cysteine switch mechanism may afford some flexibility in the mode of activation of the metallopeptidase. It may be that different activators are more or less efficient at mediating the disassociation of the relevant cysteine, or that different activators have different efficiencies in different cell or tissue types. These mechanisms allow some flexibility in the activation of the peptidase (Chakraborti et al., 2003), and could present interesting avenues of research for DA1.

1.4.2.2 *The LIM and LIM-like domain*

The LIM (Lin11, Isi1 and Mec-3) domain (PROSITE: PS00478) is a multiple zinc-finger domain with a role in the mediation of highly specific protein-protein interactions (Schmeichel and Beckerle, 1994; Agulnick et al., 1996; Kadrmaz and Beckerle, 2004). This supports its importance in the interaction of DA1 with its substrates – though not in the formation of DA1 homo-oligomers (DA1 forms homo-oligomers, and hetero-oligomers with other members of the DA1 family for example DA1-RELATED1, in a LIM-independent manner (Dumenil, 2013)). LIM domains generally comprise 55 amino acids, of which eight cysteine and histidine residues are highly conserved among functional domains in different species. The general structure is as follows: CX₂CX₁₆₋₂₃HX₂CX₂CX₂CX₁₆₋₂₁CX₂{C/H/D} (Schmeichel and Beckerle,

1994; Schmeichel and Beckerle, 1997). The number and spacing of the cysteine and histidine residues allows the binding of the two zinc ions in a tandem zinc-finger pattern (Michelsen et al., 1994), with an invariant two-residue spacer between the two which seems to be necessary for LIM domain function (Schmeichel and Beckerle, 1997). The remainder of the sequence (as indicated by X above) is more variable and allows the LIM domain to have high functional specificity.

The role of LIM domains as protein-protein interaction mediators is well established (Schmeichel and Beckerle, 1994), although as yet no conserved sequence preferences for LIM binding have been identified (Kadrmaz and Beckerle, 2004). Interestingly, members of the DA1 family also have a LIM-like domain with a degenerate zinc finger domain that has functional significance (Figure 1.4). Mutation of a cysteine in the central Zn finger domain in DAR4/CHS3/WRR5B leads to constitutive defence responses (Yang et al., 2010). A similar mutation in DA1, the DA1^{C274Y} mutation in the LIM-like domain, is not able to be ubiquitinated by BB, and consequently showed no evidence of peptidase activity, indicating a putative role for the LIM-like domain in the UIM-mediated ubiquitination and activation of the DA1 peptidase (Dong et al., 2017).

1.4.2.3 *The UIM domains*

The UIM domains are necessary for ubiquitination of DA1, and subsequent activation of the zinc metallopeptidase domain (Dong et al., 2017). It has been shown that the UIM2 is able to bind mono-ubiquitin, suggesting either that UIM1 may be a non-functional relic, or that it has a diverged function and has a more specific ubiquitin-binding role, for example binding poly-ubiquitin chains, or those attached to specific substrate proteins (Dumenil, 2013). Mono-ubiquitination can affect the properties of proteins by inhibiting their ability to bind to, and therefore control, their ubiquitinated targets. This has been demonstrated among the endocytic proteins Sts1, Sts2, Eps15 and Hrs, which are no longer able to bind to their ubiquitinated targets, resulting in reduced control of trafficking in the cell (Hoeller et al., 2006). DA1^{R358K} has a similar ubiquitin-binding ability to DA1 wild-type, indicating that the *da1-1* mutation does not affect the gene's ubiquitin binding ability (Dong et al., 2017).

1.4.2.4 *Domains in other members of the DA1 family*

DAR4/CHS3/WRR5B encodes a disease resistance (R) protein (Yang et al., 2010), and includes three domains not found in other members of the DA1 family - the NB-ARC domain, the LRR domain, and the CCR domain. The NB-ARC domain is a nucleotide-binding sequence conserved in many R proteins with a proposed function as a molecular switch to define the

activation state of the R protein (van Ooijen et al., 2008). DAR4/CHS3/WRR5B also includes a LRR (leucine-rich repeat) domain, another domain strongly conserved in proteins involved in innate immunity which functions to recognise pathogen-associated molecular patterns (PAMPs) (Ng and Xavier, 2011). Finally, the TIR (Toll/interlukin-1 receptor/resistance) domain in DAR4/CHS3/WRR5B is another protein domain commonly found in proteins involved in the innate immunity pathway, and functions in protein-protein interactions (Ve et al., 2015). DAR5/WRR7 codes for a CC-NB-LIM type of R protein (Cevik et al., 2016), and contains a CCR (coiled-coil related to RPW8) domain. CCR domains are involved in the generation of plant defence responses (Collier et al., 2011), although little is known about their precise functions.

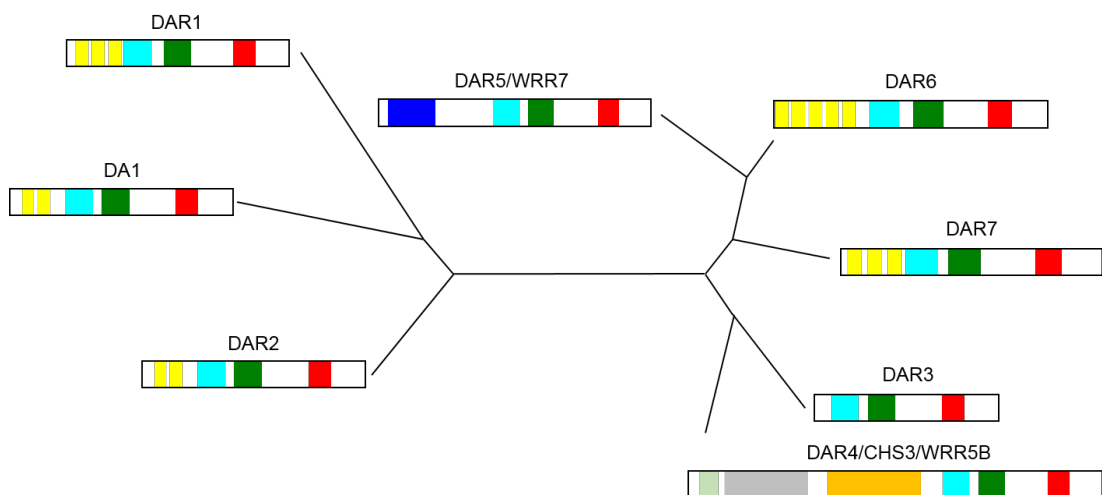


Figure 1.4 The DA1 gene family

Schematic representation of the 8 members of the DA1 gene family. Protein domains: zinc-metallopeptidase active site, red; LIM domain, cyan; LIM-like domain, dark green; UIM, yellow; NB-ARC domain, grey; LRR domain, orange; CCR domain, blue; TIR domain, light green.

1.4.3 The *da1-1* phenotype

Several studies have described the phenotypic effects of the *da1-1* negative interfering allele, which was originally identified in a mutant screen (Li et al., 2008). It is reported as resulting in increased seed mass, seed and ovule volume, embryo size, cotyledon area, flower size, silique size, leaf area and stem thickness - in short, affecting nearly every organ of the plant (Li et al., 2008; Dong et al., 2017; Vanhaeren et al., 2017). The effect on seed size was found to be maternal, as seeds produced by a *da1-1* mother regardless of the genotype of the pollen donor were significantly larger than those produced by a wild type mother, even where the pollen donor to the wild type mother was *da1-1* (Li et al., 2008).

This increase in organ size was found to result from an increase in cell number, rather than in cell area, as cell area was maintained in *da1-1* relative to wild type, and cell number was increased. Analyses of growth indicated that *da1-1* plants have a longer duration of growth than wild type, and have a longer life-span. This was proposed to be as a result of an increased duration of cell proliferation, based on analysis of *pCYCB1:1::GUS* expression in *da1-1* and wild type leaves. Analysis of the expression levels of a *pDA1::GUS* construct revealed that it is expressed most strongly during early leaf, petal, integument and embryo development, which would support the proposal of a role for DA1 in the control of cell proliferation (Li et al., 2008). However, more recent cellular analysis has showed that leaves of the *da1-1* mutant are larger than those of wild type as early as 7 days after stratification - this was found to be as a result of an increased cell number (Vanhaeren et al., 2017).

Although the overexpression of *DA1* alone does not generate a leaf size phenotype (Peng et al., 2015; Vanhaeren et al., 2017), *35S::GFP-DA1* plants exhibit reduced leaf, flower and silique size, as well as greater serrations in the leaf margins - although there is no change in seed weight. These size differences are as a result of a decrease in cell number (Vanhaeren et al., 2017).

Knowledge of extracellular signalling affecting *DA1* is limited. *DA1* expression is promoted by abscisic acid, although other phytohormones and growth regulators including jasmonates, auxin, cytokinins, brassinosteroids, gibberellins and glucose were not found to induce expression. Further analysis revealed a potential mechanism for abscisic acid to negatively regulate the duration of cell proliferation via the regulation of *DA1* expression (Li et al., 2008).

Transcriptomic analyses reveal that genes involved in the promotion of cell proliferation for example *GIF1/AN3*, *ANT* and *CYCB1;1* are upregulated in the *da1-1* mutant relative to wild type between 6 and 10 days after stratification, whereas genes such as *KRP1*, involved in the control of the arrest of cell proliferation, are repressed (see Section 1.2.3). These findings were suggested to show a putative “developmental shift” of *da1-1* plants, indicating that the tissue was at a younger developmental stage than wild type leaves of the same age, despite their larger size (Vanhaeren et al., 2017).

1.4.3.1 *DA1* genetic interactions

DA1 has been shown to genetically interact with the two E3 ligases that are able to ubiquitinate it, *BIG BROTHER (BB)* and *DA2* (Li et al., 2008; Xia et al., 2013).

1.4.3.1.1 *BB*

The *BB* protein includes a C-terminal RING-finger domain, and functions as an E3 ubiquitin ligase (see Section 1.5.4) (Disch et al., 2006). In *bb-1* knockout mutants, the petal, sepal and stems are increased in size relative to wild type, whereas in the *bb-2* T-DNA knockdown mutant exhibit an intermediate phenotype (Disch et al., 2006). Overexpression of *BB* results in a reduction in petal, sepal, stem and leaf size (Disch et al., 2006; Vanhaeren et al., 2017). Cell area in petals, sepals and the stem is not affected in either the *bb-1* or *bb-2* mutants, or in the overexpressor lines, indicating that *BB* controls organ size by limiting cell proliferation (Disch et al., 2006), although in leaves cell area is increased (Vanhaeren et al., 2017). Similarly to *DA1*, it has been proposed that this reduction in cell number is via a limitation in the duration of cell proliferation, based on kinematic analyses (Disch et al., 2006). Further research indicates that *BB* has a largely similar function in roots as in the shoot, with a *bb* mutant with a point mutation in the RING finger domain exhibiting increased root meristem size due to increased cell number, and a longer duration of cell proliferation - although this does not translate to a longer root under normal conditions (Cattaneo and Hardtke, 2017).

In a genetic screen for modifiers of the *da1-1* phenotype, *eod1-1* (*enhancer of da1-1*) was identified. The *da1-1eod1-1* double mutant was found to exhibit significantly larger organ size than *da1-1*. *EOD1* was subsequently mapped to the *BB* locus, and it was found that in *da1-1eod1-2/bb-2* mutants, seed and petal measurements exhibited a synergistic enhancement relative to the *da1-1* mutation alone, suggesting a genetic interaction and that the two genes may work together and in parallel pathways to control organ size (Li et al., 2008). Further investigation has shown that the *da1-1eod1-2/bb-2* mutant shows a synergistic enhancement in the final size of leaves as well as petals and seeds, as well as being significantly larger than wild type at 7 days after stratification due to a combination of more, and larger cells. The *eod1-2/bb-2* mutant (hereafter referred to as *bb*) exhibits an intermediate leaf phenotype at 7 days after stratification, as a result of an increase in cell area relative to wild type, but not cell number. Finally, measurements of ploidy levels in *da1-1bb* leaves over time revealed that the endoreduplication index of cells was significantly decreased between 13 and 23 days after stratification, relative to wild type, indicating a delay in the arrest of cell proliferation and the onset of cell expansion in *da1-1bb* mutants (Vanhaeren et al., 2017).

1.4.3.1.2 *DA2*

Like *BB*, *DA2* encodes a RING E3 ubiquitin ligase (see Section 1.5.4) (Xia et al., 2013). The *da2-1* T-DNA insertion mutant generates larger and heavier seeds than wild type, as well as an

increased number of seeds per silique and weight of seeds per plant - although there was no increase in the number of seeds per plant. *da2-1* plants are also taller than wild type, and exhibit larger leaves and flowers with an increased number of cells rather than an increased cell area, relative to wild type (Xia et al., 2013).

In a *da1-1da2-1* double mutant, the *da2-1* mutation synergistically enhanced the organ size phenotypes of the *da1-1* mutant, indicating a genetic interaction and that *DA1* and *DA2* could function together in a common pathway to control organ size. However, a *da2-1bb* double mutant exhibited only an additive effect on organ size relative to the *da2-1* and *bb* phenotypes, indicating that the interaction between *DA1* and *DA2* is independent of *BB* (Xia et al., 2013). Reciprocal cross experiments determined that, similarly to *DA1* (Li et al., 2008), the effect of *DA2* on seed size is maternal (Xia et al., 2013).

1.4.3.2 Substrates of *DA1*

As described in Section 1.4.1, several targets for *DA1*-mediated cleavage have been identified, all of which are known to have roles in the control of organ development. These are presented in Dong et al., 2017.

1.4.3.2.1 *BB*

Incubation of purified ubiquitinated Flag-tagged *DA1* with His-tagged *BB* for four hours resulted in the cleavage of *BB*-His and the production of a ~35kDA cleavage product. This was also observed when expressing tagged *DA1* and *BB* in *da1-ko dar1-1* protoplasts, but no cleavage product was produced when Flag-*DA1*-pep was used in the place of Flag-*DA1*, indicating peptidase-dependent cleavage of *BB* by *DA1* (Dong et al., 2017).

Identification of the target site in *BB* was carried out using Edman sequencing of the purified *BB*-His cleavage product. The Edman sequencing indicated a neo-N-terminal amino acid sequence that was a unique match to six amino acids at the predicted cleavage site of *BB*, based on the molecular weight of the cleavage product. This suggested a putative *DA1*-mediated cleavage site for *BB* between A_{60} and Y_{61} . Using site-directed mutagenesis, two mutant forms of *BB* were produced that were predicted not to be cleaved - a mutation of *AY* to *GG* (*AY*-*GG*), and a complete deletion of the four amino acids surrounding the predicted cleavage site (Δ *NAYK*). Cleavage assays in *da1-ko dar1-1* protoplasts found that these mutant forms of *BB* were not cleaved by *DA1*, showing that *DA1* cleaved *BB* between A_{60} and Y_{61} . A cleaved form of *BB*, *MY61*-*BB* was produced, with an initiator methionine followed by the C-terminal cleaved fragment, beginning with Y_{61} . Constitutive expression of this was not able

to complement the *bb* mutant phenotype, indicating a role for DA1-mediated cleavage in the reduction of *BB* activity (Dong et al., 2017).

1.4.3.2.1.1 *N-end rule degradation*

Although for the above elucidation of the *BB* cleavage site the cleaved product of *BB* was sufficiently stable to be purified in relatively large amounts for Edman sequencing, in cell-free degradation assays *MY61-BB* was less stable than wild type, un-cleaved *BB*. By expressing the cleaved fragment of *BB* with three different N-termini (Y, G and MY) and observing their stability, it was found that *G61-BB* was stable in a cell free degradation system, whereas *Y61-BB* was not. Interestingly, *MY61-BB* was also unstable in a proteasome-independent system, where the proteasome inhibitor MG132 was present. The mechanism surrounding this is as yet unclear (Dong et al., 2017). The neo-N-terminal sequence of the cleavage fragment of *BB* begins with *YK*, a sequence which has previously been shown to be a destabilising N-terminal sequence involved in the N-end rule pathway for ubiquitin-mediated degradation (Varshavsky, 2011).

The destabilising N-terminal sequence of a protein degraded via the N-end rule pathway is a key part of the *N-degron*, or signal that activates the N-end rule pathway. The *N-degron* is recognised by an *N-recognin*, an E3 ubiquitin ligase (see Section 1.5.4) which, in conjunction with an E2 ubiquitin conjugating enzyme, polyubiquitinates the N-end rule substrate and targets it for degradation in the 26S proteasome (Varshavsky, 2011). The N-end rule pathway therefore provides a mechanism for the destabilisation of proteins with specific N-terminal amino acid sequences, such as cleavage products.

The *PRT1* E3 ligase is known to be an *N-recognin* for similarly aromatic N-terminal amino acid residues (Potuschak et al., 1998). Binding assays found that *PRT1* binds preferentially to Y residues, and luciferase assays revealed that the activity of *BB-LUC* with an N-terminal Y residue was reduced in wild type protoplasts, but not in *prt1* protoplasts - an observation not made with *BB-LUC* with an N-terminal G residue. This suggests that the stability of *BB* fragments with an N-terminal tyrosine, such as the identified cleavage product, is mediated by *PRT1* via the N-end rule pathway (Dong et al., 2017).

1.4.3.2.2 *DA2*

Incubation of purified ubiquitinated Flag-tagged *DA1* with His-tagged *DA2* for four hours resulted in the cleavage of *DA2-His* and the production of a ~25kDA cleavage product, although this cleavage product was less strong than that of *BB-His*. This was also observed when expressing tagged *DA1* and *DA2* in *da1-ko dar1-1* protoplasts, but no cleavage product

was produced when Flag-DA1-pep was used in the place of Flag-DA1, indicating peptidase-mediated cleavage of DA2 by DA1. Due to the low stability of the DA2 cleavage fragment, it has not yet been possible to purify sufficient protein to carry out Edman sequencing to determine the DA1-mediated cleavage site. However, the molecular weight of the C-terminal cleavage product indicates that the cleavage site may be located in the C-terminus of DA2 (Dong et al., 2017).

1.4.3.2.3 UBP15

UBP15 is a member of the highly conserved *UBP (Ubiquitin-Specific Protease)* family which control protein de-ubiquitination in eukaryotes. De-ubiquitination enzymes (DUBs) have two distinct roles - either cleaving mature ubiquitin from ubiquitin precursors or from other linked ubiquitin molecules, or by cleaving ubiquitin from its attached target protein (Nijman et al., 2005; Liu et al., 2008). *UBP15* is expressed widely throughout all organs in the plant, but semi-quantitative RT-PCR reveals that it is expressed most highly in rosette leaves and in inflorescence tissue, and that within the rosette leaf expression is highest in later leaf developmental stages, and in the leaf margins. *GFP* fusions indicated that *UBP15* expression may be localised at the sub-cellular level to the cytosol and the nucleus (Liu et al., 2008).

In the *ubp15-1* and *ubp15-2* T-DNA insertion mutants, there is a reduction in the leaf area relative to wild type, primarily in relation to leaf width. The leaf margins of the *ubp15-1* and *ubp15-2* mutants are also more serrated than wild type, relating to the observed expression patterns described above. In addition to this, the *ubp15-1* and *ubp15-2* mutants also exhibit shorter roots relative to wild type at early developmental stages, as well as smaller flowers and siliques, and are shorter overall. Finally, the mutants also produce fewer rosette leaves than wild type before flowering, and therefore flower earlier. Overexpression of *UBP15* results in larger plants with larger, rounder and more curled rosette leaves, relative to wild type - in general, the abnormalities observed in the *UBP15* are the opposite of those observed in *ubp15-1* and *ubp15-2* (Liu et al., 2008). In addition to this, *UBP15* is, similarly to DA1 and DA2 (Li et al., 2008; Xia et al., 2013), known to maternally regulate seed size, and seed size and weight is reduced in *ubp15-1* mutants (Du et al., 2014).

Cellular analyses in leaves indicated that, while the number of cells in leaves of wild type, *ubp15-1*, *ubp15-2* and *UBP15* overexpressors are similar at the beginning of development, over time the mutant *ubp15* plants exhibited gradually fewer cells than wild type, and the *UBP15* overexpressor exhibited an increase in cell number (Liu et al., 2008). This cell proliferation phenotype is consistent with the observation that *ICK1*, a repressor of the rate

of cell proliferation (Cheng et al., 2013), is upregulated in *ubp15-1* mutants (Liu et al., 2008), suggesting that UBP15 may be involved in promoting the rate of cell proliferation. This finding is supported by studies in budding yeast, which have found that de-ubiquitination of an S-phase cyclin, CLB5, by yeast UBP15 promotes timely entry into the S-phase of mitosis (Ostapenko et al., 2015).

Mutations in *UBP15* are able to repress the large organ phenotype of *da1-1*, and overexpression of *UBP15* results in a similar seed, leaf and flower phenotype to *da1-1*, including at the cellular level. Analysis of *da1-1ubp15-1* mutants showed that mutations in *UBP15* are epistatic to *da1-1* in the integument, supporting the proposition of a common pathway for *DA1* and *UBP15* working antagonistically in the control of cell proliferation, especially in the maternal integuments (Du et al., 2014).

Using *in vitro* pull-down assays and *in vivo* co-immunoprecipitation assays, it was found that DA1 and UBP15 physically interact, which, together with findings that UBP15 protein levels were higher in *da1-1* mutants, suggests that there could be a role for DA1 in modulating UBP15 stability (Du et al., 2014). It was subsequently confirmed that UBP15 is cleaved by DA1 in the C-terminus, although the precise cleavage site has not yet been identified (Dong et al., 2017).

1.4.3.2.4 TCP family members

First described in 1999, the TCP gene family is characterised by the TCP domain, a basic helix-loop-helix (bHLH) motif that mediates protein-protein and nucleotide binding activity. The TCP domain was named for four genes in which it was originally identified - *TEOSINTE BRANCHED1*, *CYCLOIDEA* and *PROLIFERATING CELL FACTOR1/2*, found in maize, *Antirrhinum* and rice, respectively. The TCP family in Arabidopsis falls into one of two subfamilies - class I, where the bHLH motif is most closely related to those in PCF1 and PCF2, and class II where the bHLH motif most closely resembles those of CYC and TB1 (Cubas et al., 1999). The TCP gene family, including members from Arabidopsis and a number of other species, is shown in Figure 1.5.

Since 1999, TCPs have been identified as transcription factors with consensus DNA-binding sites specific to each class (Martin-Trillo and Cubas, 2010). Dimerisation is required for DNA binding, and TCPs may form either homo- or hetero-dimers (among members of the same class), although hetero-dimerisation has been found to elicit a higher efficiency of DNA binding than homo-dimerization (Kosugi and Ohashi, 2002).

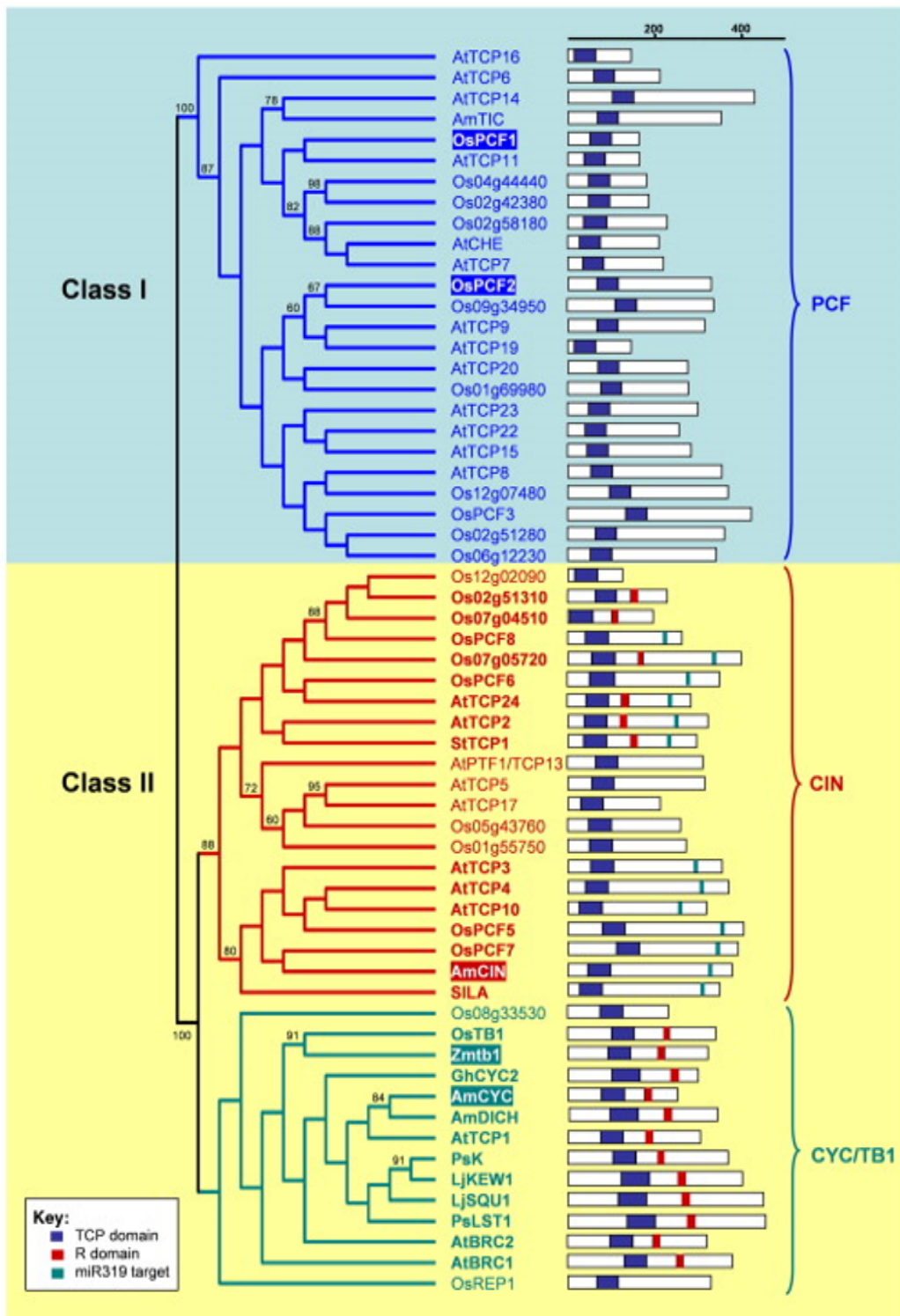


Figure 1.5 The TCP gene family

Phylogenetic tree showing predicted TCP family members from *Arabidopsis thaliana* and a range of other species, including *Oryza sativa*, *Antirrhinum majus*, *Lotus japonicus*, *Solanum lycopersicum*, *Gerbera hybrida*, *Solanum tuberosum*, *Pisum sativum* and *Zea mays*. Protein structures including conserved motifs are shown. From Martin-Trillo and Cubas, 2010, with permission.

It is widely suggested that class I and class II TCPs may act antagonistically in the control of cell growth and proliferation, with class I TCPs promoting growth and division, and class II TCPs inhibiting growth and proliferation (Martin-Trillo and Cubas, 2010). However, while there is a significant body of evidence supporting this in class II TCPs, less is known about the role of class I TCPs in the promotion of growth and proliferation - primarily as a result of the high levels of functional redundancy among the family - although the body of evidence is increasing.

There are 13 members of the class I family of TCP genes in Arabidopsis, as shown in Figure 1.5 (Martin-Trillo and Cubas, 2010). *TCP14* and *TCP15* show significant functional redundancy, and are proposed to have a role together in the promotion of cell proliferation in stem internodes while repressing cell proliferation in leaves and floral tissue, indicating that the effects of TCP family members could be tissue-dependent (Kieffer et al., 2011). Further functional redundancy is also found between *TCP8*, *TCP15*, *TCP21*, *TCP22* and *TCP23*, where even a pentuple mutant elicited little change in leaf phenotype, relative to wild type (Aguilar-Martinez and Sinha, 2013) - although expression of *TCP7* and *TCP23* fused to the repressor domain SRDX (Hiratsu et al., 2003) does result in smaller and more curved leaves, as a result of changes in cell growth (Aguilar-Martinez and Sinha, 2013). Overexpression experiments in *TCP20* showed that it also has a role in the control of early seedling development and the promotion of cell growth (Hervé et al., 2009).

The class II family of TCP genes in Arabidopsis includes 11 members, and is divided further into two clades - the CIN-like TCPs, and the TB1-type TCPs. Many of the CIN-like TCPs (*TCP2*, *TCP3*, *TCP4*, *TCP10* and *TCP24*) are regulated by miR319, a microRNA produced at the *JAW* locus. In *jaw-D* mutants defective at this locus, leaves are more curved than wild type, and have an uneven leaf shape and leaf margin (Palatnik et al., 2003). Of these, *TCP4* is the best characterised. Some class II TCP family members appear to restrict cell proliferation by regulating transcription of cell cycle control genes, for example *TCP24* works in a complex with ABAP1 to restrict the transcription of genes required for entry into the S-phase (Masuda et al., 2008). In addition, some class II TCP family members interact with phytohormone signalling pathways, including cytokinins and auxin (Suzuki et al., 2001; Koyama et al., 2010). Finally, a number of class II TCP family members have been shown to affect the expression of NAC-domain transcription factors such as the *CUP-SHAPED COTYLEDON (CUC)* genes, although there are some reports of conflicting observations. A potential mechanism for this is via the regulation of miR164 activity, which is known to repress *CUC* expression (Palatnik et al., 2003; Koyama et al., 2007).

1.4.3.2.4.1 *TCP4*

As described above, class II family member *TCP4* expression is negatively regulated by miR319, although *TCP4* alleles with point mutations at their miR319 binding sites provide an opportunity to observe the phenotypic effects of increases in *TCP4* expression - these are termed *soj* lines. Increases in *TCP4* expression both in this way, and via constitutive *TCP4* expression under a *35S* promoter, resulted in smaller plants with smaller leaves, relative to wild type - although they did not exhibit the crinkly leaf phenotype observed in *jaw-D* mutants. While there was no difference between the cell areas of the wild type and the two lines with increased *TCP4* expression, there was a reduction in cell number in the mutants, indicating that *TCP4* has a role in the limitation of cell proliferation. In addition, in the *soj* lines the leaf margins were smoother than in wild type, indicating that the regulation of *TCP4* by miR319 is important for the control of leaf serration (Schommer et al., 2014).

TCP4 is known to regulate leaf development by modulating the activity of a number of other factors, including *YUCCA5* (Challa et al., 2016), *GRFs* via miR396, and *ICK1/KRP1* (Schommer et al., 2014), each of which are known to have a role in the control of cell elongation, cell proliferation, or the cell cycle. *TCP4* has recently been shown to undergo DA1-mediated cleavage (Caroline Smith, unpublished), although similarly to DA2 and UBP15, the precise site of this cleavage is unknown.

1.4.3.2.4.2 *TCP15*

TCP15 is a member of the TCP class I family. In *tcp15-3* T-DNA insertion mutants, there is a slight but significant reduction in inflorescence height, although the most severe developmental phenotypes are observed in *tcp14tcp15* double mutants, due to the high functional redundancy of *TCP14* and *TCP15*. In this double mutant, internode length was also reduced relative to wild type, and this was found to be as a result of decreased cell proliferation rather than decreased cell area. This suggests that together *TCP14* and *TCP15* promote growth by cell proliferation in the stem internode. However, *TCP15* may also limit cell proliferation in leaves and petals, in particular in the margin, indicating that its activity is tissue-specific (Kieffer et al., 2011). Other evidence points to a role for *TCP15* in the control of cell area, as the repression of *TCP15* using a SRDX repressor domain (Hiratsu et al., 2003) has been shown to result in plants with smaller rosette leaves at earlier stages, as a result of smaller epidermal cells (Li et al., 2012; Uberti-Manassero et al., 2012). While cell division and cell area are strongly linked factors in organ development, these somewhat contradictory findings make it difficult to define a clear role for *TCP15* in organ development - other than

that it is of significant importance to the formation of morphologically correct plant organs, when taken together with *TCP14*.

Downstream of *TCP15*, it is known to suppress endoreduplication, potentially via the modulation of expression of genes involved in the cell cycle. For example, in plants where *TCP15* is repressed and endoreduplication is enhanced, the cell cycle control genes *CYCA2;3* and *RBR* - involved in the progression of the cell cycle (Desvoyes et al., 2006; Imai et al., 2006) - are repressed (Li et al., 2012), while positive regulators of endoreduplication are upregulated. It was also found that *TCP15* binds to the promoter regions of *CYCA2;3* and *RBR*, providing a mechanism for the indirect regulation of endoreduplication by *TCP15* (Li et al., 2012).

Both *TCP15* and the closely related *TCP14* were found to physically interact with *DA1* and other members of the *DA1* family, *DAR1* and *DAR2*. In addition, *TCP15::GUS* and *TCP14::GUS* expression levels were increased in *da1kodar1-1dar2-1* mutant protoplasts, relative to the level of expression in wild type protoplasts, indicating that there may be a role for members of the *DA1* family to control *TCP15* and *TCP14* levels (Peng et al., 2015). The *DA1*-mediated cleavage of *TCP15* was later confirmed, although a cleavage product could not be reliably observed for *TCP14* (Dong et al., 2017).

1.4.3.2.4.3 *TCP22*

Another member of the *TCP* class I family, *TCP22* is known to have high levels of functional redundancy with other members of this class. When taken as part of a pentuple mutant, *tcp8tcp15tcp22tcp23tcp21*, the leaves are slightly wider and larger overall than wild type, and fewer rosette leaves are produced, while not exhibiting a strong phenotypic difference (Aguilar-Martinez and Sinha, 2013). In this pentuple mutant, some genes involved in the control of SAM maintenance (*STM*, *BP*), leaf form (*AS1*), and the control of the cell cycle (*CYCA1;1*, *CYCA2;3*) are also up-regulated - indicating that *TCP22* may have a role in the repression of the cell cycle and therefore cell proliferation, although with the high level of functional redundancy in the family, it is difficult to attribute a function to a single gene (Aguilar-Martinez and Sinha, 2013).

1.5 The ubiquitin system

The ubiquitin system has a major regulatory role in controlling protein levels and activities (Komander and Rape, 2012). It involves the covalent attachment of the 8kDa ubiquitin protein to other proteins, often as ubiquitin polymers, which target proteins for degradation in the 26S proteasome. These target proteins include cyclins and inhibitors of cyclin-

dependent kinases (Hershko and Ciechanover, 1998), indicating a central role for ubiquitination in the control of the cell cycle in both plants and animals and a potential role in determining organ size.

1.5.1 Ubiquitin

Ubiquitin, named due to its ubiquitous nature in eukaryotes, is a small protein of around 8.5kDa, comprised of 76 amino acid residues (Schimke, 2006). The ubiquitin family is encoded by 14 genes in Arabidopsis, including ubiquitin-like and ubiquitin extension genes (Hatfield et al., 1997). Ubiquitin is synthesised by the ribosome in polymeric form, and is cleaved by deubiquitinating enzymes at the terminal glycine residue in order to release active monomers. These are then covalently linked via a C-terminal isopeptide bond to a lysine residue on substrates by a cascade of ubiquitin activation and conjugation enzymes called E1, E2 and E3 (Hershko and Ciechanover, 1998). The structure of the ubiquitin protein is important to its function. The terminal glycine residue at which cleavage occurs to separate monomers from the polymer forms part of the protruding C-terminus of the protein, where the carboxyl group is the initiation site of covalent linkage of the ubiquitin to targets. The pool of ubiquitin molecules is often recycled within the cell, rather than being synthesised newly for every use. NEDD and SUMO are small proteins related to ubiquitin that are also conjugated to proteins to modify their activities (Kerscher et al., 2006).

1.5.2 E1 ubiquitin activating enzymes

Ubiquitin is activated by E1 enzymes that form an initial thioester linkage with ubiquitin and start the cascade to the final ubiquitination of the target protein. Arabidopsis has two genes encoding E1 enzymes: *AtUBA1* and *AtUBA2* (Hatfield et al., 1997). These 123kDa proteins have an amino acid sequence homology of 81%, and maintain a 44-75% sequence identity similarity with E1 enzymes from other organisms. They have largely similar enzymatic properties, and are co-expressed with in most Arabidopsis tissues, though their expression is highest in the most metabolically active cells (Hatfield et al., 1997). The active site of the enzyme contains a conserved cysteine residue, forming part of a nucleotide binding motif that is able to bind activated ubiquitin by interacting with ATP-Ub or AMP-Ub. The E1 enzyme passes the activated ubiquitin via a thioester linkage to the active site cysteine residue of an E2 ubiquitin conjugating enzyme. A key link to plant growth is provided by evidence of an E1-related protein in Arabidopsis, AXR1, which has a mutant form *axr1* that is defective in auxin sensitivity. The AXR1 protein exhibits homology with the N-terminal portion of Arabidopsis E1 enzymes and lacks the active site cysteine. This suggests that the conserved cysteine has a role not only in ubiquitin binding but also in the auxin response (Hatfield et al., 1997).

1.5.3 E2 ubiquitin conjugating enzymes

The next stage of the ubiquitin signalling cascade is catalysed by E2 ubiquitin conjugating enzymes. In common with E1s, their active site has a conserved cysteine residue surrounded by a “core” of 150 amino acids, while there is variation in the surrounding N- and C-termini in order to confer specificity to E3 ubiquitin ligases. 37 E2 enzymes have been identified in *Arabidopsis* (Vierstra, 1996), grouped into 12 subfamilies (Sadanandom et al., 2012). E2 conjugating enzymes may then either transfer the ubiquitin to the E3 ubiquitin ligase enzyme, or onto the substrate directly – depending on the type of E3 ligase in question.

E2 enzymes themselves have been shown to impact on developmental processes, for example in the regulation of *FLC* expression. *Arabidopsis* E2 conjugating enzymes AtUBC1 and AtUBC2 function redundantly to regulate mono-ubiquitination of histone H2B, both via the E3 ligases HUB1 and HUB2, and independently (Xu et al., 2009). This pathway is able to subsequently upregulate the expression of *FLC* and other genes involved in the control of flowering time, repressing the floral transition (Gu et al., 2009).

1.5.4 E3 ubiquitin ligase enzymes

The final step of ubiquitination involves enzymes called E3 ubiquitin ligases. There are 1,406 different E3 ligases in *Arabidopsis* (Vierstra 1996). This provides a wide diversity of substrate specificity on ubiquitination reactions. E3 ligases have been grouped into three main classes: HECT (Homology to E6-AP C-Terminus) E3 ligases, those having a RING (Really Interesting New Gene) domain, and finally the CUL4 (CULLIN-type) E3 ligases. The HECT and RING classes differ in structure in that HECT E3 ligases are formed from a single subunit containing the 350 amino acid domain which gives it its name (Huibregtse et al., 1995) whereas the modular nature of RING E3 ligases means that they can act independently or in a complex with other factors that are thought to confer specificity. There are only seven HECT E3 ligases currently identified in *Arabidopsis* (Vierstra, 2009), compared to 469 RING E3 ligase proteins (Stone et al., 2005). An example of a RING E3 ligases-containing complex is the SCF complex, variations of which have central role in direct perception of and responses to phytohormones such as auxin (Gray et al., 1999), jasmonic acid (Xu, 2002), and ethylene (Potuschak et al., 2003). CULLIN-type E3 ligases are formed by the binding of a member of the cullin family to a RING protein (either ROC1 or ROC2), resulting in a cullin-RING E3 ligase (CRL). There are thought to be up to nine cullins in *Arabidopsis*, giving a wide possible range of E3 ligase specificities. CRLs do not bind to the substrate directly, but are linked to substrate recruiting receptors such as F-box or BC-box proteins that bind the substrate. The ubiquitinated E2 is bound to

the RING protein, and the transfer of ubiquitin from the E2 to the substrate is jointly facilitated by the proteins in the complex (Jackson and Xiong, 2009).

1.5.4.1 RING E3 ligases

The E3 ligases known to ubiquitinate DA1, BIG BROTHER and DA2, are RING E3 ligases. A conserved cysteine and histidine at the centre of the RING domain coordinates with two zinc atoms in order to maintain the overall structure of the RING E3 (Deshaies and Joazeiro, 2009; Sadanandom et al., 2012). Originally described by Freemont et al., the RING finger domain is rich in cysteine and has a basic sequence of Cys-X₂-Cys-X₍₉₋₃₉₎-Cys-X₍₁₋₃₎-His-X₍₂₋₃₎-Cys-X₂-Cys-X₍₄₋₄₈₎-Cys-X₂-Cys (Freemont, 1993). The cysteines and histidine are buried in the centre of the 3D protein structure, producing an interleaved rigid globular basis for protein-protein interaction (Borden, 2000).

Compared to HECT E3 ligases, RING E3 ligases have a different mechanism of transferring the ubiquitin from the E2 to the substrate. Rather than the E3 being ubiquitinated before passing the ubiquitin to the substrate, the RING domain binds directly to the E2 and facilitates the direct transfer of ubiquitin from the E2 to the substrate in this manner. This transfer arises most likely as a result of the proximity of the ubiquitinated E2 and the substrate, rather than as a direct catalytic function of the RING domain, as it is too distant from the active site of the E2 to play this kind of role in the reaction (Zheng et al., 2000; Zheng et al., 2002). The RING domain may also cause a conformational change in the E2, which encourages it to discharge the ubiquitin. Further evidence that the RING domain does not bind ubiquitin in order to transfer it to the substrate is provided in that the active cysteine residue is not on the surface of the RING domain, probably preventing it from forming a thioester-linked catalytic ubiquitinated intermediate.

RING E3 ligases are divided into three groups: monomeric, dimeric (both heterodimers and homodimers), and multi-subunit RING E3 ligases. Multi-subunit RING E3 ligases have subunits separate from the main ubiquitin ligase for substrate recognition, for example as shown in the SCF complex. The SCF complex is named for its components SKP1, CUL1 and the F-box, which are bound to the small RBX1 protein, which contains a RING finger domain (Zheng et al., 2002).

There are two potential mechanisms by which RING E3 ligases may facilitate E2-mediated ubiquitination of substrates. The first of these is sequential addition, whereby the substrate is bound to the E3, and a succession of E2s, each with a single ubiquitin molecule, bind to the E3 and transfer a single ubiquitin onto the growing chain on the substrate (Hochstrasser,

2006). The second is known as *en bloc* addition, whereby the substrate is bound to the E3, and two E2s, each with a single ubiquitin also bind to the substrate. Instead of each transferring their single ubiquitin straight to the substrate however, one of the E2s transfers its ubiquitin to the other, then disassociates from the E3 in order to make room for a third E2, again with a single ubiquitin. This then transfers its ubiquitin onto the growing chain on the first E2 that has remained bound to the E3 all along. This continues until a polyubiquitin chain of sufficient length is produced on the first E2, which then transfers the whole chain directly to the substrate (Li et al., 2007).

The activities of RING E3 ligases are regulated in several different ways (reviewed in Deshaies & Joazeiro 2009). Firstly, the ubiquitination activity of RING E3 ligases is regulated by substrate modification. In common with many biological processes, phosphorylation is able to influence the activity of the enzyme by affecting either the substrate, the E2 or the E3 – substrate modification being the best understood of these. In the case of some SCF ligases, the substrate must be phosphorylated before it can bind to the E3 and hence be ubiquitinated. This was elucidated by studies in budding yeast, and via SCF^{Cdc4}, which has a role in the control of the cell cycle (Feldman et al., 1997; Skowyra et al., 1997; Verma et al., 1997). Secondly, chemical modification of the E3 ligase itself also has an effect on activity, for example acetylation of residues in the RING domain can inhibit ubiquitin ligase activity of the enzyme, although the precise mechanism involved remains to be discovered (Wang et al., 2004). In addition, RING E3 ligases can be regulated by their conjugation with members of the ubiquitin family – whether ubiquitin, or ubiquitin-like. For example, autoubiquitination by the E3 could cause it to be targeted for degradation by the proteasome, hence inhibiting its activity. This has been demonstrated in SCF E3 ligases where the E2 bound to the RING domain transfers ubiquitin to the F-box subunit (Zhou and Howley, 1998; Galan and Peter, 1999). Alternatively, autoubiquitination can activate signalling in some cases. Ubiquitin-like proteins such as Nedd88 can be conjugated to subunits of RING E3 ligase complexes, which may increase the efficiency of ubiquitination by increasing the flexibility of the complex and therefore allowing closer proximity of E2 and substrate (Duda et al., 2008). The binding of small proteins to the E3 can also control its activity, for example the binding of CAND1 protein to cullins inactivates them and can be reversed by the conjugation of Nedd88 (Liu et al., 2002; Zheng et al., 2002; Bornstein et al., 2006). Another mechanism of regulation involves the binding of small molecules such as auxin to the F-box protein TIR1 to the active substrate-binding site, which facilitates the stable binding of protein substrates to the F-box receptor protein (Tan et al., 2007). This is a common mechanism by which plant hormones

are perceived by the cell – similar mechanisms are also used for the recognition of gibberellins and jasmonate (Spartz and Gray, 2008). Finally, substrate competition has been found to have a role in the control of E3 ligase activity – for example the anaphase promoting complex (APC) has a large range of substrates but processes them in order, with those most easily processed being targeted for degradation before those less easily processed (Marangos and Carroll, 2008).

Apart from DA1, a further example of RING E3 ligases in the control of organ development is TIE1-ASSOCIATED RING-TYPE E3 LIGASE1 (TEAR1), which targets TCP INTERACTOR-CONTAINING EAR MOTIF PROTEIN1 (TIE1) for degradation. TIE1 is an important repressor for CIN-like TCP family members, therefore positioning TEAR1 as a positive regulator of CIN-like TCP family members via their de-repression by TIE1, and is consequently a repressor of cell proliferation (Zhang et al., 2017)

1.5.5 Consequences of ubiquitination

1.5.5.1 Proteasomal degradation

When poly-ubiquitinated proteins are targeted for degradation in the proteasome, they are transported to the 26S proteasome within the cell. A large structure of 2MDa, the 26S proteasome is formed from 31 subunits, and divided into the 20S core protease and the 19S regulatory particle (Wolf and Hilt, 2004). The narrow pore opening limits entry into the proteasome to only proteins that have unfolded specifically for entry (Hartmann-Petersen et al., 2003). The regulatory particle forms a lid over the end of the core protease, and confers ATP dependence and polyubiquitin recognition onto the system. It has been proposed that a poly-ubiquitin chain composed of four ubiquitin monomers is the optimum signal for recognition by the proteasome (Thrower et al., 2000).

1.5.5.2 Changes in protein functionality

Not all ubiquitinated substrates are targeted for degradation in the proteasome. Mono-ubiquitination and multiple mono-ubiquitination (such as that observed in the DA1 system) are known to have a role in the changing of biochemical functions of proteins. For example, mono-ubiquitination of the histone H2B in yeast is required for mitosis and normal cell growth. In addition, plasma membrane protein activity is regulated in yeast and mammalian cells by mono-ubiquitination as a signal to promote internalisation into endocytic vesicles (Hicke, 2001). DA1 is the first ubiquitin-activated peptidase to be identified, but this could pose a new function for mono-ubiquitination and multiple mono-ubiquitination in other studies.

1.6 Aims for this thesis

This chapter has summarised current knowledge of the control of organ size in plants, and particularly via the DA1 regulatory system. This thesis takes a multidisciplinary approach to answer further questions about the function of DA1 at the molecular, cellular and whole organ level.

Chapter 2 uses *in vivo* protoplast assays to focus on the identification of novel substrates for DA1-mediated peptidase activity, as well as the identification of a conserved cleavage site in known substrates of DA1. Chapter 3 describes more in-depth whole-organ phenotyping than has been carried out before now, revealing new insights into the leaf shape of *da1-1*, *bb*, and *da1-1bb* mutants. In addition to this, confocal imaging is used to analyse all cells in wild type, *da1-1*, *bb*, and *da1-1bb* leaves during a time-series in early development. Scanning electron microscopy is also used to analyse cellular properties of these mutants in mature leaves, creating a greater understanding of the cellular basis of the large organ phenotype observed in these mutants. Finally, Chapter 4 utilises innovative live-cell imaging and analysis to produce a rich dataset, allowing the identification of a range of cellular parameters in tracked cells. For the first time, empirical observations of cell divisions in plants carrying the *da1-1*, *bb*, and *da1-1bb* mutations have been made, which may prompt novel directions for future work exploring the dynamics of cell division and organ growth.

This thesis aims to answer a number of questions about the activity of *DA1* and *BB* in the control of organ size in *Arabidopsis*:

- Are there further substrates for the DA1 peptidase?
- Is it possible to identify a conserved cleavage site for the DA1 peptidase?
- How are the phenotypes of *da1-1*, *bb* and *da1-1bb* leaves different from that of wild type, and how are these differences created at a cellular level?
- Are there differences in the control of cell division in *da1-1*, *bb* and *da1-1bb* leaves relative to wild type, and how do these differences contribute to the overall phenotypes of the mutants?

2 ANALYSING THE PEPTIDASE ACTIVITY OF DA1

2.1 Introduction

2.1.1 The biochemical function of DA1

The identification of DA1 as a ubiquitin-activated peptidase (Dumenil, 2013; Dong et al., 2017) has prompted a search for novel substrates among proteins involved in the control of cell proliferation and cell expansion. These classes of proteins were selected due to the biological role of DA1 in limiting the duration of cell proliferation during organ growth (Li et al., 2008). In *da1-1* plants, petal area increases for longer to a larger final size compared to wild type, and leaf area increases faster and for longer, leading to increased final size. In addition to this, the mitotic index of *da1-1* petals is higher than that of wild type petals, and remains higher, reaching 0% at around 150 hours old, rather than at around 100 hours old in wild type. *CYCB1;1* activity is also higher in *da1-1* plants than wild type at nine days after emergence, which suggests a role for *DA1* in the control of cell proliferation or transition to expansion (Li et al., 2008; Yu and Yao, 2008).

To date, 847 known or putative peptidases in *Arabidopsis thaliana* have been identified (Rawlings and Barrett, 1996; Rawlings et al., 2016). Zinc metallopeptidases such as DA1 form a large group, and are among the most diverse of the six catalytic types of protease (Schaller, 2004). A key question in understanding the wider biological role of DA1 is to identify its substrates and determine the biological functions of DA1-mediated cleavage.

Previous studies have shown that DA1 is a ubiquitin-activated peptidase, and is multiply-monoubiquitinated by E3 ligases BIG BROTHER (BB) and DA2. This ubiquitination activates the latent peptidase activity of DA1, and enables it to cleave substrates, which we have shown to include BB and DA2 (Dong et al., 2017). A number of other proteins involved in the control of organ size and development have already been identified as substrates for DA1, and are described below.

2.1.1.1 BIG BROTHER

As one of the E3 ligases involved in the ubiquitination and therefore activation of DA1, the cleavage of BB establishes a negative feedback loop, providing a mechanism for fine-tuning DA1 protein levels in the cell. Prior to the identification of DA1 as regulator of organ size in *Arabidopsis*, BB was shown to limit final organ size in a dosage-dependent manner. The *bb-1* knockdown mutant exhibits larger petals and sepals than wild type, while the heterozygote shows an intermediate phenotype with just under half of the wild type expression of BB. The

bb-2 T-DNA insertion mutant has *BB* levels of around 20% of that of wild type plants, and displays a *bb-1/BB* heterozygote-like phenotype (Disch et al., 2006).

The DA1 peptidase cleavage site of *BB* was identified by performing Edman sequencing of the cleaved product (Dong et al., 2017). The predicted cleavage site was then confirmed using site-directed mutagenesis. Two mutations were made to confirm the precise cleavage site by site-directed mutagenesis: a four-amino acid deletion surrounding the A₆₀-Y₆₁ cleavage site predicted by the Edman sequencing (Δ NAYK) and a substitution of A₆₀-Y₆₁ to GG (AY-GG). Neither of these mutants were able to be cleaved by DA1.

When transformed into *eod1-2* (Li et al., 2008), a loss of function allele of *BB* identified in a genetic screen for enhanced *da1-1* large organ phenotypes, a cleaved form of *BB* was unable to rescue the *eod1-2* large leaf and petal phenotype, indicating that cleavage of *BB* by DA1 reduces its biological activity. The cleavage product of *BB* is targeted by the E3 ligase PRT1 (Potuschak et al., 1998; Stary et al., 2003; Dong et al., 2017) and subsequently degraded via the N-end rule pathway (Varshavsky, 2011; Dong et al., 2017).

2.1.1.2 *DA2*

In addition to *BB*, the E3 ligase *DA2* is also known to ubiquitinate *DA1*, and has also been identified as a negative regulator of organ size in a study by Xia et al., 2013. The *da2-1* T-DNA insertion mutant exhibits a significant increase in seed size and weight relative to wild type plants, as well as being taller and with larger flowers and leaves. In addition to characterising the *da2* mutant phenotypes, this study also revealed using reciprocal crossing that *DA2* acts maternally to regulate seed growth (Xia et al., 2013).

The DA1 peptidase cleavage site has not yet been identified in *DA2* as the cleavage products are unstable and it has not been possible to purify sufficient cleaved product to perform Edman sequencing. However, this does support the hypothesis that one of the functions of protein cleavage by DA1 may be to promote the N-end-rule mediated degradation of DA1 peptidase cleaved substrates (Dong et al., 2017), although it is not clear if this is a general mechanism.

2.1.1.3 *UBP15*

UBP15 is a de-ubiquitination enzyme that has been shown to be a positive regulator of organ size (Liu et al., 2008). Knockout mutants exhibit smaller final organ sizes, with narrow and serrated leaves. They also produce fewer rosette leaves before bolting, and display an early flowering phenotype. The narrower leaves are caused by a decrease in cell number,

indicating that UBP15 can affect leaf shape by having a role in the control of cell proliferation (Liu et al., 2008).

The identification of UBP15 as a target for DA1-mediated cleavage (Dong et al., 2017) is supported by the discovery of increased levels of UBP15 protein in *da1-1* mutants (Du et al., 2014) indicating that DA1 peptidase activity has a role in controlling the levels of UBP15 in the cell.

2.1.1.4 *TCP4*

The TCP family of genes have been divided into class I and class II types. *TCP4* is a member of class II, which primarily has a role in promoting the arrest of the cell cycle and transition to the endoreduplicative phase of growth (Kosugi and Ohashi, 2002; Schommer et al., 2014). Loss of function mutants of *TCP4* have slightly enlarged leaves, as well as producing on average seven more leaves than wild type plants before reaching the flowering stage (Schommer et al., 2008). In plants expressing *35S:TCP4* there was a reduction in overall plant size (Schommer et al., 2014). *TCP4* is negatively regulated by miR319, a micro RNA known to target a number of TCP family members. *TCP4* mutants with deletions at the miR319 binding site are resistant, and plants expressing this modified *TCP4* display a further reduced organ size phenotype (Schommer et al., 2008), thus positioning *TCP4* as a negative regulator of organ size.

TCP4 has been identified as a target for DA1-mediated cleavage (Caroline Smith, unpublished), although how cleavage by DA1 affects its role is unknown.

2.1.1.5 *TCP15*

TCP15 is a member of the class I TCP family, closely related to another member of the class I TCPs, *TCP14*. Due to high functional redundancy, their phenotypes are often studied in tandem. There is considerable uncertainty in the literature regarding the overall function of *TCP15* in organ growth and development, and drawing definitive conclusions from the wide range of different and unconnected observations can be difficult.

TCP15 (along with *TCP14*) is expressed in leaf primordia, where the expression pattern recedes from the tip to the base of the leaf as the organ develops, appearing to follow the pattern of cell proliferation (Kieffer et al., 2011; Uberti-Manassero et al., 2012). There is evidence that, in conjunction with the expected function of a member of class I, *TCP15* promotes organ size: together with *TCP14* in a *tcp14tcp15* double mutant, internode length is reduced, contributing to an overall much shorter plant (Kieffer et al., 2011). In addition,

the fusion of *TCP15* to a SRDX repressor domain (Hiratsu et al., 2003) results in plants with smaller rosette leaves at earlier stages, as a result of smaller epidermal cells (Li et al., 2012; Uberti-Manassero et al., 2012), suggesting a role for *TCP15* in the promotion of growth, potentially by controlling cell expansion at early stages.

In contrast to these observations, another study has shown that inducible overexpression of *TCP15* results in a reduction in epidermal cell size in leaves (Li et al., 2012), providing a direct contradiction and evidence for *TCP15* as a growth inhibitor. It is possible that *TCP15* could have alternating roles, and that its activity is tissue-dependent or is controlled by another factor - for example its cleavage by DA1. The identification in Dong et al. 2017 of *TCP15* as a target for DA1 presents an opportunity for further work to elucidate the precise function of DA1 cleavage on a complex member of the highly redundant TCP family. This has already been explored in part by Peng et al. who have identified a role for *DA1*, *DAR1* and *DAR2* in the regulation of the endoreduplication pathway with *TCP14* and *TCP15* (Peng et al., 2015).

2.1.1.6 *TCP22*

TCP22 is a member of the highly functionally redundant class I TCP family, and is part of a distinct clade within this family, comprising *TCP7*, *TCP8*, *TCP14*, *TCP15*, *TCP21*, *TCP22* and *TCP23* (Aguilar-Martinez and Sinha, 2013). *TCP22* is primarily expressed in the young leaves of seedlings, and at a subcellular level, expression is observed in the nuclei. As a single knockdown mutant, the *tcp22-1* allele shows no discernible difference in phenotype from wild type plants: indicating previously described high redundancy. A quadruple mutant *tcp8tcp15tcp22tcp23* and a pentuple mutant *tcp8tcp15tcp22tcp23tcp21* also shows a largely similar phenotype to wild type, although the number of rosette leaves is reduced and the leaves are slightly wider and overall larger in area (Aguilar-Martinez and Sinha, 2013). *TCP22* may therefore have a role, along with other members of the class I TCP family, in controlling leaf initiation and organ growth.

In addition, the pentuple mutant described above exhibited higher expression levels of genes involved in the control of SAM maintenance and leaf development, such as *SHOOT MERISTEMLESS (STM)*, *BREVIPEDICELLUS (BP)* and *ASYMETRIC LEAVES1 (AS1)*. The cell-cycle genes *CYCA1;1* and *CYCA2;3* are also upregulated in this mutant background, providing an explanation for the larger leaf blades observed (Aguilar-Martinez and Sinha, 2013). The putative role of *TCP22* and related redundant class I TCP family members in the control of meristem maintenance and cell proliferation provides a potential explanation of the function of DA1-mediated cleavage, as identified in Dong et al. 2017.

2.1.2 Finding new substrates of the DA1 peptidase

The *da1-1* mutant displays a wide range of organ size-related phenotypes, including larger leaves and petals, larger cotyledons, and increased seed size (Li et al., 2008). Following the identification of a number of substrate proteins of DA1 that are known to be involved in the control of cell proliferation and expansion, I aimed to identify further substrates that may also be involved in plant growth. In addition, several of the substrates already identified are within the highly redundant TCP family (Danisman et al., 2013). Only a limited number of proteins within this family have been screened, and it is plausible, given their high redundancy, that DA1 is able to cleave additional TCP proteins. This idea is strengthened as DA1 appears to cleave both classes of TCP protein.

Identification of further substrates of DA1 will allow us to better understand how the cleavage activity of DA1 results in the observed reduced organ size phenotypes, and explain the increased organ size phenotype of the *da1-1* mutant. In addition, with every confirmed substrate protein of DA1, we are closer to being able to identify a conserved cleavage site and therefore the ability to perform a proteome screen to identify new candidates for DA1-mediated cleavage.

Previously, Dr Jack Dumenil initiated a systematic screening of potential DA1 target proteins by yeast-2-hybrid. A yeast-2-hybrid screen is a method of identifying *in vivo* physical protein interactions, first described in 1989. He utilised the native yeast GAL4 protein, which has both an N-terminal DNA binding domain and a C-terminal transcriptional activator domain. These two domains can be cloned and fused to bait and prey proteins, respectively. If the bait and prey proteins physically interact, the two GAL4 fragments are in sufficiently close proximity to interact, resulting in a functional version of GAL4 being reconstituted (Fields and Song, 1989). In this screen, the bait protein was a truncated version of DA1, with the N-terminal 162 amino acids removed. This left both the LIM domain and the C-terminal peptidase domain, while deleting the UIMs, reducing the risk of false positives based on interactions between endogenous yeast ubiquitin and the DA1 UIMs (Dumenil, 2013).

The proteins in the screen by Dr Dumenil which were found to interact physically with DA1 are listed below in Table 2.1.

Locus	Gene name	Gene description	Predicted location
AT2G22230		Beta-Hydroxyacyl-ACP Dehydratase, Putative	CW, CH
AT4G00270		DNA-Binding Storekeeper Protein-Related	CH
AT1G30460	ATCPSF30	Cleavage and Polyadenylation Specificity Factor Subunit	NU
AT5G35100		Peptidyl-Prolyl Cis-Trans Isomerase	CH
AT5G60390		Elongation factor Tu family protein	PM, VC, MT, NU, CY
AT4G36260	SHR2, STY2	SHI Related Sequence 2	NU
AT4G13640	UNE16	Unfertilized Embryo Sac 16	NU
AT1G69690	TCP15	TCP Family Transcription Factor	CH
AT2G15890	MEE14	Maternal Effect Embryo Arrest 14	CH
AT2G28790		Osmotin-Like Protein, Putative	CW
AT4G28750	PSAE-1	PSA E1 Knockout,	CH
AT2G30110	ATUBA1	Ubiquitin-Activating Enzyme 1	CY, NU, PM, PD
AT1G67090	RBCS1a	Ribulose Bisphosphate Carboxylase Small Chain 1a	CH
AT3G23750	TMK4	LRR-RLK Family Protein	PM
AT3G04120	GAPC1	Glyceraldehyde-3-Phosphate Dehydrogenase C Subunit	CY, MT, CH, NU, PM, AP
AT5G38410	RBCS3B	Ribulose Bisphosphate Carboxylase Small Chain 3B	CH
AT1G74030	ENO1	Enolase 1	CH
AT5G65950		Unknown Protein	Unknown
AT2G23350	PAB4	Poly(A) Binding Protein 4	CY
AT3G15360	ATHM4	Arabidopsis Thioredoxin M-Type 4	CW, CH
AT1G54630	ACP3	Acyl Carrier Protein 3	CH
AT1G36390		Co-Chaperone Grpe Family Protein	CH
AT1G60950	ATFD2	Ferredoxin 2	CH
AT5G60670		60S Ribosomal Protein L12	RB
AT5G08160	ATPK3	Arabidopsis Thaliana Serine/Threonine Protein Kinase 3	Unknown
AT5G49460	ACLB-2	ATP Citrate Lyase Subunit B 2	CY, PM
AT2G18030		Peptide Methionine Sulfoxide Reductase Family Protein	EM
AT4G32880	HTHB8	Homeobox Gene 8	NU
AT3G02550	LBD41	Lob Domain-Containing Protein 41	NU
AT5G24490		30S Ribosomal Protein, Putative	RB, CH
AT3G04940	ATCYSD1	Cysteine Synthase D1	CW, CH

Table 2.1 List of DA1-interacting proteins identified from the first round of the yeast-2-hybrid screen

From Dumenil, 2013 with permission (CY=cytosol; CW=cell wall; NU=nucleus; CH=chloroplast; PM=plasma membrane; PD=plasmodesmata; MT=mitochondria; AP=apoplast; RB=ribosome; VC=vacuole; EM=endomembrane system).

In order to understand the biological context of these yeast-2-hybrid interactions, I carried out protoplast transient expression cleavage assays to determine whether these DA1 interactors are substrates for cleavage by DA1. The proteins selected for inclusion in this study were AT4G36260 (*STYLISH2*, *STY2*), AT2G15890 (*MATERNAL EMBRYO ARREST14*, *MEE14*) and AT3G23750 (*TRANSMEMBRANE KINASE4*, *TMK4*). The reasons for these choices are described below.

2.1.2.1 *STY2*

STY2 is a member of the *SHORT INTERNODES (SHI)* family, which is known to have a role in the gibberellin signal transduction pathway, but also has high levels of functional redundancy (Fridborg et al., 2001). The first *sty2* phenotype was observed in the gynoecium, where it was observed to enhance the *sty1-1* mutant phenotype when combined as a *sty1-1sty2-1* double mutant, exhibiting reduced amounts of stylar and stigmatic tissues. Although the *sty2-1* mutant alone has no visible phenotype, this suggests that *STY1* and *STY2* are partially redundant and promote gynoecium development, in particular style and stigma formation (Kuusk et al., 2002). Their phenotypes and functions will therefore be discussed together here.

Aside from its function in promoting cell expansion in the stamen (Staldal et al., 2012) and other effects in the gynoecium, *STY1* also has an effect on the size and shape of leaves. Overexpression of *STY1* under the 35S promoter generates plants with smaller, narrower epinastic leaves compared to wild type, lacking in serrations. Supporting this, *sty1sty2* mutant leaves have increased serration, though maintain approximately the same overall leaf area as wild type (Kuusk et al., 2002), indicating a role for *STY1* in the inhibition of leaf blade width, as well as for *STY1* and *STY2* in the control of serrations, perhaps via genes controlling the leaf boundary or auxin homeostasis.

STY1 is potentially of interest despite not being identified in the yeast-2-hybrid screen because of its activity as a transcriptional activator of genes involved in auxin biosynthesis, a hormone known for its role in regulating cell proliferation and growth (Sohlberg et al., 2006; Perrot-Rechenmann, 2010). In particular, *STY1* is known to upregulate *YUCCA4 (YUC4)* (Sohlberg et al., 2006). *YUC4* is a member of the *YUCCA* family, a family of flavin monooxygenases that show overlapping functions in the control of auxin biosynthesis. Mutations in multiple *YUCCA* family genes result in smaller leaves and rosettes and decreased overall plant height, as well as defects in floral development and the differentiation of vascular tissue. These mutant phenotypes can be complemented by a

bacterial auxin biosynthesis gene, highlighting the role of the *YUCCA* family in auxin biosynthesis and hence organ development (Cheng et al., 2006). In addition to this, *STY1* is involved in the control of auxin transport, as the effects of altered auxin transport or signalling are enhanced in the *sty1-1* mutant (Sohlberg et al., 2006).

A binding site for the *STY1* transcriptional activator has been identified in the promoter region of *YUC4* and a second member of the *YUCCA* family, *YUC8*. The consensus sequence of this binding site is *ACTCTA(C/A)* respectively. Interestingly, this binding site can also be found upstream of *DA1* (Figure 2.1), which may indicate that *STY1* is also able to regulate *DA1* expression.

```

aaagttaatagcatgcagagcatttagcatattctcaagggacatcaaattccccagagtgaatagaaatttgatcag
taactgaatcggttaataataaaaacacagatagagttatatccctgtaaaaaattgacagactacctaaatgaatt
aaaatttccccaaatgtgaagaagaagaagaagctaaacatagtttaacgggtcacatatctataaaagactctacga
ccaaatgatcaaacgatttagcaaaaatattacaaaagtcacacttttatatcgataggagcataatggttcaaaata
ataatgggctatagaaaaaatcgaggccatttaactttctcttgagatgtaaaaaataaaatgagtggtgtgtgta
acttgtgagataaggtaatttgcaacttcatgaaactttaaataagcagaagacatgaaatataataagcgtaac
tagttgaaatgggttagtagagcttctgtaaaaaaagaacgaggtcaaatgatttcagtattacaaacaaaatgag
gtatgaagtaataatacaagttgtatcacataaaagaacaactgttcatgacaaacccaaactcagctatctcaaga
atgtaaatagtagtaaatagctaaatcgctcggatccaatagacggctagtggttaagtaatgtatgcgggtttatataaa
ggctcgtggttactggttagaaacataatgaagtaaaaaattgttacataatgagcttataaagcctataaacgagat
acgatttttttacattcaaaaataaacgggctgtgaaagccataaaagctatcacttccggtggtcaccgtaact
tccgaggtgtataaagaagaattcacatacttaattacaaatatttcggttaataatattgtaagtgatgatga
acgatcacattgtgacattgacactcacatagtagttataatattatgaattcatgtaagtaataatcgtagctgt
atgctaaattataatgtcaataaggtaaacatgattgaaacttttactttttgctataaaatcaacaaatctcttcc
atcttttttccctctatacttttacttttcaattttaaaagttagatataaaatataaaatgtgtttgctgttaa
tattttaacaaaaccagcctcaccaactttttcctaatcttttcttcaacttttttcttggttgctaccttttctg
ataggaataagtaataacatcatttaattcattatattgtagcttctcttttcaattttttcttctcattcttagc
tttctgctgaattatttggcaattggtaaaattacaaatcacgctgaaaagccaaaaggttaaaataatatttttcat
atcaataaaatgtgagtgagttatgggagcctagatttgggtcaaatacaatctaatatcgtagttgggttaaaaaa
tctatcaactaaaatcgataaacttgacaatttaattgaaacaacaacggtttaaacagtttaattagtagttatatacatt
tttcttgtattttatgctgttttgggtttgtagtttagaaaaacacacataataaaaaatataatataatattgat
tataaatttattttttgtgttttacaattttctattattctaaatcaatgataaataaactatttttttagaaaat
tacaattcactaataattatccaataaatttgcataaaaaatttaaaagattaatcttttagaaaataaatcatttagt
aataaagaaaatataatattataaaataattttacaatttagtggaataataaaaaaataatatttaattgttttcta
gcaaaaatataaaaatcttattagaattagaccggacaatccggataaaatgcttacgattgtagaagatttgggt
ttaaggctgaagcaataatataatataatctagatatttgcataaacggtgcaaaatggaagaaattgcca
acaaaataatatttgacttttaaatgctgaatagtagataattataatctctttctatctcaaatcacagcgtggg
gaacgttttttctggaagaagaagaagagctcaacaagctcaacgacccaaaaaacttcggacacgaagactttt
taattcatttctctcttttctgttttttctgttccaaaatattcgatactctcgatctcttctctgtgatcctcattaa
ataaaaatcagatttttattctttttttgtgagtgccaaaatttttgactttggattagcgtagaattcaagcaca
ttctgggtttattcgtgtatgagtagacattgattttgtcacaagttgcattcttttatataaaaaaagtttaatttcc
tttttcttttcttttcttttttttttttttttttttttttttttttttttttttttttttttttttttttttttttt
actaaagagtcctttttgagattcttttctgcttcccttctgcttgattagatcatttttggattctggattttgtgg
gggttctggaagcttattgggattcttctgattcaggatttttctcaaggtaaagggacgatcttttagcttctttgc
agctgcaattacttgataatccatgctctgattctaaatttcatgggttttttgaaaaaaacaaaaacaaatccg
tttggaactcgtttgcttaatgggtgacaggttttaggtgtgttagttatgtgttagattcaaaagtgctattgttc
tgtggcttttgatgtttggaagtgaacaagttgttttgggtttttgctaatcagagatgattcgcagcattttgacg
gctgcattgcccgtatgagcagatagttttatttaggcattATG

```

Figure 2.1 Sequence upstream of *DA1*

The *STY1* transcription activator binding site sequence is highlighted in yellow, and the initiation codon of *DA1* is in orange. Red indicates the 5' UTR, purple indicates an intron, and orange indicates an exon. The position of the *ACTCTAC* site suggests that it may be within the promoter region of *DA1*.

STY1 and STY2 show high levels of similarity at two positions in their amino acid sequences, with overall similarity between the two at 43%. The first is a cysteine/histidine-rich sequence C-X₂-C-X₇-C-X-H-X₂-C-X₂-C-X₇-C-X₂-H, which is found in the N-terminus of all *SHI* family members and shows 90% amino acid similarity between STY1 and STY2. This sequence is similar to that of a zinc binding RING finger motif, the function of which is to mediate protein-protein interactions (Freemont, 1993; Lovering et al., 1993; Borden, 2000; Kuusk et al., 2002). This could provide a possible site for the interaction of STY2 with DA1. The second region of high sequence similarity between STY1 and STY2 is referred to as the IGGH domain due to four residues highly conserved across all members of the family (Fridborg et al., 2001), and is required for homo-/hetero-dimerisation within the family (Eklund et al., 2010). This sequence shows an amino acid similarity of 67% between STY1 and STY2 (Kuusk et al., 2002).

Because of this high level of sequence similarity and functional redundancy between STY1 and STY2, and the identification of a *STY1* binding site in the *DA1* promoter region, I became interested in assaying STY1 as well as STY2 for cleavage by DA1.

Although the *DA1* promoter has not yet been functionally defined, it is possible that STY1 could bind in the promoter region of *DA1*, increasing *DA1* expression and resulting in a negative feedback loop, if it was able to cleave STY1 or STY2. This would reduce the inhibiting effect of STY1 on the growth of the leaf lamina, a phenotype that would support my observation that there is a significant increase in the width of the leaf lamina in *da1-1* mutants. A negative feedback loop seems like a likely mechanism for this interaction, as we already observe putative feedback loops of a similar nature with BB and DA2, both of which promote the peptidase activity of DA1 but are subsequently cleaved by it.

2.1.2.2 *MEE14*

MEE14 was initially identified as part of a screen for mutants defective in female gametophyte development and function. In the *mee14* mutant, in addition to the arrest of embryogenesis, the development of the endosperm was also aborted (Pagnussat et al., 2005). In a subsequent study, *MEE14* was renamed *CCG BINDING PROTEIN1 (CBP1)*, and a role identified for it in the control of pollen tube guidance. *MEE14/CBP1* was found to either fulfil the role of the Mediator subunit or another regulator of transcription initiation. Although to date the effects of *MEE14/CBP1* expression has primarily been studied in the reproductive organs, it is also expressed in the seedling, leaf, and inflorescence (Li et al., 2015), and this expression pattern is widely overlapping with that of *DA1*. A leaf phenotype has not yet been investigated in *mee14/cbp1* mutants. However, the seed development

phenotype renders it worthy of investigation, as the end goal for this fundamental research is to improve yields through crop improvement – and a better understanding of the genes involved in the pathway to the development of a larger, fuller seed with fully developed endosperm and embryo is important for this. The *da1-1*, *bb*, and *da1-1bb* mutants all exhibit a seed size phenotype (Li et al., 2008), so there is the possibility that *MEE14/CBP1* could be a transcriptional activator for either or both of *DA1* and *BB*, and as previously described result in a negative feedback loop following its cleavage.

2.1.2.3 *TMK4*

The *TMKs* form a small family of receptor-like kinases (RLKs), involved in the control of cell expansion and cell proliferation. In animals, the structurally-similar receptor tyrosine kinase (RTK) genes play important roles in cell proliferation, expansion, differentiation, and survival (van der Geer et al., 1994; Robertson et al., 2000). In plants, the RLKs are also thought to act as receptors for external signals, such as phytohormones (Dai et al., 2013), as well as in disease resistance, where pattern-recognition receptors (PRRs) detect pathogen-associated molecular patterns (PAMPS) and initiate a plant defence mechanism, PAMP-triggered immunity (PTI). RLKs are characterised by the presence of an extracellular receptor domain and a transmembrane domain. Most RLKs also have an intracellular protein kinase domain for signalling, although one third are non-receptor kinases or receptor-like proteins that lack the internal kinase domain (Afzal et al., 2008).

Many roles for RLKs in plant organ growth have already been identified. Their functions include, among others, the brassinosteroid signalling pathway, meristem development, cell wall signalling (including cell elongation and expansion), and inflorescence development (Dai et al., 2013). A good example of an RLK involved in the perception of external stimuli is *BRASSINOSTEROID INSENSITIVE1 (BRI1)*, the brassinosteroid signalling receptor. *BRI1* has an extracellular leucine rich repeat (LRR) domain containing 25 LRRs, as well as a 70-amino acid island between the 21st and 22nd LRRs. This island is required, in conjunction with LRR 22, to directly bind to brassinolide (Kinoshita et al., 2005). When brassinolide binds to the extracellular domain, *BRI1* is autophosphorylated (Wang et al., 2001). This alone is sufficient for *BRI1* to transphosphorylate downstream substrates when *BRI1* is in a homodimer complex, and generate a basal level of brassinosteroid signalling. However, when *BRI1* forms a heterodimer with *BRASSINOSTEROID INSENSITIVE1-ASSOCIATED RECEPTOR KINASE1 (BAK1)*, *BRI1* transphosphorylates *BAK1*, which enhances the downstream phosphorylation activity and therefore increases the brassinosteroid response (Wang et al., 2008).

Sequence analysis of TMK1 reveals structural features suggesting a receptor-like kinase function, for example the LRR domain, the transmembrane domain and the intracellular protein kinase domain (Chang et al., 1992). Four members of the *TMK* family have subsequently been identified, although high functional redundancy within the group means that double or triple mutants are required for strong developmental abnormalities to be observed. The *tmk1tmk4* double knockout mutant exhibits strongly reduced organ size, slower growth, a delay in development and reduced fertility (Dai et al., 2013). These phenotypes are further enhanced in the *tmk1tmk3tmk4* triple mutant, and in the *tmk1tmk2tmk3tmk4* quadruple mutant there is an additional complete loss of fertility. In leaves, the reduction in organ size is primarily as a result of decreased cell number: the *tmk1tmk4* double mutant has 90% smaller leaves than wild type, but only a 15% reduction in cell size indicating that there are fewer cells than in wild type. This, and further data exploring the rate of cell division at early stages of leaf development, suggests that the *TMK* family controls the rate of cell proliferation in early leaf development (Cheng et al., 2006). Conversely, cell size was significantly reduced in *tmk1tmk4* mutant roots, hypocotyls, and stamen filaments, indicating both an additional role for the *TMK* family in the rate and duration of cell expansion, and that their role is tissue-dependent (Dai et al., 2013).

TMKs have wide ranging interactions with other RLKs in many parts of the plant, particularly those which control cell numbers. For example, the functional redundancy of the TMKs with *ERECTA*, a gene functioning to control cell numbers in inflorescence tissues, could indicate why single *tmk* mutants show no mutant phenotype in the inflorescence, despite their high expression. TMKs also interact with CLV1 and CLV3 in the shoot meristem, maintaining the population of undifferentiated cells (Dai et al. 2013).

Members of the *TMK* family have also been proposed to have a role in auxin responses. The *tmk1tmk4* and *tmk1tmk3tmk4* mutants exhibit reduced sensitivity to auxin in the case of the double mutant, and none in the case of the triple mutant (Dai et al., 2013). Many phenotypic aspects of *tmk* double and triple mutants are also observed in mutants of genes involved in the auxin signalling and transduction pathway, for example single cotyledons with fused leaf-cups, as observed in *pin1-1* mutants. The PINs are involved in auxin transport, and have a key role in auxin gradients and organ development (Krecek et al., 2009). Furthermore, polar PIN1 localisation is aberrant in *tmk1tmk2tmk3tmk4* mutants, indicating a functional link between the *TMK* family and PIN localisation (Xu et al., 2014). There are also links to the putative auxin cell-surface sensor ABP1, for example *abp1* mutants show the same effects on PIN1 localisation as the quadruple *TMK* mutant, and a partial loss of function *abp1* allele

abp1-5 is able to enhance the aforementioned cotyledon defects in the quadruple *tmk* mutant (Xu et al., 2014). TMK1 is known to localise at the cell membrane (Dai et al., 2013), and quadruple *TMK* mutations have similar phenotypes to those exhibited by mutations of the ROP2 and ROP6 GTPases involved in auxin perception and signalling. TMK1-GFP coimmunoprecipitates with ABP1, and this interaction is promoted at higher concentrations of auxins. These results suggest a role for TMK1 and potentially other TMK family members in the ABP1 auxin-sensing complex at the plasma membrane (Xu et al., 2014).

A recent study using CRISPR technology has cast doubt on the role of *ABP1* in auxin signalling by creating a viable null mutant *abp1-c1*, which exhibited no defects in growth, development or the auxin response (Gao et al., 2015). In addition, a subsequent study by Enders et al. found that the weak *abp1-5* mutant most commonly used in ABP1 studies also contains a null mutation in *PHYTOCHROME B (PHYB)* and significant portions of the Wassilewskija ecotype genome, despite being in a Columbia background. Together, these findings go some way to explaining the mild auxin resistance and long hypocotyl in red light phenotype of *abp1-5*, as the Wassilewskija ecotype has a natural lower sensitivity to auxin, and the *phyB* mutation could explain the hypocotyl phenotype (Enders et al., 2015). Taken together, these data suggest that the original *ABP1* studies were conducted without proper testing of the mutant alleles used, and that any auxin response deficiency may have been as a result of off-target effects - such as that of *phyB* as previously described. These recent discoveries cast doubt over the links drawn between the auxin response phenotypes observed in *tmk* mutants and in *abp1* mutants in the Dai et al. paper, and suggest that *TMK* family members may not be involved in the auxin transduction pathway via ABP1. However, there is still strong evidence that *TMK* family members are involved in some way in the auxin response, as the mutants *tmk1tmk4* and *tmk1tmk3tmk4* exhibit reduced or eliminated auxin sensitivity (Dai et al., 2013). The mechanism for this is as yet unknown. *TMK4* has also been identified as *BAK1-ASSOCIATING RECEPTOR-LIKE KINASE1 (BARK1)*, and found to bind specifically to *BRI1-ASSOCIATED RECEPTOR KINASE1 (BAK1)*, a leucine-rich repeat receptor kinase which forms half of the brassinosteroid receptor heterodimer, by binding to *BRASSINOSTEROID1 (BRI1)* (Belkhadir and Chory, 2006; Kim et al., 2013). Evidence suggests that the effect on *BARK1* expression by brassinosteroid signalling depends on the intensity of the signal, with low or moderate signalling producing up-regulated *BARK1* expression, and high-level signalling resulting in the down-regulation of gene expression (Kim et al., 2013). This pattern of gene expression in response to phytohormone signalling can also be observed with auxin,

while abscisic acid, gibberellic acid and cytokinins largely decrease *BARK1* expression. *BARK1* overexpression also leads to increased root length (Kim et al., 2013).

I selected *TMK4* and its closely related family member *TMK1* to test for cleavage by the DA1 peptidase as they could provide a putative link between DA1 function in growth control and the well-described roles of auxin and brassinosteroids in regulating plant growth.

2.1.3 Prediction of a conserved DA1 peptidase cleavage site

The prediction of a conserved target site for DA1-mediated cleavage was made by Dr Benguo Gu, a postdoctoral researcher in the Bevan laboratory. A conserved target site would, if known, enable the screening of the proteome for putative substrates for the DA1 peptidase. The results from this screen could then be narrowed down, using a range of filters such as cellular localisation, expression patterns, and known functions in growth and development, to produce a pool of candidates for testing via the protoplast cleavage assay.

A further aim, therefore, for this Chapter was to test this prediction of a conserved cleavage site by testing new potential substrates containing the predicted consensus sequence predicted to be cleaved by DA1, and by identifying the cleavage site in two known substrates of DA1, TCP15 and TCP22. Dr Gu searched within the amino acid sequences of known cleavage substrates for DA1 for the NAYK known cleavage site in BB, but it was not found in any other known targets. However, NA sequences were found in all, with a number of intermediate amino acids and either lysine, as in BB, or arginine, which is a similar amino acid: both are strongly positively charged. These sequences have not been confirmed as the peptidase cleavage sites, however.

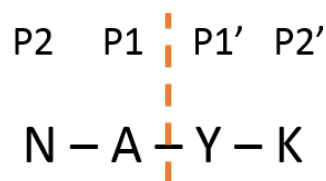


Figure 2.2 Annotation of peptidase cleavage sites

According to a system established by Schechter and Berger, 1967-68. The cleavage site is designated as being between P1 and P1', with numbering proceeding towards the N-terminus (in the manner P2, P3, P4 etc.) and the C-terminus (in the manner P2', P3', P4' etc.). The site shown is for DA1-mediated cleavage of BB (Dong et al., 2017).

As the cleavage site for BB has been previously identified (as described in Chapter 1 and earlier in this Chapter), these predictions were able to provide a framework for the identification of a putative cleavage site. The consensus sequence is asparagine, alanine, up

to three neutral amino acids, and then lysine or arginine, both of which are strongly positively charged (NAX₀₋₃(K/R). This is described in Table 2.2.

Substrate	P1	P2	P1'	P2'	P3'	P4'	Substrate cleaved?
BB	N	A	-	-	Y	K	Yes
-61BB	-	-	-	M	Y	K	No
BB AY-GG	N	G	-	-	G	K	No
BB ΔNAYK	-	-	-	-	-	-	No
TCP4_1-1	N	A	-	K	P	R	Yes
TCP4_1-2	N	A	-	-	-	K	Yes
UBP15	N	A	-	-	D	R	Yes
TCP15	N	A	-	A	Y	R	Yes
TCP22	N	A	-	S	L	R	Yes
DA2	N	A	S	V	V	R	Yes
Putative consensus sequence	NH ³⁺	Me				NH ³⁺	

Table 2.2 List of DA1 substrates and putative cleavage sites

Peptidase cleavage sites are often difficult to define, with over 2500 peptidases in the MEROPS database (Rawlings et al., 2016) not yet having an identified substrate (Rawlings, 2016). In the same study of the MEROPS database, a table of the preferred amino acids (if known) in each binding pocket from P4 to P4' shows that even for peptidases with many known substrates with the cleavage site identified, a consensus of often only one binding pocket can be achieved, and that this is often only a member of a particular group of amino acids rather than one in particular. Many of the listed peptidases have such a loose or unknown cleavage site, despite identified substrates of over 1000 in some cases, that they can only be described as having negative specificity for some amino acids at particular binding pockets (Rawlings, 2016). A proteomics approach taken to identify cleavage sites of the caspase enzyme found that the sites identified were more diverse than expected (Enoksson et al., 2007). Because of this, it could be important to expect only a loose consensus between DA1 peptidase cleavage sites in different substrates, and this was reflected in the breadth of potential substrates that were identified among the TCP family.

The amino acid sequences of both class I and class II TCP genes were searched for potential variants of the putative target site described above. In addition to the expected putative cleavage sites in TCP4, TCP15 and TCP22, further sites were identified within the class I family members TCP8, TCP11, TCP21 and TCP24, as well as the class II family member TCP3. I selected *TCP8* and *TCP21* for the cleavage assays, as these TCP family members are those that were included in the pentuple *TCP* mutant described earlier in this chapter and shown

to exhibit a leaf size phenotype (Aguilar-Martinez and Sinha, 2013). *TCP3* was selected for its closely relatedness to *TCP4*, already identified as a substrate for DA1 cleavage (Martin-Trillo and Cubas, 2010).

2.1.3.1 *TCP3*

TCP3 is closely related to *TCP4*, a gene already known to be a target for DA1, with amino acid similarity of 61%. *TCP3* knockout and over-expressor plants exhibit no clear phenotype difference from wild type (Li and Zachgo, 2013), due to the high functional redundancy within the TCP family, and the targeting of *TCP3* by miR319. *TCP2*, *TCP3*, *TCP4*, *TCP10* and *TCP24* are targeted by miR319, (Koyama et al., 2007) which is necessary to reduce *TCP* expression and maintain a wild type phenotype. When miR319 is absent or not able to target *TCP* family members, mature leaves are shorter, wider, and have strongly crinkled margins (Palatnik et al., 2003). The overexpression of a dominant repressive version of *TCP3* fused to the SRDX repression domain (Hiratsu et al., 2003) gives a similar crinkled phenotype to that of miR319 mutants. Overexpression of a modified version of *TCP3* in which the miR319 binding site is mutated inhibits leaf blade development and generates a very narrow leaf (Koyama et al., 2010), positioning *TCP3* as a negative regulator of organ growth. In addition to this, *TCP3* is thought to indirectly reduce the expression of boundary-specific genes including *CUC1* and *CUC2* by directly activating miR164, which targets *CUC1* and *CUC2* (Koyama et al., 2007; Koyama et al., 2010).

Along with *TCP1* and *TCP2*, *TCP3* has been shown to bind in the promoter region of the *NGATHA* (*NGA*) transcription factor family, activating its expression. The *NGA* family of genes act redundantly in a range of developmental processes, including the control of lateral organ size, where *NGA* overexpression results in smaller, narrower leaves and petals (Kwon et al., 2009; Ballester et al., 2015). *NGA* genes are also known to have a role in the control of auxin biosynthesis and transport, and upregulate local auxin biosynthesis (Trigueros et al., 2009; Martínez-Fernández et al., 2014). This, and other known interactions with downstream targets related to the control of organ size (Koyama et al., 2010), suggests *TCP3* is an important regulator of organ growth, and therefore an interesting candidate for testing for DA1 cleavage. The predicted cleavage site is NAK, which is the same as the predicted cleavage site for its close family member and known target of DA1, *TCP4*.

2.1.3.2 *TCP8*

TCP8 forms part of a clade within the class I TCPs, also including *TCP7*, *TCP14*, *TCP15*, *TCP21*, *TCP22* and *TCP23*. A function in the coordination of the expression of mitochondrial and

nuclear genomes has been identified (Hammani et al., 2011), but an organ size phenotype has also been observed, in conjunction with other TCP family mutations. In common with several other TCP family mutants, the *tcp8-1* single knockout exhibits a phenotype indistinguishable from the wild type. In conjunction with *tcp15-1*, *tcp22-1* and *tcp23-1*, the quadruple mutant has larger leaves than wild type, particularly in length. The pentuple mutant with the addition of *tcp21-1* shows an additional increase in leaf blade area (Aguilar-Martinez and Sinha, 2013). *TCP8* is therefore an interesting candidate to test for DA1 cleavage, as a regulator of organ growth in conjunction with other closely related family members. The predicted cleavage site of *TCP8* is NAVEH.

2.1.3.3 *TCP21*

Little is known about *TCP21*, but it is also within the same clade as *TCP7*, *TCP8*, *TCP14*, *TCP15*, *TCP22* and *TCP23*. The pentuple phenotype described above (*tcp8tcp15tcp21tcp22tcp23*) exhibits longer leaves compared to wild type, with an increase in leaf blade area (Aguilar-Martinez and Sinha, 2013). The closely relatedness of *TCP21* to known targets of DA1, *TCP15* and *TCP22*, means that it is an important potential substrate to investigate. The predicted cleavage site of *TCP21* is NAVK.

2.1.4 Finding the cleavage site in known substrates of DA1

Using site-directed mutagenesis, the putative cleavage site according to Dr Benguo Gu's prediction was deleted from both *TCP15* and *TCP22*. If the mutated forms of *TCP15* and *TCP22* are still cleaved by DA1, this means that DA1 does not act at the predicted site. In addition to these mutations, a further 10-amino acid deletion was generated for each of *TCP15* and *TCP22*, at a different position in the protein sequence, as shown in Figure 2.3 and Figure 2.4.

```

MNQNSSVAEATLQLNSGKPSPGSIPFISSGQHGNISTSATSSTSTSSGSALAVVKSA
VKKPTKDRHTKVDGRGRIRIMPAMCAARVFQLTRELGHKSDGETIEWLLQQAEP
IIASTGTGTIPANFSTLNASLRSGGGSTLFSQASKSSSSPLSFHSTGMSLYEDNNGTN
GSSVDPSRKLNSAANAAVFGFHHQMYPPIMSTERNPNTLVKPYREDYFKEPSSAA
EPSESSQKASQFQEQELAQGRGTANVVPQPMWAVAPGTTNGGSFAFWMLPMSG
SGGREQMQQQPGHQMWAFNPGNYPVGTGRVVTAPMGSMMLGGQQLGLGV
AEGNMAAAMRGRGDGLAMTLDQHQLQHQPNSQASENGGDDKK

```

Figure 2.3 Amino acid sequence of *TCP22*

Predicted cleavage site is shown in red, secondary 10 amino acid deletion is shown in green.

```
MDPDPDHNHRPNFPLQLLDSSTSSSTSLAIISTTSEPNSPKKPPPKRTSTKDRHT
KVEGRGRRIRMPAMCAARVFQLTRELGHKSDGETIEWLLQQAEPAVIAATGTGTI
PANFTSLNISRSSRSLAAHLRTTPSSYFFHSPHQSMTHHLQHQQVRPKNESH
SSSSSSQLLDHNQMGNYLVQSTAGSLPTSQSPATAPFWSSGDNTQNLWAFNIN
PHHSGVVAGDVYNPNSSGGSGGGSGVHLMNFAAIALFSGQPLASGYGGGGGGG
GGEHSHYGVLAALNAAYRPAETGNHNNNQNRDGDHNNHQEDGSTSHHS
```

Figure 2.4 Amino acid sequence of TCP15

Predicted cleavage site is shown in red, secondary 10 amino acid deletion is shown in green.

These further deletions were made because the putative cleavage site does not explain the sizes of the cleavage products on a Western blot. The full-length TCP15 protein is 34.76kDa, while the TCP22 protein is 39.61kDa. If TCP15 is cleaved at the NAAAYR predicted site, the cleavage product with an N-terminal FLAG tag would be 30.68kDa but on a Western blot this product appears smaller, around 25-30kDa (Dong et al., 2017). In addition to this, if the TCP22 protein is cleaved at the NASLR predicted site, the product would be 13.61kDa, but the product observed by Western blotting appears to also be around 25-30kDa (Dong et al., 2017). For this reason, the 10-amino acid deletion shown in green was produced at a site that could generate a cleavage product of the expected size. However, proteins often run at different sizes to their true molecular weight on Western blots – an example of this is DA1, which appears to be 70kDa but according to its amino acid sequence has a molecular weight of only 60.37kDa. This could explain why the observed cleavage product size of TCP15 and TCP22 is different from that of the predicted site, but by making deletions at this and another site based on expected size, we expected to be able to narrow down the cleavage site.

2.1.5 Aims for this Chapter

In this Chapter, the aim was to identify new substrates for the DA1 peptidase and to gain a greater understanding of the target site for DA1-mediated cleavage, in order to understand more about how DA1-mediated peptidase activity leads to altered organ growth. I used a transient expression protoplast cleavage assay system to test potential substrates identified both from the pool of physical interactors listed in Table 2.1 selected based on their biological roles, and also from the *TCP* family based on the presence of a variation on the predicted consensus cleavage site in their amino acid sequence. In addition, I also used the same system to test members of the *TCP* family known to be cleaved by DA1, *TCP15* and *TCP22*, for the position of their cleavage site, initially based on the predicted consensus cleavage site. I was able to further explore this by using 10-amino acid deletions around the expected cleavage site based on the perceived molecular weight of the cleavage product determined by Western blotting.

This Chapter aims to answer the following questions:

- Are any further of the putative DA1 interactors identified by Dr Jack Dumenil a substrate for DA1-mediated cleavage?
- Can a prediction for a conserved cleavage site for DA1 be confirmed, either through the identification of novel substrates in the TCP family known to contain a variant of the conserved site, or by testing mutated versions of known substrates?

2.2 Materials and Methods

2.2.1 RNA extraction

RNA was extracted using the Qiagen RNeasy Plant Mini Kit (Cat. No. 74903) according to the supplied protocol. Tissue was disrupted using a mortar and pestle in liquid nitrogen, provided Buffer RLT was used with 20µl 2M dithioeitol (DTT) (Melford. Cat. No. MB1015), and the product was eluted in 30µl of RNase-free water. RNA was extracted from rosette leaf tissue of plants at the flowering stage, the vegetative stage, and from seedlings in order to obtain a wide range of possible gene expression timescales. RNA was extracted for cDNA synthesis, as described below.

2.2.2 cDNA synthesis

cDNA was produced from RNA by reverse transcription using the Qiagen QuantiTect Reverse Transcription Kit (Cat. No. 205310) according to the supplied protocol.

2.2.3 PCR amplification of DNA

All PCR protocols in this thesis use dNTPs from a 100mM solution of dATP, dGTP, dCTP and dTTP (New England Biolabs. Cat. No. N0446S) and were carried out in an Eppendorf Mastercycler^R pro (Cat. No. 6321000019) thermocycler.

2.2.3.1 Amplification of target open reading frames from cDNA

All genes cloned in this chapter were amplified from cDNA using Phusion[®] High-Fidelity DNA Polymerase (New England Biolabs. Cat. No. M0530) according to the supplied protocol.

Component	Volume for 20µl reaction (µl)	Temperature (°C)	Time (seconds)
Nuclease-free water	11.8	98	30
5X Phusion GC buffer	4	98	10
10mM dNTPs	0.4	~60	30
10µM forward primer	1	72	30 per kb
10µM reverse primer	1	30x repeat of steps 2-4	
Template DNA	1	72	300
DMSO	0.6		
Phusion DNA polymerase	0.2		

Table 2.3 Phusion High Fidelity PCR protocol

2.2.3.2 Colony PCR to confirm clones

All colony PCRs were carried out with the Qiagen Taq Master Mix Kit (cat. No. 201443) using a slightly modified protocol.

Component	Volume for 30µl reaction (µl)	Temperature (°C)	Time (seconds)
Nuclease-free water	12	95	300
Taq Master Mix	15	95	30
DMSO	1	~50	30
10µM forward primer	1	72	30 per kb
10µM reverse primer	1	40x repeat of steps 2-4	
		72	600

Table 2.4 Colony PCR protocol

2.2.4 Gel extraction DNA purification

DNA fragments were extracted from agarose gels using the QIAquick Gel Extraction Kit (Qiagen. Cat. No. 28704) according to the supplied protocol.

2.2.5 Subcloning

2.2.5.1 *In-Fusion cloning*

Cloning for *TMK1*, *TMK4*, *STY1*, *MEE14* and *TCP3* was carried out using the In-Fusion® HD Cloning Kit (TaKaRa Bio. Cat. No. 121416) according to the supplied protocol.

2.2.5.2 *Gateway cloning*

Cloning for *STY2*, *TCP8* and *TCP21* was carried out using the pENTR/D-TOPO cloning system (ThermoFisher Scientific. Cat. No. K240020) and inserted into Gateway vectors (as detailed in Table 2.5 later in this Chapter) using the Gateway LR Clonase enzyme mix (ThermoFisher Scientific. Cat. No. 11791019), according to the supplied protocol. I was assisted in the cloning of *STY2* by Neil McKenzie.

2.2.5.3 *GeneArt*

The deletions in *TCP15* and *TCP22* were produced using the GeneArt™ Site-Directed Mutagenesis System (ThermoFisher Scientific. Cat. No. A13282) according to the supplied protocol. This work was carried out by Neil McKenzie.

2.2.6 Bacterial transformation

2.2.6.1 *Bacterial strains used*

E. coli Stellar™ Competent Cells (TaKaRa. Cat. No. 636763) were used for plasmid expression for protoplast transformation for all genes cloned by the In-Fusion method. One Shot™ TOP10 Chemically Competent *E. coli* cells (ThermoFisher Scientific. Cat. No. C404010) were used for all TOPO cloning. Library Efficiency™ DH5α™ Competent Cells (ThermoFisher Scientific. Cat. No. 18263012) were used for all genes cloned by the Gateway method.

2.2.6.2 Chemical transformation of bacteria

E. coli were transformed using the heat-shock method. 50µl of competent cells were incubated on ice with 1-10µg of DNA for 30 minutes. The tube was heat-shocked at 42°C for 30 seconds (Stellar™ Competent Cells and One Shot™ TOP10 Chemically Competent *E. coli*) or 45 seconds (Library Efficiency™ DH5α™ Competent Cells) before being returned to ice. 250µl of pre-warmed S.O.C medium (provided with cells) was added to each tube, and these were incubated for one hour at 37°C with shaking at 220 rpm, without antibiotics. Cells were then spread on LB (Lysogeny Broth medium: 10% w/v tryptone (Sigma-Aldrich. Cat. No. T7293), 5% w/v yeast extract (Sigma-Aldrich. Cat. No. Y1625, 10% w/v NaCl (Sigma-Aldrich. Cat. No. 433209), 15% w/v agar (Sigma-Aldrich. Cat. No. A1296), adjusted to pH7.5 with NaOH) selection plates with the appropriate antibiotic (kanamycin 50µg.ml⁻¹, ampicillin 100µg.ml⁻¹ or spectinomycin 50µg.ml⁻¹, all from Sigma-Aldrich), and incubated for 12-16 hours at 37°C.

2.2.7 Sequencing

Sequencing was carried out using the GATC Biotech LIGHTRUN NightXpress service (www.gatc-biotech.com) and primers as listed in the primer table below.

2.2.8 Protoplast assays

2.2.8.1 Plasmid purification

Large quantities of plasmid were purified from *E. coli* using the Qiagen Plasmid Maxi Kit (Cat. No. 12162). The DNA pellet was re-suspended in 100µl TE buffer (10mM Tris-HCl (Melford. Cat. No. T1513), 1mM EDTA (Sigma-Aldrich. Cat. No. EDS).

2.2.8.2 Protoplast production

The protoplast transient assay for DA1-mediated was developed by Caroline Smith and Hui Dong, and adapted from a published protocol by Wu et al. as described below (Wu et al., 2009). The plants used for protoplast isolation were *da1dar1* double knockouts to reduce endogenous DA1 family member peptidase activity.

Leaves from four to five-week-old plants were used for protoplast isolation. The leaves were stuck by their upper epidermis to Sellotape™, and Magic™ tape (Scotch) was pressed onto the lower epidermis. The Magic™ tape was removed, exposing the mesophyll cells. The Sellotape™ with the adhering leaves was cut into short strips, placed in a petri dish containing 10ml enzyme solution (20mM MES (pH5.7) (Sigma-Aldrich. Cat. No. M2933), 20mM KCl (Sigma-Aldrich. Cat. No. P9541), 0.4M D-mannitol (Sigma-Aldrich. Cat. No. 63559),

1% cellulase R10 (Cellulase Onozuka R-10, Yakult Pharmaceuticals), 0.25% macerozyme (Macerozyme R-10, Duchefa Biochemie. Cat. No. M8002), 10mM CaCl₂·2H₂O (Sigma-Aldrich. Cat. No. C3306) and incubated with shaking at room temperature for three to five hours.

The crude protoplast preparation was filtered through a 100µm mesh into a 50ml centrifuge tube, and centrifuged for three minutes at 100xg. The supernatant was discarded, the cells washed in 10ml of cold W5 solution (2mM MES (pH 5.7), 150mM NaCl, 125mM CaCl₂·2H₂O, 5mM KCl) and centrifuged again. The cells were then re-suspended in 5ml of cold W5 and incubated on ice for 30 minutes. The protoplasts were re-suspended in cold MMg (4mM MES (pH 5.7), 0.4M D-mannitol, 15mM MgCl₂ (Sigma-Aldrich. Cat. No. M8266)) to a concentration of 2-5x10⁵ cells/ml, using a haemocytometer to count cells.

2.2.8.3 *Protoplast transformation*

10µg of each plasmid to be transformed in a total 20µl solution was added to a 2ml microcentrifuge tube. Using a cut-off pipette tip, 200µl of protoplasts suspended in MMg was added to each tube, then 220µl of PEG/Ca solution (4g PEG (Sigma-Aldrich. Cat. No. 81242) 4ml 0.5M D-mannitol, 500µl 1M CaCl₂·2H₂O). The microcentrifuge tubes were inverted gently several times to mix the solutions, and allowed to incubate for ten minutes at room temperature. The solutions were diluted slowly with 1ml of cold W5 solution, and centrifuged for one minute at 100xg. The supernatant was discarded, and the protoplasts re-suspended in 250µl of cold W5 with 50µM Mg132 proteasome inhibitor (Z-Leu-Leu-Leu-al, Sigma-Aldrich C2211). The protoplasts were transferred using a cut-off pipette tip to a 24-well plate (Nunc 24-well plate, round. ThermoFisher Scientific. Cat. No. 144530), where the wells had been coated in 1% (w/v) BSA (Sigma-Aldrich. Cat. No. A2058), before being incubated overnight in a growth chamber.

2.2.8.4 *Protein extraction from protoplasts*

The protoplasts were transferred to 1.7ml microcentrifuge tubes using a cut-off pipette tip, and centrifuged for three minutes at 1,300xg. The supernatant was discarded, and the pellet re-suspended in 45µl of denaturing buffer (50mM Tris-HCl (pH 7.5), 150mM NaCl, 4M urea (Melford. Cat. No. U1363), 1% NP40 (CalBiochem. Cat. No. 492015), 1mM PMSF (Sigma-Aldrich. Cat. No. PMSF-RO ROCHE) and vortexed for 10 seconds. The solution was then centrifuged for five minutes at 14,000xg at 4°C, and the supernatant recovered.

2.2.9 Western blotting

Samples were boiled with 4x Laemmli Sample Buffer (Bio-Rad. Cat. No. 1610747) for five minutes then stored on ice before loading into a precast 12-well 4-12% gradient SDS gel

(RunBlue SDS Protein Gels 4-12%. Expedon. Cat. No. NXG41212) in SDS buffer (RunBlue SDS Run Buffer. Expedon. Cat. No. NXB50500). A protein molecular weight ladder was also loaded (PageRuler™ Plus Prestained Protein Ladder, 10 to 250kDA. ThermoFisher Scientific. Cat. No. 26619). The gel was run for an initial 20 minutes at 80V, then a further hour at 160V.

The gel was then loaded into a cassette for transfer with PVDF membrane (Sigma-Aldrich. Cat. No. 03010040001-ROCHE) between two pieces of filter paper and two sponges. The transfer took place in the cold-room, in 1x transfer buffer (1.44% (w/v) glycine (Melford. Cat. No. G0709), 0.302% (w/v) Tris (Melford. Cat. No. B2005), 20% (v/v) ethanol (VWR International GmbH)) either overnight at 30V or for 90 minutes at 90V.

The PVDF membrane was blocked in 20ml 5% milk (Marvel Original Dried Skimmed Milk, Premier Foods) in PBST (8mM Na_2HPO_4 (Sigma-Aldrich. Cat. No. S3264), 150mM NaCl, 2mM KH_2PO_4 (Sigma-Aldrich. Cat. No. P9791), 3mM KCl, 0.1% (v/v) TWEEN-20 (Sigma-Aldrich. Cat. No. P9416)) for one hour at room temperature, with shaking. It was then probed with either α FLAG (Sigma-Aldrich. Cat. No. A8592) or α HA (ThermoFisher Scientific. Cat. No. 261830HRP) monoclonal peroxidase antibody (1:1000 ratio) in 10ml 5% milk in PBST for 90 minutes at room temperature, with shaking.

The membrane was washed three times in PBST for one hour at room temperature, with shaking. Chemiluminescent substrate (SuperSignal™ West Femto Maximum Sensitivity Substrate. ThermoFisher Scientific. Cat. No. 34096) was applied to the membrane, 300 μ l each of luminol and the peroxide buffer, and incubated for five minutes before being lightly blotted on tissue and used to expose UV/blue-sensitive film (Super RX. Fujifilm). These films were developed using a medical film processor (SRX-101A. Konica Minolta. Cat. No. 1051/2).

2.2.10 Vectors and primers

Vector identity	Vector type	Tags	Source
Modified pEarleyGate 103	Binary vector	FLAG tag	Dr Hui Dong, JIC
pw1266	Binary vector	FLAG tag	Dr Phil Wigge, SLCU
pENTR/D-TOPO	Gateway entry vector	N/A	ThermoFisher Scientific. Cat. No. K240020

Table 2.5 Vectors used in Chapter 2

Primer identity		Primer sequence
In-Fusion cloning		
TMK1 C-term N-Flag	F	CGACAAGATCTCTAGAGAGAGGAATGAAGTCTTC
TMK1 C-term N-Flag	R	TAATTAAGTCTCTAGATCATCGTCCATCTACTGAAGTG
TMK4 C-term N-Flag	F	CGACAAGATCTCTAGAAAATTTGTTATGAAGAGGAAGTATG
TMK4 C-term N-Flag	R	TAATTAAGTCTCTAGATCACCGACCATCAGCTGAATCGAAAG
STY1 N-Flag	F	GATGACGACAAGATCTCTAGAATGGCGGGTTTTCTCGC
STY1 N-Flag	R	GTCTTAATTAAGTCTCTAGATCATGATCTTGGGTTGGGAAAG
MEE14 N-Flag	F	GATGACGACAAGATCTCTAGAATGATAAAATCAGTGACTCTTCG
MEE14 N-Flag	R	GTCTTAATTAAGTCTCTAGATCAGTCGGTTTCGTGGTCAGGAG
TCP3 C-Flag	F	CATTGGAGAGGACACGCTCGAGATGGCACCAGATAACGACCATTTC
TCP3 C-Flag	R	TATAATCCATCTCGAGATGGCGAGAATCGGATGAAGCAGAGGACG
Gateway cloning		
TCP8 N-Flag	F	caccATGTCTGACGACCAATTCCATCA
TCP8 N-Flag	R (STOP)	TCAATGGCGAGAAATAGAGGAAG
TCP21 N-Flag	F	caccATGGCCGACAACGACGG
TCP21 N-Flag	R (STOP)	TCAACGTGGTTCGTGGTCG
STY2 N-Flag	F	caccATGGCTGGGATATTCTCATTA
STY2 N-flag	R (STOP)	TCAAGATCTTGGTGGATTTTGATAGA
Sequencing		
T7	F	AATACGACTCACTATAGG
T7	R	GCTAGTTATTGCTCAGCG
M13	F	GTAAAACGACGGCCAG
M13	R	CAGGAAACAGCTATGAC
GeneArt		
TCP15 ΔNAAYR	F	CCATTATGGAGTTTTAGCGGCGTTGCCGGTGGCGGAGACGGGGAACCATA
TCP15 ΔNAAYR	R	TATGGTTCCCGTCTCCGCCACCGGCAACGCCGCTAAAACCTCATAATGG
TCP15 Δ136-145	F	ATCTTCTCTCTGCTGCTCATCTTTCACCACATCAGTCCATGACTCATC
TCP15 Δ136-145	R	GATGAGTCATGGACTGATGTGGTAAAAGATGAGCAGCAGAGAGAGAAGAT
TCP22 ΔNASLR	F	GATCCCGGCGAATTTCTCAACACTTAGTGGTGGTGGCTCCACCTGTTTT
TCP22 ΔNASLR	R	AAAACAAGGTGGAGCCACCACCTAAGTGTGAGAAATTCGCCGGGATC
TCP22 Δ161-170	F	GCCACTCTCGTTTCATAGCACTGGAAACGGATCATCGGTAGATCCTTCTA
TCP22 Δ161-170	R	TAGAAGGATCTACCGATGATCCGTTTCCAGTGCTATGAAACGAGAGTGCC

Table 2.6 Primers used in Chapter 2

All primers used in this Chapter were supplied by Sigma Genosys (Sigma-Aldrich).

2.3 Results

In this Chapter, a protoplast cleavage assay system was used to test potential substrates for DA1-mediated cleavage. The protoplast system was used rather than an *in vitro* system because protoplasts retain most of their native physiological responses and cellular processes when compared to intact plants (Sheen, 2001; Yoo et al., 2007). This gives a greater biological relevance to results generated via this system compared to results generated in a more artificial *in vitro* system. The protoplast system also generates results more quickly than a transient expression in *Nicotiana benthamiana*, with results generated within 24 hours. By contrast, transient expression in *N. benthamiana* can take 4 days or more, including *Agrobacterium tumefaciens* growth (Shamloul et al., 2014).

All protoplast experiments were carried out using mesophyll protoplasts isolated from *da1dar1* knockout plants. This provides a much cleaner system within which to work, removing any endogenous effects of *DA1* and *DAR1* from the experiment. The double knockout was used rather than the single *da1* knockout because *DAR1* has high functional redundancy with *DA1* and could have affected the experiment. By using a knockout plant and transfecting a controlled amount of *DA1* into the cells separately, we were more able to control the inputs to the experiment.

These experiments are designed with two negative controls. By not transfecting samples with *DA1*, we are able to conclude that the observed result in the sample that does contain *DA1* is as a result of the addition of *DA1*. In addition to this, by transfecting samples with a version of *DA1* with a mutation in the peptidase domain rendering it non-functional (here identified as *DA1-pep*), we are able to conclude that the observed result is due to the activity of the peptidase domain of *DA1*. BB cleavage is provided as a positive control, except for the deletions of TCP15 and TCP22, where a wild type version of the gene is shown as a positive control.

2.3.1 Assaying for new targets of DA1

In this section, five potential substrates were selected based on evidence from a yeast-2-hybrid screen or functional similarity, and subsequently assayed for cleavage by DA1 in an Arabidopsis protoplast system and subjected for Western blot analysis.

Based on the evidence from these protoplast assays (Figure 2.5), it is not possible to say that any of TMK4, TMK1, STY2, STY1 or MEE14 are cleaved by DA1. Although it remains possible that DA1 could cleave other potential substrates from the pool identified by yeast-2-hybrid, the identification of a predicted cleavage site for DA1 led to the decision to not test any further substrates from this pool at this time.

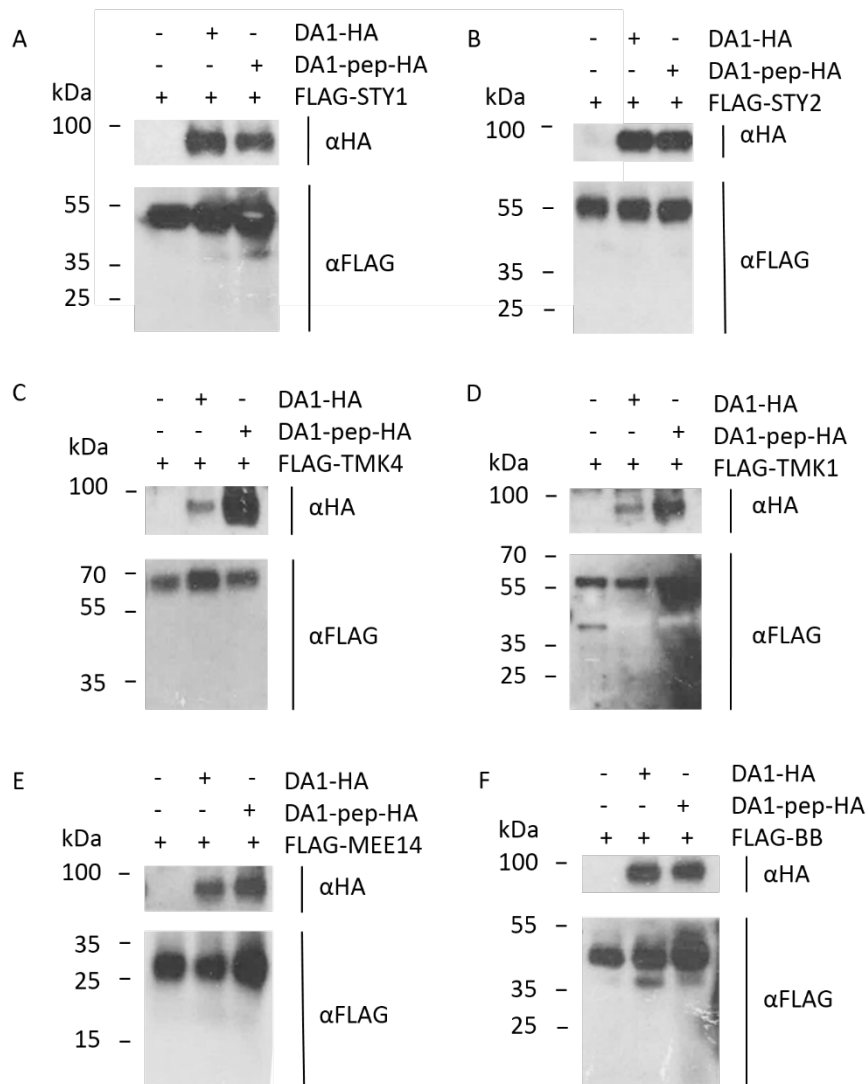


Figure 2.5 STY1, STY2, TMK4, TMK1 and MEE14 are not cleaved by DA1

Protoplast assay for DA1-mediated cleavage of STY1 (A), STY2 (B), TMK4 (C), TMK1 (D), MEE14 (E) and BB (F). FLAG-STY1, FLAG-STY2, FLAG-TMK4, FLAG-TMK1, and FLAG-MEE14 are not cleaved in a protoplast system by DA1-HA. FLAG-BB is cleaved by DA1-HA (lane 2) but not in the absence of DA1 (lane 1) or when DA1-HA is replaced with DA1-pep-HA, the peptidase mutant (lane 3).

2.3.2 Testing a predicted cleavage site for DA1

In this section, three members of the TCP family found to have a variant of the predicted cleavage site in their amino acid sequence (as described in Section 2.1.3) were assayed for cleavage by DA1 using the protoplast system (Figure 2.6).

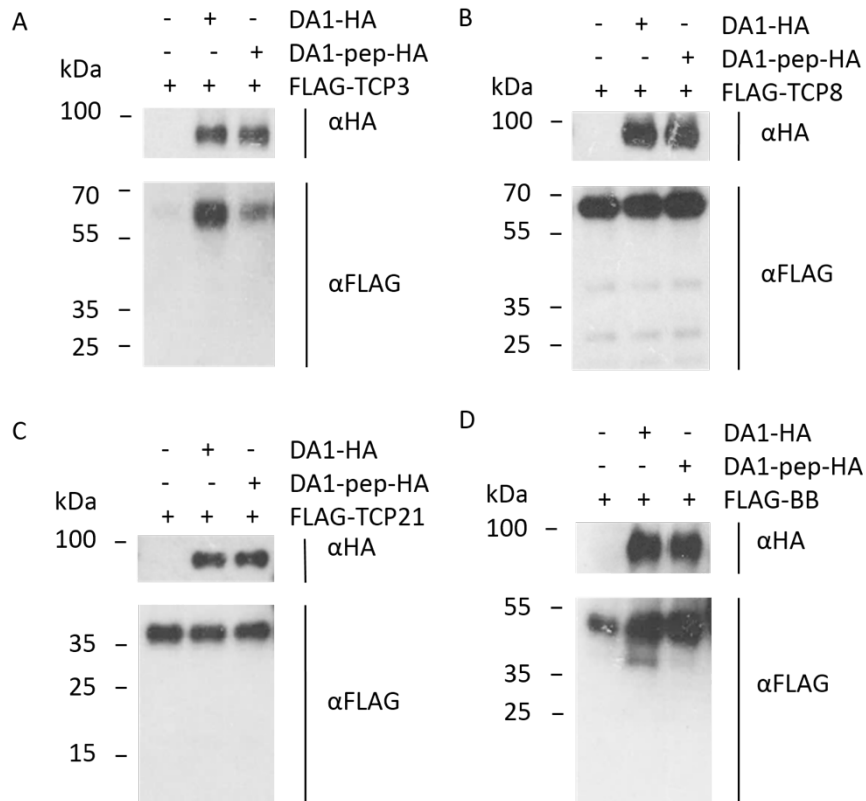


Figure 2.6 TCP3, TCP8 and TCP21 are not cleaved by DA1

Protoplast assay for DA1-mediated cleavage of TCP3 (A), TCP8 (B), TCP21 (C) and BB (D). FLAG-TCP3, FLAG-TCP8, and FLAG-TCP21 are not cleaved in a protoplast system by DA1-HA. FLAG-BB is cleaved by DA1-HA (lane 2) but not in the absence of DA1 (lane 1) or when DA1-HA is replaced with DA1-pep-HA, the peptidase mutant (lane 3).

Based on the evidence from the subsequent Western blotting, it is not possible to say that TCP3, TCP8 and TCP21 are targets for the DA1 peptidase, whether at the predicted NAX₀₃(K/R) site or at any other site detectable using the gel-based system. For this reason, it was decided to test the predicted cleavage site more directly, in substrates known to be cleaved by DA1, as detailed in the next section.

Interestingly, TCP3 protein levels were consistently dramatically lower in the absence of DA1 or DA1-pep (Figure 2.6A). This could potentially indicate that some aspect of DA1 functionality other than its peptidase activity could be involved in the maintenance of TCP3 stability, or promotion of its expression.

2.3.3 Finding the cleavage site in known targets

2.3.3.1 TCP15

The cleavage of TCP15 by DA1 has been reported in Dong et al, 2017, producing a ~25kDa N-terminal fragment. In this section, this result was replicated and a predicted cleavage site was tested.

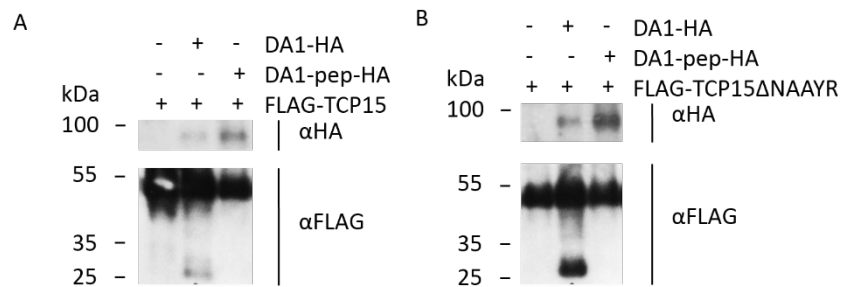


Figure 2.7 Deletion of a predicted cleavage site in TCP15 does not inhibit cleavage by DA1

Protoplast assay for DA1-mediated cleavage of FLAG-TCP15 (A) and FLAG-TCP15 Δ NAAAYR (B). (A) FLAG-TCP15 is cleaved by DA1-HA (lane 2) but not in the absence of DA1 (lane 1) or when DA1-HA is replaced with DA1-pep-HA, the peptidase mutant (lane 3). (B) FLAG-TCP15 Δ NAAAYR is cleaved by DA1-HA (lane 2) but not in the absence of DA1 (lane 1) or when DA1-HA is replaced with DA1-pep-HA, the peptidase mutant (lane 3).

There appear to be two cleavage bands for FLAG-TCP15 (Figure 2.7A), with the band of slightly lower molecular weight being stronger. This was also observed in Dong et al. 2017. The signal at the cleavage band of FLAG-TCP15 Δ NAAAYR (B) is stronger than in (A) so it is difficult to confirm that there are two cleavage bands present in (B), but the depth of the band suggests that two bands are present, representing the same cleavage pattern as in (A). From these observations, it is possible to conclude that the cleavage site of TCP15 is not at NAAAYR, as cleavage of TCP15 is not affected when these amino acids are deleted.

In addition to this, a 10-amino acid deletion based on the estimated cleavage site according to the molecular weight of the cleavage fragment was also tested, FLAG-TCP15 Δ 136-145. The preliminary data from this was inconclusive, and it is not possible to determine whether or not this deletion affects DA1-mediated cleavage of TCP15.

2.3.3.2 TCP22

In addition to TCP15, the cleavage of TCP22 by DA1 has been reported in Dong et al, 2017, producing a ~25kDA N-terminal fragment. In this section, this result was replicated and a predicted cleavage site based on the molecular weight of the cleavage fragment was tested.

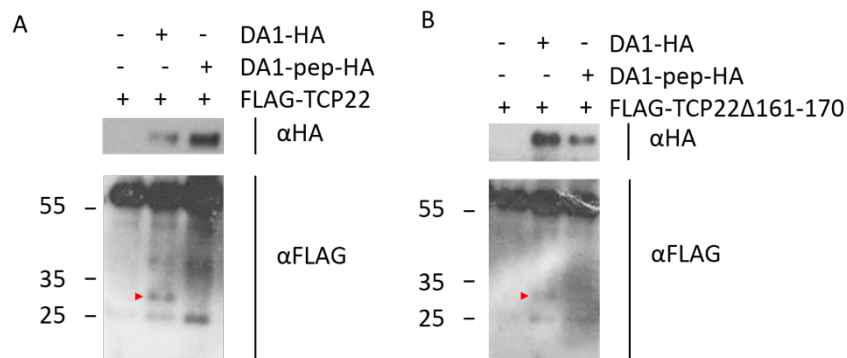


Figure 2.8 Deletion of a predicted cleavage site in TCP22 does not inhibit cleavage by DA1

Protoplast assay for DA1-mediated cleavage of FLAG-TCP22 (A) and FLAG-TCP22Δ161-170 (B). (A) FLAG-TCP22 is cleaved by DA1-HA (lane 2) but not in the absence of DA1 (lane 1) or when DA1-HA is replaced with DA1-pep-HA, the peptidase mutant (lane 3). (B) FLAG-TCP22Δ161-170 is cleaved by DA1-HA (lane 2) but not in the absence of DA1 (lane 1) or when DA1-HA is replaced with DA1-pep-HA, the peptidase mutant (lane 3).

From these observations, it is possible to conclude that the cleavage site of TCP22 is not within amino acids 161-170, as cleavage of TCP22 is not affected when these amino acids are deleted.

In addition to this, a deletion based on the putative cleavage site according to Dr Benguo Gu's prediction was tested, FLAG-TCP22ΔNASLR. The preliminary data from this was inconclusive, and it is not possible to determine whether or not this 5-amino acid deletion affects DA1-mediated cleavage of TCP22. However, as the equivalent site in TCP15 did not affect cleavage, it seems likely that the NAX₀₋₃(K/R) consensus sequence is not a conserved site for DA1-mediated cleavage.

2.4 Discussion

In this Chapter I tested potential substrates for DA1-mediated cleavage, and made progress towards the identification of a target site for proteins known to be cleaved by DA1. I did not find any evidence for the cleavage of the potential substrates tested in this work using the protoplast transient expression system.

The interactors identified in the yeast-2-hybrid screen that I tested were found not to be cleaved by DA1. Yeast-2-hybrid screens are known to produce a large proportion of false positives (Bruckner et al., 2009), so it is possible that some or all of those candidates tested were not true interactors of DA1. The reasons for the high rate of false positives found in yeast-2-hybrid screens vary widely according to the type of screen used. One reason is that the bait and prey proteins may be being expressed highly in a subcellular compartment that is not native for the target protein, which may result in it behaving biochemically differently. In addition, prey proteins may interact with the reporter protein or membrane anchors that are fused to the bait, creating an apparent interaction. Thirdly, proteins may be more generically “sticky”, or be incorrectly folded as a result of the fusion, and therefore result in aberrant physical interactions (Bruckner et al., 2009).

In addition to this, it is possible that these proteins may interact with DA1 but in a way other than as a target substrate for cleavage. For example, they may be upstream acting as regulators of DA1 protein activity, perhaps binding to DA1 protein to promote or inhibit its peptidase activity, or affect the specificity of the peptidase. These factors could present possible explanations as to why these proteins may have shown a physical interaction with DA1 but do not appear to be cleaved by DA1 in a protoplast cleavage assay.

By contrast, the TCP family members that were assayed for cleavage were identified for testing as a result of their having the putative cleavage site in their amino acid sequence. Despite being positive candidates, it is not possible to conclude that TCP3, TCP8 and TCP21 are cleaved by DA1, whether at the putative cleavage site or elsewhere.

One potential avenue for searching for further targets of DA1 is to continue screening the yeast-2-hybrid interactors list detailed earlier in this chapter. *TCP15* was initially identified as a gene of interest from this table, and is now known to be cleaved by DA1 (Dong et al., 2017), therefore there is still the potential for further substrates to be found.

Alternatively, a more targeted search among genes involved in the control of cell division could be possible. Most of the known substrates for DA1 (UBP15, TCP15, TCP22) have a

function linked to the control of cell proliferation and so it is likely that if the role of DA1 is to modulate part of the transition from cell division to cell expansion, there could be further targets to identify in this area. A range of candidates more specific to cell division rather than general organ development (as explored in the initial yeast-2-hybrid screen by Dr Dumenil) could be screened by yeast-2-hybrid to identify physical interactors.

However, given the low efficiency of both the yeast-2-hybrid screening that some of the work in this chapter is based on, and the search for proteins with the putative target site, it could have been more effective to take a wider approach, by testing for differential protein levels in *da1-1* or *da1-1* transformed with DA1-pep plants compared to wild type. This technology is now available via the iTRAQ method (isobaric tag for relative and absolute quantification). This technology is able to label all peptides in biological samples, which can then be analysed using mass spectrometry and differential protein levels identified between samples. This method has recently been successfully used to identify proteins involved in the response to heat stress in rice (Zhang et al., 2017) and grain size in wheat (Yang et al., 2017). Analysis of differential protein levels could be expanded using the N-terminal iTRAQ tagging to identify new N-termini in proteins where cleavage had occurred, in comparison to the original N-terminus. This has allowed extensive identification of cleavage sites in substrates of the caspase protease (Enoksson et al., 2007).

The methods by which cleavage sites in peptidase substrates may be identified can broadly be divided into three groups. The first of these is based on making and testing deletions of known substrates, such as the approach taken in this Chapter. In this Chapter, deletions were tested based on a predicted conserved sequence for cleavage, as well as deletions based on the observed molecular weight of cleavage products, as visualised on a Western blot. There are advantages and disadvantages to this approach. The proteins can be expressed transiently and at low levels in a protoplast system, which is quick and cheap, and can be tested on any number of substrates. There is also a very high chance that the cleavage site can be gradually identified through successive rounds of experimentation. However, these successive rounds of experimentation may occupy the researcher's time for some time, and if the prediction is found to be false, then little has been gained. Due to the frequent poor translation between migration on an SDS gel and true molecular weight, it can also be difficult to estimate the cleavage site based on the migration of the cleaved product. Therefore, this approach, while being simple and cheap, can be very time-consuming.

The second option is via an Edman sequencing approach. Edman sequencing was used to identify the cleavage site of BB (Dong et al., 2017). This method required the purification and cleavage of a large amount of the substrate protein, and subsequent purification of the cleaved fragment. The N-terminus of this purified cleavage product was then sequenced using Edman sequencing, giving a short amino acid sequence that could be aligned to the substrate amino acid sequence to determine the cleavage site. While this gives an accurate and direct result, Edman sequencing requires a very large amount of protein. This method was only able to be used in the identification of the DA1-mediated cleavage site in BB as the cleaved fragment was sufficiently stable. In other examples, for example DA2, the cleaved fragment is not sufficiently stable to be able to purify large quantities of it, rendering Edman sequencing impossible (Dong et al., 2017).

Finally, novel mass spectrometry-based methods have been successfully applied to the search for peptidase cleavage sites (Kleifeld et al., 2010) and protein sequencing (Gevaert et al., 2003; Venne et al., 2013). Mass spectrometry analysis of peptidase cleavage sites involves the digestion of the cleaved substrate protein using a peptidase, usually trypsin (Saveliev et al., 2013), and the separation of the resulting fragments according to their molecular weight by HPLC (high-performance liquid chromatography). These fragments can then be aligned to a scaffold of the un-cleaved substrate, allowing the identification of a putative cleavage site. By contrast to Edman sequencing, mass spectrometry analysis can be carried out with much less purified sample, analysing the molecular weight of amino acids to determine sequences of cleavage products. Other advantages of mass spectrometry analysis over Edman sequencing include the ability to perform quantitative analysis on cleavage products, for example if there are multiple cleavage sites but one is more frequent than the other. However, mass spectrometry relies on variation in molecular weight of amino acid residues to identify them separately, and, as some amino acids have the same molecular weight, it may be less accurate than Edman sequencing.

With these experiments, I have made progress in identifying cleavage sites in TCP15 and TCP22, by showing that the approach based on predicting peptidase cleavage sites may not be productive. Although some of the preliminary data surrounding targeted deletions in these proteins is unclear, with further work and exploration of additional 10-amino acid deletions in this area, the cleavage site will be able to be identified – perhaps in the same manner as the cleavage site of BB (Dong et al., 2017). This would involve narrowing down the 10-amino acid sequence to a smaller deletion, and confirming this by substituting amino acids for glycines, and producing “always cleaved” and “never-cleaved” versions (based on

mutations at the known cleavage site) for genetic analyses of the role of DA1 mediated substrate cleavage.

The biological function of DA1 and DA1-mediated cleavage remains unknown. DA1 is a negative regulator of growth, with the *da1-1* negative interfering allele exhibiting an enlarged final organ size compared to wild type (Li et al., 2008). Based on the *DA1* phenotype of reduced organ growth, if the function of DA1 cleavage is only to render substrates unstable and target them for degradation, then it would be expected that DA1 would only cleave substrates that are positive regulators of organ growth, such as *UBP15* (Liu et al., 2008), inhibiting their growth-promoting activity. However, DA1 is known to cleave both growth promoters and growth inhibitors, including members of both classes of the TCP family which act antagonistically to finely control organ size (Aguilar-Martinez and Sinha, 2013). In addition, *TCP15* has a tissue-dependent effect on organ growth, and can act as either a promoter or inhibitor of growth (Kieffer et al., 2011; Li et al., 2012; Uberti-Manassero et al., 2012). Together, these variable effects on growth by known DA1 substrates indicate that simple inactivation or degradation is not the sole function of DA1-mediated cleavage.

A number of other potential roles for DA1-mediated cleavage are possible. For example, proteolytic processing is known to have a role in mitochondrial translation whereby the *m*-AAA protease initiates proteolysis of MrpL32, a subunit of the mitochondrial ribosome (Bonn et al., 2011; Anand et al., 2013). In the absence of cleavage by *m*-AAA, MrpL32 is unable to assemble into mitochondrial ribosomes. Proteolytic processing can also be required for signalling, for example signal transducer and activator of transcription (STAT) proteins in animals. STAT proteins have a role in the regulation of cell proliferation, and are therefore of interest in cancer research (Hendry and John, 2004). Cleavage of STAT proteins removes their transactivation domain and changes their biological activity, as they become functionally dominant-negative signalling proteins. These alternative functions of protein cleavage in altering the biological properties or functions of the cleaved substrate provide alternate means for DA1 to affect organ growth, aside from degradation via the N-end rule pathway. This may explain why the DA1 peptidase is able to cleave substrates that both promote and inhibit organ growth. The development of transgenic plants expressing “always cleaved” and “never cleaved” versions of known DA1 substrates would provide further insights into the biological context of DA1-mediated cleavage.

2.4.1 Summary

In summary, evidence presented in this Chapter has not been able to show that any further of the putative physical interactors of DA1 (as shown by Dr Jack Dumenil) are subject to

cleavage by DA1, neither does the evidence show that any further members of the TCP family are targets for DA1-mediated cleavage. However, this does not mean that other proteins detailed in Table 2.1, or other members of the TCP family, could not in the future be found to be substrates of DA1. Additionally, while data presented in this Chapter do not present a putative conserved target site, the approach taken in this Chapter and others as described above would, in the future, allow for further work to identify one.

3 QUANTITATIVE ANALYSES OF *DA1* AND *BB* FUNCTION IN LEAF GROWTH

3.1 Introduction

The large organ phenotype of *da1-1* mutants is exhibited in almost all organs of Arabidopsis, including the seed. Whole plant seed weight is increased by approximately 17% in the *da1-1* mutant relative to wild type, and individual seeds are on average 55% larger (Li et al., 2008). The *DA1* system therefore presents a potential avenue for exploration in the search for increased crop yields. Wheat and rice orthologues of the E3 ligase *DA2* described in Chapter 1 have been found to limit grain size (Song et al., 2007; Simmonds et al., 2016), a phenotype that is reflected in Arabidopsis, where the *da2-1* mutant exhibits seeds that are larger and heavier than wild type (Xia et al., 2013). In addition, a recent study by Brinton et al. 2018 found differential regulation of genes involved in the ubiquitin-mediated degradation pathway in wheat near isogenic lines (NILs) known to have increased grain size (Brinton et al., 2017; Brinton et al., 2018). The seed size increase in Arabidopsis exhibited in *da1-1* mutants is larger than that of *da2-1* mutants, at 136% of wild type and 107% of wild type, respectively (Xia et al., 2013). Overexpression of *AtDA1*^{R358K} has also recently been shown to increase seed weight and size in *Brassica napus* (Wang et al., 2017), and in the *Zea mays* elite line DH4866, over-expression of *Zmda1* (using the same single nucleotide polymorphism as the *Arabidopsis thaliana da1-1* or *R358K* mutant) and *Zmdar1* resulted in increased ear length, kernel number and weight (Xie et al., 2017). Taken together, these findings suggest that the *DA1* growth regulatory system could be a significant opportunity for yield increase in important food and biofuel crops.

In this thesis, the phenotyping work is carried out not in seeds, but in leaves. Leaves are an ideal system in which to study organ growth, due to their high tractability, larger overall size, and the possibility of analysing growth for the complete organ at a cellular level using confocal and scanning electron microscopy. In addition, leaves permit the tracking of growth and development including even the earliest developmental stages, which would be much more complex in seed development, as this organ is hidden in a gynoecium. The effects of mutations in *DA1*, *BB* and *DA2* on seed size are largely reflected in the leaf phenotype, making leaves an ideal opportunity to study the effects of mutations in these genes of organ growth at the cellular level. In addition, in some food crops such as members of the Brassica family, the vegetative tissues rather than the seeds are the parts of the plant that are harvested as food, such as in cultivars of the *Brassica oleracea* species including kale,

cabbage and Brussels sprouts. In these species, enhancing leaf growth would increase the useful yield. Therefore, it is relevant and beneficial to undertake these studies in leaves rather than seeds.

3.1.1 Leaf growth

The growth and development of Arabidopsis leaves is well documented in the literature and has been described in detail in Chapter 1. The initiation of a leaf primordium from the shoot apical meristem is promoted by local auxin maxima (Reinhardt et al., 2000; Reinhardt et al., 2003). The developing primordia becomes an auxin sink, which in turn initiates auxin concentration heterogeneity within the shoot apical meristem, allowing the initiation of further primordia (Reinhardt et al., 2003).

The first phase of leaf growth is driven by cell proliferation. The number of cells produced during this proliferative period is a critical determinant of final organ size (Czesnick and Lenhard, 2015). The arrest of cell proliferation is thought to be controlled by the movement of a putative arrest front from the tip to the base of the leaf (Nath et al., 2003). Studies have shown that the frontier of the wave of proliferation arrest moves through the leaf and remains at a constant distance from the base of the leaf for some time, before the abrupt arrest of proliferation in all cells and the collapse of the proliferation zone (Kazama et al., 2010; Andriankaja et al., 2012). This arrest of proliferation is finely controlled by networks of genes and phytohormonal signalling promoting and inhibiting cell division, as reviewed in Andriankaja et al. 2012, among which *DA1* and *BIG BROTHER (BB)* have been proposed to play a role.

Subsequent cell growth is controlled by both phytohormones and genetic factors, and is driven by increases in cytoplasmic mass of the cell, and the loosening of the cell wall (Czesnick and Lenhard, 2015). Another feature that has been associated with cell growth is endoreduplication, whereby DNA replication occurs in the absence of mitosis, and the ploidy levels of the cell increase. Higher cell ploidy levels in shoot tissues of Arabidopsis is thought to result in larger cells, contributing to overall organ growth (Perrot-Rechenmann, 2010).

The stomatal lineage in leaves is formed from meristemoid cells that require the activity of three closely-related basic helix-loop-helix (bHLH) protein genes - *SPEECHLESS*, *MUTE* and *FAMA* - to differentiate their fate from those of a normal epidermal pavement cell (Ohashi-Ito and Bergmann, 2006; MacAlister et al., 2007; Pillitteri et al., 2007). Proliferation of these meristemoid cells persists for longer than pavement cells, and is arrested in a further,

secondary wave of proliferation arrest (Czesnick and Lenhard, 2015), when stomatal differentiation is completed.

Overall final organ size therefore emerges from a combination of the extent of cell proliferation and the final sizes of cells. A central question in the study of growth is how each of these cellular activities contribute to the final characteristic sizes of determinate organs.

There are three possible primary mechanisms in leaf growth that could control how the correct final size is achieved. The first mechanism is the control of the number of cell divisions that occur during the cell proliferation phase of growth. Changes to this could be as a result of a shortened or lengthened cell cycle and the resulting increase or decrease in the rate of cell proliferation, or by the changes in the spatial or temporal control of the division zone, for example changes that increase the duration of cell proliferation during leaf growth. The second mechanism is the control of the rate of cell growth during organ development. The third mechanism is the control of the duration of the cell growth phase, leading to larger cells. Together, modulation of these three aspects of leaf growth regulates the final organ size that is reached.

It has previously been shown that *DA1* has a role in the limitation of cell proliferation and hence final organ size (Li et al., 2008), and we have proposed that *DA1* could contribute to determining the duration of cell proliferation by cleaving proteins that directly promote cell proliferation such as TCP transcription factors and the de-ubiquitinase UBP15 (Dong et al., 2017). The peptidase activity of *DA1* is explored in more detail in Chapters 1 and 2. This positions *DA1* as a possible regulator of the first of the three mechanisms – control of the duration of cell division during leaf growth – and precisely how *DA1* and *BB* regulate cell division or any other mechanism for leaf growth is a key question for this thesis.

3.1.2 The *DA1* regulatory system in the control of whole organ size

3.1.2.1 *DA1*

The *da1-1* mutation was identified in a genetic screen by Li et al. in 2008. This initial study showed that the *da1-1* mutation promoted an increased final organ size relative to wild type (Li et al., 2008). Average seed weight is increased by approximately 30%, and the whole plant seed weight is also increased by approximately 16%. Mutant plants also exhibit enlarged cotyledons, petals and siliques than wild type, and leaves were larger and rounder. In addition, kinematic analysis showed that petals and leaves grow for longer and reached a larger final size, with leaves also growing at an increased rate (Li et al., 2008). A later study

by Vanhaeren et al., 2017 found that overexpression of the *da1-1* allele in 17 diverse accessions of *Arabidopsis thaliana* showed an increased leaf area, indicating that the function of DA1 is conserved across a range of genetic backgrounds in *Arabidopsis* (Vanhaeren et al., 2017). The increase in seed size observed in *da1-1* mutants of *Arabidopsis thaliana* is also reflected in *Brassica napus* and *Zea mays*. In *Brassica napus*, over-expression of AtDA1^{R358K} promotes increased seed weight and size, and total yield per plant (Wang et al., 2017), and in *Zea mays*, over-expression of *Zmda1*, an allele containing the same single nucleotide polymorphism as *Atda1-1*, promotes increased kernel size and number, total yield per plant, and increased starch content (Xie et al., 2017), indicating that the effects of the DA1 mechanism are conserved both within *Arabidopsis* and between *Arabidopsis* and several crop species. In wheat, a TILLING mutant influencing thousand grain weight (TGW) was shown to be due to a mis-splicing allele of *TaGW2-A1* (Simmonds et al., 2016). This gene encodes an ortholog of the *Arabidopsis* E3 ubiquitin ligase DA2, which ubiquitylates DA1 (Xia et al., 2013). The allele increases TGW by 6.6%. However, overall wheat yields were not significantly increased in this case. This observation emphasises the need to consider two main developmental components of yield, namely seed size and seed yield, in research aimed at increasing seed yields in crop species. In some cases there is an inverse relationship between seed size and seed number which has been explained at a physiological level by limiting resource availability. Recently, strategies for increasing rice grain yields and quality have pyramided multiple alleles affecting grain size and grain number to increase overall yields (Zeng et al., 2017).

3.1.2.2 BIG BROTHER

Disch et al., 2006 characterised the *bb-1* and *bb-2* mutant alleles of *BB* and described their phenotypes. The *bb-2* knockdown mutant is allelic to the *eod1-2* (*enhancer of da1-1*) allele identified in the modifier screen carried out by Li et al., 2008 and is a T-DNA insertion line, whereas the *bb-1* allele is a chromosomal reorganisation knockout mutant, resulting in the deletion of *BB* and two neighbouring genes. The *bb-1* mutant phenotype can be completely rescued by transformation with a wild type copy of *BB*, indicating that the phenotype is caused by the deletion of *BB* and not the neighbouring genes (Disch et al. 2006). It was found that *bb-1* mutants exhibited increased petal and sepal size relative to wild type, while the *bb-2* mutant showed an intermediate phenotype. Kinematic analysis of petal growth showed that *bb-1* petals grew for longer, yet at the same rate as wild type, reaching an increased final size. *BB* over-expressor lines tested by Disch et al. showed strongly reduced leaf areas. Leaf area was not affected in *bb-1* or *bb-2* mutants, although leaf shape was altered,

generating wider yet shorter leaves (Disch et al., 2006). Studies in roots have shown that *bb-2* mutants have slightly increased primary root length (Cattaneo and Hardtke, 2017).

Together, these analyses indicate that *BB* acts to limit organ size in leaves, petals and roots, by limiting the duration of growth. In addition to this, there may be a role for *BB* in the control of leaf shape, as evidenced by the wider, shorter leaves exhibited by *bb-1* and *bb-2* mutants.

3.1.3 The DA1 regulatory system in the control of cellular phenotypes

3.1.3.1 *DA1*

3.1.3.1.1 Cell number

The 2008 study by Li et al. found that epidermal cell numbers in stem cross-sections were increased by approximately 80% in *da1-1* plants relative to wild type. In addition, they also observed increased levels of *pCYCB1;1::GUS*, a marker of cell proliferation activity, in *da1-1* mutant leaves compared to wild type at nine days after germination. Furthermore, the mitotic index, or the proportion of cells in a population undergoing mitosis, in *da1-1* mutant petals remained higher for longer (Li et al., 2008). Building on these findings, Vanhaeren et al., 2017 found that plants with the *da1-1* mutation (including *da1-1bb-2* plants) also exhibited an increased number of cells per leaf relative to wild type at 7 days after stratification (Vanhaeren et al., 2017).

In addition, the same study found that plants over-expressing *DA1* under the constitutive *35S* promoter exhibit reduced cell numbers in comparison to wild type in mature leaves (Vanhaeren et al., 2017).

These observations provide evidence for a role for *DA1* in limiting cell numbers in the leaf, at least in part by limiting the duration of cell proliferation. The evidence for increased cell number at 7 days after stratification also raises the possibility that there is another, separate process controlled by *DA1* to limit cell number. At 7 days after stratification few to none of the cells in the leaf have exited the proliferative phase (Vanhaeren et al., 2017), and so the explanation for increased cell number at this early stage cannot be an increased duration of proliferation. Possible mechanisms for increased cell number at such early stages could include an increased rate of early cell proliferation, or a larger leaf primordium resulting in a larger meristematic zone in the leaf.

3.1.3.1.2 Cell size

Li et al., 2008 found that there was no significant difference in cell area between wild type and *da1-1* plants in either embryos, petals or leaves at final size (Li et al., 2008). During leaf

development between 10 and 12 days after stratification, *da1-1* and *da1-1bb-2* lines exhibited smaller pavement cells than the wild type. By 13 days after stratification, there was no statistically significant difference in cell area between wild type and the double mutant (Vanhaeren et al., 2017). The same study found that the overexpression of *DA1* does not promote increased pavement cell areas in mature leaves (Vanhaeren et al., 2017).

These data suggest that *DA1* does not have a role in the control of cell area. The reduced cell areas observed in *da1-1* and *da1-1bb-2* leaves during leaf development may be due to the extended period of cell proliferation in the *da1-1* mutant. If cells remain in the proliferative phase for longer in *da1-1* and *da1-1bb* mutants, it is more likely than in wild type plants that the population of cells measured for these analyses would include cells that had only recently exited the proliferative phase. These cells would therefore have been in the expansion phase of growth for less time than cells in the wild type plant, leading to a reduced cell size in *da1-1* and *da1-1bb* relative to wild type. There is no indication that the duration of cell expansion and endoreduplication is limited in *da1-1* or *da1-1bb* mutants, as this phase would not be complete while the leaf is still growing.

3.1.3.2 *BIG BROTHER*

3.1.3.2.1 Cell number

Although cell number was not directly measured by Disch et al., their study found that the mitotic index remained higher for longer throughout development in *bb-1* petals than in wild type petals, indicating that more cells in the petal are proliferating for longer, resulting in increased cell numbers (Disch et al., 2006). Observations in roots support these findings, where a *bb* loss-of-function mutant displayed increased meristematic cell number (Cattaneo and Hardtke, 2017).

The Vanhaeren et al. study found that there was no increase in cell number in plants with the *bb-2* mutation alone (as opposed to in conjunction with *da1-1*) at 7 days after stratification. However, plants over-expressing *BB* under the constitutive *35S* promoter exhibited reduced cell number in comparison to wild type at 21 days after stratification (Vanhaeren et al., 2017).

These observations suggest that *BB* may act to limit final cell number by limiting the duration of proliferation. The observation that there was no increase in cell number in *bb-2* at 7 days after stratification means that *BB* does not appear to control early cell numbers like *DA1*, reinforcing the conclusion that *bb* mutants have more cells due to an increase in the duration of cell proliferation.

3.1.3.2.2 Cell area

Despite having no more cells than the wild type plant at 7 days after stratification, the *bb-2* mutant has a larger leaf phenotype. This can be explained by the observation that plants with the *bb-2* mutation (including *da1-1bb-2*) had an increased cell size relative to wild type. However, during later leaf development, plants with only the *bb-2* mutation did not have a cell area significantly different from that of wild type plants (Vanhaeren et al., 2017). This is supported by the findings of Cattaneo et al., whereby a loss-of-function mutation in *bb* did not cause a change in root mature cell length (Cattaneo and Hardtke, 2017). Conversely, Disch et al. found that cell area is only slightly influenced by knockdown or knockout mutations in *BB*, and in over-expressor lines - with the exception of one over-expressor line in which *BB* expression was 5.9 times more than in the wild type, where leaf and petal cell area were reduced to 40% and 80% of wild type respectively (Disch et al. 2006). Conversely, *BB* over-expressor plants were found to exhibit larger pavement cells in the mature leaf by Vanhaeren et al.

The evidence on the effect of *BB* on cell area is somewhat contradictory. On one hand, it seems that *BB* may have an early effect of limiting cell area in leaves. On the other, *BB* may promote either larger or smaller cells in the mature leaf and petal. Disch et al. observed that, while one of the over-expressor lines they observed did exhibit smaller cells than wild type in leaves and petals, this could be as a result of the interplay between cell growth and cell division. Cells normally grow to a specific size before they are competent to divide (Johnston et al., 1977; Kellogg, 2003), and it may be that the activity of *BB* in this over-expressor line was primarily to repress cell growth, which indirectly inhibits cell division (Disch et al., 2006). This provides a potential mechanistic framework for the activity of *BB* in the limitation of organ size.

These analyses of cellular growth provide convincing evidence for the role of *DA1* and *BB* in the control of cell number via the duration of cell proliferation, and some further evidence for a role for *BB* in the control of cell area. There is also evidence that *DA1* and *BB* have some other, separable, effects on organ size at very early stages, although the mechanisms for this have not yet been defined.

Although no direct studies were made on the presence or absence of a compensation mechanism, as described in Chapter 1, the lack of a significant reduction in cell size in *da1-1* mutants suggests that there is no compensation mechanism involved in the *da1-1* phenotype. The evidence surrounding a compensation mechanism in *BB* mutants is less

clear, with conflicting observations - although these observations have been made in different organs of the plant, and there may be a tissue-specific aspect to *BB* activity.

3.1.4 Advances in plant phenotyping

This thesis is one of the first studies to segment and computationally analyse all the cells within a leaf. Whole-organ cellular analyses have previously been carried out in roots (Di Mambro et al., 2017), however to date most studies in leaves have been limited to a small area of cells within the leaf, such as in Vanhaeren et al. 2017. In contrast, Andriankaja et al. 2012 measured a significant proportion of cells in the leaf blade of a wild type plant by segmenting by hand and analysing. In this thesis, we have been able to quantitatively extend this type of analysis by using a semi-automated cell segmentation tool (as described in Section 3.2.6.2) to analyse all accurately measurable cells in the leaf, or of one leaf blade, and by comparing the effects of mutations thought to control aspects of cell proliferation and expansion.

The approach taken by Vanhaeren et al. 2017 and others measures only the cells in the tip of the developing leaf, therefore it does not record information such as the distribution of cell sizes and densities across the whole leaf. In order to determine the differences in the growth pattern of mutants in cell proliferation and expansion such as *da1-1* and *bb* compared to wild type, it is important to consider the proportion of the cells in the leaf that have the competence to divide compared to those that have lost the competence to divide and are committed to cell growth and differentiation. Without an integrated view of all observable cells in an organ during growth it is not possible to attribute an observation of reduced cell area in the tip of the developing leaf, for example, to either a true effect for the gene in question on cell area, or that simply the cell in question has more recently exited the proliferative phase and is smaller due to having had a shorter time to undergo cell expansion at that time. The ability to analyse the distribution of cell attributes such as area, circularity and relative density throughout the length and breadth of the leaf is important to understand how growth patterns may vary between genotypes, and this is not something that can be accomplished using only cell measurements from small sections in the tip of the leaf.

There is a variety of automated and semi-automated phenotyping software available for whole plants, whole organs, and within those organs also at the cellular level. Many of these software packages are detailed on the Plant Image Analysis website (Lobet et al., 2013).

3.1.4.1 Whole plant phenotyping

Quantification of the plant rosette of leaves can bring new insights into aspects of plant growth and development such as phyllotaxy, petiole length and rosette area. Examples of the software currently developed for this purpose include rosettR (Tomé et al., 2017), Rosette Tracker (De Vylder et al., 2012), Phentyping^{4D} (Apelt et al., 2015) and PhenoPhyte (Green et al., 2012). Some of these packages include the additional ability to track a time-course at macroscopic growth scales in the rosette.

3.1.4.2 Whole organ phenotyping

Automated and semi-automated analysis of a whole leaf is useful because it can be high throughput, and may generate more data than simple measurements of leaf width, length and area, for example an overall shape parameter, or serration phenotypes. Examples of the software currently developed for this purpose include Leaver (Borianne and Brunel, 2012), LeafAnalyser (Weight et al., 2008), LeafProcessor (Backhaus et al., 2010), LAMINA (Bylesjö et al., 2008) and Easy Leaf Area (Easlon and Bloom, 2014). In this thesis, I did not use automated software to analyse leaf length, width and area. This is because many of the software packages above are designed for use with flat leaves, which would be characteristic of *Arabidopsis* plants grown on soil, as seen in Figure 3.1.

However, leaves of *Arabidopsis* grown on plates such as I used in my experiments are differently shaped, and tend to be curved at later stages. This necessitates cutting of the leaf boundaries in order to flatten the leaf, which could distort measurements such as shape. In addition, folded areas of the leaf can be taken into account using manual measurements, which would not be possible using automated measurement. The plants in these experiments were grown on media, rather than on soil, in order to ensure consistency between the chapters of this thesis - in Chapter 4, where live cell imaging was used, growing plants on media was necessary to maintain sterile conditions. As a result of these growth conditions and the physiology of the leaves, I carried out my leaf measurements using ImageJ, as described in Section 3.2.5.1.

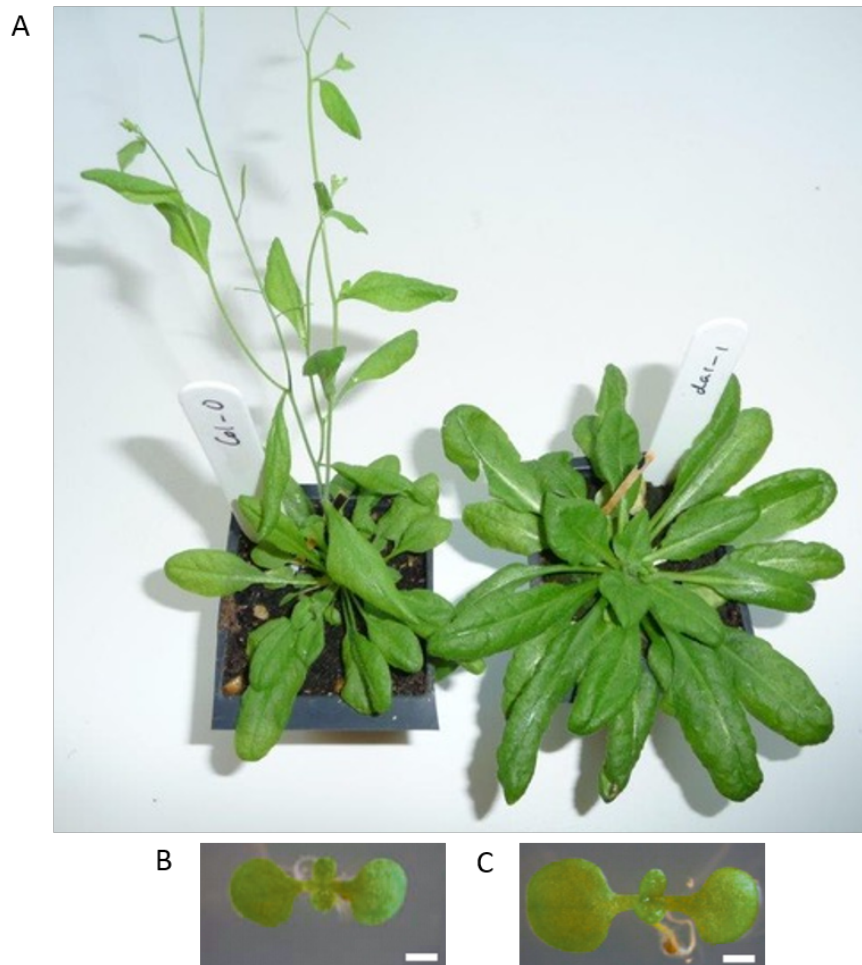


Figure 3.1 Comparison of wild type and *da1-1* plants grown on soil and on media

(A) Wild type (left) and *da1-1* (right) plants grown on soil, aged 6 weeks. Photograph by Caroline Smith. (B) and (C) show wild type and *da1-1* seedlings respectively, grown on media at 9 days after stratification (scale bars 1mm, adapted from Li et al., 2008 with permission).

3.1.4.3 Cellular analysis

The two primary semi-automated software packages available for cellular image analysis are MorphoGraphX (Barbier de Reuille et al., 2015) and LithoGraphX (Barbier de Reuille et al., 2015; Barbier de Reuille et al., 2015), both originating from the same lead developer, where LithoGraphX is a derivative of the MorphoGraphX project. These software packages are very powerful and designed for analysing 3D structures such as shoot apical meristems and developing embryos (Bassel et al., 2014; Shapiro et al., 2015). In addition to this, a recent paper by Möller et al. describes a novel tool for cell segmentation specifically designed for plant epidermal pavement cells (Möller et al., 2017), developed as a plugin for the widely distributed ImageJ image analysis package. PaCeQuant is designed specifically for segmenting epidermal pavement cells, with their highly complex shapes. LithoGraphX and

MorphographX have only to date been used successfully on tissues where cells are of regular shapes, for example the cuboid cells found in root cell files or in embryos. PaCeQuant is designed to segment and interpret the complex shapes of epidermal pavement cells. However, it is only able to segment small patches of cells, rather than cells across a whole leaf, as is the aim for this project. For this reason, a collaboration was formed to develop a new software package that could fulfil all the requirements for this project.

3.1.5 Aims for this Chapter

This Chapter describes quantitatively the growth of the *da1-1*, *bb*, and *da1-1bb* mutants, by phenotyping them at two levels. At the whole organ level, I measured leaf width, length and area over time. By comparing these data to the wild type growth trajectory, I aimed to establish quantitative growth parameters of the duration and rate of growth, particularly in the *bb* and *da1-1bb* mutants where this has not yet been studied. At the cellular level, by segmenting and analysing almost all pavement and stomatal cells in the leaves through time, I aimed to understand at the cellular level in growing leaves how the *DA1* regulatory system influences growth and determines final organ sizes.

This Chapter aims to answer the following questions:

- Is there more to be learnt about the growth trajectory or mature phenotype of *da1-1*, *bb* and *da1-1bb* leaves, at the whole organ level?
- How do the cellular phenotypes of *da1-1*, *bb* and *da1-1bb* leaves differ from wild type, throughout growth?
- How is the increased mature leaf area observed in *da1-1*, *bb* and *da1-1bb* relative to wild type achieved? Is this as a result of increased cell area, or increased cell number?

3.2 Materials and Methods

3.2.1 Plants used in this Chapter

<i>Arabidopsis thaliana</i> line	T-DNA/mutation
Col-0	n/a
<i>da1-1</i>	SNP mutant (Li et al., 2008)
<i>bb</i>	SALK_045169
<i>da1-1bb</i>	Formed by crossing of above (Li et al., 2008)

Table 3.1 Plant lines used in Chapter 3

3.2.2 Transformation of *Agrobacterium tumefaciens*

The *pAtML1::mCitrine-RC12A* plasmid was kindly provided by Dr Emily Abrash at Stanford University, with the permission of Dr Adrienne Roeder at Cornell University (Roeder et al., 2010). In this construct, the mCitrine fluorescent protein is fused to RC12A, localised in the plasma membrane, and is expressed under the AtML1 promoter, restricting expression to the epidermal cell layer only. This restriction of mCitrine expression to the epidermal cell layer reduces the confounding effects of sub-epidermal fluorescence and makes images easier to segment.

This plasmid was used to transform *Agrobacterium tumefaciens* (GV3101). 2µl of plasmid DNA was mixed with 50µl of cells thawed on ice, and carefully pipetted into a chilled electroporation cuvette (Bio-Rad. Cat. No. 165-2089), avoiding the formation of bubbles. This was placed in the electroporation machine (MicroPulser Electroporator. Bio-Rad. Cat. No. 165-2100), and electrocuted using the following settings: pulse controller 400 ohms, voltage 1.8kV, capacitance 25mF. Cells were removed from the cuvette using 1ml SOC medium into a 1.5ml tube, and incubated with shaking for one hour at 28°C. 20µl of cells were spread on LB agar plates with the appropriate antibiotics (rifampicin 25µg.ml⁻¹, gentamycin 5µg.ml⁻¹ and spectinomycin 25µg.ml⁻¹, all from Sigma-Aldrich) and the remainder spun down and plated separately. The plates were incubated for two days at 28°C.

3.2.3 *Arabidopsis thaliana* transformation

3.2.3.1 *Arabidopsis thaliana* floral dip

Arabidopsis thaliana plants were transformed using the floral dip method (Clough and Bent, 1998). *Agrobacterium tumefaciens* cells transformed with the appropriate plasmid were incubated in 500ml LB solution with the appropriate antibiotics (rifampicin 25µg.ml⁻¹, gentamycin 5µg.ml⁻¹ and spectinomycin 25µg.ml⁻¹, all from Sigma-Aldrich) at 28°C for 48 hours. The cells were spun down in a centrifuge and a solution of 5% sucrose (w/v) (Melford.

Cat. No. S0809), 0.25% v/w MS salts (Sigma-Aldrich. Cat. No. M5534) and 0.05% MES (Sigma-Aldrich. Cat. No. M0164) with 0.05% (v/v) Silwet L-77 (Fisher Scientific. Cat. No. NC0138454) was used to re-suspend them to an OD₆₀₀ of 0.80. T0 Arabidopsis plants were grown with 20 individuals per pot in order to maximise the number of potential transformants. When the plants reached flowering age, any siliques that had already formed were removed to reduce the number of non-transformants. The *Agrobacterium* suspension was put into a beaker and the pots of Arabidopsis inverted into it and agitated for 30 seconds. The dipped plants were covered with clear plastic for 24 hours in order to retain high humidity levels and increase the rate of transformation. This process was repeated with the same plants three days later in order to increase the rate of transformation. Plants were bagged following silique formation, harvested when dry, and hand-threshed.

3.2.3.2 Selection of transformants

Seeds from T0 plants were screened using BASTA (Sigma-Aldrich. Cat. No. 45520) selection to identify T1 individuals. Seeds were spread over seed trays and stratified for three nights at 4°C, before being placed in the glasshouse to germinate. Propagator lids were removed once seedlings were large enough. Seedlings were sprayed once per week for three weeks with BASTA solution. Leaf tissue was sampled from T1 survivors and sent to iDna Genetics (<http://www.idnagenetics.com>) for copy number analysis. iDna Genetics used quantitative real time PCR to estimate the numbers of transgene copies in individual plants, similar to an approach previously taken in barley (Bartlett et al., 2008).

Individuals with one T-DNA insertion were transplanted and self-fertilised to generate T2 seeds. T2 individuals were sown in 24-pot trays and stratified as above. Samples were sent to iDna Genetics for copy number analysis, and individuals with two insertions of the BASTA resistance gene (indicating a single copy, homozygous genotype) were bagged and harvested as described above. For each genotype, 2-5 independent single copy, homozygous transformants were identified. Of these, the line with the brightest fluorescence was selected for use in these experiments.

3.2.4 Plant growth conditions

3.2.4.1 Glasshouse

All soil-grown Arabidopsis plants were grown on compost composing of eight parts peat-based compost (Levington F2 soil, N150:P200: K200mg/L, pH=5.3-5.7) and one part grit.

For plants to undergo the floral dip, 20 seeds were sown into FP9 pots and stratified for three nights at 4°C, before being moved to glass-house conditions (16h light / 8h dark cycle supplemented with 120 $\mu\text{mol m}^{-2} \text{s}^{-1}$ fluorescent lighting, 21-23°C day, 16°C night).

For the identification of T1 transformants by BASTA selection, seeds were sown into seed trays and stratified for three nights at 4°C, before being moved to glass-house conditions (16h light / 8h dark cycle supplemented with 120 $\mu\text{mol m}^{-2} \text{s}^{-1}$ fluorescent lighting, 21-23°C day, 16°C night). Single copy, homozygous transformants were individually transplanted to cells of a P24 tray to mature and be bagged and harvested.

3.2.4.2 *Controlled Environment Room*

Threshed seed was sterilised by shaking in a 1.5ml tube containing 1ml sterilisation solution (50% (v/v) ethanol and 0.625% (w/v) dichloroisocyanuric acid (Sigma-Aldrich. Cat. No. 35915) for 20 minutes. The sterilisation solution was immediately removed and the seeds washed three times with 1ml 100% ethanol. Seeds were left to dry in a laminar flow hood on sterile filter paper. When dry, 5 seeds per plate were sown evenly spaced onto plates with 25ml GM agar (0.43% (w/v) Murashige and Skoog, 1% (w/v) sucrose, 0.01% (w/v) inositol, 10ppm (w/v) thiamine, 50ppm (w/v) pyridoxine, 50ppm (w/v) nicotinic acid, 0.05% (w/v) MES, 9% (w/v) agar, pH 5.7). The plates were sealed with micropore tape (3M. Cat. No. 1530-0) and the seeds stratified for 3 nights at 4°C before being moved to a Controlled Environment Room (20°C, 16 hours light, 8 hours dark).

3.2.5 Plant imaging

3.2.5.1 *Light microscopy*

For the whole-organ phenotyping and growth curve measurements, leaf 1 was dissected from each plant using forceps (Dumont #5) and placed on a microscope slide (VWR. Cat. No. 631-0110) in a droplet of water, with the abaxial side facing upwards. A coverslip (BDH. Cat. No. 405/0187/35) was placed on top. At later stages, when leaves were too large or curled to lie flat, a razor blade (GEM. Cat. No. 62-0178) was used to cut the leaf margin to allow the leaf to lie flat, and double-sided tape was used to secure the leaf to the slide. Eight to ten plants were sampled every two days from each genotype, from five days after stratification to 35 days.

Leaves were imaged in bright field using a Leica M205FA microscope fitted with a Leica DFC310FX colour camera, controlled using the Leica LAS AF software. The same microscope was also used for leaf dissection at early stages.

3.2.5.2 *Confocal microscopy*

For the cellular imaging, leaf 1 was dissected from each plant using forceps (Dumont #5) and placed on a microscope slide in a droplet of water, with the abaxial side facing upwards. A coverslip was placed on top. At later stages, when leaves were too large or curled to lie flat, a razor blade was used to cut the leaf margin to allow the leaf to lie flat, and double-sided tape was used to secure the leaf to the slide. Five plants were sampled every day from each genotype, from seven days after stratification to eleven days after stratification.

Leaves were imaged using either a Leica SP5 (II) or a Leica TCS SP8X confocal scan head mounted on a Leica DM6000 microscope, controlled using the Leica LAS AF software. A 20x air objective was used on both microscopes. The argon laser excitation was set to 514nm, and the fluorescence emission was collected in the 520-600nm range using a HyD detector.

3.2.5.3 *Scanning electron microscopy*

The scanning electron microscopy sample preparation and image collection was carried out by Kim Findlay, Head of Bioimaging at the John Innes Centre.

3.2.5.3.1 **Sample preparation**

For the SEM imaging, leaf 1 was dissected from each plant using forceps (Dumont #5). The leaf was frozen in a liquid nitrogen slush and sputter coated with platinum metal to a thickness of 15nm to prevent charging in the microscope and increase the signal to noise ratio.

3.2.5.3.2 **Imaging**

The leaves were imaged at 33 days after stratification using the FEI NovaNano450 scanning electron microscope, at a voltage of 3kV. A patch of cells was imaged at the tip, middle and base of the leaf blade for each leaf. Eight to 11 plants were sampled from each genotype.

3.2.6 **Image analysis**

3.2.6.1 *Light microscopy*

Leaf blade width, length and area were measured manually using the FIJI software package based on ImageJ 1.50d (Rasband, 1997-2016).

All numerical data were analysed in R 3.3.3 (www.r-project.org).

3.2.6.2 *Confocal microscopy*

The fluorescent images generated in this Chapter were analysed using the Leaf Analysis Toolkit software developed by Dr Ross Carter, Dr Athanasuis Marée, and Dr Veronica

Grieneisen. The combination of an epidermal specific fluorescent marker line in the leaves and the flattening effect of a Gaussian projection meant that we were able to segment flattened leaf images in 2D and extract specific parameters that were required for subsequent analyses. The Leaf Analysis Toolkit software used here is available by contacting Dr Ross Carter, and is stored at www.github.com/rosscarter3/leaf_analysis_toolkit, commit a61c6a50c51f9f0fb35114278bf94adde1b04b53. These scripts will be made public upon publication of these data. A version of this software has been used in a recently published study (Carter et al., 2017).

The analysis was carried out on a 2016 Apple Macbook Pro.

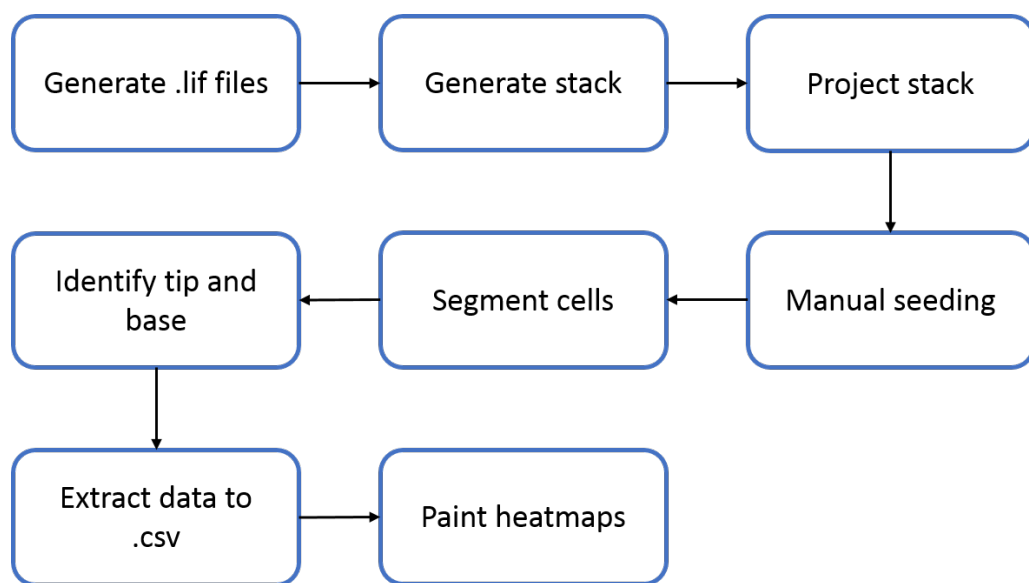


Figure 3.2 Leaf Analysis Toolkit pipeline

3.2.6.2.1 Generation of .lif files

The first step of the pipeline was the generation of the .lif files produced by the confocal microscope. Each .lif file includes several images, each made up of a number of Z-slices due to the natural curvature of the leaf, even when flattened on a microscope slide.

3.2.6.2.2 Generation of image stacks

The stacks were generated using the “lif2stack.py” script. This extracted the images from the .lif file, and created a separate directory for each one. Within each directory, there was a folder containing the Z-slices extracted as individual .png files, as well as a “dims.txt” file containing the image metadata (dimensions, number of Z-slices, and voxel (3D pixel) size).

3.2.6.2.3 Generation of projections

Projections were generated from the stacks using the “stack2proj.py” script. This generated three .png files in the image directory, as shown in Figure 3.3. Projections convert the 3D stack of Z-slices to a 2D image that can be segmented. The maximum Z projection of the stack projects the voxels (3D pixels) of maximum intensity in each location. This generates a bright image, but one which might include a significant amount of noise distracting from the abaxial epidermis of the leaf - for example bleed-through into mesophyll cells, or even the adaxial epidermis if the tissue is very thin. The surface projection of the stack projects the uppermost surface of the leaf, by using a “Gaussian projection”, a method developed by Dr Matthew Hartley (Scientific Computing, John Innes Centre). The Gaussian projection aims to reduce the effect of the previously described noise in the image from mesophyll cells or the adaxial epidermis, by identifying the upper surface (abaxial epidermis) of the sample. The image is blurred in 3D and the Z-index with the greatest signal closest to the top of the stack is identified, which is the upper surface of the sample. A surface is created from this Z-index by blurring in the X-Y directions. This projection is used to inform the other two projections. The G3D projection is generated by performing a maximum Z projection only in a small Z-section around the surface projected in the Gaussian projection. This generates a high-quality image where there is little to no noise from other cell layers. This is the projection that is used for segmentation.

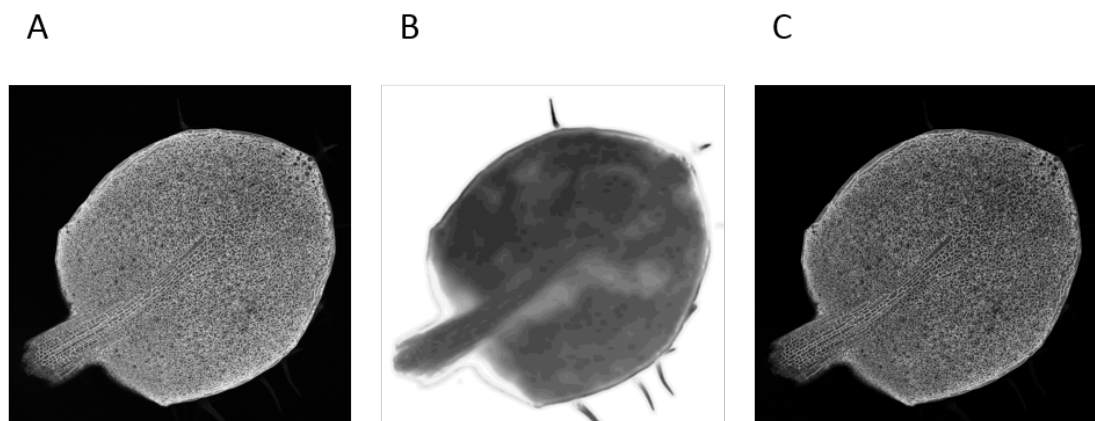


Figure 3.3 Projections generated by Leaf Analysis Toolkit

Maximum Z projection (A), surface projection (B), and G3D projection (C).

3.2.6.2.4 Manual seeding

Manual seeding was carried out using GIMP 2.8.16. A single red point was placed in each cell of the leaf. This manual seeding allows Leaf Analysis Toolkit to identify each cell, and it is

subsequently able to define cell outlines by watershedding. I was assisted in this work by Josie Lett, Heppy Robb and Jayden Endean.

3.2.6.2.5 Segmentation

Segmentation was carried out using the “ws_segment_from_dir.py” script. This script identifies cell outlines by watershedding from the manual seeds, and generates a .png image overlaying the segmentation onto the G3D projection, so it can be checked for accuracy.

3.2.6.2.6 Identification of the leaf tip and leaf base

The tip and base were identified in order to generate coordinates for each cell within the leaf. The G3D image was opened in GIMP 2.8.16 and the X-Y coordinates for both the tip of the leaf and the base of the leaf blade (where it meets the petiole) were recorded in a new .txt file, “tip.txt”.

3.2.6.2.7 Extraction of data

The cell data from the segmented image was extracted using the “extract_celldata.py” script. This generates a “data.csv” file in which each cell is given a unique identifier, and parameters such as location in the leaf, cell area, circularity, cell perimeter, and relative cell density are recorded.

3.2.6.2.8 Generation of heatmaps

Heatmaps were produced using the “heatmaps.py” script. This generates .png files in which cells in a map of the cells in the leaf are painted according to their value of any of the parameters listed in the “data.csv” file. The heatmaps use the Viridis colour scheme (van der Walt and Smith, 2015), which is perceptually-even and suitable for colour-blindness.

All numerical data were analysed in R 3.3.3.

3.2.6.3 Scanning electron microscopy

Cell area and cell perimeter were measured manually using the FIJI software package based on ImageJ 1.50d (Rasband, 1997-2016). Up to 20 cells were measured per image. I was assisted in this work by Jayden Endean.

All numerical data were analysed in R 3.3.3.

3.3 Results

3.3.1 Whole organ phenotype

To further elucidate the whole organ phenotype of *da1-1*, *bb*, and *da1-1bb*, Arabidopsis seedlings were grown on plates and sampled on every second day from five days after stratification to 39 days after stratification. The width, length, and area of the first leaf of each seedling was measured as shown in Figure 3.4. It is important to note that leaves are 3D structures, and in this study, parameters such as fresh weight or thickness of the leaves or cells were not measured. The use of the area parameter as a proxy for organ size is therefore a limitation to these experiments, as it is not a full measurement of total growth of the leaf. Nevertheless, it is used here as a reasonable measure of the 2D growth of the leaf, if not 3D.

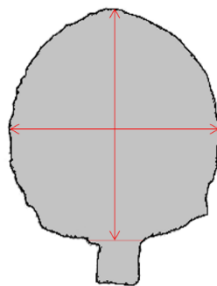


Figure 3.4 Leaf dimensions.

Width and length measurements were made along the longest axes of the leaf, excluding petiole (red arrows). Length measurements were made from the tip of the leaf to the petiole boundary, along the midvein. Width measurements were made at a 90° angle from the midvein, at the widest part of the leaf. Area measurements were made of the whole leaf, excluding the petiole.

From these data, I assessed quantitatively how the width, length and area of the first leaf of *da1-1*, *bb* and *da1-1bb* mutants change throughout growth, as well as determining their final size and a range of other parameters relating to organ size and growth. Some of these data have been published in Dong et al. 2017.

3.3.1.1 *da1-1*, *bb* and *da1-1bb* mutants exhibit increased final organ size relative to wild type

Measurements were taken from 29 days after stratification to 39 days after stratification to measure the final sizes of all four genotypes. This pooled sample amounted to around 50 individual leaves per genotype.

The *da1-1* and *bb* mutants exhibited increased final leaf width in the first leaf relative to wild type plants, at 123% and 110% of wild type respectively. The *da1-1bb* mutant demonstrated a synergistic interaction between the *da1-1* and *bb* mutations, with a final width of 148% of wild type. Leaves of all three mutants were significantly wider than wild type (Figure 3.5).

The effect of the *da1-1* and *bb* mutations on final leaf length was not as great as on final leaf width, exhibiting final lengths of 112% and 105% of wild type respectively. In common with the final width measurements, the *da1-1bb* double mutant also showed a synergistic increase in final length, at 130% of wild type. The *bb* mutant did not exhibit a significant increase in final length relative to wild type, but both *da1-1* and *da1-1bb* showed a strongly significant increase (Figure 3.5).

The largest effects on leaf phenotype were observed in the final leaf area, which is to be expected as a multiplier of width and length. The *da1-1* mutants exhibited a final leaf area of 140% of that of wild type, while *bb* mutants were 117% of wild type. As with final width and length, the final area of *da1-1bb* mutants exhibited a synergistic increase, at 196% of wild type. All three mutants were significantly larger than wild type (Figure 3.5).

Figure 3.5 also shows the levels of variation of final size within genotypes. For all three of width, length and area, mutants showed increased variation within the samples than wild type, as demonstrated by the heights of the box and whiskers plots.

In addition to this, Figure 3.6 demonstrates how leaf shape is affected in each of the mutants. By calculating a ratio of leaf length to leaf width, a measure of the roundness of the leaf is created. A score of 1 represents a perfectly circular leaf, scores greater than 1 indicate a leaf that is longer than it is wide, while a score less than one indicates a leaf that is wider than it is long. Figure 3.6(A) shows the ratio on raw, untransformed data, indicating that all three of the mutants are significantly wider than they are long, but that this difference is more extreme than in wild type. By Log₁₀ transforming the data (Figure 3.6(B)), it is possible to identify that, as the differences between genotypes are maintained (with the exception of the difference between *da1-1* and *da1-1bb*), that this is a true difference between genotypes and not merely an artefact of early exponential growth rates exaggerating pre-existing differences in the mutants. This indicates that growth in the mutants is anisotropic in comparison to growth in wild type leaves, suggesting that the increase in leaf area is likely to be primarily as a result of the greater increase in leaf width, than in leaf length.

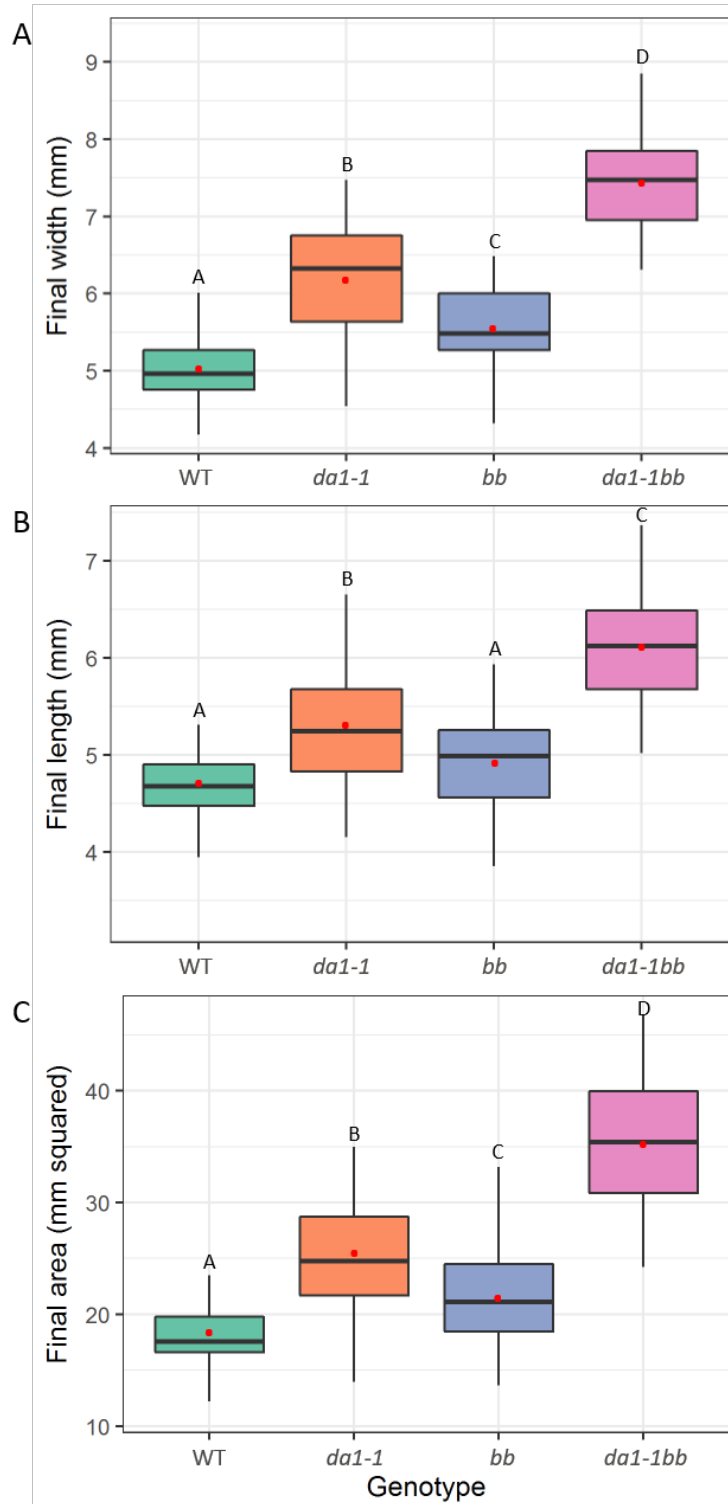


Figure 3.5 Mature leaf size in *da1-1*, *bb*, and *da1-1bb* mutants

Boxplot of final width (A), length (B), and area (C) of the first leaves of wild type, *da1-1*, *bb* and *da1-1bb* plants. Samples pooled from 29DAS - 39DAS (n = 50). Red points indicate means of samples. Small letters indicate significance groups according to ANOVA with a post-hoc Tukey pairwise comparison (variances were equal, p = 0.05).

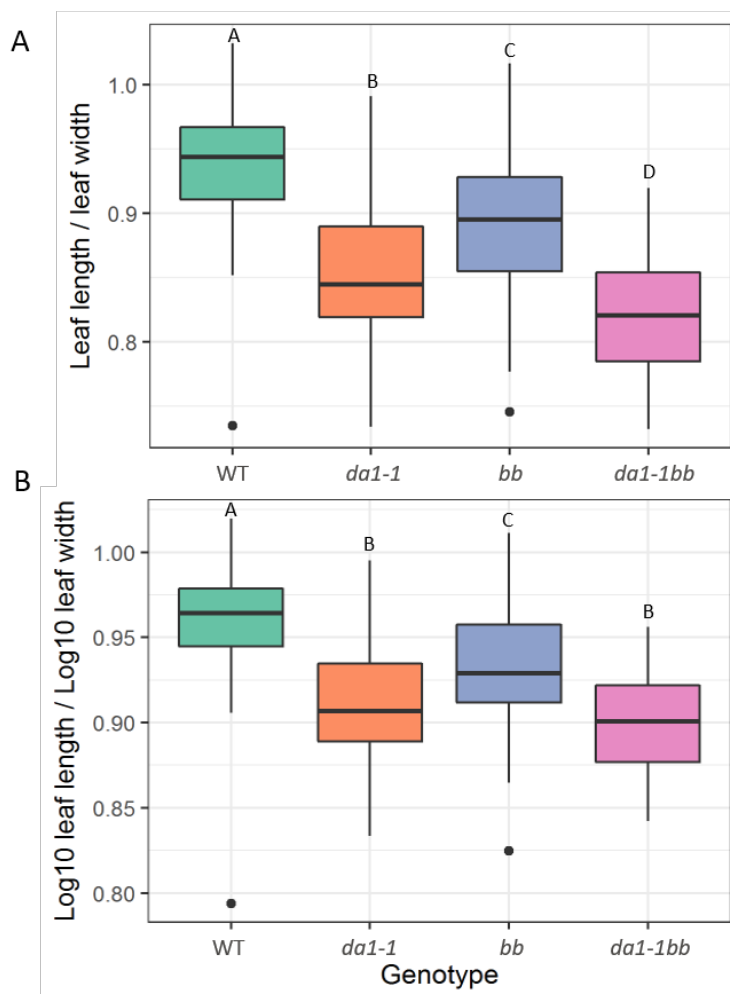


Figure 3.6 Mature leaf shape in *da1-1*, *bb*, and *da1-1bb* mutants

Boxplot of final leaf length / leaf width (A) and Log10 final leaf length / Log10 leaf width (B) of the first leaves of wild type, *da1-1*, *bb* and *da1-1bb* plants. Samples pooled from 29DAS - 39DAS (n = 50). Small letters indicate significance groups according to ANOVA with a post-hoc Tukey pairwise comparison (variances were equal, p = 0.05).

3.3.1.2 *da1-1* and *da1-1bb* mutants exhibit an increased duration of growth

Measurements of the first leaf were taken every second day from 5 days after stratification to 39 days after stratification, when all four genotypes tested had reached their final size. Eight to ten plants were sampled per genotype, per day. Logistic curves were fitted to the data (Figure 3.7) according to the Boltzmann or Logistic function, as shown in Equation 3.1 (pers. comm., Samantha Fox).

In the Boltzmann or Logistic function, A is final leaf size (width, length or area), t is time, t_m is the time of inflection at which 50% of growth has taken place, and k is the early exponential

growth rate. These parameters were manually adjusted where necessary to achieve the most representative fit for each of width, length, and area; and each genotype analysed. The best fitting parameter values for each of the above are shown in Table 3.2.

$$y = \frac{-A}{1 + e^{(t-t_m)k}} + A$$

Equation 3.1 The Boltzmann or Logistic function

Genotype	Width			Length			Area		
	A	t_m	k	A	t_m	k	A	t_m	k
wild type	5.0	290	0.025	4.7	315	0.018	18.1	365	0.030
<i>da1-1</i>	6.2	330	0.018	5.3	340	0.015	25.3	380	0.025
<i>bb</i>	5.5	310	0.019	4.9	310	0.017	21.2	360	0.027
<i>da1-1bb</i>	7.4	330	0.019	6.1	310	0.018	35.4	370	0.028

Table 3.2 Logistic function parameter values for curve fitting

The curves were also transformed with the natural log (Ln) (Figure 3.8) which allows a more realistic representation of the size differences at early stages. At early stages, the curve is plotted at a higher value than the measurements made, as at five days after stratification the leaves have a high degree of topology and a light microscopy image may not give a full indication of the curved surface and therefore total width, length or area of the leaf.

Figure 3.7 and Figure 3.8 show that *da1-1*, *bb*, and *da1-1bb* plants have an increased final size relative to wild type, and that in *da1-1* and *da1-1bb* mutants this is at least in part due to an increased duration of growth. Table 3.3 shows the day at which the leaf reaches 95% of its final size, and demonstrates that *da1-1* in particular grows for longer than wild type plants, and that *da1-1bb* and *bb* increase in width for a longer duration than wild type, but not length or area.

Genotype	Time at final width (DAS)	Time at final length (DAS)	Time at final area (DAS)
wild type	17	20	20
<i>da1-1</i>	21	23	21
<i>bb</i>	20	20	20
<i>da1-1bb</i>	20	20	20

Table 3.3 Time at final size of wild type, *da1-1*, *bb*, and *da1-1bb* leaves

3.3.1.3 *da1-1*, *bb*, and *da1-1bb* mutants exhibit significant increases in leaf size relative to wild type throughout growth

The first leaves of *da1-1*, *bb*, and particularly *da1-1bb* mutants are significantly larger than wild type at many points throughout development, as shown in Table 3.4, in which asterisks indicate significance of difference relative to wild type (* = $p < 0.05$, ns = not significant), according to ANOVA with a post-hoc Dunnett test (variances were equal).

Days after stratification	<i>da1-1</i>			<i>bb</i>			<i>da1-1bb</i>		
	Width	Length	Area	Width	Length	Area	Width	Length	Area
5	*	ns	ns	*	*	*	*	*	*
7	ns	*	ns	*	*	*	*	*	*
9	ns	ns	ns	*	*	*	*	*	*
11	ns	ns	ns	ns	ns	ns	*	ns	*
13	*	ns	*	*	*	*	*	*	*
15	*	*	*	*	*	*	*	ns	*
17	ns	ns	ns	*	ns	*	*	*	*
19	*	ns	ns	ns	ns	ns	*	*	*
21	*	ns	ns	ns	ns	ns	*	ns	*
23	*	*	*	*	*	*	*	*	*
25	*	ns	*	ns	ns	ns	*	*	*
27	ns	ns	ns	ns	ns	ns	*	*	*
29	*	*	*	*	ns	*	*	*	*
31	ns	ns	ns	ns	ns	ns	*	*	*
33	*	ns	ns	ns	ns	ns	*	*	*
35	*	*	*	ns	ns	ns	*	*	*
37	*	*	*	*	*	ns	*	*	*
39	*	ns	ns	ns	*	ns	*	*	*

Table 3.4 Significance of difference of *da1-1*, *bb*, and *da1-1bb* from wild type through leaf growth

Table 3.4 shows that *bb* and *da1-1bb* mutants exhibited a more often significant increase in organ size relative to wild type at early stages than the *da1-1* single mutant, which showed little or no significance before 13 days after stratification. Conversely, as expected based on the findings in Section 3.3.1.1, *da1-1*, and in particular *da1-1bb*, exhibited more often a

significant increase in organ size compared to wild type than *bb* in the later stages of growth and at final size.

In *da1-1*, *bb*, and *da1-1bb* mutants, the least frequently significant effect throughout growth was on the length of the leaf. Length was the only parameter for which the *da1-1bb* double mutant exhibited any non-significant differences at any time-point. It was also the least frequently significant parameter for *da1-1* mutants, and in *bb* mutants it was the joint least frequently significant parameter, with leaf area. This is to be expected, as the increase in leaf length at final size was less than the increase in leaf width or area, as shown in Section 3.3.1.1. In all three mutants, the most frequently significant effect throughout growth was on the width of the leaf.

3.3.1.4 *da1-1bb* mutants exhibit a synergistic increase in leaf size throughout growth

Figure 3.7 shows that for width, length, and areal measurements of leaf size in the first leaf, the *da1-1bb* double mutant exhibited a synergistic increase in size at almost all times from nine days after stratification onwards. The exceptions were 15 and 23 days after stratification, which exhibited anomalous results across all four genotypes, and 37 days after stratification in length only.

The increase in size of *da1-1bb* in comparison to wild type was not synergistic at very early stages because the *bb* mutant is nearly as large, or larger than, the double mutant at these early stages.

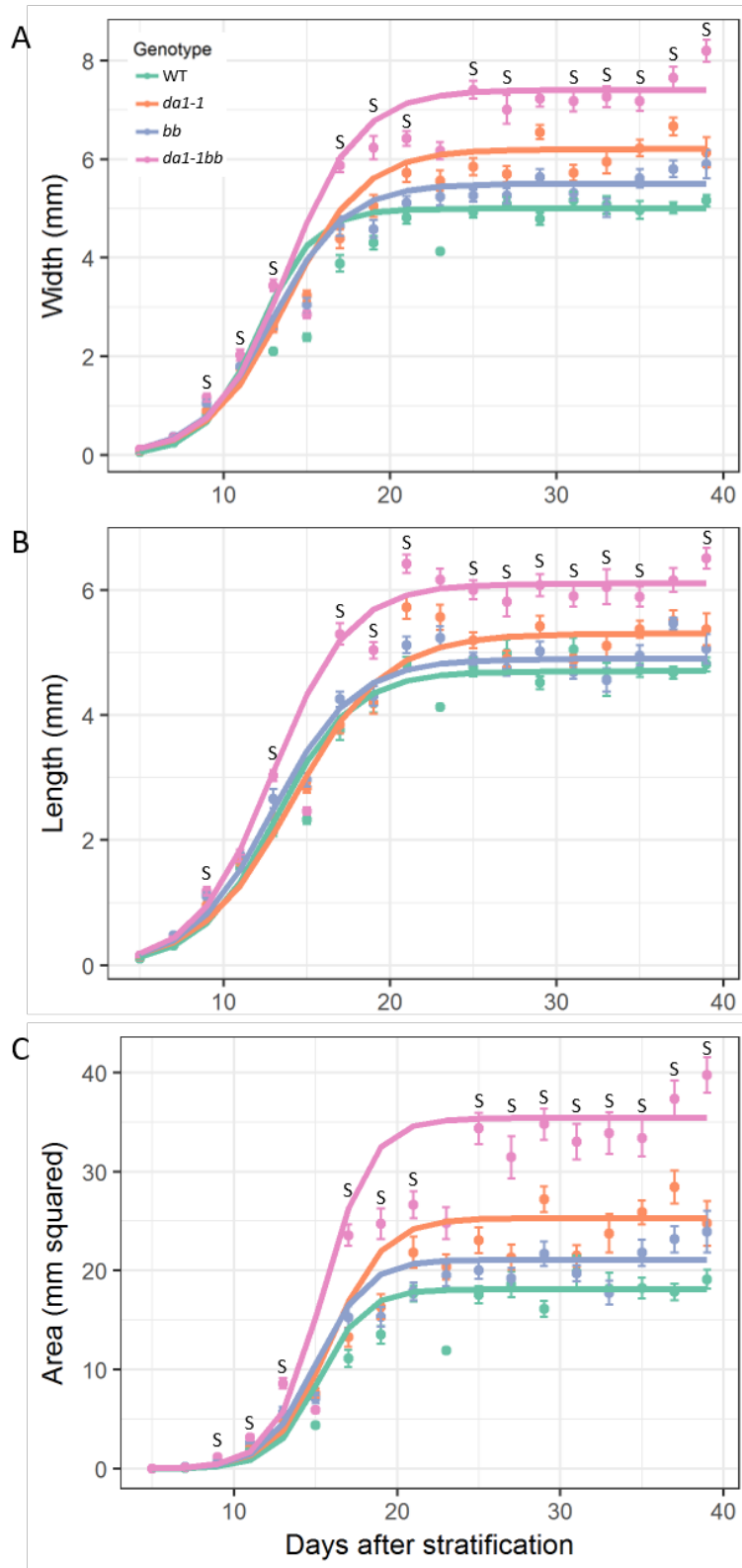


Figure 3.7 Growth curve of wild type, *da1-1*, *bb*, and *da1-1bb* leaves

Width (A), length (B), and area (C) of the first leaf of wild type, *da1-1*, *bb*, and *da1-1bb* plants from five to 39 days after stratification. Standard error shown (n=8-10). "S" denotes a synergistic increase in *da1-1bb* leaf size.

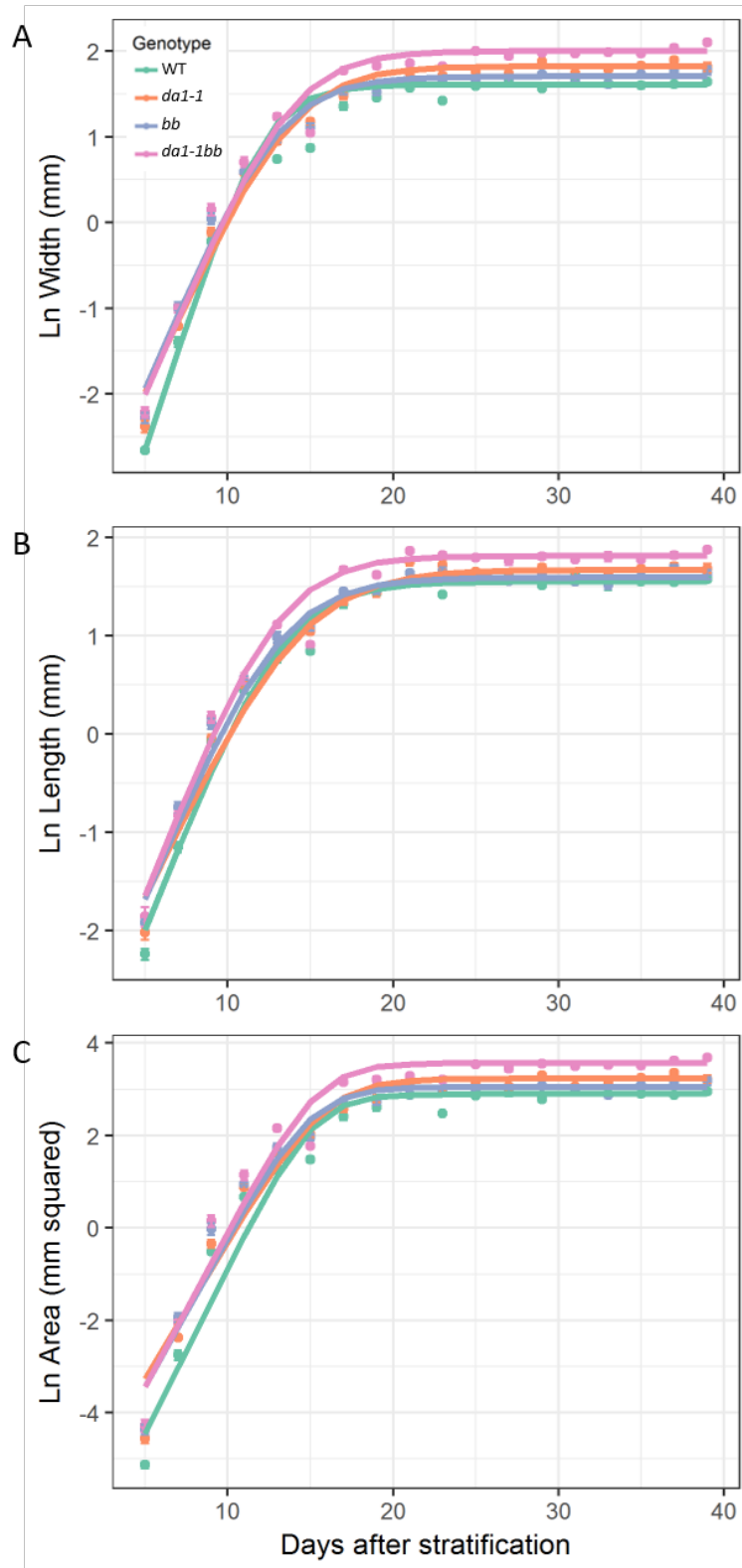


Figure 3.8 Natural log growth curve of wild type, *da1-1*, *bb*, and *da1-1bb* leaves

Width (A), length (B), and area (C) of the first leaf of wild type, *da1-1*, *bb*, and *da1-1bb* plants from five to 39 days after stratification. Data transformed with the natural log, standard error shown (n=8-10).

3.3.1.5 *da1-1bb mutants grow at an increased rate during the linear phase of growth*
Between 9 and 17 days after stratification, the growth of the first leaf was linear, as demonstrated in Figure 3.9. From this linear phase of growth, it is possible to calculate overall rates of growth and determine from this whether the *da1-1*, *bb*, or *da1-1bb* mutants grow faster than wild type plants, which would provide an alternative or additional mechanism for the increased final size observed in the mutants relative to wild type. The data for 15 days after stratification was removed as an anomalous timepoint.

Using t-tests to compare the rates of increase in width between the four genotypes revealed that *da1-1* ($p = 0.0301$), *bb* ($p = 0.0417$), and *da1-1bb* ($p < 0.0001$) all increased in width more quickly than the wild type plants. In addition to this, *da1-1bb* exhibited an increased rate of growth relative to *da1-1* ($p < 0.0001$) and *bb* ($p = 0.0003$), while *da1-1* and *bb* showed no significant difference in rate of increase in width, relative to each other ($p = 0.6327$). Comparing the rate of increase in length showed that while *da1-1* and *bb* did not separately show an increased rate of growth relative to wild type ($p = 0.7563$ and $p = 0.0690$, respectively), the *da1-1bb* double mutant had a strongly increased rate of increase in length ($p < 0.0001$). Additionally, *da1-1bb* exhibited an increased rate of growth relative to both the *da1-1* ($p < 0.0001$) and the *bb* ($p < 0.0001$) single mutants. The *da1-1* and *bb* single mutants were themselves not significantly different in rate of increase in length from each other ($p = 0.1473$). Finally, comparison of the rate of areal increase revealed that *da1-1* ($p = 0.0067$), *bb* ($p < 0.0001$) and *da1-1bb* ($p < 0.0001$) all showed an increased rate of areal increase relative to wild type. In addition to this, *bb* exhibited an increased rate of growth relative to *da1-1* ($p < 0.0001$), and *da1-1bb* grew more quickly than either *da1-1* or *bb* ($p < 0.0001$ for both comparisons).

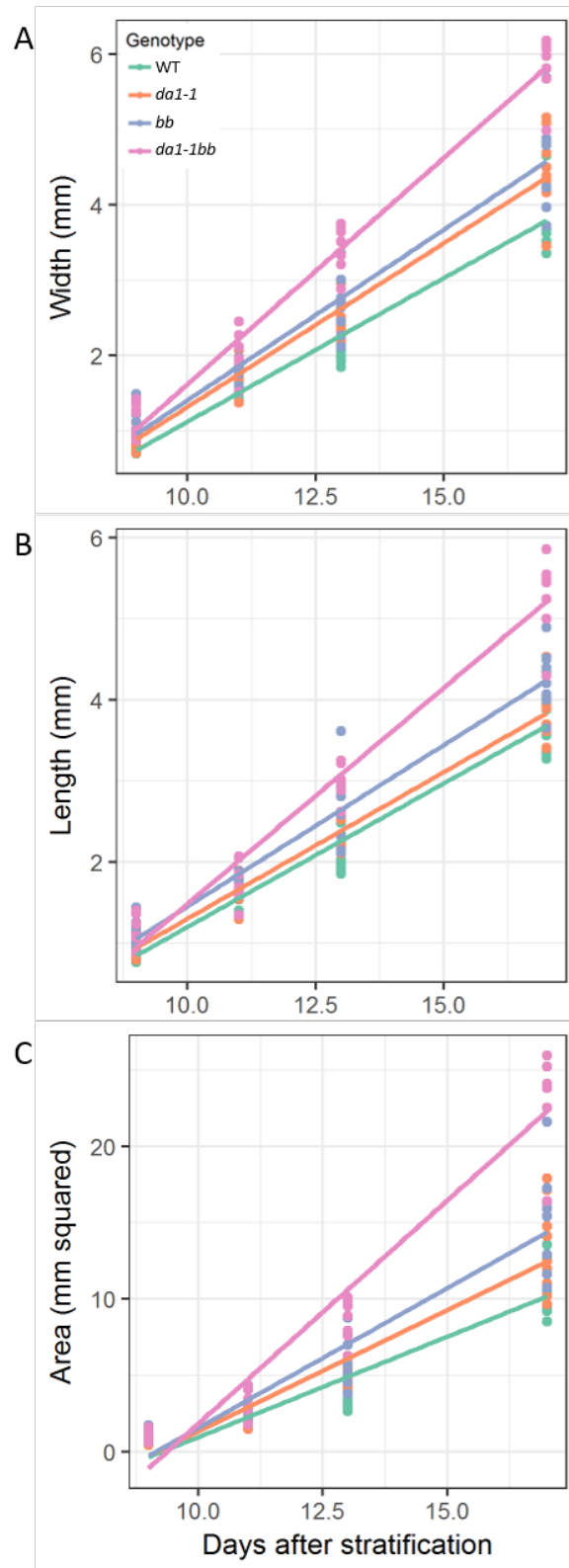


Figure 3.9 Linear phase growth of wild type, *da1-1*, *bb*, and *da1-1bb* leaves

Width (A), length (B), and area (C) of the first leaf of wild type, *da1-1*, *bb*, and *da1-1bb* plants from nine to 17 days after stratification. Anomalous data at 15 days after stratification removed (n = 8-10).

3.3.2 Cellular phenotype in growing leaves

To determine the total number of cells, and key parameters regarding those cells in a growing leaf, confocal microscopy was used to image whole leaves of 5 to 7 leaves per genotype per day, between 7 and 11 days after stratification. The *pAtML1::mCitrine-RCI2A* plasmid was used to mark the cell membrane, as described previously in Section 3.2.1 (plants expressing *pAtML1::mCitrine-RCI2A* will hereafter be referred to as *pAR169*). For the largest leaves at the latest stages of growth, one half of the leaf blade was imaged rather than the whole leaf (as in Andriankaja et al., 2012) and taken as a representative sample of the leaf. As the expression of the cell membrane marker begins to fade at later stages of growth, imaging one half of the leaf blade allowed the generation of a high quality, representative sample, rather than a poorer quality image of the whole leaf. Throughout, the first leaf was used.

Semi-automatic cell segmentation using Leaf Analysis Toolkit as described in Section 3.2.6.2 was carried out on 3 representative leaves per genotype, per timepoint. The large cells in the leaf margin, and cells in the midvein were excluded from the segmentation and analyses as they exhibit very different cell size and shape compared to the adjacent pavement cells (Figure 3.10), and were therefore a confounding factor in this study.

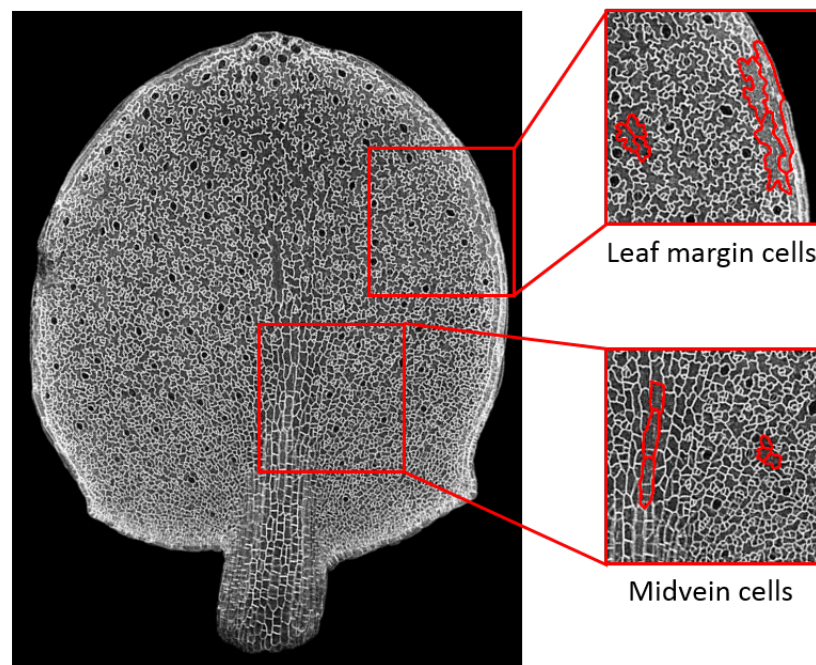


Figure 3.10 Exclusion of leaf margin and midvein cells from segmentation

Red outlines show three cells each in the leaf margin and midvein, in comparison to three nearby pavement cells, for shape and size comparison.

These cells were excluded by defining them as part of the background of the image, so they were not assigned a cell identification number. Positional data as well as area, relative cell density and circularity values were extracted for each cell.

3.3.2.1 Cell number in growing leaves

Total cell number (excepting midvein and leaf margin cells as described in Figure 3.10) was measured in each of the segmented leaf images, and a mean taken from the three samples per genotype, per time-point. Where only half of the leaf had been segmented due to its size (as detailed in Section 3.3.2), the measured cell number was doubled to produce an estimate of the total cell number in a whole leaf.

As shown in Figure 3.11, in all genotypes the mean cell number increased in an approximately linear fashion between 7 and 11 days after stratification. Throughout this time period, *da1-1*, *bb*, and *da1-1bb* leaves had more cells than wild type leaves. These differences were statistically significant (according to Student's t-test) at all time-points for all three mutants, with the exception of *da1-1bb* at 7 days after stratification, and *da1-1* at 9 days after stratification.

At every time-point except 7 days after stratification, the *da1-1bb* double mutant exhibited the largest increase in cell number relative to wild type, with total cell number at 11 days after stratification around 240% of that of wild type, compared to 187% for *da1-1* and 182% for *bb*. The *da1-1bb* mutant also had a significantly increased cell number relative to the *da1-1* and *bb* single mutants at several points throughout the sampling period, particularly at later stages: it was significantly increased relative to *da1-1* at 9 days after stratification ($p = 0.0161$), relative to *da1-1* and *bb* at 10 days after stratification ($p = 0.0033$ and $p = 0.0316$ respectively) and relative to *da1-1* and *bb* at 11 days after stratification ($p = 0.0337$ and $p = 0.0212$ respectively). However, these increases in cell number did not demonstrate a synergistic interaction, as is observed in overall leaf area at 9 and 11 days after stratification (as shown in Figure 3.7).

Using t-tests to compare the rates of increase in cell number of the four genotypes revealed that *da1-1* ($p = 0.0007$), *bb* ($p < 0.0001$), and *da1-1bb* ($p < 0.0001$) all had a faster rate of increase in cell number than the wild type. In addition to this, *da1-1bb* also exhibited an increased rate of cell number increase compared to *da1-1* ($p = 0.0003$) and *bb* ($p = 0.0004$), although *da1-1* and *bb* did not exhibit a significant difference in rate from each other ($p = 0.5040$).

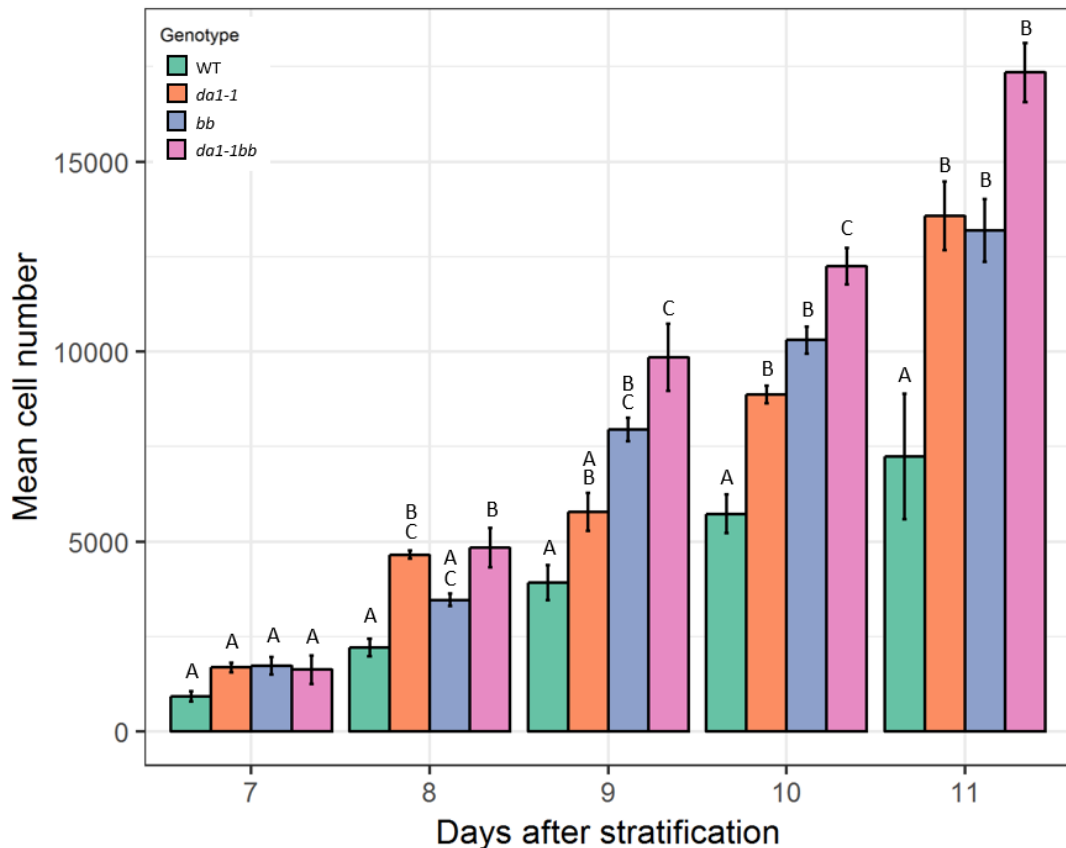


Figure 3.11 Total cell number of wild type, *da1-1*, *bb*, and *da1-1bb* leaves

Total cell number of wild type *pAR169*, *da1-1 pAR169*, *bb pAR169*, and *da1-1bb pAR169* leaves from 7 to 11 days after stratification. Standard error shown ($n=3$). Small letters indicate significance groups according to ANOVA with a post-hoc Tukey pairwise comparison (variances were equal, $p = 0.05$). Cells in the midvein and the leaf margin are excluded from these data. Where leaves were very large (at 11DAS), some data represent an estimation of the total cell number based on the total cell number from half the leaf blade, doubled.

3.3.2.2 Cell area in growing leaves

Areal data was collected for each cell in each of the segmented leaf images, and a mean taken from each sample. A mean was then taken from the three samples per genotype, per timepoint.

In all genotypes, the mean cell area increased in a largely linear manner between 7 and 11 days after stratification (Figure 3.12). Mean cell areas were generally decreased in the *da1-1*, *bb*, and *da1-1bb* mutants relative to wild type. The most pronounced differences in mean cell area from wild type were exhibited by the *da1-1* and *da1-1bb* mutants throughout the 5 days sampled, though increasing in later timepoints. By contrast, *bb* mutants exhibited a small, but non-significant reduction in mean cell area relative to wild type throughout the sampling period.

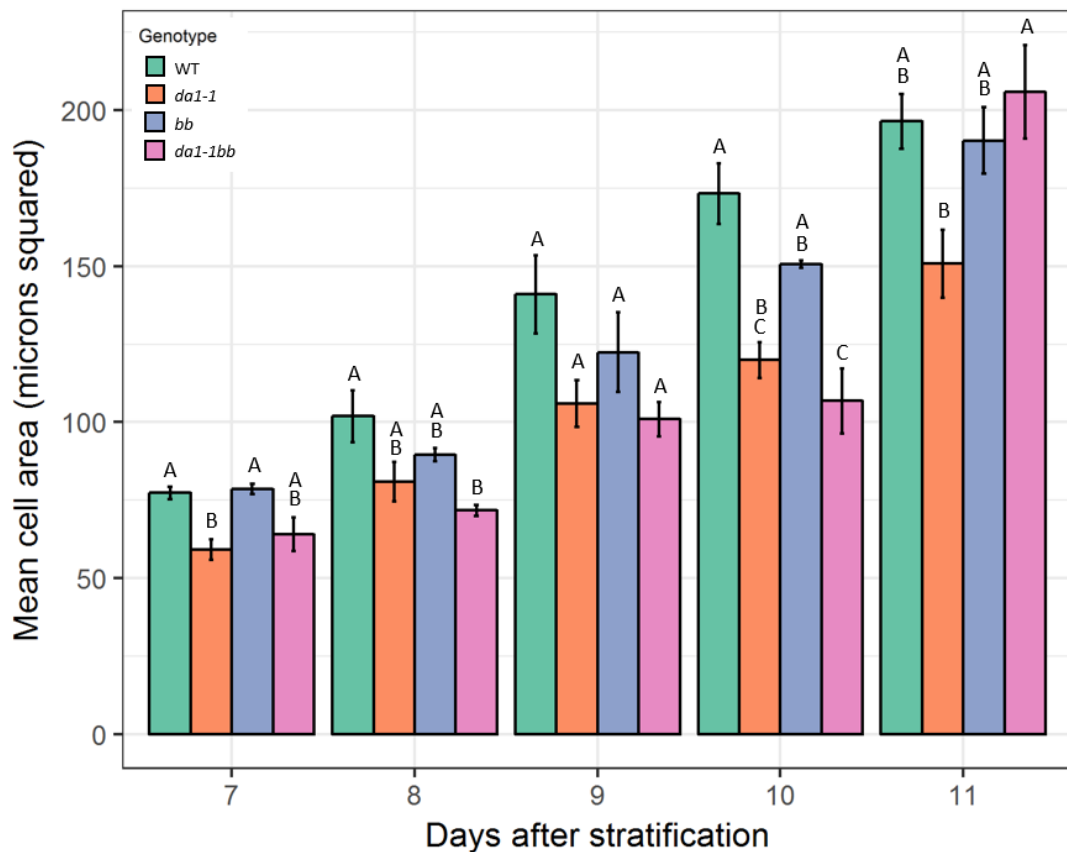


Figure 3.12 Mean cell area of wild type, *da1-1*, *bb*, and *da1-1bb* leaves

Mean cell area of wild type *pAR169*, *da1-1 pAR169*, *bb pAR169*, and *da1-1bb pAR169* leaves from 7 to 11 days after stratification. Standard error shown (n=3). Total cells analysed > 370,000. Small letters indicate significance groups according to ANOVA with a post-hoc Tukey pairwise comparison (variances were equal, $p = 0.05$). Cells in the midvein and the leaf margin are excluded from these data.

Figure 3.13 shows the distribution of cell areas spatially within the leaf, by relative distance from the leaf tip. The slopes of the linear regression lines fitted to this data show the location of the smallest and largest cells, in each genotype and at each timepoint. At 7 days after stratification, *da1-1bb* exhibited the shallowest slope, indicating the most uniform distribution of cell areas along the length of the leaf. The slope of *da1-1bb* was significantly less steep than all three of wild type ($p = 0.0160$), *da1-1* ($p = 0.0244$), and *bb* ($p = 0.0005$). The steepest slope, and therefore least uniform distribution of cell areas along the leaf, was found in the wild type leaf, although this slope was not statistically significantly steeper than either *da1-1* or *bb*. However, *bb* was found to have a significantly steeper slope than *da1-1* ($p = 0.0155$), and therefore exhibited a less uniform distribution of cell areas along the leaf.

At 8 days after stratification, all genotypes exhibited a steeper gradient of cell areas from the tip to the base of the leaf than at the previous timepoint, 7 days after stratification (wild type: $p = 0.0052$, *da1-1*: $p = 0.0029$, *bb*: $p = 0.0029$, *da1-1bb*: $p = 0.0001$). Within the 8 days after stratification timepoint, wild type leaves showed the steepest gradient, which was significantly steeper than all three of *da1-1* ($p = 0.0129$), *bb* ($p = 0.0071$) and *da1-1bb* ($p = 0.0003$). The shallowest slope was found in *da1-1bb*, which was also found to be significantly shallower than *bb* ($p = 0.118$), although not *da1-1* ($p = 0.0720$).

At 9 days after stratification, all genotypes again showed an increased gradient of cell areas than at the previous timepoint (wild type: $p = 0.0439$, *da1-1*: $p = 0.0037$, *bb*: $p = 0.0318$, *da1-1bb*: $p = 0.0004$). The shallowest slope was still found in the *da1-1bb* mutant, which was significantly less steep than wild type ($p = 0.0086$) and *da1-1* ($p = 0.0035$), although not *bb* ($p = 0.0744$). The steepest slope was found in *bb*, although this was not significantly steeper than the slope of any other genotype.

At 10 days after stratification, only *da1-1bb* showed a significantly increased gradient of cell areas relative to 9 days after stratification ($p = 0.0107$). The steepest gradient within the 10 days after stratification timepoint was found in wild type plants, although this was not significantly different to any other genotype. The shallowest gradient was found in *da1-1bb* leaves, which was significantly less steep than *bb* ($p = 0.00163$) but no other genotype. Finally, at 11 days after stratification none of the four genotypes exhibited a difference in the slope, relative to 10 days after stratification. In addition to this, there were no significant differences observed between genotypes within 11 days after stratification.

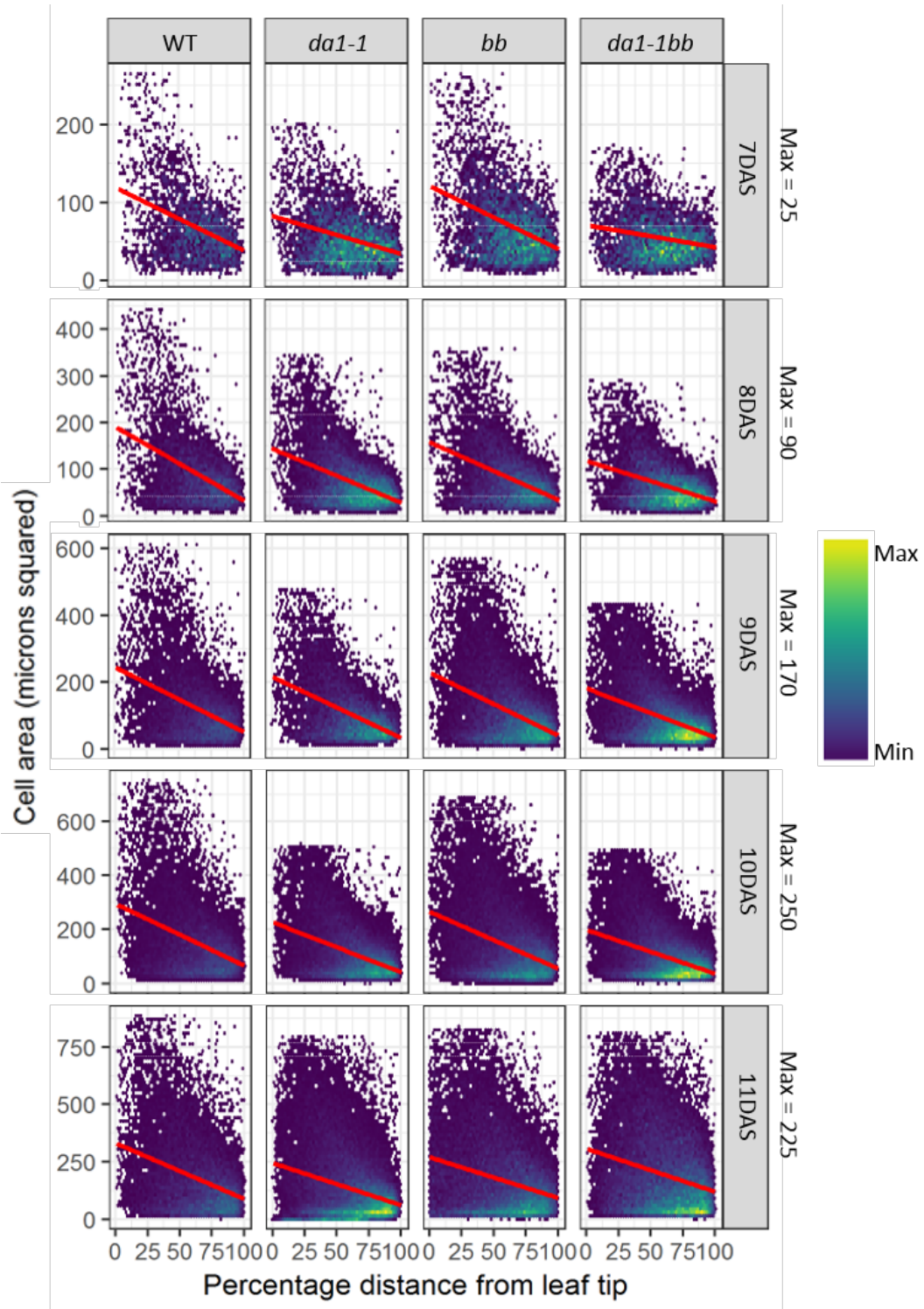


Figure 3.13 Cell area distributions within wild type, *da1-1*, *bb*, and *da1-1bb* leaves

Binned hex-plots of cell areas by relative distance from the leaf tip in wild type *pAR169*, *da1-1 pAR169*, *bb pAR169*, and *da1-1bb pAR169* leaves from 7 to 11 days after stratification. Each heatmap represents three pooled independent samples. Data within three standard deviations of the mean of each pooled sample are shown. Red lines indicate linear regressions. Cells in the midvein and the leaf margin are excluded from these data. Total cells analysed > 370,000.

Figure 3.14 shows the frequency distribution of cells binned by area, where the bin width is 60 microns squared. This data gives a more detailed insight into the structure of the cell population than Figure 3.12, and how that varies between genotypes and over time.

At all timepoints, and for all genotypes, the greatest proportion of cells are found in the 30-90 μm^2 range. However, this proportion falls from 60-70% of all cells at 7 days after stratification, to under 30% of all cells at 11 days after stratification. This is as a result of the flattening and widening of the frequency distribution of cell areas over time due to the appearance of more large cells at later timepoints. The frequency distributions for wild type showed that the proportion of smaller cells dropped quickly, from 60.2% at 7 days after stratification, to 56.2% at 9 days after stratification and 28.8% at 11 days after stratification. Over the same time period, the right-hand tail of the wild type distribution extended significantly from 210-270 μm^2 at 7 days after stratification, to 870-930 μm^2 at 11 days.

The *da1-1* mutant showed a similar reduction in the proportion of cells in the 30-90 μm^2 range over the 5 days sampled, although at every timepoint the proportion of cells in that bin was larger than for wild type. In addition to this, the proportions of cells in the higher bins of *da1-1* was also lower than for wild type at each timepoint, and at every timepoint the right-hand tail of the distribution did not extend as far as for wild type. At 11 days after stratification, the maximum extent of the *da1-1* right-hand tail was 750-810 μm^2 .

As with *da1-1*, the *bb* mutant exhibited a similar pattern in reduction of the population of smaller cells over time. The changes in the *bb* distribution, however, were more similar to wild type, with only a slight reduction in the length of the right-hand tail of the *bb* distribution relative to wild type.

The strongest difference in the shape of the frequency distribution from wild type was observed in the *da1-1bb* mutant. The distribution at 7 days after stratification was very narrow, with 68.6% of all cells in the 30-90 μm^2 range, and no cells in any bins higher than the 150-210 μm^2 range. Similarly to *da1-1*, the distribution extended at the right-hand tail more slowly than wild type and *bb*, and at 11 days after stratification, the maximum extent of the tail was 750-810 μm^2 .

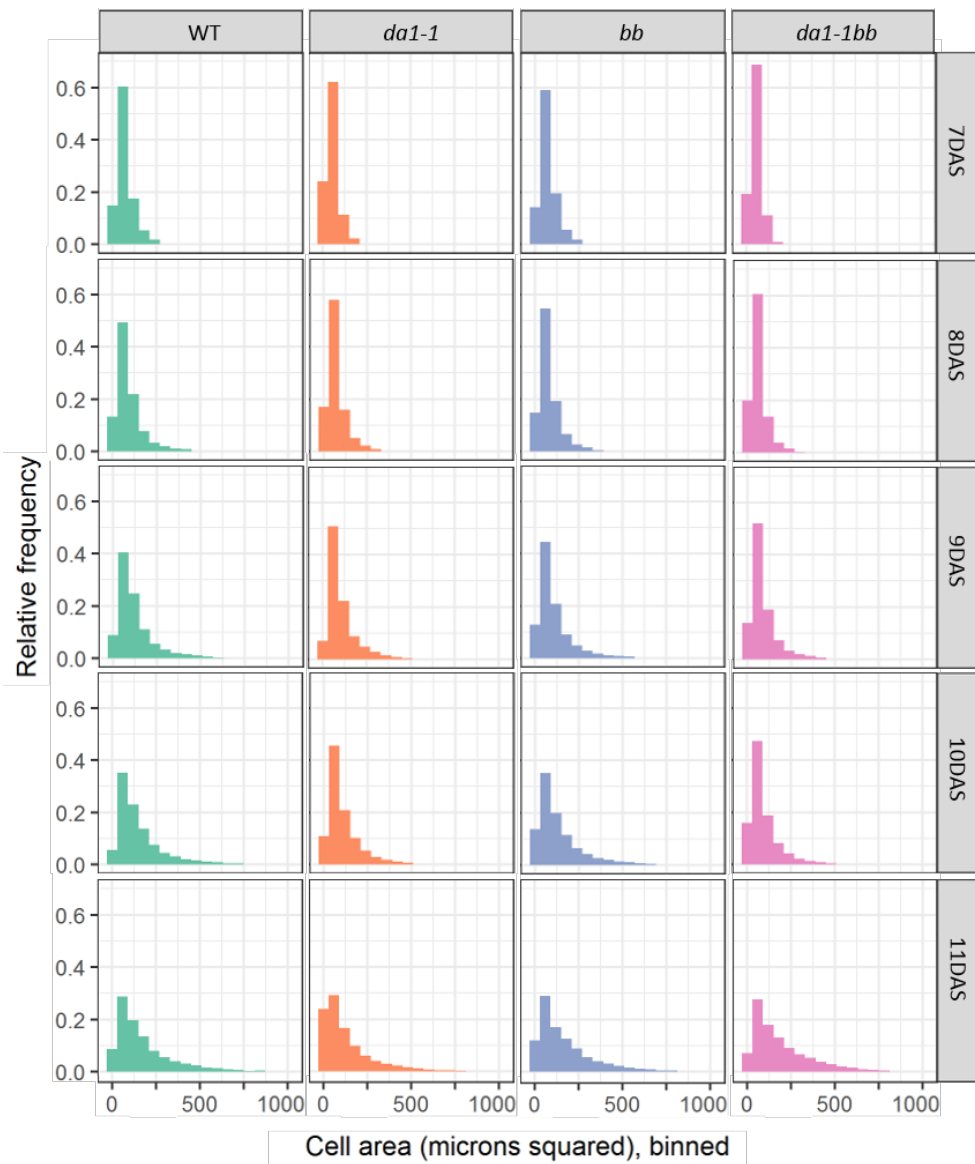


Figure 3.14 Frequency distributions of cell areas in wild type, *da1-1*, *bb*, and *da1-1bb* leaves

Histograms of relative frequency of cell areas in wild type *pAR169*, *da1-1 pAR169*, *bb pAR169*, and *da1-1bb pAR169* leaves from 7 to 11 days after stratification. Bin width = 60. Each histogram represents three pooled independent samples per genotype. Data within three standard deviations of the mean of each pooled sample are shown. Cells in the midvein and the leaf margin are excluded from these data. Total cells analysed > 370,000.

3.3.2.3 Cell density in growing leaves

Cell density was calculated using the total number of cells in the leaf, divided by the total area of all cells in the leaf, in each segmented leaf image. A mean was then taken from the three samples per genotype, per time-point.

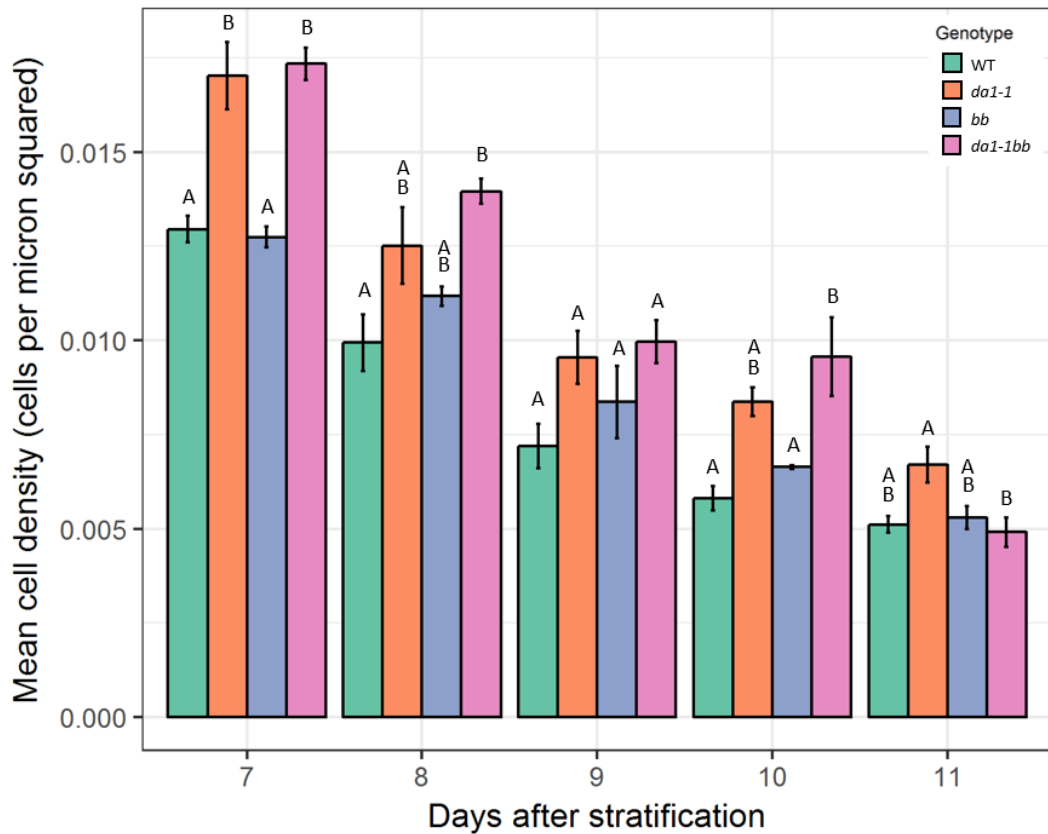


Figure 3.15 Mean cell density of wild type, *da1-1*, *bb*, and *da1-1bb* leaves

Mean cell density of wild type *pAR169*, *da1-1 pAR169*, *bb pAR169*, and *da1-1bb pAR169* leaves from 7 to 11 days after stratification. Standard error shown (n=3). Total cells analysed > 370,000. Small letters indicate significance groups according to ANOVA with a post-hoc Tukey pairwise comparison (variances were equal, $p = 0.05$). Cells in the midvein and the leaf margin are excluded from these data.

Mean cell density decreased over time in all four genotypes between 7 and 11 days after stratification, as shown in Figure 3.15. Mean cell density was generally increased in *da1-1* and *da1-1bb* relative to wild type, with the greatest difference at 7 days after stratification, where the cell densities were 31.5% and 33.9% higher, respectively. Although the absolute differences in cell densities decreased over time, the percentage differences remained approximately the same. At 11 days after stratification, the mean cell density of the *da1-1bb* mutant was approximately equal to that of wild type, although the *da1-1* mutant maintained a significantly increased cell density, at 31.1% increased. By contrast, the *bb* mutant

exhibited no statistically significant difference in mean cell density relative to wild type throughout the 5 days sampled. There were no significant differences between the rates of decrease in mean cell density of any of the four genotypes.

Figure 3.17 shows the distribution of relative cell densities spatially within the leaf, by relative distance from the leaf tip. Relative cell density was calculated for each cell, based on the areas of it and its direct neighbours, giving a cell density result for each individual cell. These cell density results for each cell were used to calculate relative cell densities for each cell, by designating the cell with the highest cell density result as 1, and the lowest as 0. Each cell was therefore given a relative cell density score between 0 and 1. This data permits a comparison of the locations and frequencies of relative densities within leaves, rather than absolute cell densities. In tests on growing leaf tissue in other experiments, it was found that areas where the relative cell density was at or above 0.7 (that is, at or above 70% of the maximum cell density in the leaf, see Figure 3.16) correlated strongly with areas where most cell divisions took place (pers. comm., Ross Carter).

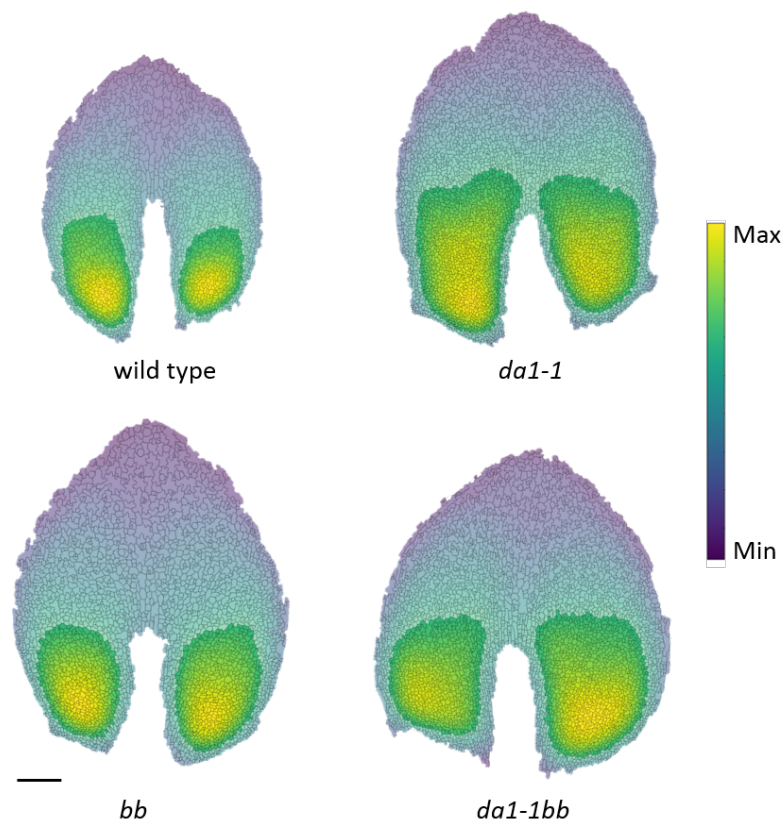


Figure 3.16 Heatmaps of relative cell density within wild type, *da1-1*, *bb*, and *da1-1bb* leaves

Heatmaps of relative cell density of wild type *pAR169*, *da1-1 pAR169*, *bb pAR169*, and *da1-1bb pAR169* leaves at 8 days after stratification. Areas of relative cell density over 0.7 are highlighted. Scale bar 100 μ m.

The slopes of the linear regressions fitted to the data in Figure 3.17 show the spatial distribution of the areas of highest and lowest relative cell density within the leaf, in each genotype and at each timepoint. At 7 days after stratification, the gradient of the slope in *da1-1bb* leaves was the shallowest, and exhibited a significant difference from each of wild type ($p = 0.0182$), *da1-1* ($p = 0.0209$), and *bb* ($p = 0.149$). Although the steepest slope was observed in *bb* leaves, there were no significant differences in the distribution of relative cell densities along the leaf between any of the other three genotypes at 7 days after stratification.

Between 7 and 8 days after stratification, the slopes of all four genotypes became significantly steeper (wild type: $p = 0.0053$, *da1-1*: $p = 0.0026$, *bb*: $p = 0.0156$, *da1-1bb*: $p = 0.0002$), indicating a greater differential between the relative cell density of cells at the tip of the leaf compared to those at the base of the leaf. At 8 days after stratification, the *da1-1bb* mutant exhibited the least steep gradient between the tip and the base of the leaf, which was significantly less steep than that of wild type ($p = 0.0126$). Wild type leaves showed the steepest gradient, although no significant difference in gradient of slope was observed between it and *da1-1* or *bb*.

At 9 days after stratification, the steepness of the slope of *da1-1bb* was significantly increased relative to 8 days after stratification ($p = 0.0482$), although there was no significant change in slope for wild type, *da1-1* and *bb*. In addition to this, there were no significant differences in slope between any of the four genotypes at 9 days after stratification, indicating that the distributions of relative cell density were largely similar.

There was no significant change in the gradient of slope of any genotype between 9 and 10 days after stratification, nor was there any significant difference between any of the genotypes within the 10 days after stratification timepoint. Finally, at 11 days after stratification, there was a reduction in the gradient of the slope of *da1-1bb* relative to the slope at 10 days after stratification ($p = 0.0185$), but none of the other genotypes. There was also no significant difference between any of the four genotypes at 11 days after stratification.

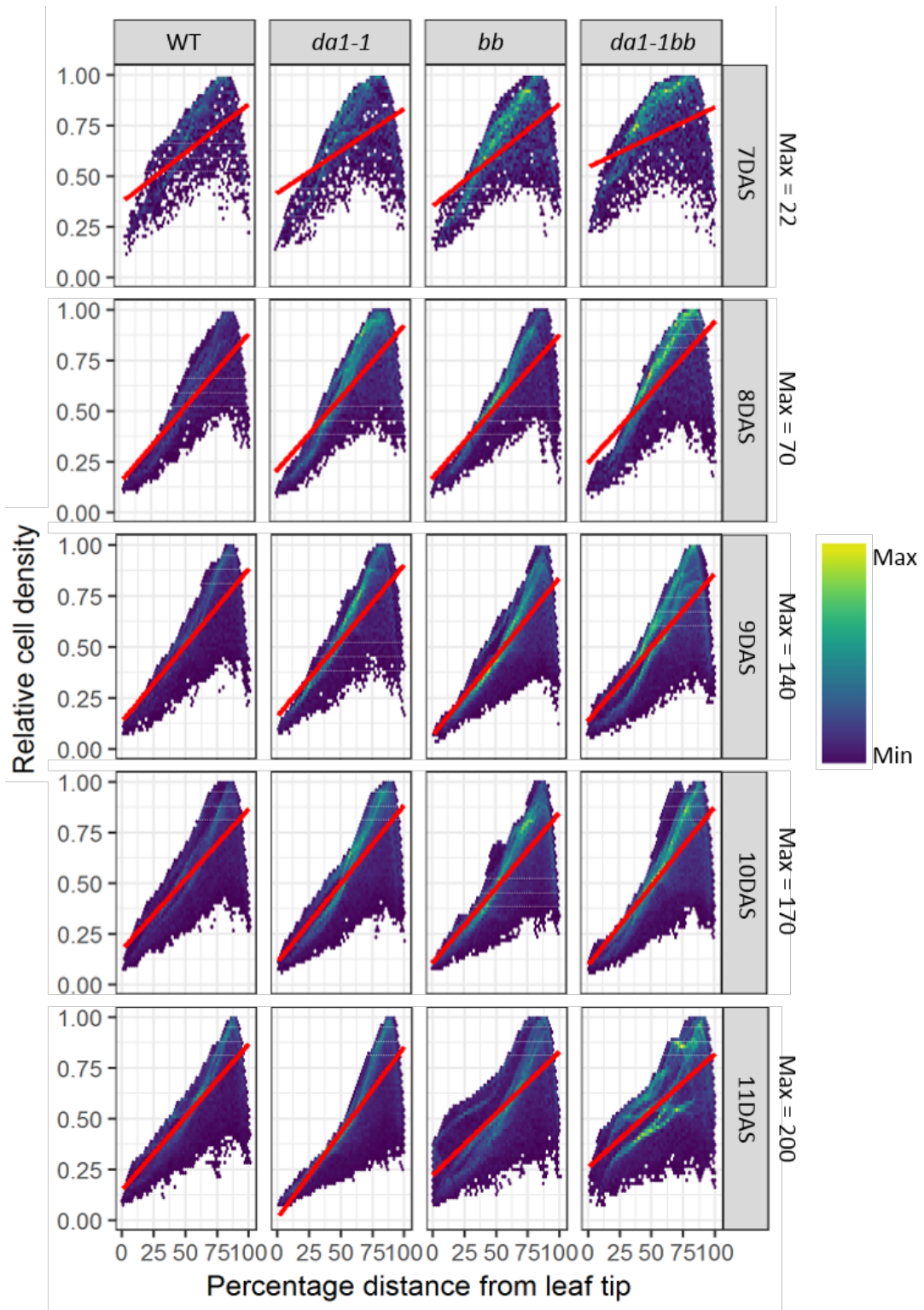


Figure 3.17 Relative cell density distributions within wild type, *da1-1*, *bb*, and *da1-1bb* leaves

Binned hex-plots of relative cell density compared to relative distance from the leaf tip in wild type *pAR169*, *da1-1 pAR169*, *bb pAR169*, and *da1-1bb pAR169* leaves from 7 to 11 days after stratification. Each heatmap represents three pooled independent samples. Red lines indicate linear regressions. Cells in the midvein and the leaf margin are excluded from these data. Relative cell density is defined as relative to the highest cell density within that leaf. Total cells analysed > 370,000.

Figure 3.18 shows the frequency distribution of cells binned by relative cell density, where the bin width is 0.1. As Figure 3.15 demonstrates, there was a general shift over time in all genotypes towards lower relative cell densities, and this is reflected in Figure 3.18 by the peak of the frequency distribution shifting to the left, over time. In addition to this, at early time points, the peaks of distributions were in general greater than at later timepoints, indicating that there was a flattening of the distribution over time and therefore a more even frequency distribution of cells with different relative cell densities, in particular at lower relative cell densities.

The greatest difference in the distributions was between wild type and both *da1-1* and *da1-1bb*. At 7 to 10 days after stratification, a greater proportion of the *da1-1* and *da1-1bb* cells were in higher relative cell density bins, than wild type. The *bb* mutant exhibited a largely similar distribution to wild type, throughout the 5 days sampled. At 11 days after stratification, all four genotypes had largely similar frequency distributions of relative cell density, indicating that leaves had approximately the same proportion of cells at high, middle and low relative cell densities.

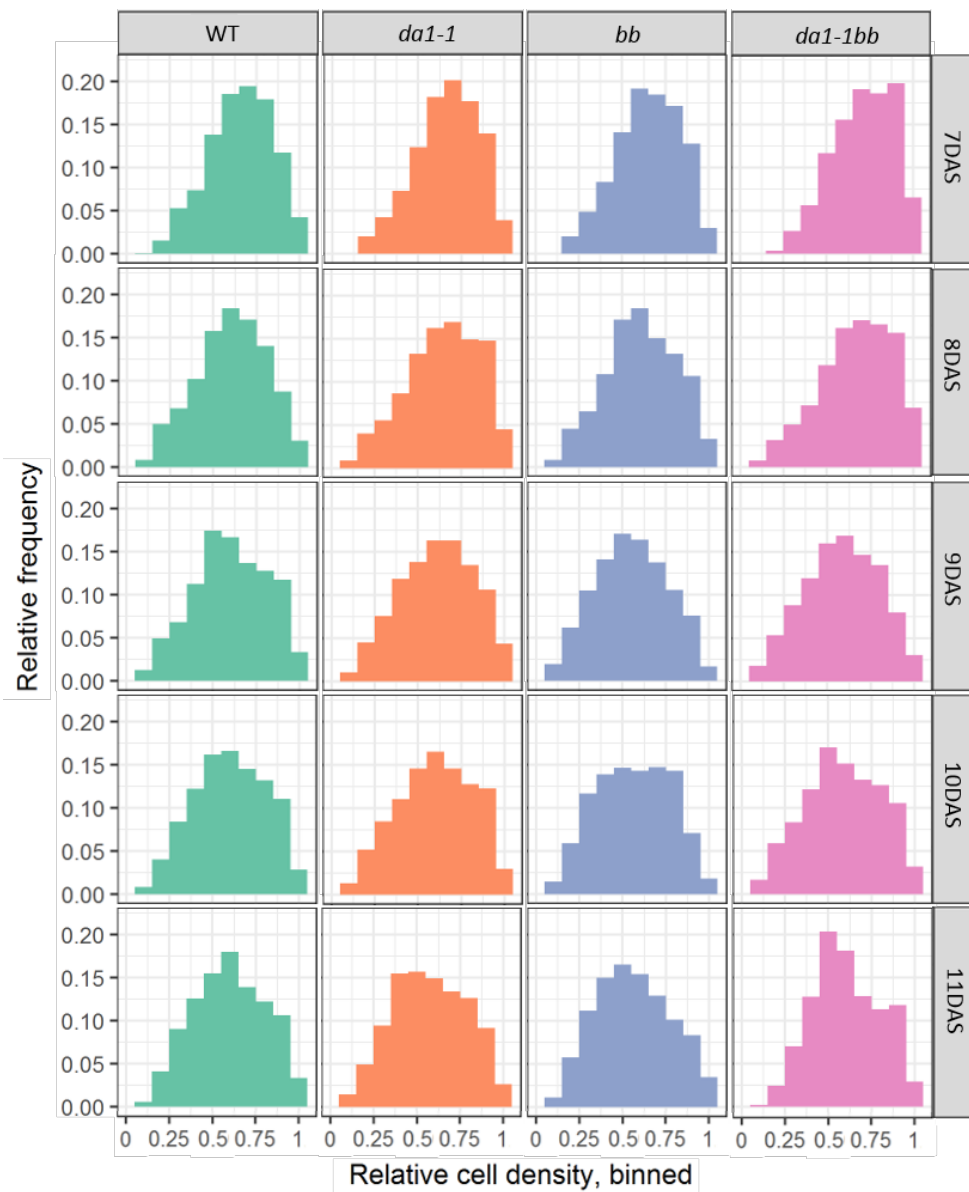


Figure 3.18 Frequency distributions of relative cell densities in wild type, *da1-1*, *bb*, and *da1-1bb* leaves

Histograms of relative frequency of relative cell densities in wild type *pAR169*, *da1-1 pAR169*, *bb pAR169*, and *da1-1bb pAR169* leaves from 7 to 11 days after stratification. Bin width = 0.1. Each histogram represents three pooled independent samples per genotype. Cells in the midvein and the leaf margin are excluded from these data. Total cells analysed > 370,000.

3.3.2.4 Cell circularity in growing leaves

Cell circularity data was extracted from the segmented leaf images, and calculated according to Equation 3.2.

$$Circularity = \frac{4\pi Area}{Perimeter^2}$$

Equation 3.2 Formula for calculating cell circularity

Cell circularity is therefore a function of the relationship between the length of the cell perimeter, and the area of the cell. Using this equation, a perfect circle has a circularity score of 1, and all other shapes are given a decimal score. Simpler shaped cells, therefore, have a higher circularity score, and a lobed cell with a more complex shape has a lower circularity score. This circularity measure is an indicator of cell growth and differentiation.

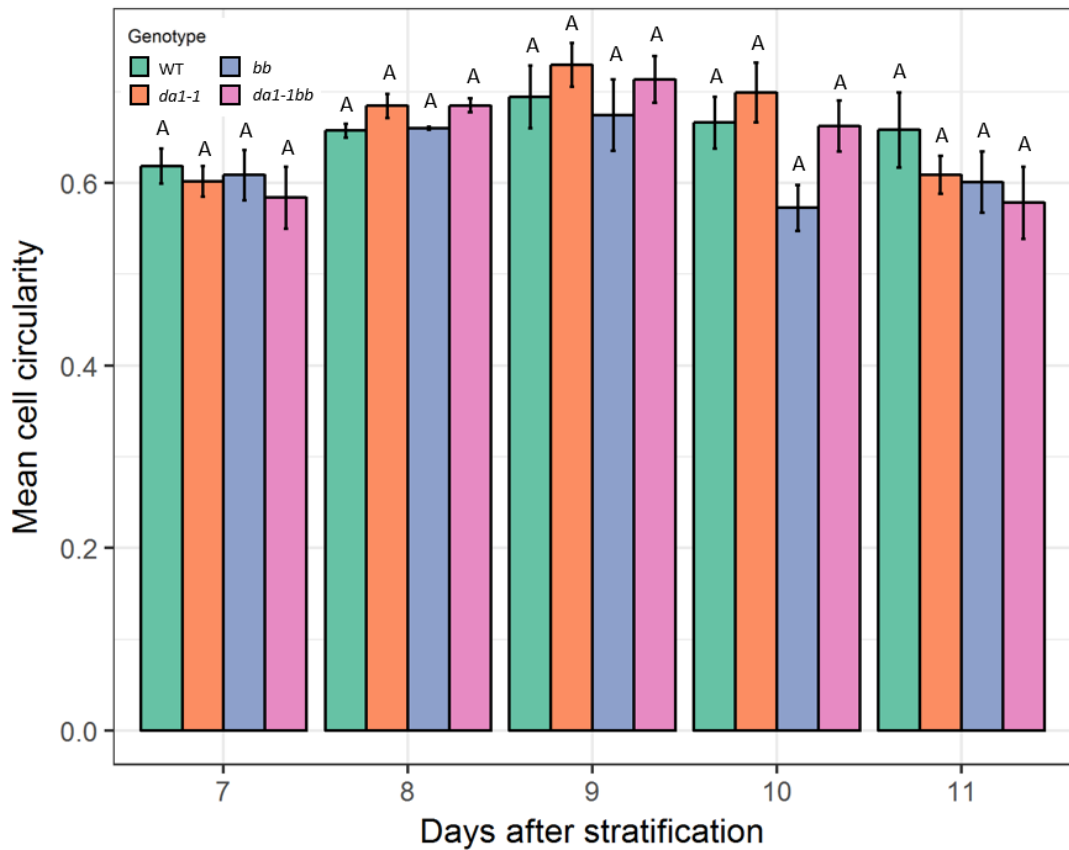


Figure 3.19 Mean cell circularity of wild type, *da1-1*, *bb*, and *da1-1bb* leaves

Mean cell circularity of wild type *pAR169*, *da1-1 pAR169*, *bb pAR169*, and *da1-1bb pAR169* leaves from 7 to 11 days after stratification. Standard error shown (n=3). Small letters indicate significance groups according to ANOVA with a post-hoc Tukey pairwise comparison (variances were equal, p = 0.05). Total cells analysed > 370,000. Cells in the midvein and the leaf margin are excluded from these data.

In Figure 3.19, the mean cell circularity was calculated from three independent samples per genotype, per timepoint, and a mean taken of these. Trends in mean cell circularity over time are not as clear as those for mean cell area or mean relative cell density. Cell circularity appears to rise from around 0.6 at 7 days after stratification in all genotypes, before peaking at 9 days after stratification at around 0.7, and falling again to 0.6 by 11 days after stratification. There were no significant differences between any of the four genotypes at any time throughout the experiment.

Figure 3.20 shows how cell circularity was distributed spatially within the leaf, by relative distance from the leaf tip. The slopes of the linear regression lines fitted to this data show the location of the most and least circular cells, in each genotype and at each timepoint. At 7 days after stratification, the slopes of all four genotypes were relatively flat, with a slight, unexpected, indication of higher cell circularity in the leaf tip than in the base of the leaf. There were no significant differences in slope between any of the genotypes. This indicated relative uniformity in cell circularity across the length of the leaf in all three mutants and the wild type.

At 8 days after stratification, wild type, *da1-1* and *da1-1bb* showed slight slopes indicating a decrease in cell circularity in the tip of the leaf relative to those cells in the base, although the difference in slope relative to 7 days after stratification was only significant in *da1-1* ($p = 0.0034$), and not wild type or *da1-1bb*. Comparatively, the slope of *bb* remained largely flat, indicating uniformity of cell circularity along the leaf. The slope of the *bb* mutant was found to be significantly flatter than both wild type ($p = 0.0103$) and *da1-1* ($p = 0.0179$).

At 9 days after stratification, all genotypes exhibited a steeper gradient of cell circularity along the leaf, indicating a greater differential between the cells in the tip of the leaf with a low circularity score, and the cells in the base with a higher circularity score. In wild type ($p = 0.0131$), *da1-1* ($p = 0.0058$) and *da1-1bb* ($p = 0.0296$) but not *bb* ($p = 0.0631$) difference in slopes from 8 to 9 days after stratification was significant. Within the 9 days after stratification time-point, *da1-1* exhibited a steeper slope than *da1-1bb* ($p = 0.0434$), although there were no other significant differences in slope between genotypes.

There was no significant change in slope for any genotype between 9 and 10 days after stratification, nor between 10 and 11 days after stratification. In addition to this, at neither 10 nor 11 days after stratification did any of the genotypes show any significant difference in slope from each other, within genotype. This indicated that the distribution of cell circularity along the leaf was uniform across genotypes, and across both time-points.

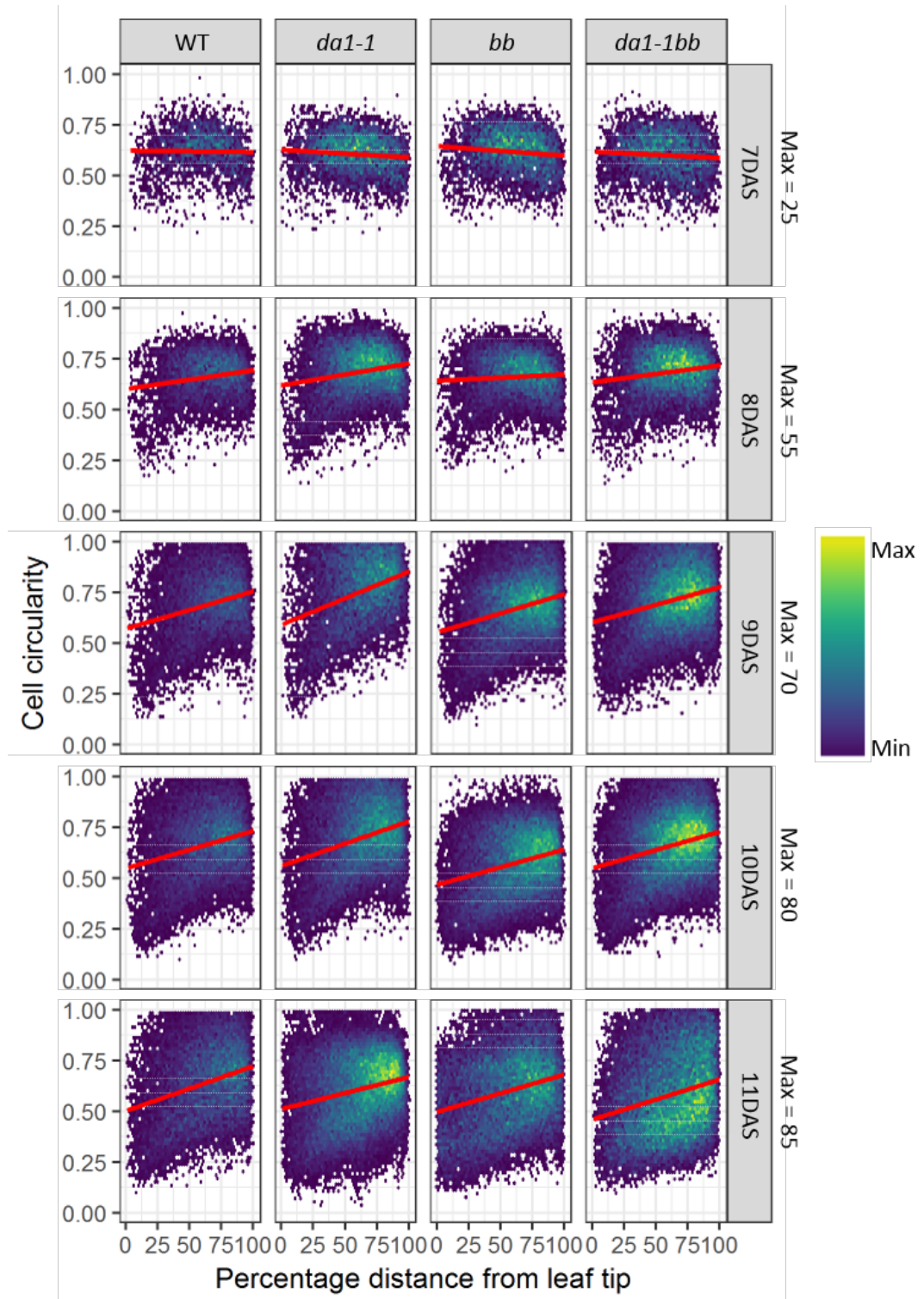


Figure 3.20 Cell circularity distributions within wild type, *da1-1*, *bb*, and *da1-1bb* leaves

Binned hex-plots of cell circularity by relative distance from the leaf tip in wild type *pAR169*, *da1-1 pAR169*, *bb pAR169*, and *da1-1bb pAR169* leaves from 7 to 11 days after stratification. Each heatmap represents three pooled independent samples. Red lines indicate linear regressions. Cells in the midvein and the leaf margin are excluded from these data. Total cells analysed > 370,000.

Figure 3.21 shows the frequency distribution of different cell circularity scores between genotypes and across the 5-day sampling period. At 7 days after stratification, in all genotypes, the bin containing the highest proportion of cells was 0.55-0.65, peaking at between 30% and 40% of cells. At 11 days after stratification, the frequency distribution of all genotypes was flatter, and the proportion of cells in each bin was more equal. The same pattern of a rise in cell circularity to 9 days after stratification, followed by a fall, as observed in Figure 3.19 may also be observed in the frequency distribution. There were no strong differences between any of the genotypes, at any time-point, in the frequency distribution of cell circularities.

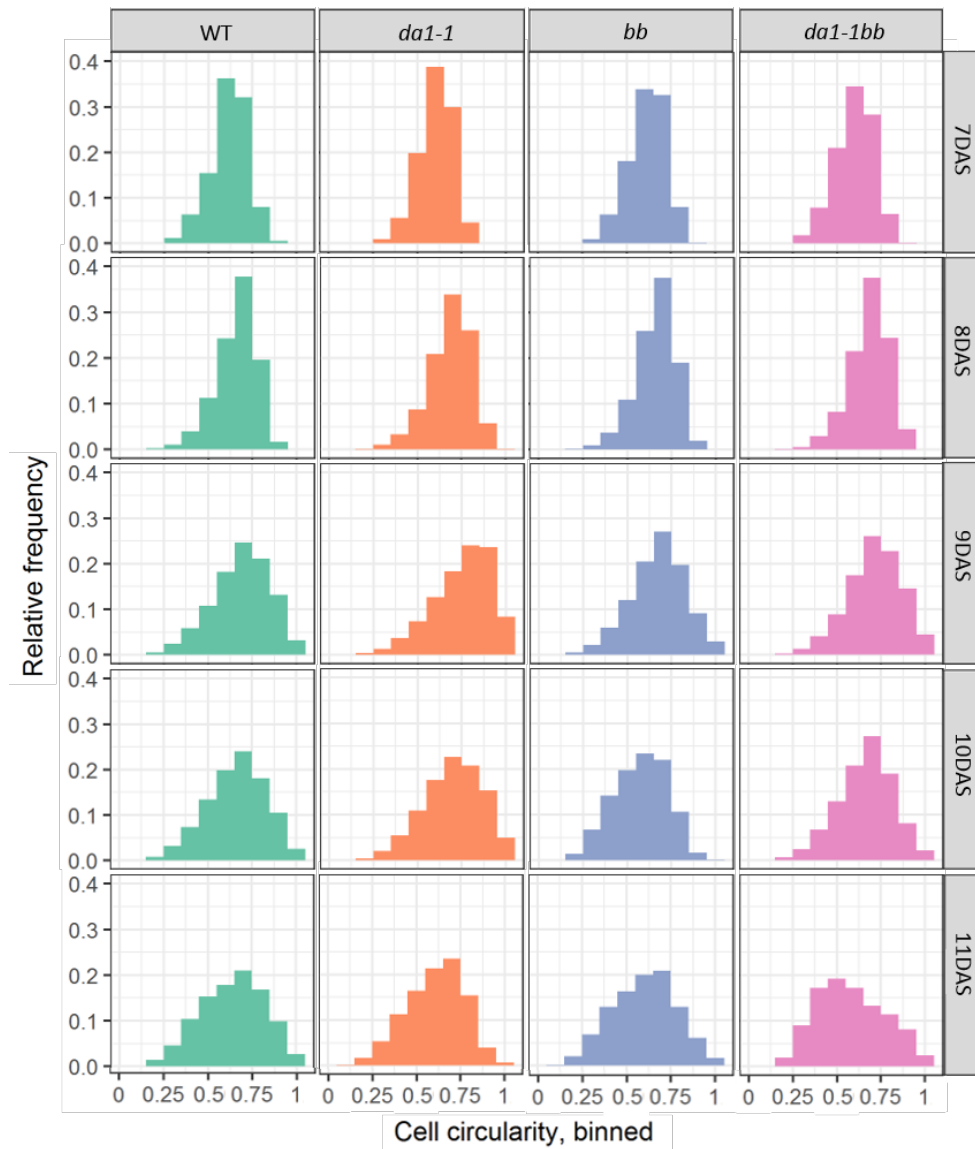


Figure 3.21 Frequency distributions of cell circularities in wild type, *da1-1*, *bb*, and *da1-1bb* leaves

Histograms of relative frequency of cell circularities in wild type *pAR169*, *da1-1 pAR169*, *bb pAR169*, and *da1-1bb pAR169* leaves from 7 to 11 days after stratification. Bin width = 0.1. Each histogram represents three pooled independent samples. Cells in the midvein and the leaf margin are excluded from these data. Total cells analysed > 370,000.

3.3.3 Cellular phenotype in mature leaves

To determine the final size and shape of cells in mature leaves, scanning electron microscopy was used to image areas of cells at the base, middle and tip of the blades of 8 to 11 leaves per genotype, at 33 days after stratification, as shown in Figure 3.22. Scanning electron microscopy was used in this experiment as it was not possible to image cells using the *pAR169* line used in Section 3.3.2. This is because, as leaves age, the brightness of the fluorescent reporter line is reduced and it was not possible to achieve high quality images using a confocal microscope.

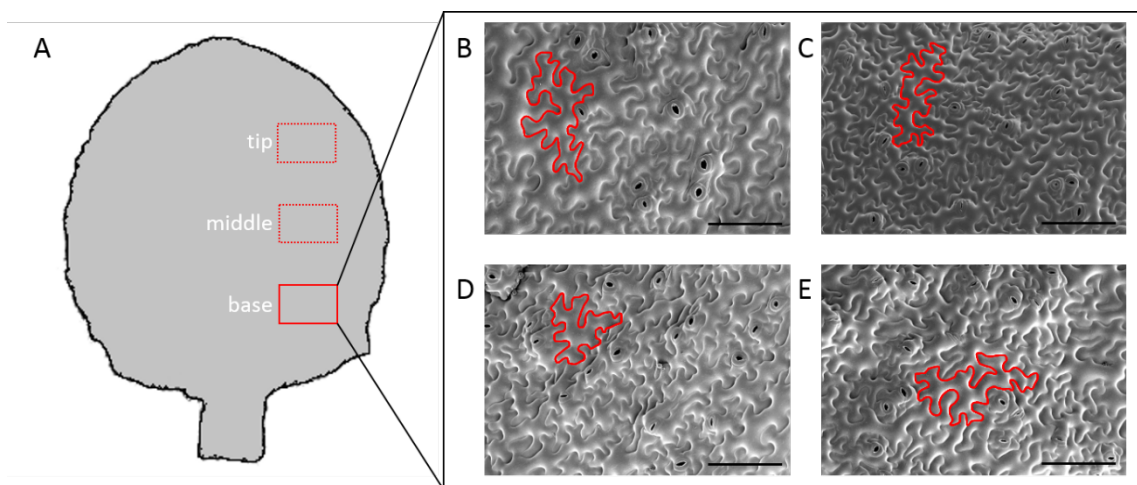


Figure 3.22 Collection of SEM images from mature leaves

Red boxes show the location of tip, middle and base images on the leaf blade (A). Images from the base of the leaf blade of the first leaf of wild type *pAR169* (B), *da1-1 pAR169* (C), *bb pAR169* (D), and *da1-1bb pAR169* (E). Leaves were imaged when mature (33 days after stratification). Scale bars represent 100 μ m. Red outlines show examples of epidermal pavement cells (not intended as representative).

The area and perimeter of approximately 20 pavement cells per image was measured manually (stomatal guard cells were excluded) using ImageJ, and the circularity of the cell calculated from these measurements according to Equation 3.2 (Section 3.3.2.4). Cell circularity is represented as a decimal, where a score of 1 denotes a perfect circle.

3.3.3.1 Cell shape and size varies between genotypes in mature leaves

For this analysis, the mean was taken of the base, middle and tip measurements from each leaf of each genotype. Each leaf represented a single biological replicate. These means were then used for the statistical analyses.

A summary of these data is represented in Table 3.5.

Genotype	Final cell area (μm^2)	Percentage of wild type	Final cell perimeter (μm)	Percentage of wild type	Final cell circularity	Percentage of wild type
wild type <i>pAR169</i>	2439.55 (+/- 111.242)	100%	394.97 (+/- 13.098)	100%	0.241 (+/- 0.008)	100%
<i>da1-1</i> <i>pAR169</i>	1937.21 (+/- 75.941)	79%	356.76 (+/- 8.285)	90%	0.254 (+/- 0.004)	105%
<i>bb</i> <i>pAR169</i>	2132.54 (+/- 92.582)	87%	382.66 (+/- 13.264)	97%	0.229 (+/- 0.006)	95%
<i>da1-1bb</i> <i>pAR169</i>	2491.21 (+/- 188.119)	102%	407.61 (+/- 21.896)	103%	0.236 (+/- 0.011)	98%

Table 3.5 Cell area, perimeter, and circularity in mature leaves

The data from mature leaves showed a reduction of final cell area in the *da1-1* mutant, where cells on average were only 79% of wild type size. This is shown in Figure 3.23. There was a weak but non-significant reduction in mean cell size in the *bb* mutant, while the cells of the *da1-1bb* mutant were approximately the same size as wild type, at 102% of wild type area. The mean cell area of *da1-1* mutants was significantly decreased relative to *da1-1bb* mutants.

Cell perimeter measurements indicated that there was no significant difference in cell perimeter between any of the genotypes. Additionally, cell circularity was not significantly different between any of the genotypes.

The variation was greater in the wild type and *da1-1bb* double mutant samples than in those of the single *da1-1* or *bb*, where the data are more closely clustered around the mean of the dataset.

Together, these data indicate that the cells in mature *da1-1* leaves are slightly more likely to be smaller, have a decreased perimeter, and to be more circular than wild type and the *bb* and *da1-1bb* mutants. The decrease in perimeter is likely to be in part as a result of the decrease in cell area.

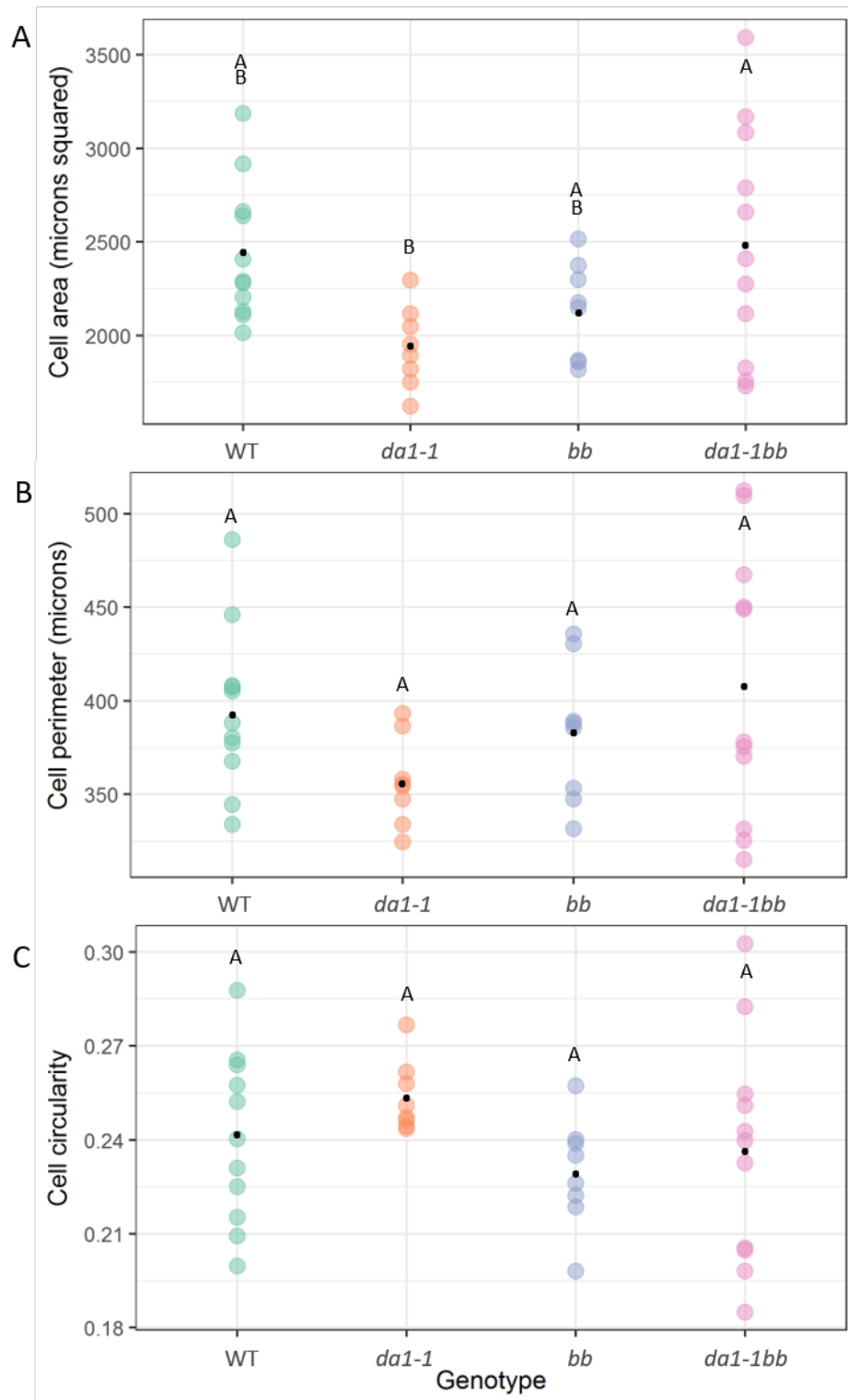


Figure 3.23 Cell area, perimeter, and circularity in mature leaves

Area (A), perimeter (B), and circularity (C) of epidermal pavement cells of wild type *pAR169*, *da1-1 pAR169*, *bb pAR169*, and *da1-1bb pAR169* mature leaves. The first leaf was sampled at 33 days after stratification. Black points indicate means of samples. Small letters indicate significance groups according to ANOVA with a post-hoc Tukey pairwise comparison (variances were equal, $p = 0.05$).

3.3.3.2 Patterning of cell size and shape across sampling positions in the leaf varies between genotypes

For this analysis, the mean was taken of each of the base, middle, and tip measurements from each leaf of each genotype. These means were then used for the statistical analyses.

As well as the variation in overall cell area, perimeter, and circularity, these data can also be further interrogated to identify variation of cell size and shape across genotypes at different sampling positions in the leaf. These data are summarised in Table 3.6.

Genotype	Cell area (μm^2)			Cell perimeter (μm)			Cell circularity		
	Base	Middle	Tip	Base	Middle	Tip	Base	Middle	Tip
wild type	2574.3	2774.6	2066.9	386.3	432.6	380.9	0.2752	0.2339	0.2176
pAR169	+/- 232	+/- 269	+/- 111	+/- 27.0	+/- 29.8	+/- 13.4	+/- 0.01	+/- 0.01	+/- 0.01
da1-1	2023.3	2066.9	1721.5	363.1	363.2	343.9	0.2624	0.2711	0.2272
pAR169	+/- 111	+/- 176	+/- 118	+/- 18.2	+/- 22.7	+/- 16.6	+/- 0.01	+/- 0.01	+/- 0.01
bb	2022.6	2223.7	2151.2	345.4	406.5	394.5	0.2565	0.2241	0.2081
pAR169	+/- 66	+/- 124	+/- 138	+/- 14.9	+/- 17.8	+/- 19.6	+/- 0.01	+/- 0.01	+/- 0.01
da1-1bb	2245.8	2755.6	2472.2	365.1	443.1	414.5	0.2656	0.2240	0.2193
pAR169	+/- 218	+/- 326	+/- 178	+/- 27.6	+/- 41.0	+/- 20.0	+/- 0.01	+/- 0.02	+/- 0.01

Table 3.6 Cell area, perimeter, and circularity across sampling positions in mature leaves

Measurements of cell area in the tip of the leaf found that, as expected based on overall cell area measurements described in Section 3.3.3.1, *da1-1* plants had the smallest cells, although this difference was only significant relative to *da1-1bb* (Figure 3.24). Samples taken from the middle and basal areas of the leaf blade reflected this trend, but the reduction in cell area of *da1-1* plants was not significant.

Cell perimeter measurements indicated that there was little variation between genotypes in the pattern of variation within a leaf (Figure 3.25). Cell perimeters in the middle and base of the leaf blade showed no significant differences across wild type, *da1-1*, *bb*, and *da1-1bb*.

Finally, cell circularity also showed little variation between genotypes at different sampling points within the leaf (Figure 3.26).

3.3.3.3 Cell shape and size varies between sampling positions, within genotypes

In all four genotypes tested, the largest cells measured were found in the middle of the leaf blade (Figure 3.24, Table 3.6). In wild type and *da1-1*, the smallest cells were in the tip of the leaf, whereas in *bb* and *da1-1bb* the smallest cells were in the base of the leaf. Although these differences are largely non-significant (with the exception of wild type, where cells in

the base were significantly larger than cells in the tip of the leaf, $p = 0.0152$), they therefore overall represent a trend across genotypes for the largest cells in the mature leaf to be in the middle of the leaf blade.

Furthermore, in all four genotypes, the cells with the longest perimeters were also found in the middle of the leaf blade, although these differences are again not statistically significant (Figure 3.25, Table 3.6). The cell perimeter in the base of *da1-1* leaves is almost exactly equal to that of the perimeter in the middle of the leaf, a pattern that is not reflected in wild type or the other mutants.

Finally, in all genotypes, the most circular cells (with scores of over 0.25) were found in the base of the leaf, and the cells in the tip of the leaf blade were statistically significantly less circular than in the base, in all genotypes (Figure 3.26, Table 3.6). However, the *da1-1* mutant maintains this higher level of cell circularity in the cells of the middle of the leaf blade, where the other mutants and wild type have cell circularity scores of around 0.225. The difference between cell circularity in the tip and in the middle of the leaf is also strongly significant in *da1-1* plants, an observation not made in the wild type or other mutants. In the tip of the leaf blade, all four genotypes have a largely equal cell circularity score.

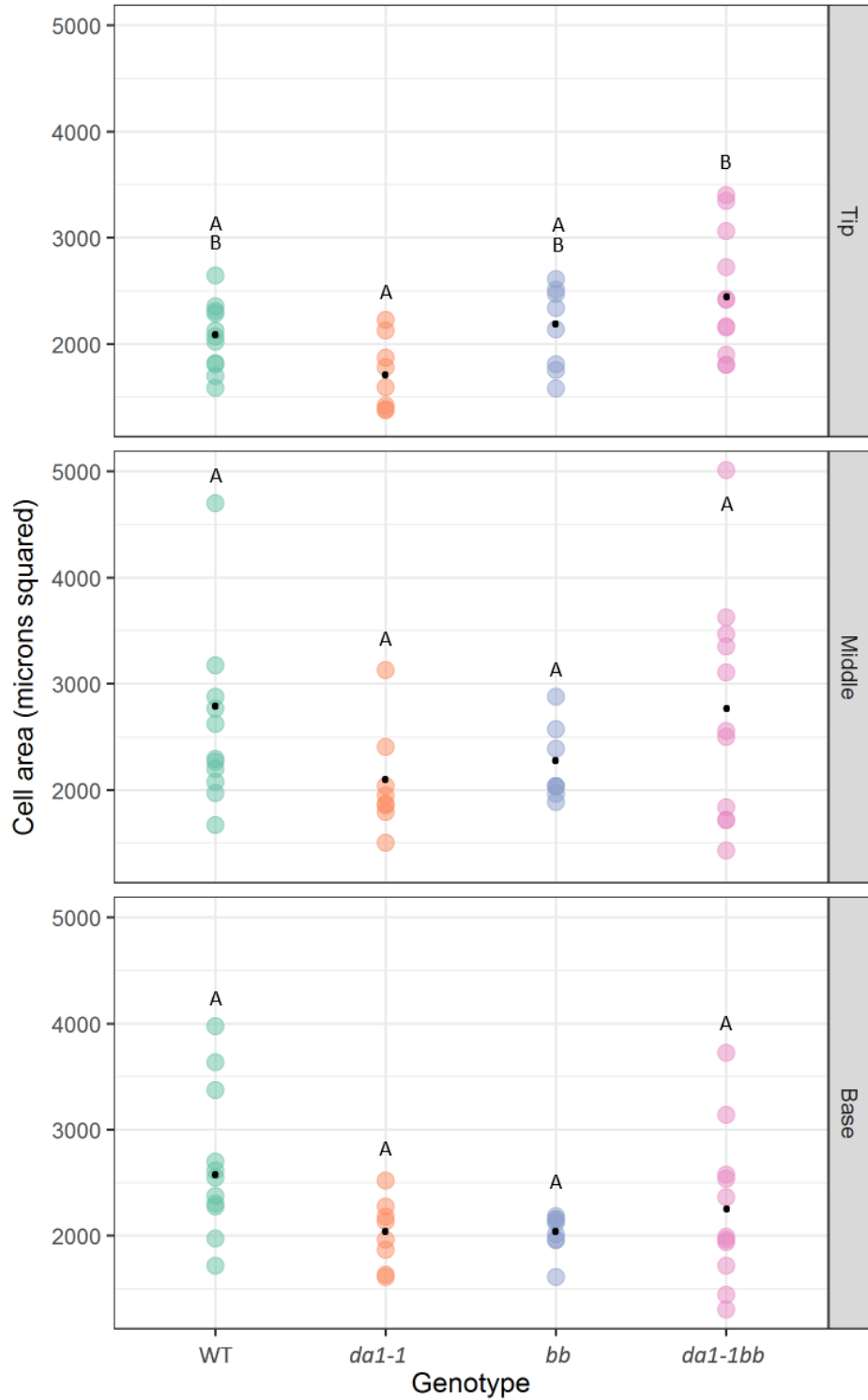


Figure 3.24 Cell area by location in mature leaves

Area of epidermal pavement cells of wild type *pAR169*, *da1-1 pAR169*, *bb pAR169*, and *da1-1bb pAR169* mature leaves in the tip, middle and base positions of the leaf blade. The first leaf was sampled at 33 days after stratification. Black points indicate means of samples. Small letters indicate significance groups according to ANOVA with a post-hoc Tukey pairwise comparison (variances were equal, $p = 0.05$).

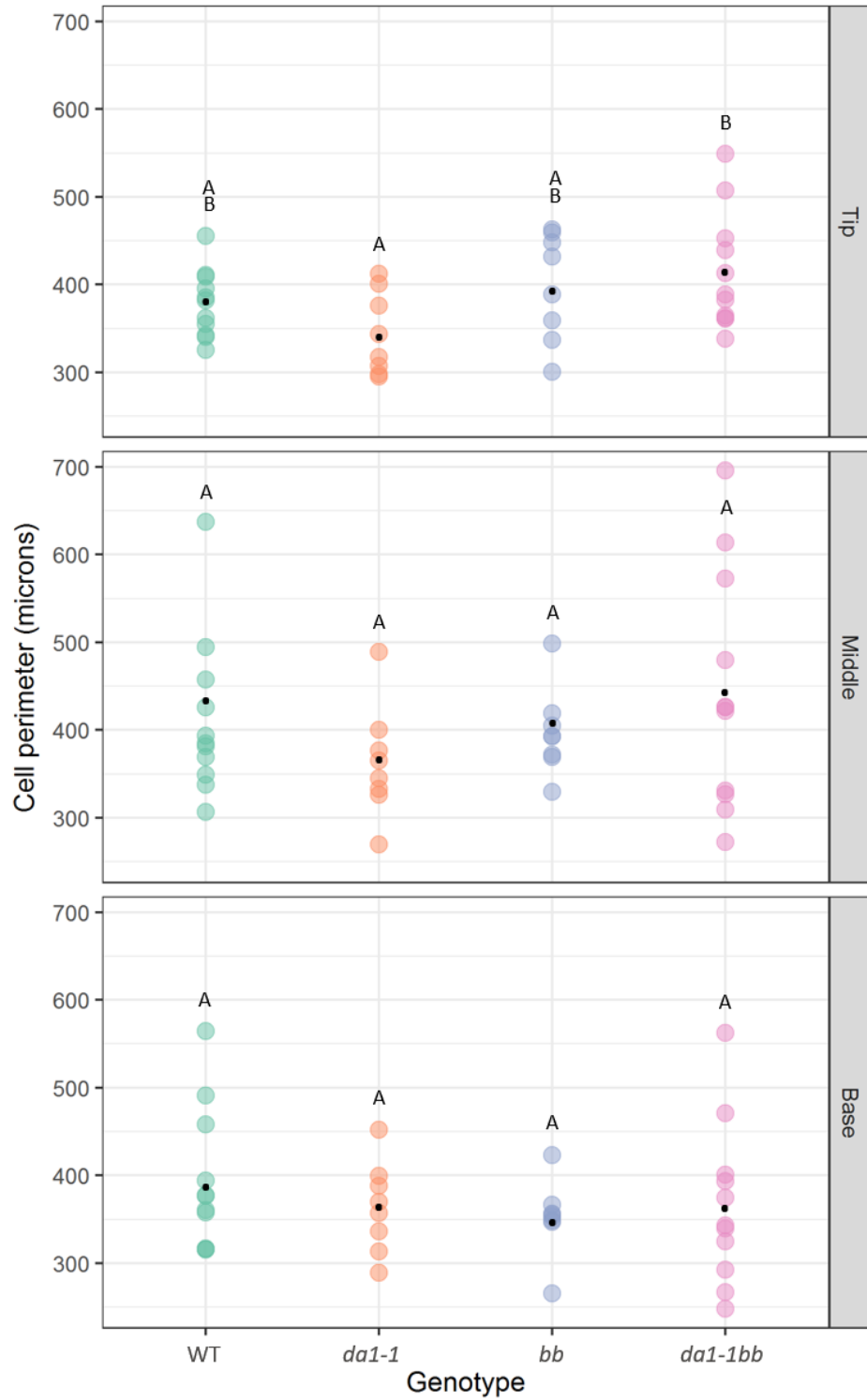


Figure 3.25 Cell perimeter by location in mature leaves

Perimeter of epidermal pavement cells of wild type *pAR169*, *da1-1 pAR169*, *bb pAR169*, and *da1-1bb pAR169* mature leaves in the tip, middle and base positions of the leaf blade. The first leaf was sampled at 33 days after stratification. Black points indicate means of samples. Small letters indicate significance groups according to ANOVA with a post-hoc Tukey pairwise comparison (variances were equal, $p = 0.05$).

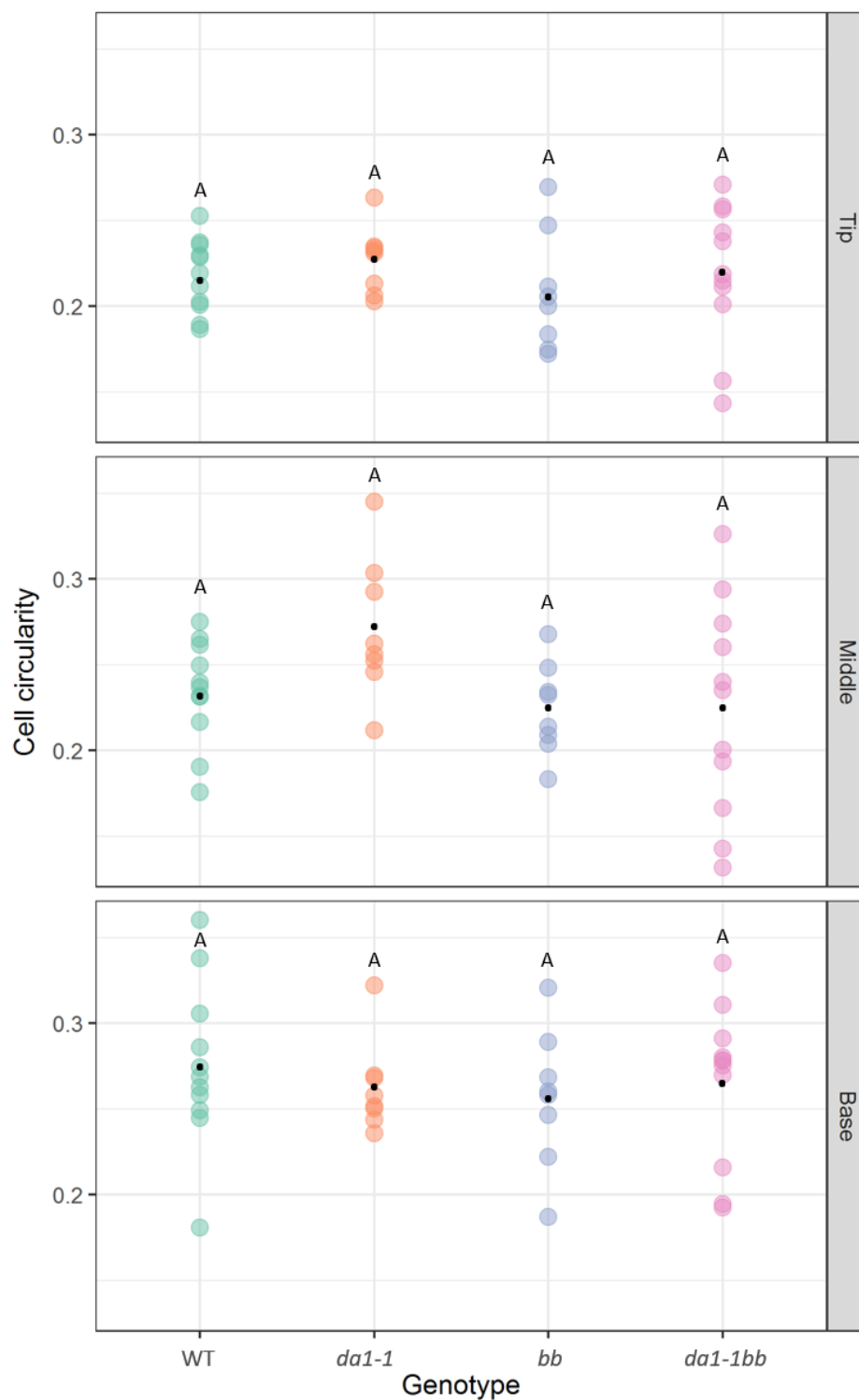


Figure 3.26 Cell circularity by location in mature leaves

Circularity of epidermal pavement cells of wild type *pAR169*, *da1-1 pAR169*, *bb pAR169*, and *da1-1bb pAR169* mature leaves in the tip, middle and base positions of the leaf blade. The first leaf was sampled at 33 days after stratification. Black points indicate means of samples. Small letters indicate significance groups according to ANOVA with a post-hoc Tukey pairwise comparison (variances were equal, $p = 0.05$).

3.4 Discussion

In this Chapter, I have quantitatively analysed parameters of growth of wild type and *da1-1*, *bb*, and *da1-1bb* mutant *Arabidopsis thaliana* at both the whole-organ and the cellular level. My findings support many aspects of the published literature on the activity of *DA1* and *BB*, while also challenging other previously published findings, and adding to our knowledge in other areas. They also provide a quantitative foundation for future studies of the functions of *DA1* and *BB* in the control of organ size and shape. Finally, this work establishes a new cellular basis for understanding the functions of other genes controlling organ growth.

3.4.1 *da1-1*, *bb*, and *da1-1bb* mutants exhibit increased leaf sizes throughout growth and at final size

Several independent studies have shown that *da1-1* mutants exhibit an increased final leaf weight and leaf area relative to wild type (Li et al., 2008; Dong et al., 2017; Vanhaeren et al., 2017), but data presented in this Chapter show that this increase in leaf area is primarily derived from an increase in leaf width. While both leaf width and leaf length were increased in *da1-1*, *bb*, and *da1-1bb* mutants relative to wild type, the greater increase was in leaf width. Li et al. observed the more rounded appearance of *da1-1* leaves relative to wild type, and this observation of increased leaf width relative to the increase in length supports this. These findings suggest that *DA1* may more strongly control growth in the mediolateral than proximodistal direction.

Previous observations have suggested that *bb-2* mutant leaves exhibited a shorter but wider leaf phenotype, although no significant increase in final leaf area. This is despite the over-expression of *BB* promoting a strong reduction in leaf area (Disch et al., 2006). Contrary to this, data shown in Section 3.3.1.1 demonstrated a small but significant increase in final width, length, and area in *bb-2* mutants, relative to wild type. One possibility to explain this discrepancy in observation is that Disch et al. used a leaf other than the first or second leaves to measure width, length, and area. Other work has shown that the increased leaf size phenotype of *bb-2* mutants is found only in the first leaf pair (Vanhaeren et al., 2017), and Disch et al. do not record which leaf was used for the measurements that they cite. Another potential explanation is that, given that the plant material in Disch et al. was grown in pots on soil rather than on GM on plates, and the considerable differences in leaf shape and size of *Arabidopsis* grown on soil and on synthetic media, the *bb-2* phenotype may be weaker in soil-grown plants than those grown on media.

DA1 and *BB* were first shown to interact synergistically to produce a greater than additive increase in final organ size in Li et al. 2008, and this was confirmed in leaf area measurements by Vanhaeren et al. 2017. The data presented in Section 3.3.1.1 adds to this by confirming that a synergistic interaction is observed in both the increases in final leaf width and length. The data presented here also showed that, while *da1-1* and *bb* showed significant increases in width, length, and area from the very earliest stages of growth, the synergistic interaction between *da1-1* and *bb* is present in the *da1-1bb* double mutant as early as 9 days after stratification, and is maintained throughout growth to final size. At very early stages, before 9 days after stratification, the interaction is not synergistic as the *bb* mutant leaf is approximately the same size, or larger, than the *da1-1bb* mutant, indicating a separable role for *BB* in controlling very early leaf growth.

The determinate final organ sizes of *da1-1*, *bb*, and *da1-1bb* have been studied extensively over more than ten years (Disch et al., 2006; Li et al., 2008; Dong et al., 2017; Vanhaeren et al., 2017), yet the data presented in this Chapter suggest that future work could include further analysis of the leaf shape phenotypes observed in these mutants. This could also include further analysis of the phenotypes of soil-grown plants. Plants grown on soil provide a more accurate representation of the true nutrient regimes in which crop plants are grown, compared to growth on plates on synthetic medium. If the differences observed in the *bb-2* final leaf area phenotype are as a result of different growth conditions, and the phenotype is less strong in soil-grown plants, this could provide insights into the interplay between genetic networks controlling the formation of determinate plant organs, and other, external factors.

3.4.2 *da1-1*, *bb*, and *da1-1bb* mutants exhibit increased rates of leaf growth

Li et al. showed that the leaf area of the *da1-1* mutant increased at a faster rate than wild type, but it was thought that the primary factor contributing to the increased final organ size was an increase in the duration of growth (Li et al., 2008). While my data confirms that there is an increase in the duration of leaf growth in *da1-1*, *bb*, and *da1-1bb* mutants relative to wild type, it also shows that there is a significant increase in the rates of leaf growth of these mutants, in the linear phase of growth (Section 3.3.1.5). As expected, based on its greatest final size, the *da1-1bb* mutant exhibited the largest and most significant increase in linear growth rate relative to wild type. In conjunction with this, Section 3.3.2.1 describes the first experiment determining the total leaf epidermal pavement cell number of wild type, *da1-1*, *bb*, and *da1-1bb* mutants over time. In this experiment it was found that, not only do all three mutants studied exhibit higher mean total cell numbers, but that they also all exhibit an

increased rate of increase in total cell number, relative to wild type. Together, these data provide the first indications that there could be a role for *DA1* and *BB* in the control of the rate of cell proliferation, as well as the duration of cell proliferation.

With knowledge of the biochemical activity of *DA1*, possible mechanisms for this include cleavage by *DA1* of positive regulators of the cell cycle, for example CDKs or cyclins. Alternatively, *DA1* could affect other regulators of cell division, for example the controller of cell size at division, whereby a smaller minimum cell volume of division could be set in the *da1-1* mutant, allowing more frequent cell divisions during the proliferative phase. As well as promoting the peptidase activity of *DA1*, as an E3 ligase *BB* could also independently target regulators of the cell cycle for degradation in the proteasome. This could happen in much the same way as the E3 ubiquitin-ligase Skp1, Cullin, F-box complex targets E2Fc, part of an inducer complex for S-phase specific CDKs in the cell cycle (Francis, 2007).

Future work in this area could include assaying *DA1* peptidase activity against a range of cell cycle regulators directly, rather than genes that may regulate the cell cycle (as was the approach in Chapter 2). Potential targets to be tested could include cyclins and CDKs involved in the promotion of progression through the cell cycle. The same set of targets could also be assayed for ubiquitination by *BB*. Using qPCR, it could be interesting to determine if the expression of these genes involved in the control of the cell cycle is affected in the *da1-1*, *bb*, or *da1-1bb* mutants in any way - for example, genes involved in promoting progression through the cell cycle could be up-regulated in the mutants relative to wild type during the cell proliferation phase, or the period of expression could be lengthened. This would confirm a direct effect for *DA1* or *BB* on the control of the cell cycle, and therefore cell division. This area of research has begun to be explored in Vanhaeren et al., 2017, but could be expanded further to focus specifically on proteins involved in the arrest of cell proliferation. Finally, a key experiment to determine the rate and duration of cell proliferation in the mutants relative to wild type is to dynamically track cells in the growing leaf, and determine the spatial and temporal characteristics of the zone of cell proliferation. Using this method could also reveal further characteristics of cell division in the mutants and in wild type, for example cell area at cell division, the symmetry of cell divisions, and the average number of division cycles each cell completes before exiting the proliferative phase. This approach has been taken in this thesis, in Chapter 4.

3.4.3 Increased mature leaf size in *da1-1*, *bb*, and *da1-1bb* mutants is due to increased cell number, not cell size

This thesis is the first study of pavement cells in mature leaves of the *da1-1* and *da1-1bb* mutants, although pavement cell area was investigated earlier by Disch et al. in *bb* mutants. It was found that *bb* mutants exhibit no significant change in cell area in mature leaves from wild type (Disch et al., 2006), an observation that the findings reported in Section 3.3.3.1 support. In addition to this, however, the data presented here show a significant reduction in cell area for *da1-1* mutants. Interestingly, this effect of the *da1-1* mutation is not reflected in the *da1-1bb* double mutant. This suggests that the presence of a functional copy of *BB* could be required to effect this reduction in final cell size, as well as that the increased mature leaf area in all three mutants is as a result of increased final cell number, rather than final cell size.

One possible model to explain the interaction of *DA1* and *BB* to control final cell size could be that normal *BB* expression promotes a smaller final cell size, but only when there is no functional copy of *DA1*, which would normally work antagonistically to *BB* and promote the wild type final cell size (Figure 3.27). This model is supported by the observations presented here: in the *da1-1bb* double mutant, the *bb* mutation does not promote smaller cells therefore final cell size is similar to wild type, and there is no need for a functional copy of *DA1* to maintain this. In the *bb* single mutant, there is no promotion of smaller cells by *BB* therefore there is no change in mature cell size. In the *da1-1* single mutant, however, the functional copy of *BB* promotes a smaller than wild type final cell size, which is not counteracted by *DA1* and therefore results in a smaller final cell size.

This model does not immediately appear to conform to a previous observation that a *35S::BB* overexpressor line exhibited significantly increased pavement cell area in mature leaves, relative to wild type (Vanhaeren et al., 2017), suggesting that *BB* could promote increased final cell area, rather than decreased. However, with the knowledge of the biochemical interactions of *DA1* and *BB*, it could be possible that constitutive overexpression of *BB* in this way promotes an abnormally high level of *DA1* activity, which could result in a more extreme response to the smaller cell areas promoted by *BB*, and finally result in increased cell area. At the same time, the *35S::GFP-DA1* overexpressor line may not have exhibited larger cells for this reason, as the E3 ligases required for its activation, *BB* and *DA2*, may not have been expressed highly enough to sufficiently enhance its activity relative to wild type.

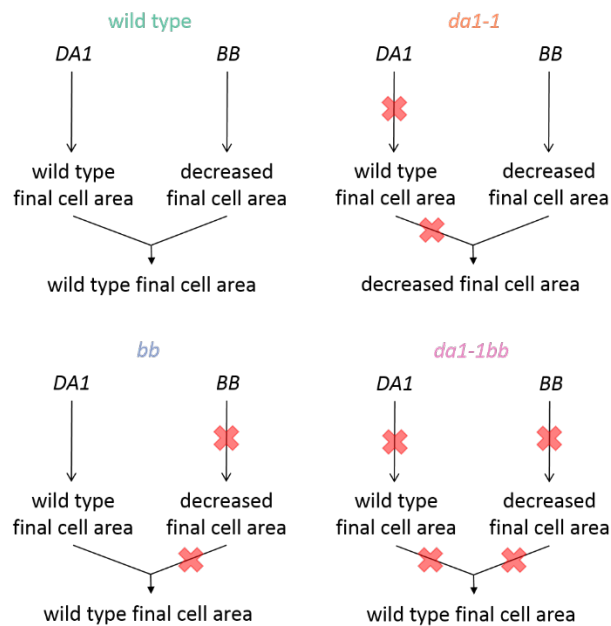


Figure 3.27 Proposed model for the activity of *DA1* and *BB* in the control of final cell area

To confirm or refute this model, a potential future course of work could be to create a *35S::BB* overexpressor line in a *da1-1* background, and a *35S::GFP-DA1* overexpressor line in a *bb* background. Based on the model proposed above, in the *da1-1 35S::BB* plants one would expect to observe an extremely small final cell size, and a final cell area comparable to that of wild type plants in *bb 35S::GFP-DA1*.

These data also raise the alternative possibility that *DA1* is somehow involved in the so-called compensation mechanism, the theory that suggests that defects in cell proliferation in certain mutants can result in subsequent changes to the cell expansion phase of growth, resulting in a final leaf area similar to that of wild type (Hisanaga et al., 2015, also explored further in Chapter 1). If *DA1* was involved in the mechanism by which leaves achieve these changes in cell expansion, mediating their final leaf area, then it could be expected that the *da1-1* mutant would exhibit some aberrant cell expansion. Investigating the expression of *DA1* by qPCR in mutants in which a compensatory effect has been observed, such as *aintegumenta*, *erecta*, or *struwwelpeter* (Hisanaga et al., 2015) could provide an insight into whether *DA1* could be partially involved in the control of cell area in the compensation mechanism.

3.4.4 Mutations in *DA1* and *BB* also affect other cell characteristics throughout growth and in mature leaves

In this Chapter, data on cell circularity throughout growth and in mature leaves is presented, as well as cell area and cell density throughout growth. By segmenting and analysing almost all cells in the leaf (with the exception of cells in the leaf margin and in the midvein, as described in Section 3.3.2), it has been possible to analyse the spatial distribution of these characteristics throughout the leaf.

3.4.4.1 *Cell circularity is not strongly affected by mutations in DA1 or BB*

Cell circularity may be used as an indicator of the developmental age of tissue - that is, those cells that remain smaller and rounder are more likely to be younger, and remain in the zone of competence to divide in the base of the leaf. Conversely, those cells with a greater perimeter to area ratio and therefore a lower circularity score are more likely to be exhibiting the characteristic “lobed” shape of a differentiated pavement cell, and are likely therefore to be developmentally older, in the tip of the leaf, and no longer able to divide. It is possible therefore, that the proportion of cells at a higher circularity in a leaf could be an indicator of the proportion of the cells in the leaf that are still in their proliferative phase.

Mean cell circularity over time exhibited no significant differences between phenotypes, and no real trend over time. The apparent rise in cell circularity in early developmental stages (7 to 9 days after stratification) could be the result of a systemic issue with the segmentation software. The perimeter of the cell in an image of a leaf must, by definition, be formed of pixels. Although to the observer the boundaries of cells appear to be smooth lines, they are in fact slightly jagged as the pixels produce curved lines. In a cell with a very large number of pixels in cell area, this jagged effect does not significantly affect the length of the perimeter in relation to the area, but where the number of pixels within the cell is very small, this can be a significant and confounding effect, resulting in a lower circularity score. As cells in the younger leaves were smaller than in the larger leaves (Figure 3.12) this impact was greater and is reflected in Figure 3.19. Some cells were affected particularly strongly by this issue, perhaps due to variation in image quality across the leaf, and generated circularity scores that were outside the mathematically expected range of 0 - 1. These cells were included in the cell counts for total cell number, but were excluded from the subsequent data analysis, and can be seen as white cells in the heatmaps.

The spatial distribution of cell circularity (Figure 3.20) shows how the gradient of cell circularity forms over time, from a relatively uniform spread at 7 days after stratification in

all genotypes, to a steeper gradient at later time-points. The *bb* and *da1-1bb* mutants both appeared to maintain a flatter gradient in cell circularity for longer than wild type and *da1-1*, indicating that there was less difference between the circularity in the base and the tip of the leaf. Conversely, the *da1-1* and *da1-1bb* mutants exhibited a higher frequency of more circular cells (Figure 3.21). In mature leaves, the data were also fairly inconclusive, revealing no strong trends between genotypes and sampling positions (Section 3.3.2.4). Together, these weak and conflicting results suggest that cell circularity may not be the most useful parameter with which to compare wild type and the mutants.

3.4.4.2 Cell area is reduced during growth in *da1-1* and *da1-1bb* mutants

Data shown in Section 3.3.2.2 shows that mean cell area is reduced relative to wild type in *da1-1* and *da1-1bb* mutants, while *bb* exhibits no significant change. However, at 11 days after stratification, *da1-1bb* mutants exhibited mean cell areas approximately equivalent to those of wild type. It is possible that some kind of transition begins to occur at around this time, beyond which the cell area fates of *da1-1* and *da1-1bb* mutants diverge, resulting in their differing final cell areas. According to the model proposed in Figure 3.27, this transition could be activated by *BB* expression, resulting in smaller cells in *da1-1* mutants but wild type size in the *da1-1bb* mutant. Figure 3.14 also shows that *da1-1* and *da1-1bb* have more small cells, and fewer large cells, than wild type and *bb*. Comparing the mutants between time-points shows that the *da1-1* and *da1-1bb* cell area frequency distributions are relatively similar to that of wild type, at one day earlier in the sampling period. This, in conjunction with the delayed appearance of a strong gradient in cell area along the leaf in *da1-1bb* mutants (Figure 3.13), suggests that *da1-1* and *da1-1bb* could be at a tissue developmental stage of one to two days younger than that of wild type and *bb*. This suggestion agrees with that of Vanhaeren et al., who describe a “developmental shift” in these mutants, relative to wild type. The finding in the same study of larger cells in *bb* and *da1-1bb* mutants at 7 days after stratification appears to contradict this theory, while my findings of largely similar, and reduced cell areas (respectively) better supports the assertion that the leaves of the mutants are developmentally “younger” than wild type, which could enable them to grow for longer.

Although the number of stomatal and meristemoid cells in leaves is low compared to the total number of pavement cells sampled, the analysis in this section could have been improved by separately identifying them, for example by seeding them in a different colour during the segmentation process. This would allow a marginally more accurate calculation of pavement cell area, as well as providing the opportunity for a number of further analyses such as the temporal and spatial distribution of stomata and meristemoid cells in wild type

and mutants, and indications of the stomatal index. The stomatal index has previously been shown to be an indicator of the developmental age of tissue (Andriankaja et al., 2012), as part of a secondary wave of cell-cycle arrest (White, 2006).

This experiment could also have been improved by extending the period sampled both earlier and later, to capture a longer period of growth, and potentially observe the end of the cell proliferation phase of development. However, time constraints caused by loss of fluorescence from the marker gene meant that a time-course extending beyond 11 days after stratification was not possible, as well as a gradual reduction in the signal from the cell membrane reporter line, as noted in Section 3.3.2. Earlier imaging was also challenging, as the seedlings were difficult to dissect without some crushing, and obtaining high quality images proved difficult. As well as extending the duration of the imaging, further work could include some imaging of the shoot apical meristem.

Given the increased seed weight observed in *da1-1*, *bb*, and *da1-1bb* mutants (Li et al., 2008), and the observations that all organs in the plant are increased in size in these mutants, it is plausible that the meristems from which these organs are formed is larger, or exhibits some other abnormality such as in the rate of cell division. If a larger meristem allocated more cells to each new leaf primordium, an initially larger leaf would be produced. The percentage increases in seed weight recorded earlier do not fully explain the percentage increases in final leaf area described in this Chapter - but together with the increased rate of cell division that could be inferred from the data in Section 3.3.2.1, this could provide a mechanism for explaining how the larger final organ sizes are produced in these mutants. The well-known *CLAVATA-WUSCHEL* pathway is a central controller of shoot apical meristem size (Somssich et al., 2016), therefore as well as analysis of cell number and cell division rates in the meristem, it could be interesting to analyse the balance of expression of members of this pathway in *da1-1* and *bb* mutants.

3.4.4.3 *Cell density is increased during growth in da1-1 and da1-1bb mutants*

Although cell density in mature leaves was not studied, inferences based on the cell area measurements and final leaf area suggest that cell density is increased relative to wild type in *da1-1* mutants, but not in *bb* or *da1-1bb* mutants. On the other hand, data presented in Section 3.3.2.3 shows that cell density is increased in both *da1-1* and *da1-1bb*, except for at 11 days after stratification, where cell density for the *da1-1bb* mutant is comparable to that of wild type. This could be as a result of the “transition” suggested above in Section 3.4.4.2, as cell area and cell density are closely linked.

The spatial and temporal distributions of relative cell densities support the proposal of a “developmental shift” as *da1-1bb* mutants continued to increase the differential between their densest and least dense areas until 10 days after stratification, whereas the other genotypes did not change significantly beyond 8 days after stratification. This suggests that a larger area of high relative cell density persisted for longer in the double mutant, supporting the theory that the tissue is developmentally younger and therefore able to grow for longer to produce a larger final organ size.

3.4.5 Summary

In summary, the data presented in this Chapter gave new insights into the anisotropic growth of the *da1-1*, *bb* and *da1-1bb* mutants, and the increased rate of growth at the whole organ level. This was supported by the increased rate of increase in cell numbers in the mutants relative to wild type, indicating an increased rate of cell division. Additionally, cells were largely smaller throughout growth in leaves of plants carrying the *da1-1* mutation, supporting the previously held hypothesis of a “developmental shift” in these plants (Vanhaeren et al., 2017). Finally, the SEM imaging confirmed that the increased leaf area in the mutants relative to wild type is due to increased cell number, while presenting an interesting question for future work surrounding the identification of smaller mature cells in *da1-1* leaves than in wild type.

4 LIVE CELL IMAGING ANALYSIS OF *DA1* AND *BB* ACTIVITY

4.1 Introduction

Live cell imaging is the visualisation of cells and cellular processes, often within a growing tissue. This allows the study of the development of that tissue over time at a cellular level, by observing cell proliferation and cell growth, as well as the observation of a wide range of biological processes such as signalling, organelle transport, and cytoskeletal changes using, for example, fluorescent proteins. The utilisation of live cell imaging allows the generation of a very rich dataset, and, following the interesting findings surrounding the activity of *DA1* and *BB* described in Chapter 3, a range of cellular and growth parameters were tested in plants carrying the *da1-1* and *bb* mutations in order to discern further differences relative to wild type, in order to explain some of these observations - as well observations previously made in a number of publications (Disch et al., 2006; Li et al., 2008; Dong et al., 2017; Vanhaeren et al., 2017).

4.1.1 Applications of live cell imaging

Live cell imaging has been successfully employed to study growth in a range of tissues, including roots, meristems, and floral organs, rendering it a powerful system for studying organ development.

The use of live cell imaging in roots is widespread, as they are transparent, all cell types are known, and their essentially singular dimension growth is readily observed. They grow rapidly, exhibiting high rates of growth of approximately 50-300 μ m per hour, with a full cell cycle taking between 10 and 35 hours in *Arabidopsis thaliana* primary roots (Von Wangenheim et al., 2017). Work presented in von Wangenheim et al. 2017 showed an innovative approach to the issue of high rates of growth and cell division in roots by developing software to automatically track root tips as they were imaged on the microscope, enabling the microscope's field of view to be automatically adjusted as the roots grew down a block of agar. This tracking mechanism was possible due to the maintained size and orientation of the root tip, as a result of the vertical orientation of the seedlings (Von Wangenheim et al., 2017). Their work showed that, within the 38-hour period for which the roots were tracked (with an imaging interval of 20 minutes), cells exhibited a high level of regularity in cell division, with each "first generation" membrane that was observed at the first time-point being separated from the next by exactly three new membranes by the end of the tracking period. They also observed evidence for the synchronisation of root stem cell initial division, as all cell divisions in this region took place within a single 10 hour period,

with an average duration of around 4 hours (Von Wangenheim et al., 2017). These observations of growth and cell division strengthen add a new dimension to our understanding of how roots grow and tissue organisation within the root tip.

The control of cell proliferation in the shoot apical meristem (SAM) is of central importance to the developing plant, as the SAM must maintain a constant cell number by replenishment, while supplying sufficient cells to new organ primordia throughout the plant's life cycle. Studies of the *CLAVATA* family, *WUSCHEL* and *SHOOT MERISTEMLESS* have elucidated a genetic network controlling the size and maintenance of the shoot apical meristem. Live cell imaging allowed Reddy et al. to observe cell division in a live SAM, and identify temporal and spatial variations in cell division parameters. It was shown that cells within L1, L2 and the corpus exhibited a coordinated pattern of variation in mitotic activity over time (Reddy et al., 2004), which did not appear to be linked to the timing at which new primordia arise, or diurnal rhythms, as had previously been described (Lyndon, 1998).

Although recent protocols include the removal of sepals to access floral buds (Prunet et al., 2016), live cell imaging has also been successfully applied to the sepals themselves by Roeder et al. 2010, in which a model using the timing of cell division to control cell size patterning in sepals was proposed. The model demonstrates that variability in the control of cell division, caused by asymmetric cell divisions and asynchronous cell cycles and cell cycle durations can result in the range of epidermal cell sizes observed in sepals. The addition of an endoreduplication factor to the model further explained the "giant cells" observed in the sepal epidermis, produced when cells enter the endocycle comparatively early (Roeder et al., 2010).

4.1.2 Modelling leaf growth through live cell imaging

Live cell imaging has recently been applied to a growing leaf, in order to gain an understanding of how tissue deforms throughout growth to produce the final leaf size and shape. In Kuchen et al. 2012, a model of tissue organiser deformation was proposed to explain the variation in growth rates observed during development. Using time-lapse imaging of the first leaf of *Arabidopsis*, the paper describes experimental observations of growth rates that were used to inform the model. At early stages of development, the growth rate in the leaf lamina followed a linear relationship from high in proximal regions to lower growth rates in more distal regions. At later stages in growth, this gradient became less steep, with the exception of a rapid decline in growth rate near the tip of the leaf. Conversely, the growth rate throughout the midvein and petiole was low (Kuchen et al., 2012). Analysis

of these data produced the model shown in Figure 4.1. PGRAD is a modelled growth promoting factor that forms a linear gradient from base to tip of the leaf. LATE is another modelled factor not shown in Figure 4.1 as it is expressed uniformly throughout the tissue, but only in later stages it inhibits the growth that is promoted by PGRAD. LAM is a factor expressed throughout the tissue, but less in the most proximal region as these cells are destined to form the leaf petiole. The MID factor marks the midline of the leaf. POLARISER forms a proximodistal gradient of a factor providing the polarity signals to inform the local directionality of growth, and is promoted in the base of the leaf by PROXORG yet degraded throughout the rest of the leaf.

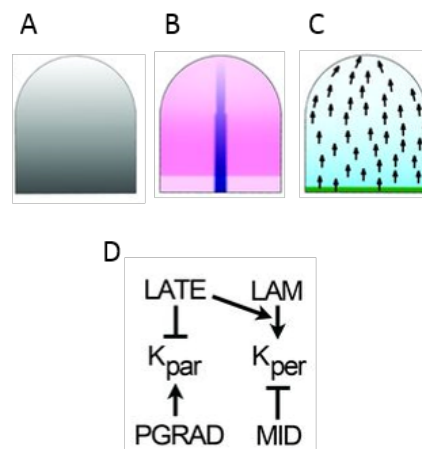


Figure 4.1 Model proposed by Kuchen et al. to explain observed growth rates in leaf development

Schematic of the spatial distribution of the factors PGRAD (A), MID (blue), LAM (pink) (B), POLARISER (cyan), and PROXORG (green) (C). Proposed interactions of described factors and impacts on growth parallel (K_{par}) and perpendicular (K_{per}) to POLARISER (D). Adapted from Kuchen et al. 2012 with permission.

Interactions between these factors as shown in Figure 4.1D are sufficient to generate computational simulations of realistic leaf growth and orientation. Kuchen et al. propose a number of candidate genes for the factors in the model, for example *LEAFY PETIOLE* and members of the *YABBY* family for LAM (Kuchen et al., 2012), which are known to promote lamina growth (van der Graaff et al., 2000; Sarojam et al., 2010), and members of the *CUP-SHAPED COTYLEDON (CUC)* family for POLARISER or PROXORG.

In a more recent study (under review) by the same team, Fox et al. integrated patterns of cell division into the model, using live cell imaging and growing the plant in an optical imaging chamber (as described in Section 4.2.4.3). To do this, a *spch* mutant was used to simplify the model by excluding stomatal lineage divisions. Further factors were added to the model as a result of this work. The first factor controls the competency of cells to divide, PMF (proximal

mobile factor). PMF is able to control both division and growth, and is involved in the maintenance of the zone of competency to divide. The second factor is CDIV, which conferred competency to divide in cells. Finally, \bar{A} represents the mean cell area at time of division (Fox et al., under review).

While *spch* mutants grown under live cell imaging conditions present a useful model for analysing cell division dynamics, it is important to note that the lack of stomata and significantly different growth conditions mean that these results cannot be compared directly to the growth of non-*spch* mutants grown on soil. The same limitation applies to the results collected in this chapter, meaning that while some interesting observations have been made, it is not possible to conclude that the *da1-1* and *bb* mutants would have precisely the same effects in wild type, soil-grown plants (for example, differences in the effect of the *bb* mutation have already been observed in Chapter 3).

Nevertheless, using the framework proposed by Fox et al., it is possible that *DA1* or *BB* could provide a further candidate gene for one or more of the proposed factors, integrating the *DA1* regulatory system into a larger growth control model.

4.1.3 Aims for this Chapter

In this Chapter, the growth of *spch*, *spch da1-1*, *spch bb*, and *spch da1-1bb* seedlings expressing an epidermal specific plasma membrane marker was tracked from 126 to 312 hours (equating to 5 to 13 days) after stratification. Cellular growth and division in these seedlings have been analysed using bespoke software. From these data, I aimed to understand more about the role that the duration, rate or other dynamics of cell proliferation could have in generating the observed phenotypes of *da1-1*, *bb* and *da1-1bb*, as well as gain a better understanding more generally of how the relationship between cell division and cell expansion may be affected in organ size mutants such as those studied in this Chapter.

This Chapter aims to answer the following questions:

- Is the duration of cell proliferation increased in the mutants relative to wild type, resulting in increased final cell number and therefore increased leaf area?
- Is there an increased rate of cell proliferation in the mutants relative to wild type, resulting in increased final cell number and therefore increased leaf area?
- Are there other differences in the cell division dynamics of the *da1-1*, *bb* or *da1-1bb* mutants relative to wild type that could result in increased final cell number

4.2 Materials and Methods

4.2.1 Plants used in this Chapter

<i>Arabidopsis thaliana</i> line	T-DNA/mutation
Col-0 <i>pAtML1::mCitrine-RCI2A</i>	As described in Chapter 3
<i>da1-1 pAtML1::mCitrine-RCI2A</i>	SNP mutant (Li et al., 2008), as described in Chapter 3
<i>bb pAtML1::mCitrine-RCI2A</i>	SALK_045169, as described in Chapter 3
<i>da1-1bb pAtML1::mCitrine-RCI2A</i>	As described in Chapter 3
<i>spch-4</i>	SALK_078595

Table 4.1 Plant lines used in Chapter 4

4.2.2 *Arabidopsis thaliana* crossing

All siliques, open flowers, and partially opened buds were removed from a shoot of the maternal plant, as well as buds that were too small to be dissected. Using a magnifying headband (Donegan Optivisor. Donegan Optical) the remaining buds were carefully opened using forceps (Dumont #5) that had been sterilised in ethanol, and all anthers were removed, leaving only the stigmata. An open flower from the paternal plant was introduced to the maternal stigmata and pollen was transferred. The bud stem was labelled using masking tape, and checked 3 days later for growth. Successful crosses were wrapped loosely in cling film to protect the developing silique, and harvested when mature.

4.2.3 *Arabidopsis thaliana* genotyping

4.2.3.1 Genomic DNA extraction

Genomic DNA was extracted using the Edwards method (Edwards et al., 1991). Leaf tissue was crushed in 400µl Edwards buffer (200mM Tris-HCl pH 7.5 (Melford. Cat. No. T1513), 250mM NaCl (Sigma-Aldrich. Cat. No. 433209), 25mM EDTA (Sigma-Aldrich. Cat. No. EDS), 0.5% SDS (Sigma-Aldrich. Cat. No. 71725) with a small pestle in a microcentrifuge tube. This was centrifuged at 14,000rpm for two minutes at 4°C, and the supernatant recovered into a new microcentrifuge tube. An equal volume of ice cold isopropanol was added to the supernatant and incubated on ice for ten minutes. This was centrifuged at 14,000rpm for 5 minutes at room temperature, the supernatant discarded, and the pellet dried. The pellet was re-suspended in 100µl TE solution.

4.2.3.2 PCR amplification of DNA

All PCR protocols in this thesis were carried out in an Eppendorf Mastercycler^R pro (Cat. No. 632100019) thermocycler.

PCR genotyping of plants was carried out using TaKaRa *Taq* (TaKaRa. Cat. No. R001A) according to the manufacturers' protocol (Table 4.2).

Component	Volume for 50µl reaction (µl)	Temperature (°C)	Time (seconds)
Nuclease-free water	39.25	94	30
10x PCR Buffer (Mg ²⁺ plus)	5	55-75	30
dNTP mixture	4	72	30 per kb
10µM forward primer	0.5	35x repeat of steps 1-3	
10µM reverse primer	0.5		
Template DNA	0.5		
TaKaRa <i>Taq</i>	0.25		

Table 4.2 TaKaRa PCR protocol

4.2.3.3 Restriction digestion

For *da1-1* genotyping, the product of the PCR was subjected to a restriction digestion to identify the *da1-1* single nucleotide polymorphism. The PCR product was digested at 37°C for 1 hour by Mnl1 (New England Biolabs. Cat. No. R0163S) using CutSmart® buffer (New England Biolabs. Cat. No. B7204S), and inactivated at 65°C for 20 minutes. The product was analysed by DNA gel electrophoresis. The *da1-1* allele is not digested by Mnl1, as the DA1^{R358K} mutation is in in the active site.

4.2.3.4 DNA gel electrophoresis

A 1% (w/v) agarose gel made with TBE buffer was used, with 0.003% (v/v) ethidium bromide. Running buffer was added to the samples, and a molecular weight ladder (either NEB 1kb ladder or NEB 2-log 0.1-10kb ladder) was loaded in the first well. The gel was run at 100V for around 20 minutes and imaged using an Alphamager EP machine (Cell Biosciences).

4.2.3.5 Copy number analysis

Leaf tissue was sampled from F2 plants and sent to iDNA Genetics (<http://www.idnagenetics.com>) for copy number analysis, and individuals with two insertions of the BASTA resistance gene (indicating a single copy, homozygous genotype) were bagged following silique formation, harvested when dry, and hand-threshed.

4.2.3.6 Primers used in this chapter

Primer identity		Primer sequence
spch	SALK_078595 LP	TATGAGGGACTCGCATTTCATC
spch	SALK_078595 RP	AAAACAAATTCGTTTGCTCCC
eod1-2	SALK_045169 LP	GAGCGATGCATCTCTAACCAC
eod1-2	SALK_045169 RP	AGTAGGAACAGAAAGCAGGGG
LBb1.3		ATTTTGCCGATTTTCGGAAC
da1-1	F	GACACCATGCAATGCCAACC
da1-1	R	CTTTGAGCCTCATCCACGCA

Table 4.3 Primers used in Chapter 4

4.2.4 Plant imaging

4.2.4.1 Plant growth conditions

Threshed seed was sterilised by shaking in a 1.5ml tube containing 1ml sterilisation solution (50% (v/v) ethanol and 0.625% (w/v) dichloroisocyanuric acid (Sigma-Aldrich. Cat. No. 35915) for 20 minutes. The sterilisation solution was immediately removed and the seeds washed three times with 1ml 100% ethanol. Seeds were left to dry in a laminar flow hood on sterile filter paper. When dry, approximately 30 seeds per plate were sown onto plates with 25ml GM agar (0.43% (w/v) Murashige and Skoog, 1% (w/v) sucrose, 0.01% (w/v) inositol, 10ppm (w/v) thiamine, 50ppm (w/v) pyridoxine, 50ppm (w/v) nicotinic acid, 0.05% (w/v) MES, 9% (w/v) agar, pH 5.7). The plates were sealed with micropore tape (3M. Cat. No. 1530-0) and the seeds stratified for 3 nights at 4°C before being moved to a Controlled Environment Room (20°C, 16 hours light, 8 hours dark).

4.2.4.2 Identification of speechless homozygous mutants

At 5 days after stratification, the plates were removed from the Controlled Environment Room. Sterilised forceps (Dumont #5) were used to transfer seedlings to sterilised dimpled slides (Sigma-Aldrich. Cat. No. BR475505-50EA) with a droplet of sterilised water. A sterilised coverslip was placed on top (BDH. Cat. No. 405/0187/35). Seedlings were phenotyped according to the presence or absence of stomata using either a Leica SP5 (II) or a Leica TCS SP8X confocal scan head mounted on a Leica DM6000 microscope, according to the imaging conditions described in Section 4.2.4.4. Seedlings lacking stomata were identified as *speechless* homozygous mutants, and placed on a fresh plate (as described in Section 4.2.4.1) while the optical imaging chamber was prepared.

4.2.4.3 Setting up the optical imaging chamber

The optical imaging chamber was developed by Grant Calder, and custom-built at the John Innes Centre (Calder et al., 2015).

The optical imaging chamber was sterilised before use by autoclave. Liquid media in the form of quarter strength MS (1.1% Murashige and Skoog medium (Sigma-Aldrich. Cat. No. M5519), 7.5% sucrose (Melford. Cat. No. S0809) in ddH₂O) was used as a medium for plant growth within the optical imaging chamber.

The chamber was positioned in a sterilised laminar flow hood. Modified caps with tubing were attached to the media bottle and the waste bottle, and the tube ends connected with the tubes of the optical imaging chamber. The joins were additionally covered with foil to promote a sterile environment within the optical imaging chamber.

The mesh upon which the seedlings were placed was positioned in the chamber, with a ring weight positioned on top to prevent the mesh from floating when media was pumped into the chamber. The pump was connected to the tube leading from the media bottle, and media pumped into the chamber until small beads formed on the surface of the mesh.

Using sterile forceps, four seedlings were positioned on the mesh such that they did not overlap, and were not likely to overlap after they had grown. They were also positioned away from the edge of the chamber, for ease of microscopy.

The ring weight was removed and the coverslip was added to the chamber, ensuring no air bubbles formed. The chamber was then sealed and placed into the Controlled Environment Room. The pump was set to a low flow rate, constantly refreshing the reservoir of media below the seedlings.

Between imaging time-points, the optical chamber was kept in a Controlled Environment Room (20°C, 16 hours light, 8 hours dark), with the pump providing constantly refreshed liquid medium. During imaging, the tubes of the optical chamber were sealed to prevent loss of the liquid medium from the chamber.

4.2.4.4 Imaging conditions

Seedlings were imaged using either a Leica SP5 (II) or a Leica TCS SP8X confocal scan head mounted on a Leica DM6000 microscope, controlled using the Leica LAS AF software. A custom attachment was used to attach the optical imaging chamber to the Leica DM6000 stage. A 20x air objective was used on both microscopes. The argon laser excitation was set to 514nm, and the fluorescence emission was collected in the 520-600nm range using a HyD detector.

4.2.5 Image analysis

4.2.5.1 *Point Tracker*

The images generated in this chapter were analysed using Point Tracker 0.6.12 rev 3373, a tool developed by Dr Pierre Barbier de Reuille during his time in Professor Enrico Coen's group at the John Innes Centre. This software was kindly provided by Samantha Fox, with the permission of Professor Enrico Coen.

High quality 2D projections were made from the .lif file produced by the microscope software, using the first steps of the Leaf Analysis Toolkit pipeline as described in Chapter 3. For each leaf to be tracked, a tracking project was created within the Point Tracker software, and the projection from each time-point was saved within the project.

Points were manually placed on each vertex of a cell in the first time-point, and these points were grouped to create a cell. These points were copied from the first time-point to the second, and adjusted to reflect the growth of the cell. If a cell division occurred between time-points, this was recorded and two new daughter cells were created from the parent cell. The locations of points and therefore the position, size, shape and other parameters of each cell, were recorded automatically in a .csv file.

4.2.5.2 *Track 'n' R*

The data was visualised using Track 'n' R, a custom ImageJ toolset comprising of macros that enable the analysis of Point Tracker data using R, developed by Dr Florent Pantin. This software was kindly provided by Samantha Fox, with the permission of Professor Enrico Coen. Track 'n' R interprets the .csv files generated by Point Tracker and can perform a range of analyses exploring the growth and division dynamics of a leaf through a time-course.

Figures were made using Adobe Photoshop CS6 and R 3.3.3.

4.3 Results

The *Arabidopsis thaliana da1-1bb* plants transformed with the *pAtML1::mCitrine-RCI2A* generated in Chapter 3 were crossed with *speechless* mutants (plants expressing *pAtML1::mCitrine-RCI2A* will hereafter be referred to as *pAR169*). The resultant F1 plants were allowed to self-fertilise, and the F2 seedlings were genotyped according to the methods detailed in Section 4.2.3. The genotypes selected were *spch pAR169*, *spch da1-1 pAR169*, *spch bb pAR169* and *spch da1-1bb pAR169*. All lines were homozygous for *pAR169* as well as at the *DA1* and *BB* loci as appropriate. As a homozygous mutation at *speechless* is lethal when grown under normal conditions, the lines were segregating at the *SPEECHLESS* locus.

For each genotype, four *speechless* homozygotes were selected according to the method described in Section 4.2.4.2, before being placed in the optical imaging chamber. The seedlings were imaged at a high temporal resolution at the start of the experiment, with the interval between time-points increasing over the course of the experiment. Seedlings were imaged every 6 hours for the first 48 hours, every 8 hours for the subsequent 48 hours, every 12 hours for the subsequent 48 hours, and every 24 hours for the final 48 hours. The images generated at the first time-point, 120 hours after stratification, have been discarded for these analyses as there is a “settling in” period for the seedlings within the optical imaging chamber (pers. comm., Samantha Fox) where growth may be abnormal. One representative leaf was chosen for each genotype (based on leaf width measurements), and the cells tracked and analysed as described in Section 4.2.5.

It is important to note that in this chapter, only a single biological replication was analysed for each genotype, due to the complexity of the analysis. Without further analysis of the other three biological replicates available, the results in this chapter should be interpreted with care. Further biological replicates will be analysed for publication in the future.

4.3.1 Maintenance of the *da1-1*, *bb*, and *da1-1bb* large organ phenotypes

By comparing width measurements of the first leaves of the *spch pAR169*, *spch da1-1 pAR169*, *spch bb pAR169*, and *spch da1-1bb pAR169* seedlings to those of wild type, *da1-1*, *bb*, and *da1-1bb* (described in Chapter 3) it is possible to determine whether mutations in *DA1* and *BB* have a similar effect on organ size in plants with a *speechless* mutation as in those without. It is important for the validity of this experiment that the organ size differences between genotypes that were observed in Chapter 3 and a range of publications (Disch et al., 2006; Li et al., 2008; Xia et al., 2013; Cattaneo and Hardtke, 2017; Dong et al., 2017; Vanhaeren et al., 2017) are reflected in the *speechless* background, despite the effects

of *speechless* in the reduction of organ size and rate of organ growth (Gray, 2007). Figure 4.2 demonstrates that the differing widths of leaves in *da1-1*, *bb* and *da1-1bb* mutants are maintained relative to wild type in the *speechless* background, as is the increase in rate of growth.

Figure 4.3 shows the increase in the width of the first leaf of the *spch pAR169*, *spch da1-1 pAR169*, *spch bb pAR169*, and *spch da1-1bb pAR169* seedlings used in this experiment (filled circles) in relation to the increase in width of the first leaf of wild type, *da1-1*, *bb*, and *da1-1bb*, as measured in Chapter 3 (open circles). Despite the difference in absolute width between the plants in a *speechless* background and those wild-type for *SPEECHLESS*, the pattern of increased organ size in *da1-1*, *bb*, and *da1-1bb* relative to wild type is maintained. In all four genotypes, the *speechless* mutants exhibit a leaf width comparable to that of those wild-type for *SPEECHLESS* until approximately 144 hours after stratification. Beyond this, the rate of growth is dramatically increased in plants without the *speechless* mutation. By contrast, the rate of growth in *speechless* mutants remains largely the same after 144 hours, resulting in decreased leaf width at 312 hours after stratification, relative to plants wild-type for *SPEECHLESS*.

In the *speechless* background, leaf widths at 312 hours were 122.2% of wild type width in *da1-1* mutants, 126.4% in *bb* mutants, and 161.1% in *da1-1bb* mutants. In plants without the *speechless* mutation, leaf widths at 312 hours were 122.6% of wild type width in *da1-1* mutants, 127.4% in *bb* mutants, and 163.7% in *da1-1bb* mutants.

These strong similarities in phenotype between the wild type and *speechless* support previous findings (Kuchen et al., 2012; Carter et al., 2017), and make it a useful tool in the understanding of cell dynamics in the growing leaf.

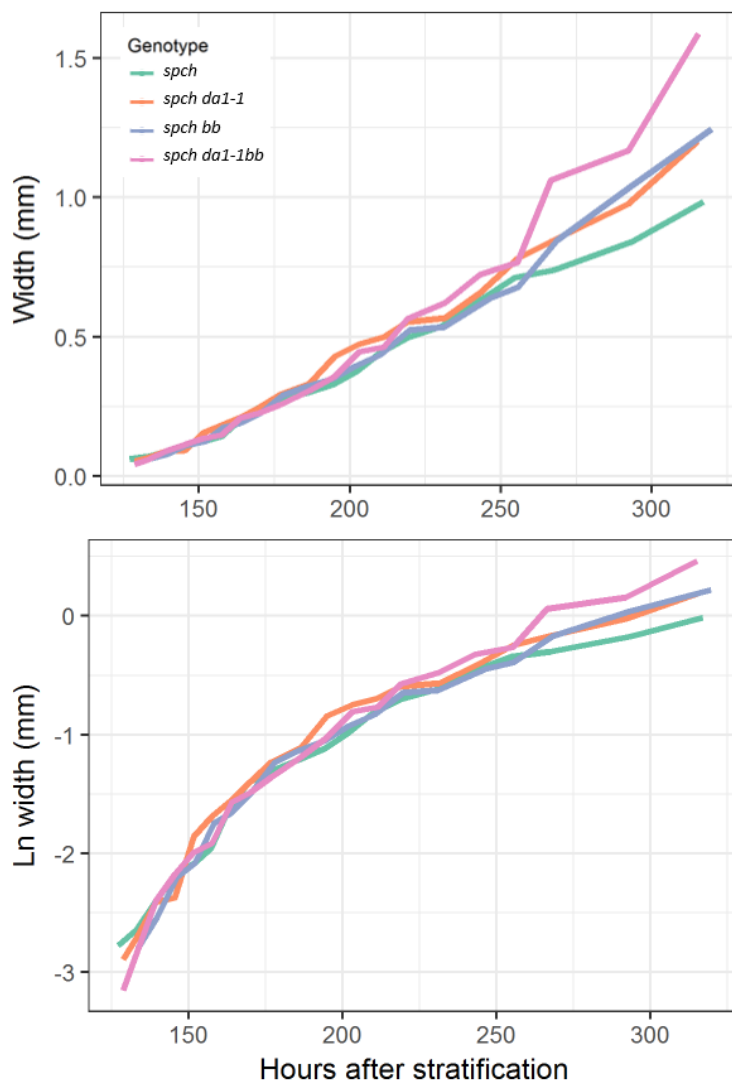


Figure 4.2 Growth of *spch*, *spch da1-1*, *spch bb*, and *spch da1-1bb* leaves

Width of the first leaf of *spch pAR169*, *spch da1-1 pAR169*, *spch bb pAR169*, and *spch da1-1bb pAR169* plants from 120 to 312 hours after stratification. Anomalous data for *spch bb pAR169* at 126hrs removed. n = 1.

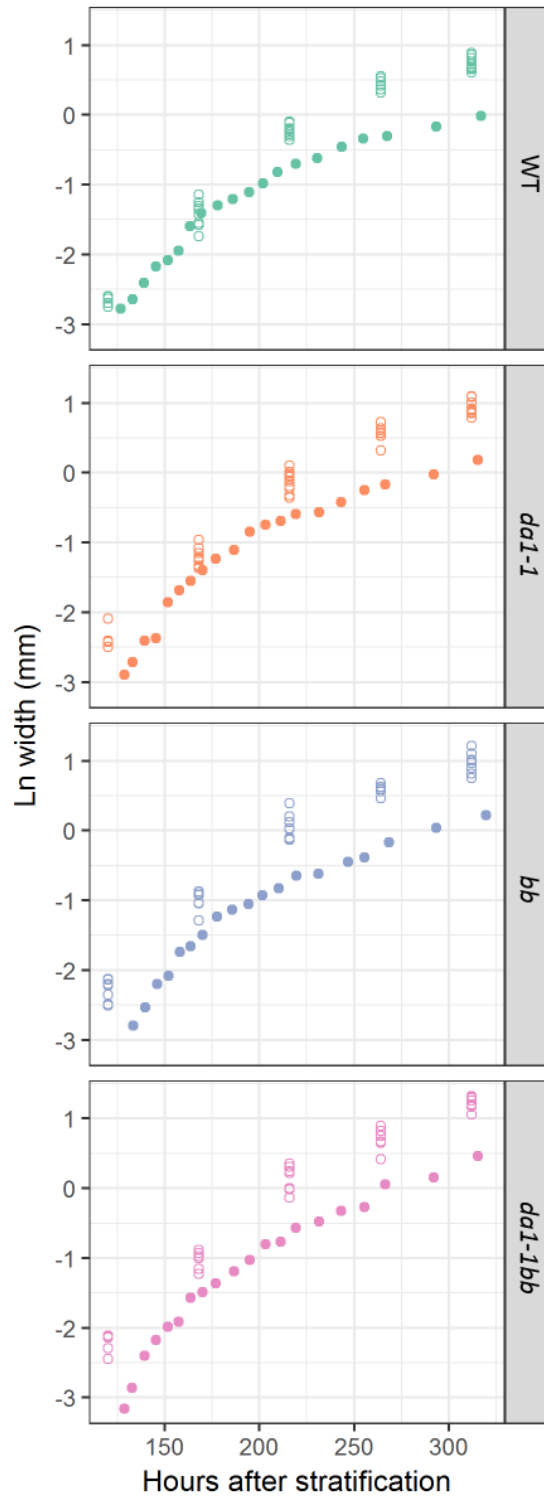


Figure 4.3 Growth of *spch*, *spch da1-1*, *spch bb*, and *spch da1-1bb* leaves relative to wild type, *da1-1*, *bb*, and *da1-1bb*

Natural log of the width of the first leaf of *spch pAR169*, *spch da1-1 pAR169*, *spch bb pAR169*, and *spch da1-1bb pAR169* plants (filled circles, $n = 1$) relative to wild type, *da1-1*, *bb*, and *da1-1bb* plants (open circles, $n = 8-10$) from 120 to 312 hours after stratification. Anomalous data for *spch bb pAR169* at 126hrs removed.

4.3.2 Competency to divide

The spatial and temporal distribution of cells with the competency to divide is critically important for the determination of final leaf area, as this determines the final cell number. For this reason, recording the location and duration of the proliferative phase (referred to as the zone of competency to divide) had the potential to offer insights into the causes of the large organ phenotype observed in *da1-1*, *bb*, and *da1-1bb* plants. Cells amenable to tracking were manually tracked throughout the time-course, and Track 'n' R was used to plot this data for comparison between genotypes, as shown in Figure 4.4, Figure 4.5, Figure 4.6, and Figure 4.7. A summary of these data at 24-hour intervals is presented in Figure 4.8. Cells amenable to tracking were defined as those that were fully visible throughout the tracking period, and did not curve away from the focal plane due to leaf curvature. In the later time-points, some cells were affected by tiling of microscope images causing some distortion, and were removed from the analyses.

From Figure 4.4, showing cell divisions in lines containing *spch*, but not the other mutations, it is evident that initially the zone of competence to divide extends to, or just below, 150 μ m from the petiole-lamina boundary. From 169 hours after stratification, this zone begins to extend towards around 300 μ m from the petiole-lamina boundary, as the growth of the tissue is faster than any reduction in the zone of competency to divide. The zone peaked at 300 μ m from the petiole-lamina boundary at between 202 and 255 hours after stratification, before receding to the base of the leaf. The last observed cell division took place during the 268-293 hours after stratification interval. In addition to defining the maximum distance that the zone of competency to divide extends to, the location of cell divisions within this zone is also of interest. No further cell divisions were observed in the leaf midvein beyond 202 hours after stratification, after which cell divisions appeared to recede from the midvein towards the leaf margin, and cease throughout the rest of the width of the leaf lamina. These data were fully consistent with previous observations of cell division dynamics (Fox et al., under review).

Figure 4.5 shows the locations of cell divisions during the same time period for the *spch da1-1* mutant. Similar to *spch*, the division zone initially extends 150 μ m from the petiole-lamina boundary, and later grows to 300 μ m. However, the zone of competency to divide in *spch da1-1* extended to 300 μ m from the petiole-lamina boundary more quickly than in *spch*, beginning to grow from 150 μ m at around 152 hours after stratification and reaching 300 μ m at 177 hours after stratification. In addition to this, between 195 and 292 hours after stratification, the cell competent to divide furthest from the petiole-lamina boundary was

outside the 300µm zone observed in *spch*. The final cell division event observed was in the 292-315 hours after stratification interval, which marked the end of the imaging period, so it is possible that further cell divisions may have occurred later. Finally, while in *spch* cell divisions were mainly constrained to the leaf margin at later stages, in *spch da1-1* cells continued to divide throughout the whole width of the leaf lamina until 292 hours after stratification, although cells in the midvein did cease division earlier.

Figure 4.6 shows the division competency of cells in a *spch bb* leaf. As with *spch* and *spch da1-1*, the zone of competency to divide extended initially to 150µm from the base of the leaf. The zone began to extend beyond 150µm from 178 hours after stratification, and reached 300µm from the petiole-lamina boundary during the 220-231 hours after stratification interval, although it did not exceed this distance at any time. Beyond 231 hours after stratification, the zone of competency receded towards the base of the leaf in a similar manner to *spch*, with the majority of divisions at the leaf margin rather than distributed across the width of the leaf lamina. As with *spch da1-1*, the final cell division events observed were in the 292-315 hours after stratification interval, which marked the end of the imaging period, so it is possible that further cell divisions may have occurred later.

Finally, Figure 4.7 shows cell divisions in *spch da1-1bb*. As with the other three genotypes, the zone of competency to divide initially extends to a maximum distance of 150µm from the base of the leaf, before beginning to extend at 176 hours after stratification. The zone reached 300µm in the 192-200 hours after stratification interval, and then extended slightly beyond 300µm until 288 hours after stratification. In the final time-point, two cell division events were observed, one of which was 300µm from the petiole-lamina boundary. Similar to *spch da1-1*, the cell division events were not restricted to the edge of the leaf blade during the later time-points observed, instead spreading across the whole width of the leaf lamina. Cell divisions also persisted in the leaf midvein until the 218-228 hours after stratification interval, whereas in the other genotypes these divisions were arrested before 200 hours after stratification.

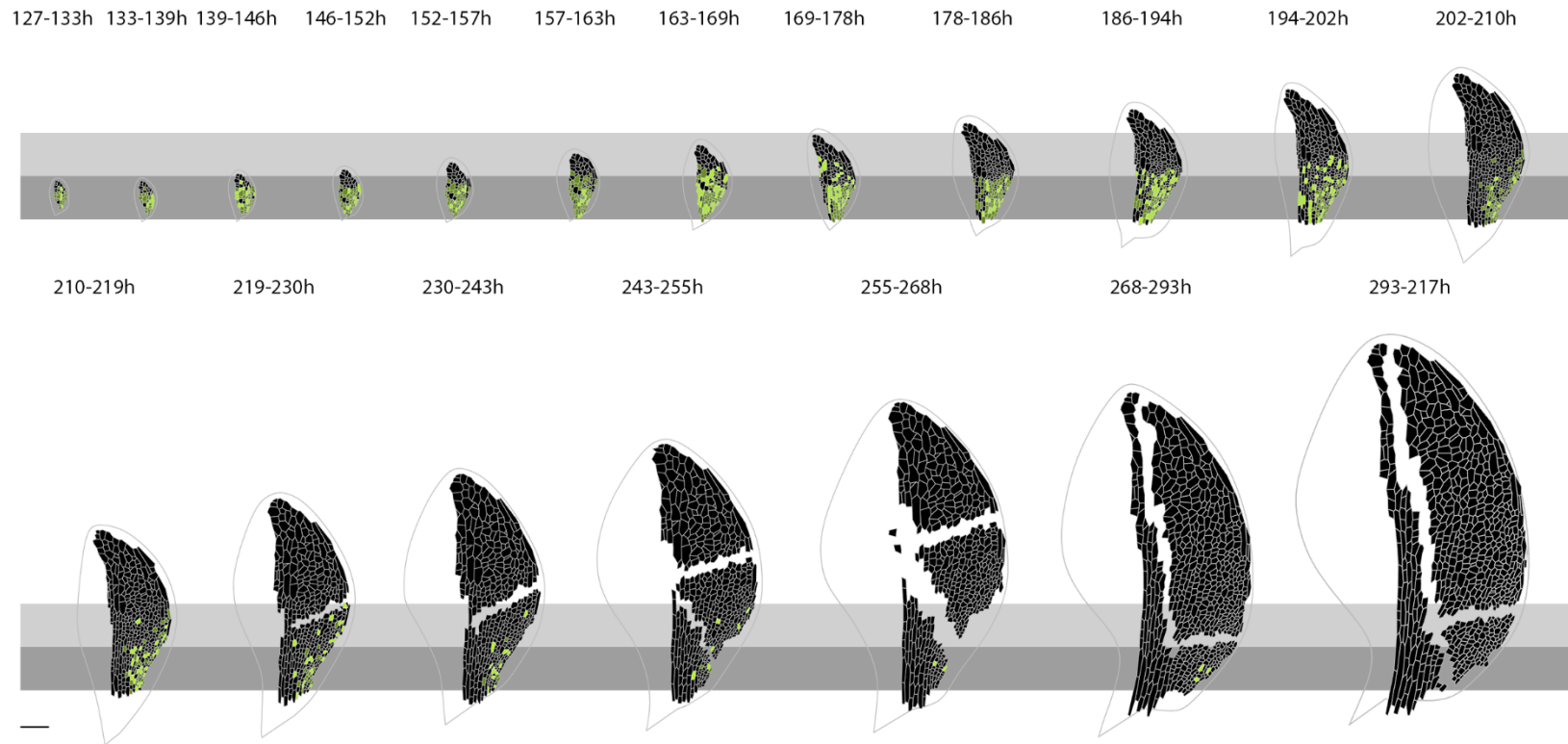


Figure 4.4 Division competency of cells in *spch*

Time-lapse imaging of the first leaf of *spch pAR169*. Cells amenable to tracking that were competent to divide are coloured green. Cells that executed division during the interval are coloured light green, and those that divided during a later interval are coloured dark green. Cells that did not divide are coloured black. Data is shown on the first time-point for each tracking interval. Leaves are aligned according to the petiole-lamina boundary. Grey boxes indicate 150µm (dark grey) and 300µm (light grey) from the petiole-lamina boundary. Scale bar 100µm.

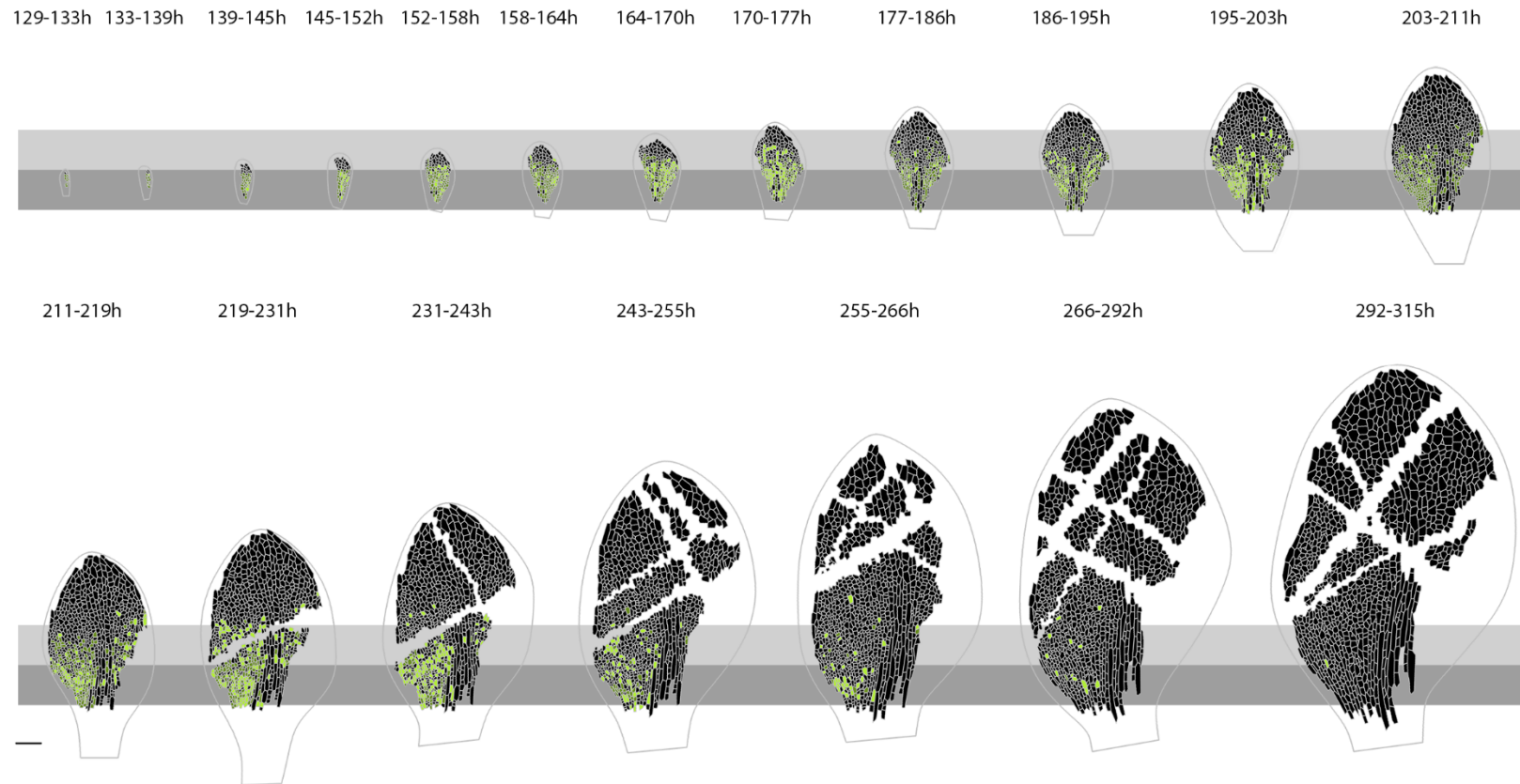


Figure 4.5 Division competency of cells in *spch da1-1*

Time-lapse imaging of the first leaf of *spch da1-1 pAR169*. Cells amenable to tracking that were competent to divide are coloured green. Cells that executed division during the interval are coloured light green, and those that divided during a later interval are coloured dark green. Cells that did not divide are coloured black. Data is shown on the first time-point for each tracking interval. Leaves are aligned according to the petiole-lamina boundary. Grey boxes indicate 150µm (dark grey) and 300µm (light grey) from the petiole-lamina boundary. Scale bar 100µm.

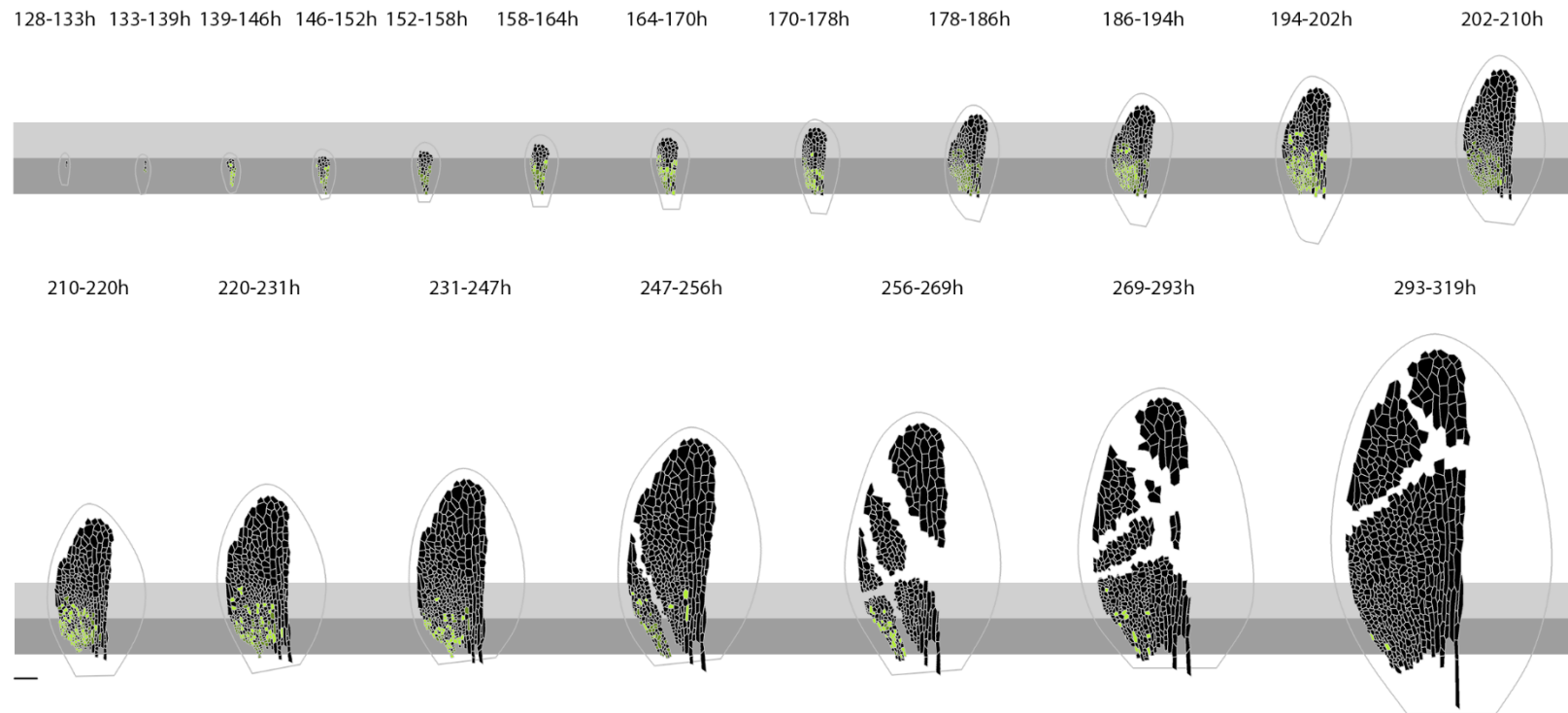


Figure 4.6 Division competency of cells in *spch bb*

Time-lapse imaging of the first leaf of *spch bb pAR169*. Cells amenable to tracking that were competent to divide are coloured green. Cells that executed division during the interval are coloured light green, and those that divided during a later interval are coloured dark green. Cells that did not divide are coloured black. Data is shown on the first time-point for each tracking interval. Leaves are aligned according to the petiole-lamina boundary. Grey boxes indicate 150µm (dark grey) and 300µm (light grey) from the petiole-lamina boundary. Scale bar 100µm.

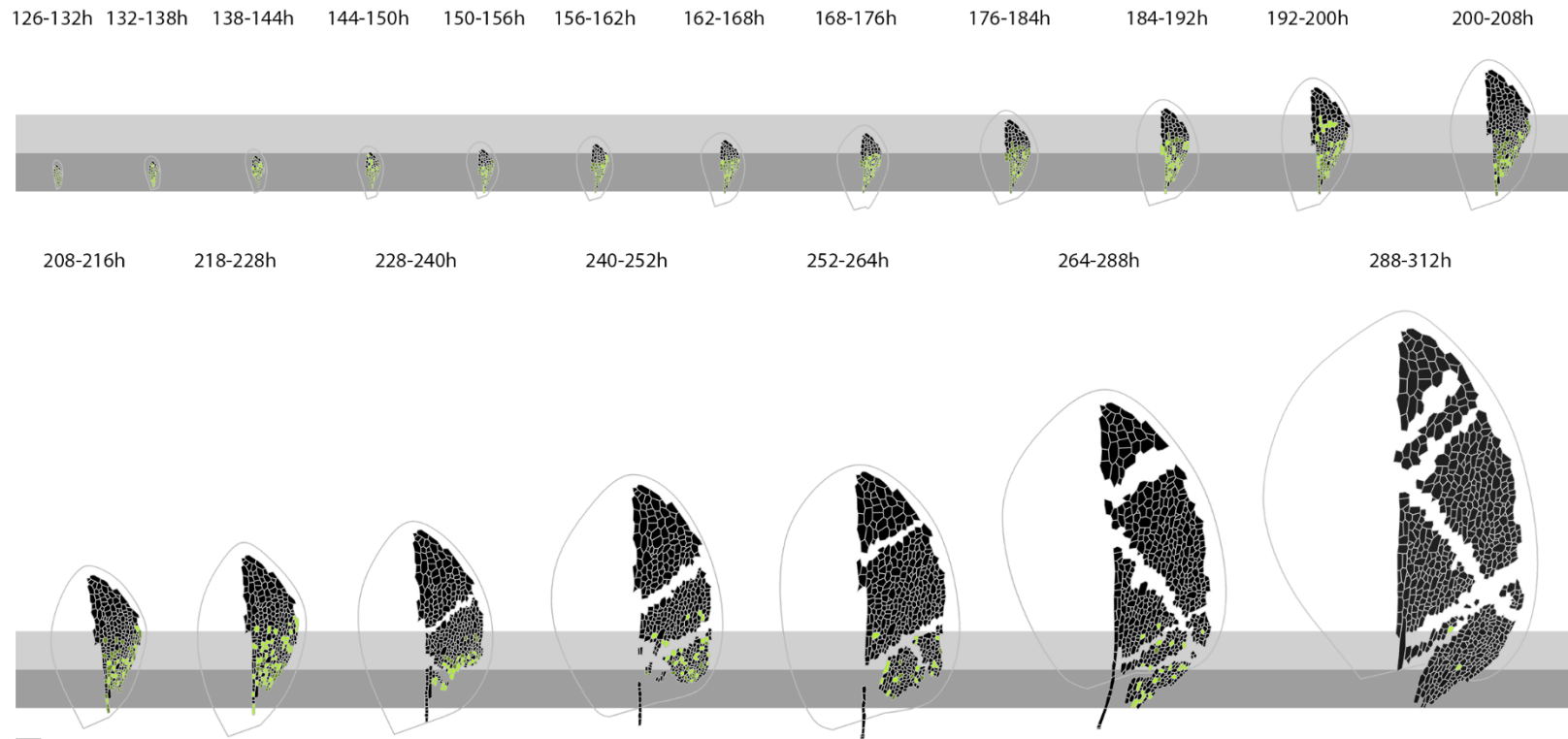


Figure 4.7 Division competency of cells in *spch da1-1bb*

Time-lapse imaging of the first leaf of *spch da1-1bb pAR169*. Cells amenable to tracking that were competent to divide are coloured green. Cells that executed division during the interval are coloured light green, and those that divided during a later interval are coloured dark green. Cells that did not divide are coloured black. Data is shown on the first time-point for each tracking interval. Leaves are aligned according to the petiole-lamina boundary. Grey boxes indicate 150µm (dark grey) and 300µm (light grey) from the petiole-lamina boundary. Scale bar 100µm.

Figure 4.8 shows a summary of the data presented in Figure 4.4, Figure 4.5, Figure 4.6, and Figure 4.7, where all four genotypes are scaled equally and the data presented at approximately 24-hour intervals for easier comparison. The most striking comparison between the genotypes is at the ~219-230 hours after stratification interval (fifth image shown), where the differences in the zones of division competency is very clear. The *spch* mutant has only a few cells retaining competency to divide, primarily in the leaf margin and not fully extending to 300 μ m from the petiole-lamina boundary. By comparison, the *spch da1-1*, *spch bb*, and *spch da1-1bb* mutants retain competency to divide in almost all cells within 300 μ m of the petiole-lamina boundary, and even slightly beyond this in the *spch da1-1* and *spch da1-1bb* mutants.

Data presented in this section therefore suggests that the duration of cell proliferation may be extended in *spch da1-1*, *spch bb*, and *spch da1-1bb* relative to *spch*. In addition, the zone of competency to divide is increased in *spch da1-1* and *spch da1-1bb* relative to *spch*, and the distribution of actual cell divisions within this zone of competency to divide is affected in *spch da1-1*, *spch bb*, and *spch da1-1bb* mutants. With further biological replicates, it would be possible to statistically analyse these differences to determine the precise impact of each mutation on the duration and location of cell proliferation.

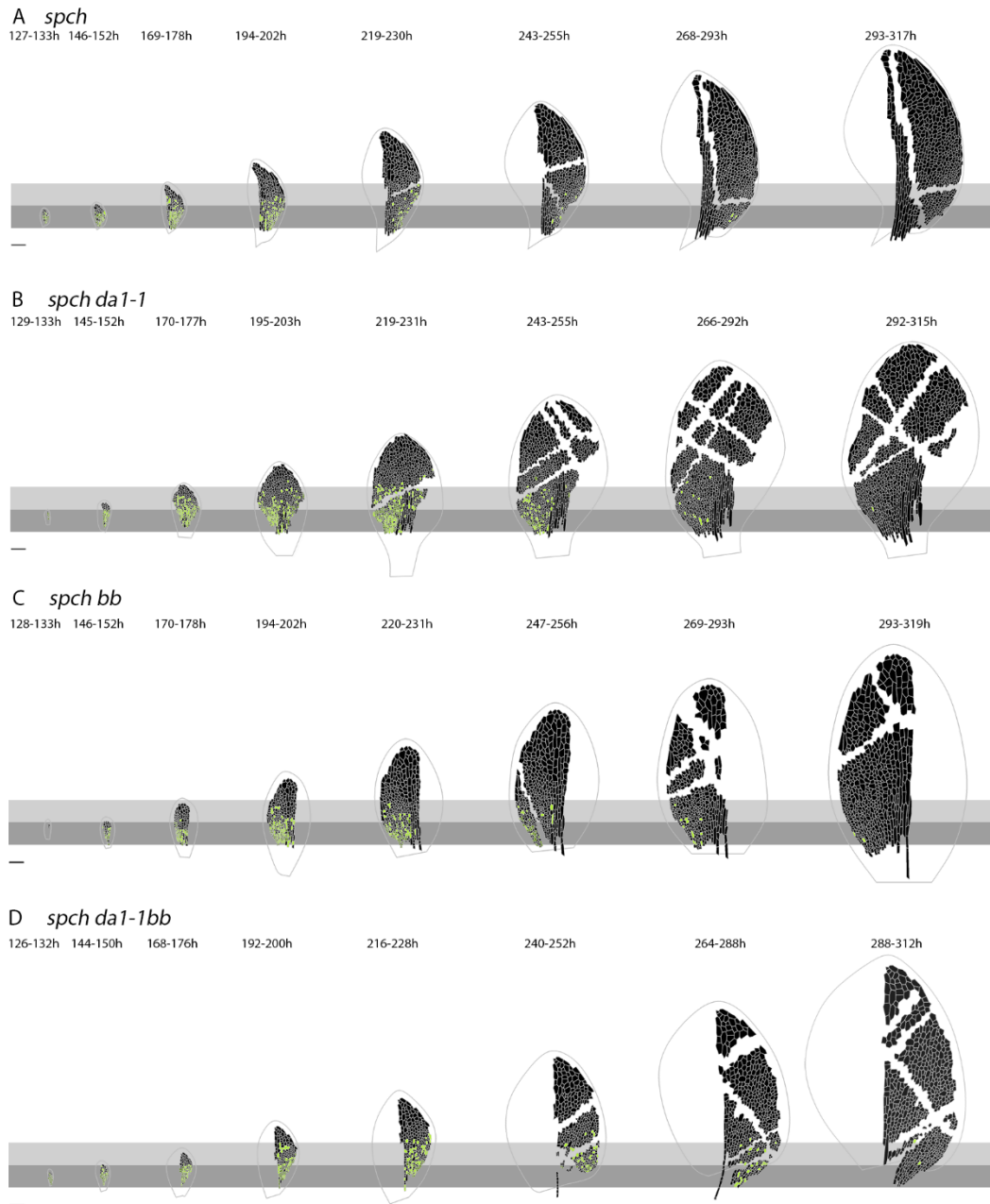


Figure 4.8 Division competency of cells in *spch*, *spch da1-1*, *spch bb*, and *spch da1-1bb*

Time-lapse imaging of the first leaf of *spch pAR169* (A), *spch da1-1 pAR169* (B), *spch bb pAR169* (C), and *spch da1-1bb pAR169* (D), shown at approximately 24-hour intervals. Cells amenable to tracking that were competent to divide are coloured green. Cells that executed division during the interval are coloured light green, and those that divided during a later interval are coloured dark green. Cells that did not divide are coloured black. Data is shown on the first time-point for each tracking interval. Leaves are aligned according to the petiole-lamina boundary. Grey boxes indicate 150µm (dark grey) and 300µm (light grey) from the petiole-lamina boundary. Scale bars 100µm.

Figure 4.9 shows the cell areas of cells in the proximal 150µm, 300µm, and 450µm zones to the petiole-lamina boundary, in the last 96 hours of the tracking period, as well as an indication of the maximum extent of the zone of competency to divide. Comparing the differences between genotypes in cell areas in these zones with the numbers of cell divisions occurring in these zones could further elucidate the relationship between cell area and cell division, and how that is affected in *da1-1*, *bb* and *da1-1bb* mutants.

At ~219 hours after stratification, all four genotypes had very small cells in the basal 150µm, although there were a few slightly larger cells towards the middle of the leaf in *spch*. In the 150-300µm zone, *spch da1-1* exhibited equally small cells, while *spch*, *spch bb*, and *spch da1-1bb* had a few slightly larger cells beginning to be present. In the 300-450µm zone, the cell areas of *spch da1-1* were comparable to those of the other mutants in the 150-300µm zone. By contrast, *spch* and *spch bb* had much larger cells in the 300-450µm zone, while *spch da1-1bb* exhibited an intermediate cell area phenotype.

At ~243 hours after stratification, again cell area of cells in the leaf lamina was similar between the four genotypes in the proximal 150µm. In the 150-300µm zone, *spch da1-1* and *spch da1-1bb* exhibited cell areas approximately equivalent to those in the more basal area, while cell areas in *spch* and *spch bb* were slightly increased. In the 300-450µm zone, *spch da1-1* again exhibited very small cells, of a comparable size to the more basal zones. The *spch da1-1bb* mutant showed a small increase in cell area, while *spch* and *spch bb* showed a greater increase in cell area in cells further from the petiole-lamina boundary.

At ~266 hours after stratification, cells in the most proximal regions of *spch* and *spch bb* were beginning to expand, leaving fewer small cells. The *spch da1-1* and *spch da1-1bb* leaves still exhibited many small cells in the proximal 150µm, and this was reflected in the 150-300µm zone in these genotypes. By contrast, *spch* and *spch bb* showed an even larger proportion of larger cells in this zone, and the cells were larger still in the 300-450µm zone in these mutants. In *spch da1-1* there was a slight increase in the number of larger cells relative to the 150-300µm zone, but some small cells remained. An intermediate phenotype was observed in *spch da1-1bb*.

Finally, at the ~292 hours after stratification timepoint, all genotypes had some larger cells among the small cells in the proximal 150µm. In the 150-300µm zone, the proportion of larger cells to smaller cells was greater in *spch* and *spch bb*, with slightly fewer larger cells in *spch da1-1* and *spch da1-1bb*. In the 300-450µm zone, the largest cells observed were in *spch*

bb, with large cells also observed in *spch*. The cells in *spch da1-1* and *spch da1-1bb* retained approximately the same proportion of larger and smaller cells as in the 150-300 μ m zone.

These observations suggest that cell divisions are more likely to occur in regions of the leaf where there is a higher proportion of smaller cells, relative to other areas of the leaf.

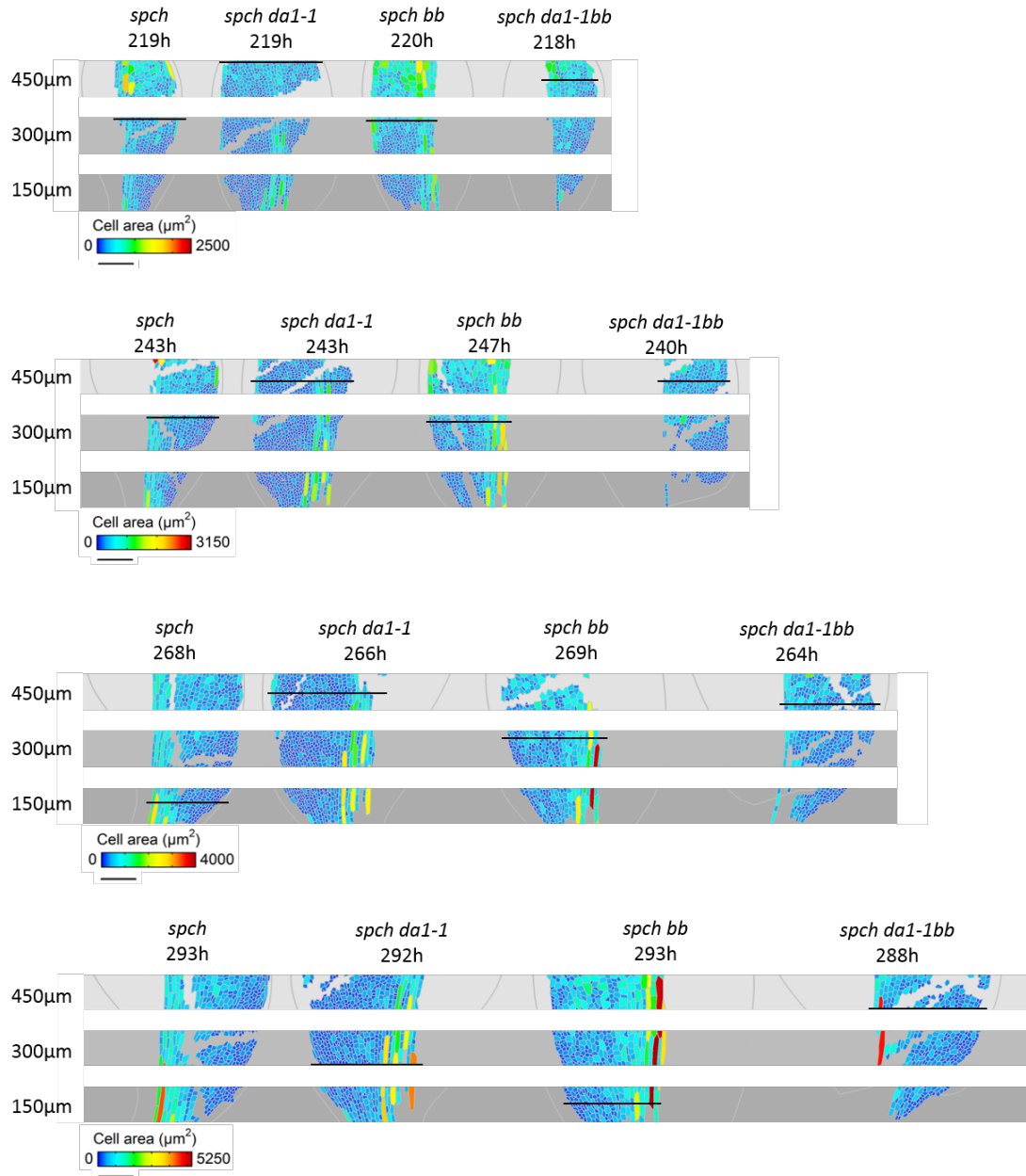


Figure 4.9 Cell area of cells in *spch*, *spch da1-1*, *spch bb*, and *spch da1-1bb*

Time-lapse imaging of the first leaf of *spch pAR169*, *spch da1-1 pAR169*, *spch bb pAR169*, and *spch da1-1bb pAR169*, shown at approximately 24-hour intervals for the final 96 hours of the tracking period. Heatmap indicates area of cells amenable to tracking. Grey bars mark 150 μ m, 300 μ m and 450 μ m from petiole-lamina boundary. Black lines mark most distal cell with competency to divide. Scale bars 100 μ m.

4.3.3 Number of cell divisions per cell

The number of cell divisions each cell underwent was counted from ~156 hours after stratification, as it was from this time-point that all four genotypes had sufficiently large numbers of tracked cells to measure. For every cell with competency to divide later during growth, the number of cell divisions it would later undertake was counted, and a mean taken of these. In *spch*, cells at 157 hours after stratification were expected to divide on average another 1.59 times before ceasing division. In *spch da1-1* at 158 hours this number was 1.52 times, in *spch bb* at 158 hours a cell could be expected to divide 1.36 further times, and finally in *spch da1-1bb* a cell at 156 hours after stratification on average divided a further 1.77 times. However, according to a Mann-Whitney U-Test, none of the differences between the genotypes are statistically significant.

When using incomplete data from ~126 hours after stratification (no sample is available for *spch bb* as none of the cells observed in the first time-point divided subsequently), *spch* cells divided on average 1.95 times in the future, *spch da1-1* cells divided 2.30 times further, and *spch da1-1bb* 1.96 times. However, these differences were again non-significant according to the Mann-Whitney U-Test.

Further biological replicates would allow a more precise statistical analysis of these data, as the different cells within each genotype are not truly independent samples.

4.3.4 Cell cycle time

Cell cycle time is defined as the number of hours between the birth of a cell (in a cell division event), and the death of a cell (when it itself divides). In this study, the imaging time intervals used mean that the exact time of cell division is not known, only the 6, 8, 12 or 24-hour time period in which it took place. For this reason, calculations of cell divisions assumed it to have taken place exactly halfway through the imaging period. Although this could potentially introduce some error into the data, cells are just as likely to have divided at the start of the time interval as at the end of it, and therefore the “mean time of birth” and “mean time of division” are reasonable metrics to estimate the times of cell birth and division. Only cells that were produced during a cell division event (as opposed to being visible at the start of the experiment, or becoming visible as leaf grew away from the cotyledons) and also divided themselves were included in these analyses, with a total of 790 complete cell cycles observed across all genotypes.

From Figure 4.10, it is clear that the time between cell divisions was increased in *spch bb* ($p < 0.0001$) relative to *spch*, at 132% of *spch*. However, the slight increases in the time of the

cell cycle observed in *spch da1-1* and *spch da1-1bb* were not significant despite being very similar in duration to *spch da1-1bb*. This could be as a result of the greater variation in cell cycle durations in *spch da1-1* and *spch da1-1bb*. In addition to this, *spch bb* exhibited a longer cell cycle time than *spch da1-1* ($p < 0.0001$), and *spch da1-1bb* ($p = 0.0006$).

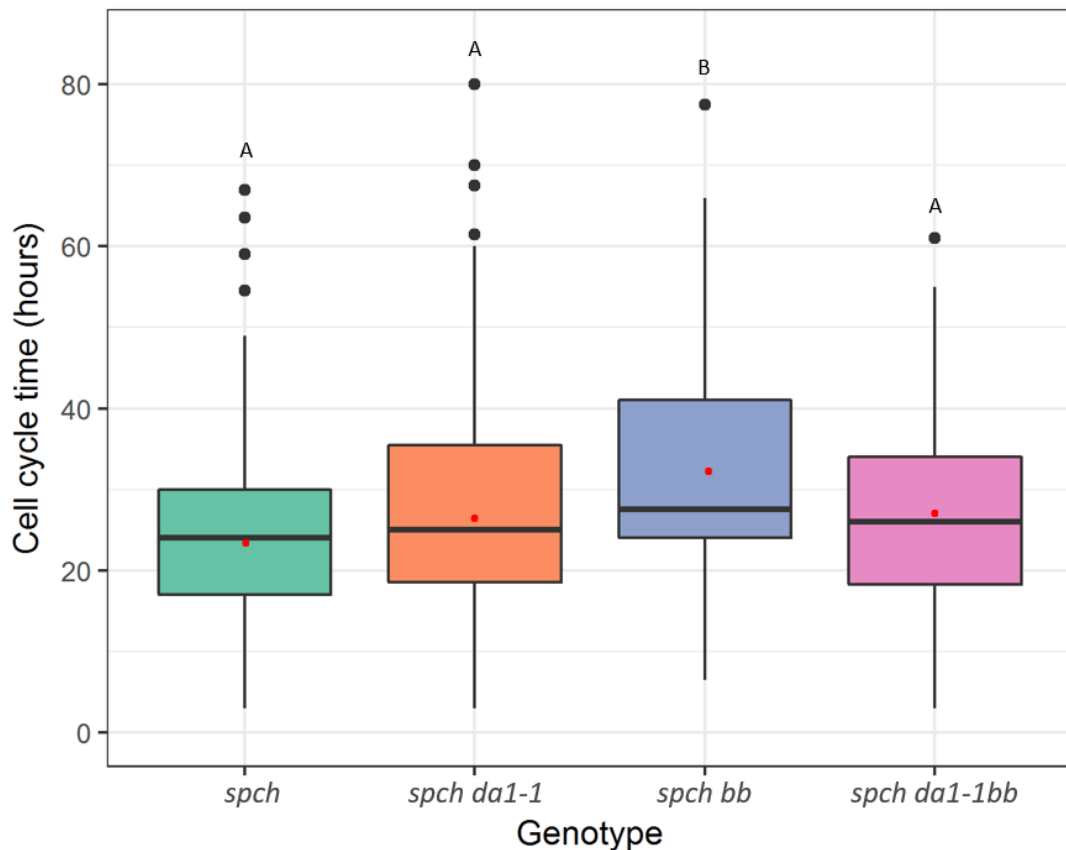


Figure 4.10 Cell cycle time in *spch*, *spch da1-1*, *spch bb*, and *spch da1-1bb* leaves

Boxplot of cell cycle time of cells in the first leaf of *spch pAR169*, *spch da1-1 pAR169*, *spch bb pAR169*, and *spch da1-1bb pAR169* leaves ($n = 1$). Total complete cell cycles observed = 790. Red points indicate means of samples. Small letters indicate significance groups according to ANOVA with a post-hoc Tukey pairwise comparison (variances were equal, $p = 0.05$). Black points indicate outliers.

Figure 4.11 shows how cell cycle time changed according to the time at which the cell divided. There is a clear difference between *spch* and the other mutants, where *spch* exhibits a steeper gradient, starting with a shorter cell cycle than the other mutants at early stages, and ending with a longer cell cycle time than the others by the end of the sampling period. By contrast, the *spch da1-1*, *spch bb*, and *spch da1-1bb* mutants all show a much shallower gradient in the change in cell cycle time, although *spch da1-1bb* exhibits the least change in cell cycle time during leaf growth. Comparing the linear regressions of the four genotypes revealed that the slope of each of *spch da1-1*, *spch bb*, and *spch da1-1bb* was significantly shallower than that of *spch* ($p < 0.0001$ for all), while *spch da1-1bb* was also significantly less steep than either of *spch da1-1* or *spch bb* ($p < 0.0001$ for both). However, the R^2 values for these slopes are very low in all four genotypes, potentially as a result of each genotype consisting of only a single biological replicate. This means that these data should be interpreted carefully, and not too great an importance placed upon the differences in the slopes, as each point does not represent an independent sample.

Observations in this section suggest that the time between cell divisions is on average increased in *bb* mutants, although the relationship between the age of the leaf and cell cycle time may be somewhat weakened relative to *spch* in all three mutants.

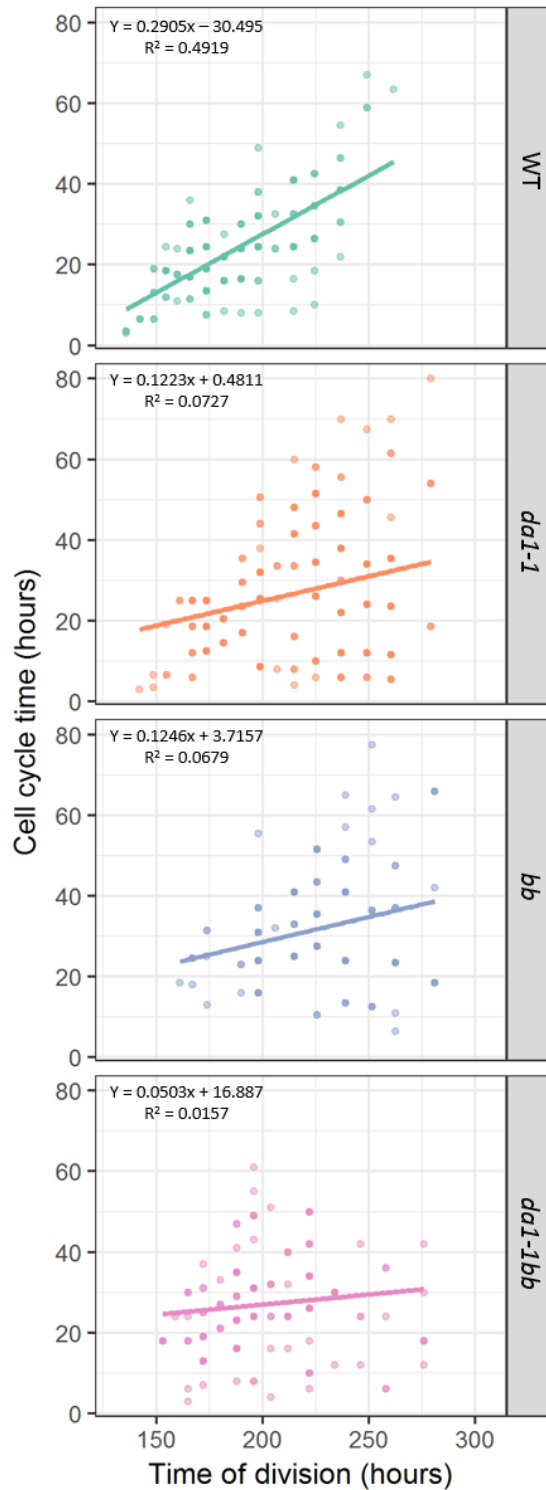


Figure 4.11 Cell cycle time over time in *spch*, *spch da1-1*, *spch bb*, and *spch da1-1bb* leaves

Cell cycle time of cells in the first leaf of *spch pAR169*, *spch da1-1 pAR169*, *spch bb pAR169*, and *spch da1-1bb pAR169* leaves, from 126 to 312 hours after stratification (n = 1). Total complete cell cycles observed = 790.

4.3.5 Cell area at time of division

Cell area at time of division was measured for all division events, of which a total of 1611 were observed across all genotypes.

Figure 4.12 shows that cell area at time of division was on average larger in *spch da1-1* ($p < 0.0001$), *spch bb* ($p < 0.0001$), and *spch da1bb* ($p < 0.0001$) than in *spch*. Cell areas at time of division were 113% of *spch* in *spch da1-1*, 134% in *spch bb*, and 139% in *spch da1-1bb*. In addition to this, cell area at time of division was increased in *spch bb* ($p < 0.0001$) and *spch da1-1bb* ($p < 0.0001$) relative to *spch da1-1*. There was no significant difference between the mean cell areas at time of division of *spch bb* and *spch da1-1bb* ($p = 0.5509$).

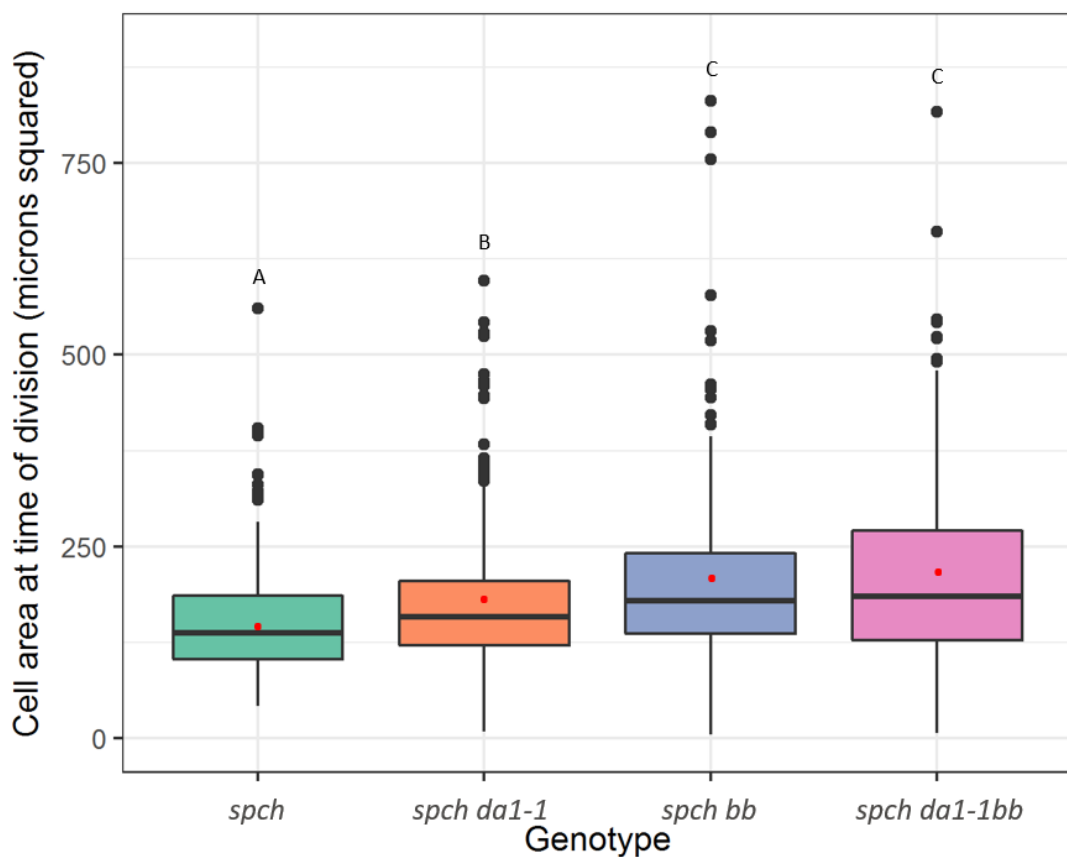


Figure 4.12 Cell area at time of division in *spch*, *spch da1-1*, *spch bb*, and *spch da1-1bb* leaves

Boxplot of cell area at time of division of cells in the first leaf of *spch pAR169*, *spch da1-1 pAR169*, *spch bb pAR169*, and *spch da1-1bb pAR169* leaves ($n = 1$). Total division events observed = 1661. Red points indicate means of samples. Small letters indicate significance groups according to ANOVA with a post-hoc Tukey pairwise comparison (variances were equal, $p = 0.05$). Black points indicate outliers.

Figure 4.13 shows how the cell area at time of division varied according to genotype through time. From Figure 4.13 it is possible to see that, while cell area at time of division increased for all genotypes throughout the sampling period, this increase was significantly greater in *spch da1-1*, *spch bb*, and *spch da1-1bb* than in *spch* ($p < 0.0001$ for each). The steepest increase in cell area at time of division was observed in *spch da1-1bb*, which was also steeper than both *spch da1-1* and *spch bb* ($p < 0.001$ for both). However, the R^2 values for these slopes are very low in all four genotypes, potentially as a result of each genotype consisting of only a single biological replicate. This means that these data should be interpreted carefully, and not too great an importance placed upon the differences in the slopes, as each point does not represent an independent sample.

Data presented in this section shows that cell area at time of division is on average increased in *spch da1-1*, *spch bb*, and *spch da1-1bb* relative to *spch*. Furthermore, the cell area at time of division may be increased in later stages of growth in *spch*, and this increase could be enhanced in the in *spch da1-1*, *spch bb*, and *spch da1-1bb* mutants.

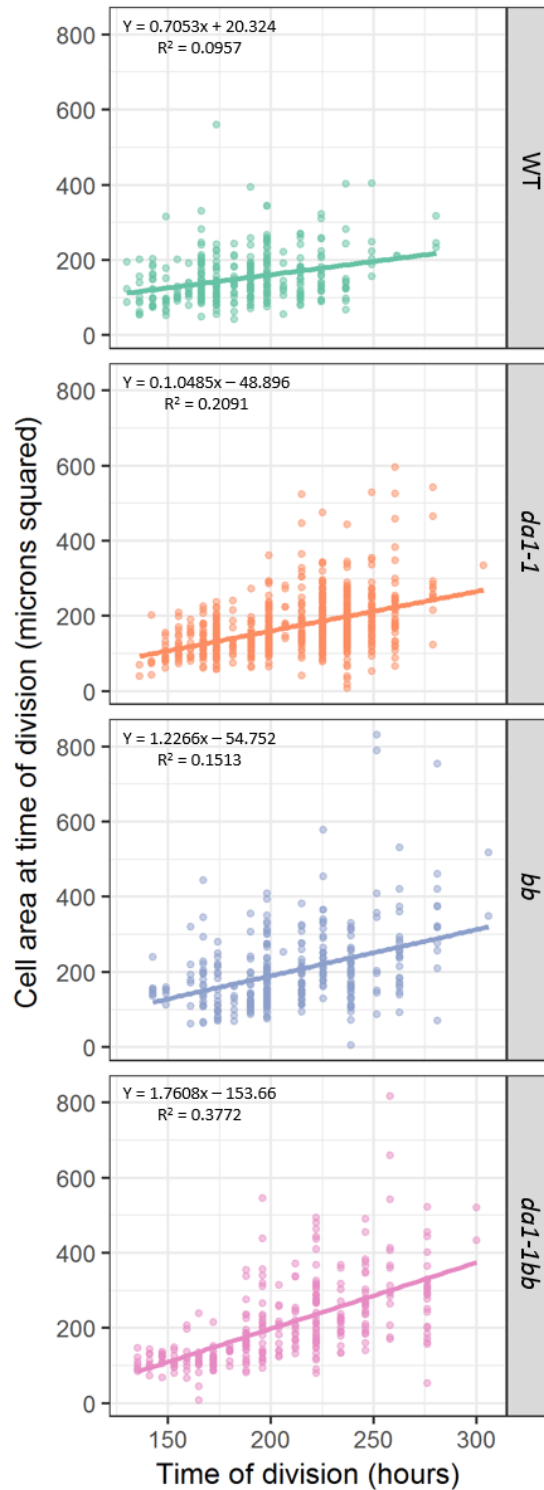


Figure 4.13 Cell area at time of division over time in *spch*, *spch da1-1*, *spch bb*, and *spch da1-1bb* leaves

Cell area at time of division of cells in the first leaf of *spch pAR169*, *spch da1-1 pAR169*, *spch bb pAR169*, and *spch da1-1bb pAR169* leaves, from 126 to 312 hours after stratification (n = 1). Total division events observed = 1661.

Figure 4.14 shows the cell area at time of division, and the spatial distribution of these divisions within the leaf. For all genotypes studied, cells that divided at a larger area were located in either more distal regions of the zone of competency to divide, or in the midvein. In addition, cells with the largest area at the time of division were observed in the later time-points, (Figure 4.13). Figure 4.14 also supports these observations by showing that slightly more of the largest cells divided in *spch da1-1*, *spch bb*, and *spch da1-1bb* than in *spch*, and as reflected in Figure 4.12, these small differences are statistically significant.

Figure 4.9 shows the cell areas of cells in the proximal 150µm, 300µm, and 450µm zones to the petiole-lamina boundary, in the last 96 hours of the tracking period. By comparing the differences between genotypes in cell areas in these zones with the numbers of cell divisions occurring in these zones could further elucidate the relationship between cell area and cell division, and how that is affected in *da1-1*, *bb*, and *da1-1bb* mutants.

At ~219 hours after stratification, all four genotypes had very small cells in the basal 150µm, although there were a few slightly larger cells towards the middle of the leaf in *spch*. In the 150-300µm zone, *spch da1-1* exhibited equally small cells, while *spch*, *spch bb* and *spch da1-1bb* had a few slightly larger cells beginning to be present. In the 300-450µm zone, the cell areas of *spch da1-1* were comparable to those of the other mutants in the 150-300µm zone. By contrast, *spch* and *spch bb* had much larger cells in the 300-450µm zone, while *spch da1-1bb* exhibited an intermediate cell area phenotype.

At ~243 hours after stratification, again cell area of cells in the leaf lamina was similar between the four genotypes in the proximal 150µm. In the 150-300µm zone, *spch da1-1* and *spch da1-1bb* exhibited cell areas approximately equivalent to those in the more basal area, while cell areas in *spch* and *spch bb* were slightly increased. In the 300-450µm zone, *spch da1-1* again exhibited very small cells, of a comparable size to the more basal zones. The *spch da1-1bb* mutant showed a small increase in cell area, while *spch* and *spch bb* showed a greater increase in cell area in cells further from the petiole-lamina boundary.

At ~266 hours after stratification, cells in the most proximal regions of *spch* and *spch bb* were beginning to expand, leaving fewer small cells. The *spch da1-1* and *spch da1-1bb* leaves still exhibited many small cells in the proximal 150µm, and this was reflected in the 150-300µm zone in these genotypes. By contrast, *spch* and *spch bb* showed an even larger proportion of larger cells in this zone, and the cells were larger still in the 300-450µm zone in these mutants. In *spch da1-1* there was a slight increase in the number of larger cells relative to

the 150-300 μ m zone, but some small cells remained. An intermediate phenotype was observed in *spch da1-1bb*.

In the final tracking interval at the ~292 hours after stratification timepoint, all genotypes had some larger cells among the small cells in the proximal 150 μ m. In the 150-300 μ m zone, the proportion of larger cells to smaller cells was greater in *spch* and *spch bb*, with slightly fewer larger cells in *spch da1-1* and *spch da1-1bb*. In the 300-450 μ m zone, the largest cells observed were in *spch bb*, with large cells also observed in *spch*. The cells in *spch da1-1* and *spch da1-1bb* retained approximately the same proportion of larger and smaller cells as in the 150-300 μ m zone.

These observations, in conjunction with those in Section 4.3.2, suggest that cell divisions are more likely to occur in regions of the leaf where there is a higher proportion of smaller cells, relative to other areas of the leaf.

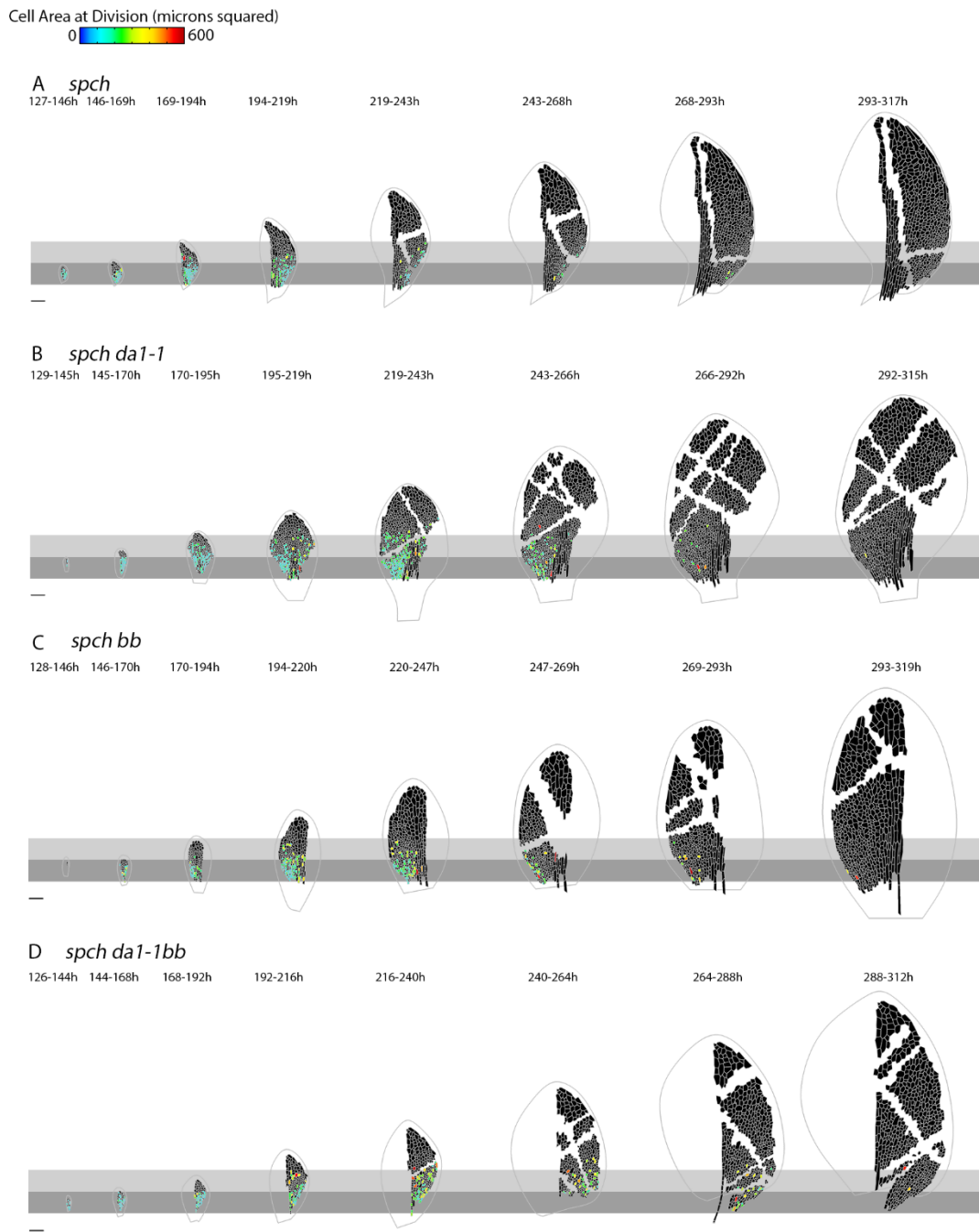


Figure 4.14 Area at time of division of cells in *spch*, *spch da1-1*, *spch bb*, and *spch da1-1bb*

Time-lapse imaging of the first leaf of *spch pAR169* (A), *spch da1-1 pAR169* (B), *spch bb pAR169* (C), and *spch da1-1bb pAR169* (D), shown at approximately 24-hour intervals. Heatmap indicates area at time of division of cells amenable to tracking at the time of the division event. Data is shown on the first time-point for each tracking interval. Leaves are aligned according to the petiole-lamina boundary. Grey boxes indicate 150 μ m (dark grey) and 300 μ m (light grey) from the petiole-lamina boundary. Scale bars 100 μ m.

4.3.6 Cell division symmetry

The symmetry of cell divisions is calculated as a ratio of the areas of the two daughter cells at the time of cell division. A cell division symmetry score of 1 denotes a cell that has divided equally, while a lower score indicates a cell that has divided unequally, resulting in one daughter cell larger than the other. Cell division symmetry was measured for all division events, of which a total of 1611 were observed across all genotypes.

Figure 4.15 shows that cell divisions were on average less symmetrical in *spch da1-1* ($p < 0.0001$), *spch bb* ($p < 0.0001$), and *spch da1-1bb* ($p = 0.0006$) relative to *spch*. The least symmetrical cell divisions were observed in *spch bb*, with a 9.8% reduction in cell division symmetry relative to *spch*. There were no significant differences in mean cell division symmetry between *spch da1-1*, *spch bb*, and *spch da1-1bb*.

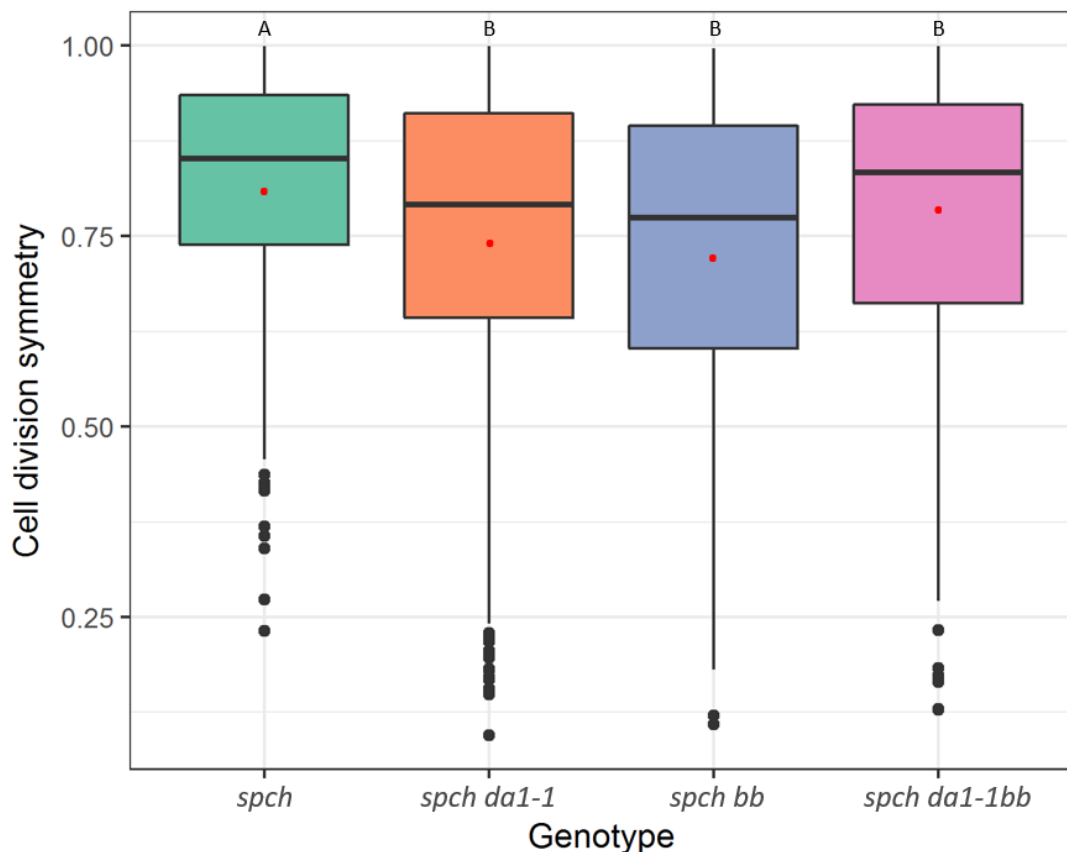


Figure 4.15 Cell division symmetry in *spch*, *spch da1-1*, *spch bb*, and *spch da1-1bb* leaves

Boxplot of cell division symmetry of cells in the first leaf of *spch pAR169*, *spch da1-1 pAR169*, *spch bb pAR169*, and *spch da1-1bb pAR169* leaves ($n = 1$). Total division events observed = 1661. Red points indicate means of samples. Small letters indicate significance groups according to ANOVA with a post-hoc Tukey pairwise comparison (variances were equal, $p = 0.05$). Black points indicate outliers.

Figure 4.16 demonstrates how cell division symmetry changes according to the time of division in each of the four genotypes. Interestingly, while cell division symmetry did not change over time in *spch* leaves, the *spch da1-1*, *spch bb*, and *spch da1-1bb* leaves all exhibited a decrease in cell division symmetry over time, with a significantly steeper slope than *spch* ($p < 0.001$). The steepest slope was observed in *spch da1-1*. However, the R^2 values for these slopes are very low in all four genotypes, potentially as a result of each genotype consisting of only a single biological replicate. However, as all the data in each genotype does trend towards 1 (total symmetry), a low R^2 value is more likely than in the other measurements made in this chapter. Nevertheless, this means that these data should be interpreted carefully, and not too great an importance placed upon the differences in the slopes, as each point does not represent an independent sample.

These data show that cells in *spch da1-1*, *spch bb*, and *spch da1-1bb* mutants divide on average significantly more asymmetrically than in *spch*. In addition, as the leaf ages, cells in *spch da1-1*, *spch bb*, and *spch da1-1bb* appear to become progressively more likely to divide asymmetrically, while the symmetry of *spch* cell divisions remains constant over time.

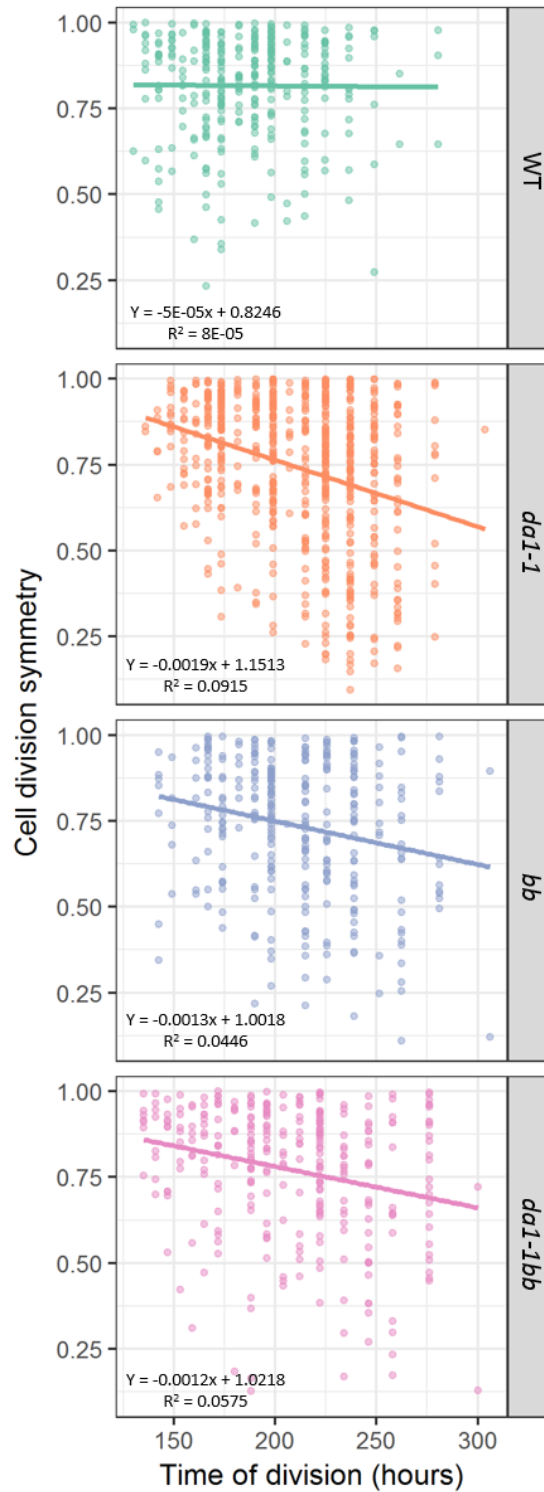


Figure 4.16 Cell division symmetry over time in *spch*, *spch da1-1*, *spch bb*, and *spch da1-1bb* leaves

Cell division symmetry of cells in the first leaf of *spch pAR169*, *spch da1-1 pAR169*, *spch bb pAR169*, and *spch da1-1bb pAR169* leaves, from 126 to 312 hours after stratification (n = 1). Total division events observed = 1661.

4.3.7 Cell growth

The rate of relative areal cell growth was calculated as an average over approximately 24-hour periods. This averaging over 24-hour periods prevents short-term variations in growth rate due to circadian rhythms from affecting overall growth rates. The same time-points are shown in Figure 4.17 for cell growth as in Figure 4.8 for cell division competency. From Figure 4.17 it is clear that in all genotypes, cellular growth rates are initially high (3-6% increase in area, per hour) before decreasing later in development. In addition to this, smaller cells in the base of the leaf were more likely to be growing more quickly than larger cells in the tip of the leaf. In all four genotypes, the highest rates of cell growth persisted for the longest in the leaf margin, with lower growth rates in the midvein at later stages. These data reflect those reported by Kuchen et al, 2012.

The primary difference between the genotypes is the low rate of cellular growth in the tip of the *spch da1-1* mutant over the penultimate and final tracking intervals, in comparison to the other genotypes. While the rate of growth was low in the distal regions of *spch*, *spch bb*, and *spch da1-1bb*, in many cells of *spch da1-1* the rate of growth was below 1% per hour, or 0. The cells in the base of the *spch da1-1* mutant at the final time-point also increased in area more slowly than for the other genotypes, at a rate of around 1% per hour, compared to 2-3% per hour in *spch*, *spch bb*, and *spch da1-1bb*, all of which exhibit largely similar spatial and temporal patterns of cellular growth rate.

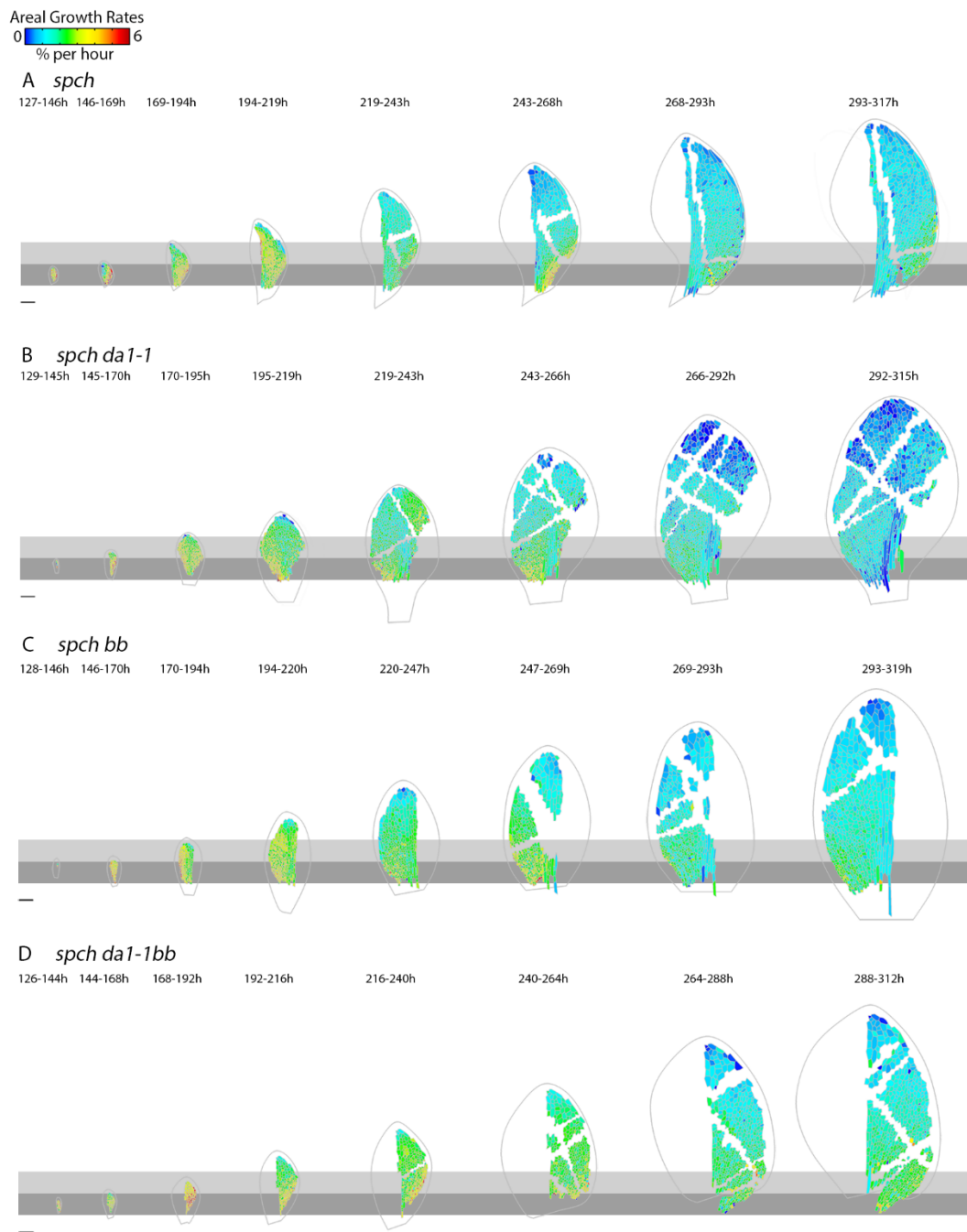


Figure 4.17 Areal growth rates of cells in *spch*, *spch da1-1*, *spch bb*, and *spch da1-1bb*

Time-lapse imaging of the first leaf of *spch pAR169* (A), *spch da1-1 pAR169* (B), *spch bb pAR169* (C), and *spch da1-1bb pAR169* (D), shown at approximately 24-hour intervals. Heatmap indicates areal growth rates of cells amenable to tracking. Data is shown on the first time-point for each tracking interval. Leaves are aligned according to the petiole-lamina boundary. Grey boxes indicate 150µm (dark grey) and 300µm (light grey) from the petiole-lamina boundary. Scale bars 100µm.

4.3.8 Anisotropy of cell growth

Anisotropic cell growth occurs when cells grow more in one direction relative to another. High levels of cell growth anisotropy could contribute to overall anisotropic growth in the leaf, changing its shape (Kuchen et al., 2012). The cell growth anisotropy was calculated as an average over approximately 24-hour periods in order to account for variations in rate due to circadian rhythms. The same time-points are shown in Figure 4.18 for cell growth anisotropy as in Figure 4.8 for cell division competency and Figure 4.17 for cell growth.

Figure 4.18 shows that there is overall a slight increase in cell anisotropy in *spch da1-1* from around 266 hours after stratification onwards, relative to all other genotypes. This increase in anisotropy is primarily located in the midvein and in some areas of the tip of the leaf. Apart from this, there are no strong differences in cell anisotropy between *spch*, *spch bb*, or *spch da1-1bb*.

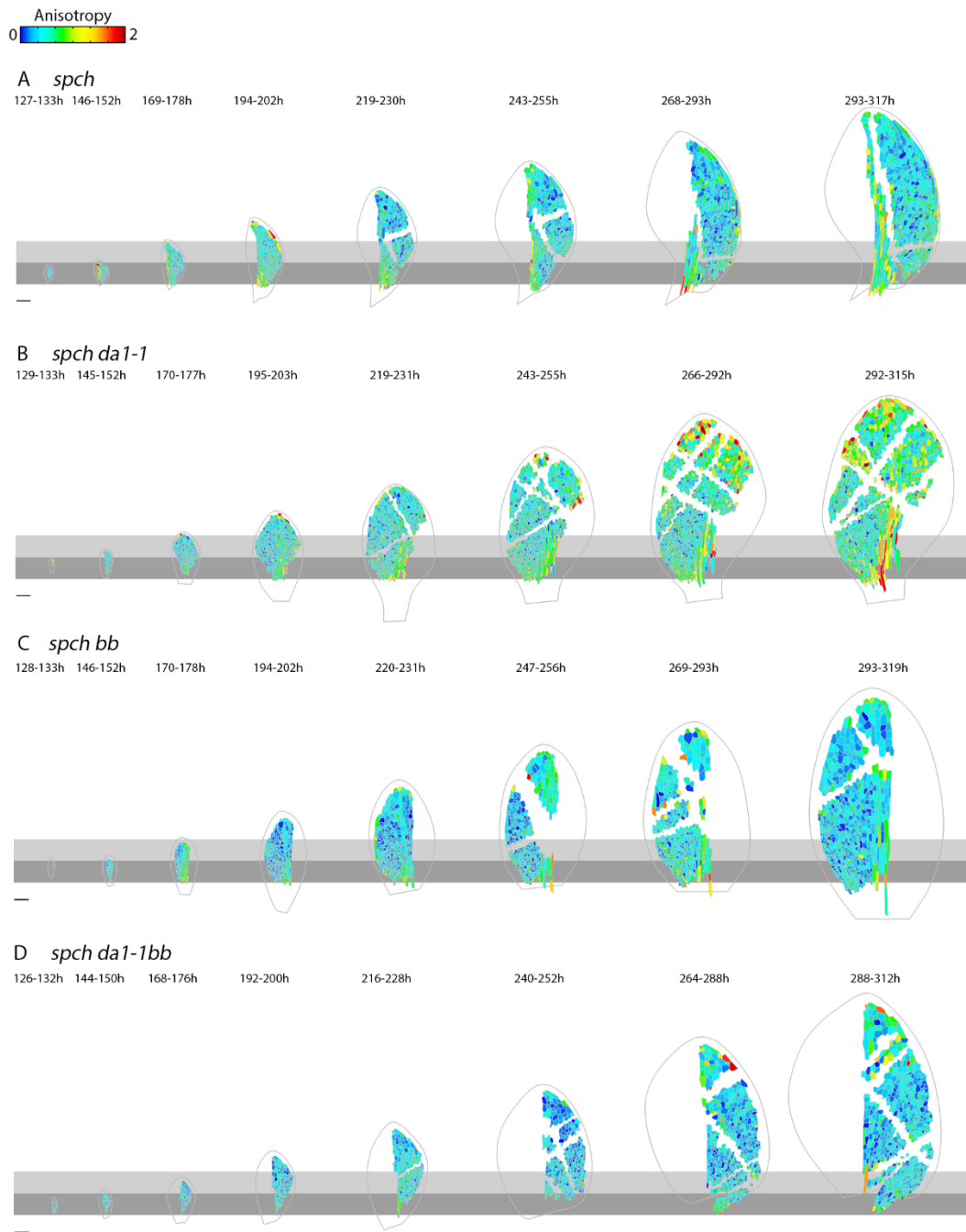


Figure 4.18 Anisotropic growth of cells in *spch*, *spch da1-1*, *spch bb*, and *spch da1-1bb*

Time-lapse imaging of the first leaf of *spch pAR169* (A), *spch da1-1 pAR169* (B), *spch bb pAR169* (C), and *spch da1-1bb pAR169* (D), shown at approximately 24-hour intervals. Heatmap indicates anisotropy of cells amenable to tracking. Data is shown on the first time-point for each tracking interval. Leaves are aligned according to the petiole-lamina boundary. Grey boxes indicate 150µm (dark grey) and 300µm (light grey) from the petiole-lamina boundary. Scale bars 100µm.

4.4 Discussion

4.4.1 Mutations in *DA1* and *BB* promote an increased duration, and population-level rate, of cell proliferation

Several studies have inferred that the *da1-1* and *bb* mutants may exhibit an extended duration of cell proliferation, based on observations of increased duration of growth, and transcriptome analysis of genes involved in cell division and cell growth (Disch et al., 2006; Li et al., 2008; Cattaneo and Hardtke, 2017; Dong et al., 2017; Vanhaeren et al., 2017). However, no studies have, before now, carried out live cell imaging analysis to observe and quantify cell divisions as they take place. In this Chapter, data presented shows quantitatively an increase in the duration of cell proliferation in *spch da1-1*, *spch bb*, and *spch da1-1bb* relative to *spch* (Figure 4.4, Figure 4.5, Figure 4.6 and Figure 4.7) of at least 24 hours. This therefore confirms qualitative estimates from previous studies, that *DA1* and *BB* have a role in limiting the duration of cell proliferation during leaf growth.

However, this new quantitative data described in this chapter also offers other new insights into the spatial patterning of cell divisions in *spch*, *spch da1-1*, *spch bb*, and *spch da1-1bb* mutants. Fox et al. (under review) showed that the maximum distal boundary of the *spch* zone of competency to divide was at 300µm from the petiole-lamina boundary, an observation that my data supports. Interestingly, *spch da1-1* and *spch da1-1bb* (although not *spch bb*) exhibit cell divisions occurring beyond this 300µm zone, indicating a potentially larger zone of competency to divide, and therefore larger population of cells proliferating for a longer period of time. Perhaps more importantly, my data also shows how cell division events are distributed within the zone of competency to divide. A much larger proportion of the cells in the leaf blade retain competency to divide for longer, in *spch da1-1*, *spch bb*, and *spch da1-1bb* compared to *spch*. The increased anisotropy found in *da1-1*, *bb*, and *da1-1bb* mutants resulting in very wide leaves (in particular at the base of the leaf) reported in Chapter 3 of this thesis can now be explained by the persistence of cell divisions in medio-lateral regions of the leaf blade of these mutants, whereas in the wild type, cell divisions are quickly restricted to the leaf margins.

Changes in these spatial aspects of cell division competency in *da1-1* and *bb* mutants had not been predicted in previous studies, and could be a major contributor to the increased final organ size. A study in roots found that an increased size of root meristem or “proliferative fraction” resulted in accelerated root growth (Beemster and Baskin, 1998). Despite clear structural differences in the 2D/3D growth of leaves compared to 1D unidirectional root

growth, it is plausible that a similar mechanism can now be applied to leaf growth, resulting in a larger final organ size, due to the maintenance of a larger “proliferative fraction” - as is shown in this Chapter. Mutations in *bb* have actually been shown to behave in this manner, accelerating growth due to a larger meristem while not affecting overall root elongation (Cattaneo and Hardtke, 2017), indicating that changes in meristem size could have different effects in different plant organs.

A number of genes other than *DA1* and *BB* have been shown to have a role in the control of organ size via the control of cell proliferation and therefore cell number. For example, ectopic expression of the auxin-inducible gene *ARGOS* promotes an increased duration of cell proliferation and organ growth, leading to a larger final organ size (Hu et al., 2003). Additionally, overexpression of *ORGAN SIZE RELATED1*, which shares a conserved protein domain with *ARGOS*, promotes increased organ size due to increased cell numbers, although also exhibits increased cell area (Feng et al., 2011), which is not observed in *da1-1* or *bb* mutants (as described in Chapter 3). *AINTEGUMENTA* is also thought to promote the maintenance of the proliferative phase in several plant organs (Mizukami and Fischer, 2000). Many of these organ size regulators act in response to auxin signals, suggesting that it will now be important to identify a mechanism that regulates *DA1* and *BB* functions, for example to down-regulate their activity during early stages of leaf growth. While this was partially investigated in Chapter 2, future work could include testing the sensitivity of mutants and overexpressor lines to a range of extracellular signals.

A limitation to the analyses in this section of this Chapter is the lack of statistical power when comparing genotypes, as a result of sampling only one leaf per genotype. Even in subsequent sections, where data was collected at a cell by cell level, the cell by cell observations are not truly independent. However, despite the dramatic variation between genotypes observed and the selection of the most representative individual within each group (based on leaf width), with the currently available data it is impossible to statistically confirm variation in the spatiotemporal distribution of cell divisions at the leaf level. In the future, more time could be spent on analysing the remaining three samples in each genotype in order to generate a larger dataset in which differences in the duration and spatial distribution of cell divisions could be formally statistically tested.

4.4.2 Mutations in *BB* and *DA1* may affect cell cycle time and cell area at division
The observation of an increased cell cycle time in *spch bb* and *spch da1-1bb* mutants relative to *spch* was unexpected, as it would not appear to be consistent with the observed increased

rate of growth. However, given the findings that cell proliferation is prolonged in these mutants relative to *spch*, and each cell may only undergo the same number of divisions in its lifetime as those in *spch* (Section 4.3.3), this is expected. More interesting is how this could interact with the observation of larger cell areas at time of division in *spch da1-1*, *spch bb*, and *spch da1-1bb*, relative to *spch*. An increase in cell cycle time could result in larger cell sizes at time of division, if cell growth was not affected, while increasing the maximum threshold for cell division could also result in an increased cell cycle period, assuming no change in cellular growth rates. Either way, increasing the potential of larger cells to divide could provide a mechanism for the spatiotemporal variation in zones of competency to divide observed in the *spch da1-1*, *spch bb* and *spch da1-1bb* mutants. Understanding which of these two factors is the main cause could provide significant insights into the fundamental mechanisms of *DA1* and *BB* activity.

In yeast, progression through the cell cycle is largely controlled by cell size checkpoints, although a number of different mechanisms have been proposed by which this size-control mechanism may be achieved in both budding yeast (Martin and Berthelot-Grosjean, 2009; Moseley et al., 2009) and fission yeast (Polymenis and Schmidt, 1997). In plants, this relationship is more complex. Willis et al. report that neither cell size checkpoints, nor minimum time elapsed, control entry into mitosis in the shoot apical meristem (SAM). Instead, cell division is controlled by a combination of critical size control and the addition of a critical increment in size from the birth of the cell, indicating that differential cellular growth rates could be important in the determination of the timings of cell division (Willis et al., 2016). Jones et al. propose that the control of cell size at time of division and cell cycle duration are controlled at two points during the cell cycle (G1/S and G2/M), and that progression through these checkpoints is dependent on a critical cell size (Jones et al., 2017) - although the possibility of a critical increment as described by Willis et al. was not explored in this study. Although the control of cell proliferation in the SAM is undoubtedly different from that in the leaf, primarily as a result of the final arrest of cell proliferation that must occur in determinate organs, these observations suggest that a more fundamental cause of the variation in cell cycle duration observed in the mutants (particularly mutants carrying the *bb* mutation) could be due to altered control of cell volume at division.

These findings highlight the importance of the careful interpretation of the data regarding the duration of cell proliferation in Section 4.3.2. In fact, knowing that the number of divisions per cell is constant between the wild type and the mutants (Section 4.3.3) and yet the time taken to complete each of those divisions is increased in the mutants (particularly

bb and *da1-1bb*), it is perhaps not surprising that the duration of cell proliferation is increased in the mutants relative to wild type - and this alone would not result in an increase in cell number leading to an increase in final organ size. More important are the dynamics of the spatial extent of the zone of competency to divide, which is larger for longer in the mutants relative to wild type, hence including a greater cell population with the competency to divide, and the likelihood of actual division within this zone, which is increased in the mutants. Together, this suggests that an increased duration of proliferation is merely a by-product of other mechanisms promoting an increase in final organ size in *da1-1*, *bb* and *da1-1bb* mutants, and not the cause.

This experiment could have been improved by the separate identification of lamina cells and midvein cells within the leaf. It seems that different cell division “rules” apply to cells in the midvein compared to those in the lamina; for example, they divide on average at a larger size (Fox et al., under review). Therefore, not only could this produce a confounding effect within each genotype, perhaps producing the outliers observed in Figure 4.12, but it could also have affected comparisons between genotypes. This is due to the different amounts of midvein that was amenable to tracking in each genotype - for example, almost all midvein cells are tracked in *spch da1-1*, while almost none are tracked in *spch da1-1bb*. While this is unlikely to have affected the overall result, due to the relatively low proportion of the total cell population made up by cells in the midvein, it is possible that if the data from these two cell types was able to be separated, further insights into the control of cell division in more cell types in the leaf could be made.

Future work to understand the convergent control of cell cycle period and cell area in *da1-1*, *bb* and *da1-1bb* mutants could include the creation of double or triple mutants with components of the cell cycle. This could include either cyclin-dependent protein kinases (CDKs) for example CDKA;1, which is known to control both the G1/S and G2/M transitions, or cyclins (Francis, 2007). Alternatively, the E2F transcription factors drive a number of G1/S phase controllers (Mariconti et al., 2002), so these could also prove to be interesting targets to investigate for genetic interactions with *DA1* and *BB*.

4.4.3 Mutations in *DA1* and *BB* promote asymmetric cell divisions in pavement cells

In plants, a number of rules have been proposed that aim to explain the observed orientation of division planes in cells, and the generally high level of symmetry in the daughter cells produced. A number of 19th century botanists proposed rules for plant cell division such as

new cell walls appearing at an angle perpendicular to the primary direction of growth (Hofmeister, 1863), intersecting existing walls at an angle of 90° (Sachs, 1878), and perhaps the most well-known, Errera's rule, which states that the division plane between the two daughter cells should be a "surface of minimum energy" - in much the same way that soap bubbles may be divided by a thin film, creating two daughter cells of equal volume (Errera, 1888). This has subsequently been developed into the "shortest wall" rule, whereby cells are predicted to divide at the shortest wall passing through the centre of the cell (Yoshida et al., 2014). While this rule is not perfect, it is the rule most frequently used in models and simulations of organ development.

Data presented in Section 4.3.6 suggests that *spch da1-1*, *spch bb*, and *spch da1-1bb* mutants may break this rule, by showing significantly asymmetric divisions in epidermal pavement cells. In addition to this, while the relative symmetry of *spch* cell divisions was maintained throughout the tracking period, the other mutants appeared to show progressively increasing cell division asymmetry over time. Asymmetric cell divisions have been linked to tumorigenesis in animals via the maintenance of a stem cell population (Knoblich, 2010), a concept which has some parallels with the ectopic cell divisions observed in the *spch da1-1*, *spch bb* and *spch da1-1bb* mutants, where a larger population of smaller cells is maintained for longer than in *spch*. The stomatal lineage is a key example of asymmetric cell divisions occurring in wild type Arabidopsis, where genes including *SPCH* and *BREAKING OF ASYMMETRY IN THE STOMATAL LINEAGE (BASL)* promote asymmetric cell divisions resulting in meristemoid cells and stomatal guard cells distributed throughout the pavement cells (Pillitteri et al., 2016). However, the research described in this Chapter was carried out in *spch* mutants, in which *SPCH* is knocked out and which do not exhibit the asymmetrical divisions that lead to stomatal development. It could be possible that *DA1* or *BB* are somehow involved in the repression of *BASL* expression in pavement cells, which could lead to the observed phenotypes. Alternatively, other cues could be affecting cell polarity, which is thought to affect the location of the preprophase band. This again links to possible role for *DA1* or *BB* in the regulation or perception of extracellular signals such as auxin, cytokinins and brassinosteroids - or indeed, the regulation of *DA1* and *BB* themselves by these signals.

Repeating this experiment with the additional application of phytohormones could determine if extracellular signalling of this kind is involved in the control of the position of the preprophase band, and therefore asymmetric cell division. In addition to this, carrying out tracking experiments of this kind on wild type, *da1-1*, *bb*, and *da1-1bb* plants would allow the inspection and comparison of stomatal and non-stomatal cell divisions in wild type and

each mutant. If there is variation between the genotypes in the patterns of division in the stomatal lineage, this opens up the possibility of a regulatory relationship between the DA1 system and genetic factors controlling the symmetry of cell divisions.

4.4.4 The increased final organ size and shape change observed in *da1-1*, *bb*, and *da1-1bb* mutants is due to cell division dynamics rather than cell growth

Based on observations in Sections 4.3.7 and 4.3.8, it appears that the overall final organ size and shape change observed in the mutants (as described in Chapter 3) are not due to changes in cellular growth rates or cell growth anisotropy. The single exception to this is the decreased rate of cell areal growth in the tip of *spch da1-1* leaves, which could explain the decreased final cell size in mature leaves of *da1-1*. If further work reveals that *DA1* interacts in some way with auxin signalling, this could affect the loosening in the cell walls promoted by auxin as proposed in the Acid Growth Theory of cellular expansion (Rayle and Cleland, 1992). If *da1-1* mutants are less receptive to auxin, this could explain their reduced cell growth.

The anisotropic tissue growth reported in Chapter 2, resulting in much wider leaves in *da1-1*, *bb*, and *da1-1bb* mutants is not as a result of anisotropic cell growth, but more likely due to the increased number of cell divisions occurring across the width of the base of the leaf lamina, as shown in Figure 4.8.

4.4.5 Two possible mechanisms promoting increased final leaf size in *da1-1*, *bb*, and *da1-1bb* mutants

Based on the observations made in this Chapter, it may be that there are two separable mechanisms involved in the control of cell proliferation in mutants carrying the *da1-1*, *bb*, and *da1-1bb* mutations. The first of these mechanisms is one controlling the size of the zone of competency to divide - that is, the maximum distance of any cell with competence to divide from the petiole-lamina boundary, and the duration at which this distance remains high. This Chapter has shown that in the *speechless* background, this zone is spatially extended in the *spch da1-1* and *spch da1-1bb* mutants, and temporally extended in *spch da1-1*, *spch bb*, and *spch da1-1bb*, relative to *spch*. The extension of this zone in these mutants strongly correlates with a larger zone of smaller cells (Figure 4.9). While the additional longevity of the zone of competency to divide, and hence duration of proliferation in *spch da1-1*, *spch bb*, and *spch da1-1bb* relative to *spch* does not result in an increase in cell number (see Section 4.4.2), the observation that the zone of competency remains larger for longer in *spch da1-1*, *spch bb*, and *spch da1-1bb* than in *spch* and reaches a greater maximal extent

in *spch da1-1* and *spch da1-1bb* does mean that there are more cells within it for longer, which then have the competency to divide. While these findings surrounding the spatiotemporal dynamics of the zone of competency to divide do present interesting opportunities to further investigate a potential role for *DA1* and *BB* in the control of the cell cycle, they do not in themselves fully explain the dramatic differences in cell numbers and final organ size between the mutants and wild type described in Chapter 3.

A second proposed mechanism may go some way towards explaining these phenotypic differences, however. Observations in Section 4.3.2 found that, while the maximal distal extent of the zone of competency to divide was increased in the *spch da1-1* and *spch da1-1bb* mutants, the proportion of the cells within that zone of competency to divide which were observed to actually divide was also greater in *spch da1-1*, *spch bb* and *spch da1-1bb* than in *spch*. This is illustrated in Figure 4.19.

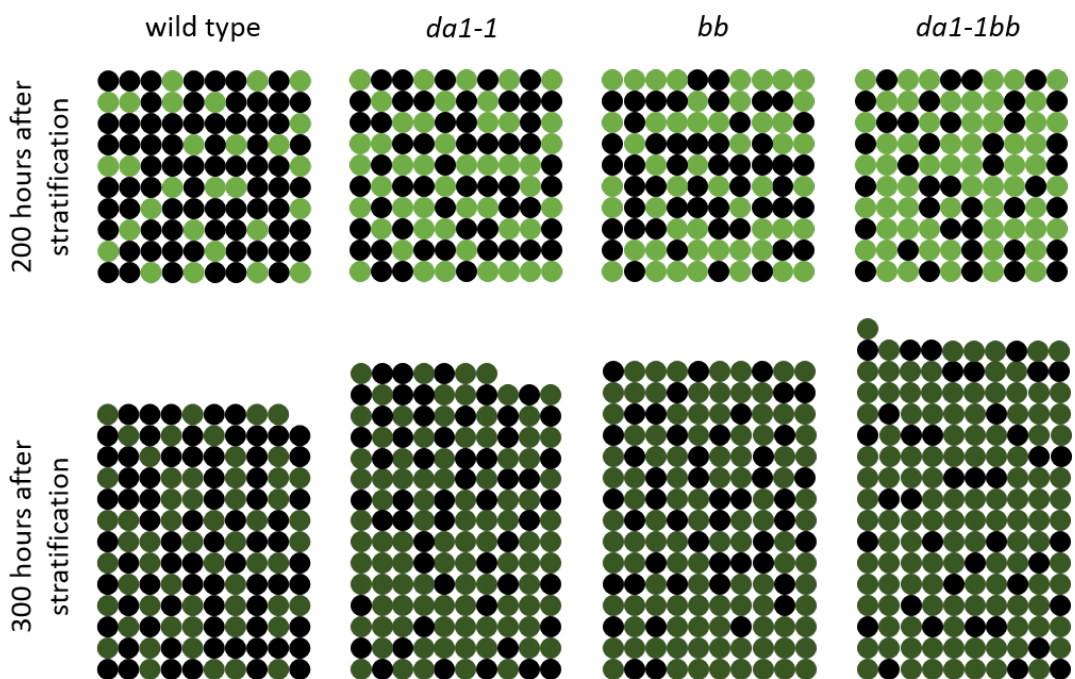


Figure 4.19 Division competency at the cell population level

Normalised 100-cell populations within the zone of competency to divide of wild type, *da1-1*, *bb*, and *da1-1bb* at 200 hours after stratification, and the predicted result of one cell division cycle in 100 hours, shown at 300 hours after stratification. Black circles indicate cells within the zone of competency to divide that do not divide. Light green circles indicate cells within the zone of competency to divide that do divide (wild type: 28.5%, *da1-1*: 47.4%, *bb*: 49.7%, *da1-1bb*: 61%). Dark green circles indicate cells produced as a result of cell divisions between 200 and 300 hours after stratification.

In Figure 4.19, data from the tracking experiment has been used to produce a population of cells, normalised to 100, with a representative proportion of black (do not divide) and light green (will divide) cells from within the zone of competency to divide, at approximately 200 hours after stratification, for each mutant and for wild type. Cells in the midvein were excluded from this, as they show a different pattern of competency to divide from lamina cells. My data suggests that cells may divide on average once within the final 100 hours of the experiment (Section 4.3.3), so each light green cell divides once before 300 hours after stratification. This produces a new population of cells - black (did not divide), and dark green (divided).

From this schematic, it is possible to see how having a greater proportion of cells within the zone of competency to divide that actually divide, could result in an increase in cell number such as that observed in Chapter 3. If the other differences observed in the mutants were added to this model, for example the increased number of cells within the zone of competency to divide, then it is possible that the differences in cell number between the mutants and wild type could be sufficient to explain the differences in overall final organ size.

The results of this model therefore highlight the importance of measuring competency to divide, and the rate of cell division, at the cell population level (in terms of the density of cell divisions in the zone of competency to divide), rather than just on a zonal or individual cellular level.

4.4.6 Modelling the effects of *da1-1* and *bb*

According to the models proposed in Kuchen et al. 2012 and Fox et al. (under review), it is possible that *DA1* or *BB* could be candidates for LATE, and have a role in limiting growth at later stages. However, LATE is not involved in the control of cell division, which appears to be the primary mechanism by which *da1-1* and *bb* mutants generate larger final organ sizes. This therefore suggests that *DA1* or *BB* could instead be candidates for controlling the sensitivity of cells to another factor such as CDIV - if there is patchy or stochastic recognition of a factor that confers actual division competency upon a cell within the zone of competency to divide, the *da1-1* or *bb* mutations could lower the threshold of the factor required for any given cell to divide. Further testing of the impacts of *da1-1* and *bb* mutations in the proposed model could further elucidate roles for *DA1* and *BB* in an integrated model of the control of cell division and cell growth.

4.4.7 Summary

In summary, the evidence presented in this Chapter suggests that, while there is an increased duration of cell proliferation in the mutants relative to wild type leaves, this is not the main reason for the increased final cell number, as cells tend to divide the same number of times in all genotypes, but more slowly in the mutants. While the rate of cell division of each individual cell is not increased in the mutants relative to wild type (it is in fact decreased), there is an increased rate of cell division at the population level, with more cells of the total population that are competent to divide, actually dividing in the mutants, relative to wild type. It seems likely that it is this effect that contributes mainly to the increase in cell numbers. A key limitation of this chapter is the lack of biological replicates for each genotype, meaning that future analysis of the three further biological replicates is imperative to fully understand the effects of these mutations on cell division.

5 GENERAL DISCUSSION

In this thesis I have taken a multidisciplinary approach to understanding the activity of *DA1* and *BB*, incorporating biochemical work and a range of innovative imaging and analysis techniques to further elucidate the biological functions of *DA1* and *BB* activity in leaf growth.

In Chapter 2, a range of potential novel substrates were tested for DA1-mediated cleavage. These included 5 proteins of interest identified based on a yeast-2 hybrid screen previously carried out by Dr Jack Dumenil, selected for their important roles in organ development in *Arabidopsis* and mutant phenotypes that would be expected based on possible cleavage by DA1. In addition to this, a prediction for a conserved cleavage site for DA1 by Dr Benguo Gu was tested in members of the TCP family, including the testing of 3 potential novel substrates. Although none of the 8 potential substrates of DA1 tested were found to be cleaved by DA1 in a transient protoplast system, progress was made on the identification of a target site for cleavage in two known substrates of DA1.

In Chapter 3, quantitative phenotyping of *da1-1*, *bb*, and *da1-1bb* leaves during growth generated new insights into how these mutations affect leaf shape as well as size. This was followed up with a whole-organ cellular analysis of leaves at early stages of growth, in which it was confirmed that the increase in leaf area in *da1-1*, *bb* and *da1-1bb* mutants relative to wild type is as a result of increased cell number. I also showed that there may be an increase in the rate of cell proliferation in the mutants in addition to the published increase in the duration of cell proliferation (Disch et al., 2006; Li et al., 2008; Vanhaeren et al., 2017). Other cell-level and leaf-level parameters such as cell area, cell density and cell circularity were also analysed, building a more complete and quantitative picture of how the *da1-1* and *bb* mutations affect leaf growth at the cellular level. In addition, scanning electron microscopy was carried out on mature leaves of wild type, *da1-1*, *bb* and *da1-1bb*, allowing the analysis of cell areas in mature leaves and leading to the proposal of a model for the interaction of *DA1* and *BB* in the control of final cell area.

Chapter 4 describes a detailed study of cell division and growth in *spch*, *spch da1-1*, *spch bb* and *spch da1-1bb* through live-cell imaging over an 8-day period. In this experiment, cell divisions have been empirically measured for the first time in plants carrying the *da1-1* and *bb* mutations, allowing a range of parameters to be determined including the spatiotemporal distribution of cell divisions, and information regarding the time between cell divisions, cell area at the time of division, and the symmetry of cell divisions. In conjunction with these cell division analyses, measurements of cellular growth rates and anisotropy revealed that the

increased final leaf size and wider leaf blade produced in *da1-1*, *bb* and *da1-1bb* is almost exclusively as a result of the zone of competency to divide staying larger for longer (rather than an absolute duration of proliferation), and a greater population-level rate of cell divisions within this zone of competency to divide (that is, a greater proportion of the cells within the zone of competency to divide may be observed to actually undergo cell division).

5.1 Building our knowledge of DA1 and BB activity

The findings in this thesis have significantly built upon the current understanding of the roles of *DA1* and *BB* in leaf growth. For example, evidence in this thesis suggests that the increased duration of growth observed in the *da1-1*, *bb* and *da1-1bb* mutant leaves compared to wild type (Disch et al., 2006; Li et al., 2008; Dong et al., 2017; Vanhaeren et al., 2017) is not as a result of the slightly increased absolute duration of proliferation, but more likely due to a larger population of cells dividing for longer, creating a larger population of small cells which then move more slowly into the expansion zone, resulting in an increased duration of leaf growth. This means that the observation of an increased mitotic index over a longer duration of leaf growth in *da1-1* plants than in wild type (Li et al., 2008) was a valid and useful metric, but this initial interpretation can now be revised in the light of these new findings concerning the density of cell divisions in the zone of competency to divide. By also observing a snapshot of *pCYCB1;1::GUS* expression rather than a time-course, Li et al. came to the valid conclusion based on the available data that the duration of proliferation was increased in the *da1-1* mutant relative to wild type. However, by utilising live-cell imaging, it is possible to achieve a more quantitative and integrated picture of the growth dynamics of a leaf. It is important to note that the *spch* mutant may affect cell division dynamics, and therefore while the results presented in Chapter 4 are comparable between themselves, it is not possible to compare the results, time-point to time-point, to previous studies in a wild type for *SPEECHLESS* background.

The finding of a larger zone of smaller cells with the competence to divide that persisted for longer is also supported by many of the findings regarding the cell area and cell density distributions in Chapter 3. While Vanhaeren et al. did carry out some cell-level analyses of *da1-1*, *bb* and *da1-1bb* mutants, the approach I took in Chapter 3 of segmenting and analysing essentially all upper epidermal pavement cells in the leaf allowed a more holistic evaluation of the spatial distributions of cell areas. In addition to this, Chapter 3 made a further new observation that cell area in *da1-1* mature leaves are reduced, relative to wild type - while *bb* and *da1-1bb* mutants maintained the same cell area as wild type. By contrast,

no change in cell area in mature leaves of *da1-1* is reported in Li et al. 2008 or Vanhaeren et al. 2017, although the extent of the sampling and analysis in these studies is unknown. This difference in final cell area prompted the suggestion of an antagonistic model of interactions for *DA1* and *BB*. Testing this model will shed light on the potential for a role for *DA1* in a compensation mechanism.

Many of the findings in both Chapter 3 and Chapter 4 point towards a role for *DA1* and *BB* in the control of the cell cycle. Already, several of the known substrates of the *DA1* peptidase are known to modulate the cell cycle - for example, *UBP15* is a histone de-ubiquitinase (pers. comm., Yunhai Li), and is thought to have a role in the promotion of the cell cycle potentially by down-regulating the cell cycle repressor *ICK1*. This is reflected in the small organ sizes and reduced cell proliferation in *ubp15* mutants (Liu et al., 2008).

Another substrate of *DA1*, *TCP15* promotes the transcription of the *CYCA2;3* and *RETINOBLASOMA-RELATED (RBR)* genes, both of which are involved in the promotion of the cell cycle (Li et al., 2012). Interestingly, *RBR* has also recently been shown to promote asymmetric cell divisions both in the stomatal lineage and in the maintenance of a stem cell population in roots (Wildwater et al., 2005; Desvoyes et al., 2014), drawing a potential link to the increased asymmetry of cell divisions in the *spch da1-1*, *spch bb* and *spch da1-1bb* mutants. Reduced *DA1* activity, such as in *spch da1-1* plants, could result in increased *TCP15* protein levels and consequently an increase in *RBR* expression, and increased cell division asymmetry. This potential mechanism to explain the increase in asymmetric cell divisions in *spch da1-1*, *spch bb* and *spch da1-1bb* relative to *spch* suggests that investigation of *RBR* expression levels in cells within *spch da1-1* plants of variable cell division symmetry could be interesting. While it seems unlikely that *RBR* is a direct target for *DA1*-mediated cleavage (as it is already regulated indirectly by *DA1* peptidase activity), the link between these two genes could still be of interest for future work in this area.

Although Chapter 2 did not identify any additional substrates for *DA1* peptidase, the work carried out in this thesis does pose two new lines of investigation into the biochemical activity of *DA1*. Firstly, work in the future seeking to identify new substrates for the *DA1* peptidase should focus primarily on genes involved directly and indirectly in the control of the cell cycle. Using quantitative proteomics methods such as the iTRAQ method (Enoksson et al., 2007; Yang et al., 2017; Zhang et al., 2017) to compare protein expression across a range of cell cycle genes in the *da1-1* mutant relative to wild type could give a clearer indication of viable candidates for cleavage than using a yeast-2-hybrid screen based on

observable phenotypes, as detailed in Chapter 2. Secondly, while the interacting proteins that were tested for cleavage were found not to be substrates of DA1, it remains possible that the yeast-2-hybrid interaction observed by Dr Jack Dumenil was still valid and they could be linked to DA1 in a way other than as a substrate for cleavage. For example, TCP3 appears to depend on the presence of DA1 (although not DA1 peptidase activity) for stability. It is possible that other domains in DA1, for example the LIM or LIM-like domains could be involved in the maintenance of the stability of, or transcriptional regulation of, genes negatively controlling growth. TCP3 is closely related to TCP4 (Martin-Trillo and Cubas, 2010), a known negative regulator of organ growth (Schommer et al., 2014), suggesting a mechanism via which increased DA1 expression would promote increased protein levels of TCP3, repressing growth. Analysing the stability and expression of *TCP3* in the presence of DA1 proteins lacking in the functional domains other than the peptidase domain, could elucidate this effect further. In addition to this, proteins physically interacting with DA1 could be part of a putative mechanism modulating DA1 activity, rather than a downstream peptidase substrate for example, which our work until now has primarily focussed on. The regulation of DA1 protein levels or peptidase activity is not well understood, but work by Dr Hui Dong is beginning to explore a mechanism for DA1 regulation by TMK1 and TMK4. TMK4 was found by Dr Jack Dumenil to interact physically with DA1 in a yeast-2-hybrid screen as well as in an *in vitro* co-immunoprecipitation experiment, but was not found in Chapter 2 to be cleaved by DA1. Dr Dong has identified a role for TMK1 and TMK4 in the phosphorylation of DA1, which represses its peptidase activity. A similar role has been identified for BAK1, the closely related brassinosteroid receptor (Hui Dong, unpublished). The identified roles of TMK1, TMK4 and BAK1 in phytohormone sensing (Li et al., 2002; Dai et al., 2013; Kim et al., 2013; Xu et al., 2014) position these observed interactions with DA1 as important steps in a potential pathway for the regulation of DA1 activity by auxin and brassinosteroids. For example, DA1 activity may be repressed by phosphorylation to maintain the competence of cells to proliferate during leaf growth.

Together, my work in this thesis has built significantly upon the fundamental understanding of the biological functions of *DA1* and *BB*, as well as identifying a new perspective on the control of cell division in organ growth which could be applied to future studies on other genes.

5.2 DA1 and BB as factors in a quantitative framework for the control of organ size and shape

In this thesis I present quantitative data that can be used in mathematical models of growth that aim to explain shape and size in leaf development, the most comprehensive of which is that described by Kuchen et al. 2012 and Fox et al. (under review). In this model, a number of quantifiable factors interact to control cell division, growth and polarity (see Chapter 1 and Chapter 4 for fuller descriptions of this model).

Before the research described in Chapter 4, it seemed most likely that *DA1* or *BB* could have been candidates for LATE, a factor expressed uniformly throughout the tissue but which only represses tissue growth at later stages (Fox et al., under review). However, it now seems that *DA1* is exclusively involved with cell proliferation, and that *BB* may be involved both with cell proliferation, and the repression of cell expansion at later stages (see Chapter 3) - but that their impact on cell division is throughout the division phase, not merely at the end to extend the duration. The additions made to the model by Fox et al. (under review) of PMF and CDIV pose the most interesting opportunities for identifying a potential role for *DA1* or *BB* in the model. PMF controls both cell division and cell growth, and is involved in the maintenance of the zone of competency to divide. CDIV confers competency to divide in cells. If PMF mediates the zone of competency to divide, and CDIV promotes the ability of cells within that zone to divide, then *DA1* could be a candidate for the repression of PMF, and either *DA1* or *BB* could be a candidate for the repression of CDIV.

Alternatively, *DA1* could be downstream of the PMF or CDIV factors. For example, as PMF is thought to be a mobile signal (proximal mobile factor) (Fox et al., under review), another candidate for this could be a phytohormone such as brassinosteroids. If PMF were brassinosteroids, which may have a role in reducing *DA1* peptidase activity (Hui Dong, unpublished), increased brassinosteroid signalling would result in decreased *DA1* activity, and the concomitant increase in the zone of competency to divide. Equally, increased CDIV as a result of increased brassinosteroids would result in reduced *DA1* activity, and potentially more cells within the zone of competency to divide that actually complete a cell division. Brassinosteroids have a well-described role in promoting epidermal growth in leaves, and are a plausible candidate for a signal that maintains the capacity of cells to proliferate during organ growth (Savaldi-Goldstein et al., 2007)

It is now possible to apply the comprehensive quantitative data on leaf growth gathered in this thesis that describe the effects of growth modifier mutants such as *da1-1* or *bb* to a

robust mathematical model such as that proposed by Kuchen et al. and Fox et al. This could identify further candidates for the growth factors discussed here, resulting in the future in a more complete quantitative description of the role of key regulatory genes in the growth and development of the Arabidopsis leaf.

5.3 A new model incorporating competence to divide within a cell population?

A recent publication used live cell imaging to visualise tissue development in *Drosophila melanogaster* and developed a simple model incorporating a number of cellular processes to characterise tissue growth and deformation during wing and thorax development (Guirao et al., 2015). These cellular processes included cell divisions (D), cellular rearrangement (R), cell shape and size changes (S), and cell apoptosis (A). The model also included other processes than cell divisions and apoptosis that would result in a change in the number of cells, such as the integration of new cells in epithelium sheets (N), the fusion (or coalescence) of existing cells (C), and cells entering or leaving the field of view of the microscope (J). Guirao et al. determined that in the absence of any of the three latter factors (N , C and J), that the growth and deformation of the tissue could be described according to Equation 5.1.

$$G = D + R + S + A$$

Equation 5.1 A model to quantify tissue development and deformation in *Drosophila melanogaster*

(Guirao et al., 2015)

While cellular rearrangement and apoptosis are a feature of *Drosophila* epithelial development (Xu et al., 2009; Guirao and Bellaïche, 2017), these do not generally occur in Arabidopsis growth. For this reason, this simple model could be modified for application to the Arabidopsis leaf growth system.

To develop a model of this type to describe Arabidopsis leaf growth and how the different mutations investigated contribute to final organ size, based on the findings described in this thesis, would require a number of factors. Two fundamental factors contribute to the final size of an organ - mature cell number, and the number of cells. Therefore, mature cell area should be the first factor, M . The number of cells in a mature leaf is based on the number of cell divisions that occur, and the number of cells in the initial primordium. As the SAM and organ initiation has not yet been studied in *da1-1*, *bb* and *da1-1bb* mutants, a proxy based on seed size could be used to indicate embryo size and therefore a potential global effect on

all tissues of the plant. This could be termed I . Data presented in Chapter 4 described the number of cell divisions per dividing cell in each of the mutants from early stages of growth. While no statistically significant differences between genotypes were observed in this study, this term (D) could be included in the model in other instances so that it could be applied to the study of other mutations. Finally, determining the number of cells within the tissue that will divide is a more complex issue, involving the maximum size of the zone of competency to divide, the time at which the zone recedes to the base of the leaf, the overall duration (or longevity) of cell proliferation, and the proportion of cells actually dividing within that zone. These could be described as Z , R , L and P , respectively. The final area of the leaf is defined as F , and the total model is shown in Equation 5.2.

$$F = M + I + D + Z + R + L + P$$

Equation 5.2 A model to predict final organ size based on cell size and division factors in *Arabidopsis thaliana*

Together, this produces a model with many factors, but which can be significantly simplified with the biological knowledge gathered in this thesis. For example, the number of divisions per dividing cell (D) is not changed in the *da1-1*, *bb* and *da1-1bb* mutants. In addition, it appears that the duration of cell proliferation (L) is not itself of significant importance to the control of final leaf size. Both of these terms could therefore be excluded from the model in this instance, and the new model used to determine whether the observed changes in the factors are sufficient to explain the differences in final leaf area.

$$F = M + I + Z + R + P$$

Equation 5.3 A simplified model for describing the effects of *da1-1*, *bb* and *da1-1bb* on leaf size

Following this model, the parameters for each genotype and the results are in Table 5.1, normalised to make wild type the standard. The figures used in Table 5.1 are based on calculations and measurements from the data shown in Chapter 3 and Chapter 4 of this thesis, and from published data. M is the mean area of epidermal pavement cells in mature leaves. I represents the mean seed weight, as described in Li et al., 2008. Z represents the most distal extension of the zone of competency to divide. R is the time at which the zone of competence to divide begins to recede towards the base of the leaf (see Supplementary

Figure S2). Finally, *P* represents the proportion of the cells within the zone of competency to divide that are actually observed to divide.

Factor	wild type	<i>da1-1</i>	<i>bb</i>	<i>da1-1bb</i>
<i>M</i>	1.0	0.79	0.87	1.02
<i>I</i>	1.0	1.32	1.05	1.69
<i>Z</i>	1.0	1.25	1.0	1.17
<i>R</i>	1.0	1.1	1.1	1.2
<i>P</i>	1.0	1.7	1.7	2.1
Prediction	5.0	6.16	5.72	7.18

Table 5.1 Calculations for a model describing the effects of *da1-1*, *bb* and *da1-1bb* on leaf size

Measurements of final leaf area in Chapter 3 showed that *da1-1* leaves are 140% of wild type area, *bb* leaves 117%, and *da1-1bb* leaves were 196% of wild type. The model described here predicts that *da1-1* leaves would be 123% of wild type, *bb* leaves 114%, and *da1-1bb* leaves 144%. Based on this, it seems that this model is sufficient to explain the trends of the effects of *BB* on leaf development, but not *DA1*, as the predictions from *da1-1* and *da1-1bb* are lower than the real value. The model does, however, predict a synergistic interaction between the mutants, which is also observed in the real measurements. This suggests that there could be a further factor affecting cell activity in mutants carrying the *da1-1* allele that is not reflected in this model. For example, this model does not include any potential impact that increased asymmetric cell divisions could have. Further analysis of the biological data, or more detailed experiments with shorter tracking intervals could begin to elucidate this in the future.

Together, the research described in this thesis both adds significantly to our knowledge of the effects of *DA1* and *BB* on leaf growth, but also poses an emergent new concept in the way of thinking about the control of cell division within a population of cells, rather than simply in a defined zone or at the single-cell level. This new concept could change the way in which growth and division is measured for not only *DA1* and *BB* but also other genes, in the future.

BIBLIOGRAPHY

- Achard P, Gusti A, Cheminant S, Alioua M, Dhondt S, Coppens F, Beemster GTS, Genschik P** (2009) Gibberellin Signaling Controls Cell Proliferation Rate in Arabidopsis. *Current Biology* **19**: 1188-1193
- Afzal AJ, Wood AJ, Lightfoot DA** (2008) Plant receptor-like serine threonine kinases: roles in signaling and plant defense. *Molecular Plant-Microbe Interactions* **21**: 507-517
- Aguilar-Martinez JA, Sinha N** (2013) Analysis of the role of Arabidopsis class I TCP genes AtTCP7, AtTCP8, AtTCP22, and AtTCP23 in leaf development. *Frontiers in Plant Science* **4**: 406-119
- Agulnick AD, Taira M, Breen JJ, Tanaka T, Dawid IB, Westphal H** (1996) Interactions of the LIM-domain-binding factor Ldb1 with LIM homeodomain proteins. *Nature* **384**: 270–272
- Alexandratos N, Bruinsma J** (2012) World agriculture towards 2030/2050: the 2012 revision. *In* ESA Working paper No. 12-03. FAO, Rome
- Alvarez JP, Goldshmidt A, Efroni I, Bowman JL, Eshed Y** (2009) The NGATHA Distal Organ Development Genes Are Essential for Style Specification in Arabidopsis. *The Plant Cell* **21**: 1373-1393
- Anand R, Langer T, Baker MJ** (2013) Proteolytic control of mitochondrial function and morphogenesis. *Biochimica et Biophysica Acta (BBA) - Molecular Cell Research* **1833**: 195-204
- Anastasiou E, Kenz S, Gerstung M, MacLean D, Timmer J, Fleck C, Lenhard M** (2007) Control of Plant Organ Size by KLUH/CYP78A5-Dependent Intercellular Signaling. *Developmental Cell* **13**: 843-856
- Andriankaja M, Dhondt S, De Bodt S, Vanhaeren H, Coppens F, De Milde L, Muhlenbock P, Skirydz A, Gonzalez N, Beemster GTS, Inzé D** (2012) Exit from Proliferation during Leaf Development in Arabidopsis thaliana: A Not-So-Gradual Process. *Developmental Cell* **22**: 64-78
- Andrietta MH, Eloy NB, Hemerly AS, Ferreira PCG** (2001) Identification of sugarcane cDNAs encoding components of the cell cycle machinery. *Genetics and Molecular Biology* **24**: 61-88
- Apelt F, Breuer D, Nikoloski Z, Stitt M, Kragler F** (2015) Phytotyping4D: a light-field imaging system for non-invasive and accurate monitoring of spatio-temporal plant growth. *The Plant Journal* **82**: 693-706

- Ariizumi T, Lawrence PK, Steber CM** (2011) The Role of Two F-Box Proteins, SLEEPY1 and SNEEZY, in Arabidopsis Gibberellin Signaling. *Plant Physiology* **155**: 765-775
- Autran D, Jonak C, Belcram K, Beemster GTS, Kronenberger J, Grandjean O, Inzé D, Traas J** (2002) Cell numbers and leaf development in Arabidopsis: a functional analysis of the STRUWWELPETER gene. *The EMBO Journal* **21**: 6036-6049
- Backhaus A, Kuwabara A, Bauch M, Monk N, Sanguinetti G, Fleming A** (2010) leafprocessor: a new leaf phenotyping tool using contour bending energy and shape cluster analysis. *New Phytologist* **187**: 251-261
- Ballester P, Navarrete-Gomez M, Carbonero P, Onate-Sanchez L, Ferrandiz C** (2015) Leaf expansion in Arabidopsis is controlled by a TCP-NGA regulatory module likely conserved in distantly related species. *Physiologia Plantarum* **155**: 21-32
- Barbier de Reuille P, Robinson S, Burian A, Summers H, Yoshida S** (2015) LithoGraphX. *In*, **Barbier de Reuille P, Routier-Kierzkowska A-L, Kierzkowski D, Bassel GW, Schüpbach T, Tauriello G, Bajpai N, Strauss S, Weber A, Kiss A, Burian A, Hofhuis H, Sapala A, Lipowczan M, Heimlicher MB, Robinson S, Bayer EM, Basler K, Koumoutsakos P, Roeder AHK, Aegerter-Wilmsen T, Nakayama N, Tsiantis M, Hay A, Kwiatkowska D, Xenarios I, Kuhlemeier C, Smith RS** (2015) MorphoGraphX: A platform for quantifying morphogenesis in 4D. *eLife* **4**: e05864
- Bartlett JG, Alves SC, Smedley M, Snape JW, Harwood WA** (2008) High-throughput Agrobacterium-mediated barley transformation. *Plant Methods* **4**: 22
- Bassel GW, Stamm P, Mosca G, Barbier de Reuille P, Gibbs DJ, Winter R, Janka A, Holdsworth MJ, Smith RS** (2014) Mechanical constraints imposed by 3D cellular geometry and arrangement modulate growth patterns in the Arabidopsis embryo. *Proceedings of the National Academy of Sciences* **111**: 8685-8690
- Baute J, Polyn S, De Block J, Blomme J, Van Lijsebettens M, Inzé D** (2017) F-Box Protein FBX92 Affects Leaf Size in Arabidopsis thaliana. *Plant and Cell Physiology* **58**: 962-975
- Beemster GTS, Baskin TI** (1998) Analysis of Cell Division and Elongation Underlying the Developmental Acceleration of Root Growth in Arabidopsis thaliana. *Plant Physiology* **116**: 1515-1526
- Beemster GTS, De Vusser K, De Tavernier E, De Bock K, Inzé D** (2002) Variation in Growth Rate between Arabidopsis Ecotypes Is Correlated with Cell Division and A-Type Cyclin-Dependent Kinase Activity. *Plant Physiology* **129**: 854-864
- Belkhadir Y, Chory J** (2006) Brassinosteroid signaling: a paradigm for steroid hormone signaling from the cell surface. *Science* **314**: 1410-1411

- Bergmann DC, Sack FD** (2007) Stomatal Development. *Annual Review of Plant Biology* **58**: 163-181
- Betsuyaku S, Takahashi F, Kinoshita A, Miwa H, Shinozaki K, Fukuda H, Sawa S** (2011) Mitogen-Activated Protein Kinase Regulated by the CLAVATA Receptors Contributes to Shoot Apical Meristem Homeostasis. *Plant and Cell Physiology* **52**: 14-29
- Bonaccorso O, Lee JE, Puaah L, Scutt CP, Golz JF** (2012) FILAMENTOUS FLOWER controls lateral organ development by acting as both an activator and a repressor. *BMC Plant Biology* **12**: 176
- Bonn F, Tatsuta T, Petrunaro C, Riemer J, Langer T** (2011) Presequence-dependent folding ensures MrpL32 processing by the m-AAA protease in mitochondria. *The EMBO journal* **30**: 2545-2556
- Borden KLB** (2000) RING domains: master builders of molecular scaffolds? *Journal of Molecular Biology* **295**: 1103-1112
- Borianne P, Brunel G** (2012) Automated valuation of leaves area for large-scale analysis needing data coupling or petioles deletion. *In IEEE Fourth International Symposium on Plant Growth Modeling, Simulation, Visualization and Applications (PMA)*, pp 50-57
- Bornstein G, Ganoth D, Hershko A** (2006) Regulation of neddylation and deneddylation of cullin1 in SCFSkp2 ubiquitin ligase by F-box protein and substrate. *Proceedings of the National Academy of Sciences* **103**: 11515-11520
- Brinton J, Simmonds J, Minter F, Leverington-Waite M, Snape J, Uauy C** (2017) Increased pericarp cell length underlies a major quantitative trait locus for grain weight in hexaploid wheat. *New Phytologist* **215**: 1026-1038
- Brinton J, Simmonds J, Uauy C** (2018) Ubiquitin-related genes are differentially expressed in isogenic lines contrasting for pericarp cell size and grain weight in hexaploid wheat. *BMC Plant Biology* **18**: 22
- Bruckner A, Polge C, Lentze N, Auerbach D, Schlattner U** (2009) Yeast two-hybrid, a powerful tool for systems biology. *International Journal of Molecular Sciences* **10**: 2763-2788
- Bylesjö M, Segura V, Soolanayakanahally RY, Rae AM, Trygg J, Gustafsson P, Jansson S, Street NR** (2008) LAMINA: a tool for rapid quantification of leaf size and shape parameters. *BMC Plant Biology* **8**: 82
- Calder G, Hindle C, Chan J, Shaw P** (2015) An optical imaging chamber for viewing living plant cells and tissues at high resolution for extended periods. *Plant Methods* **11**: 22

- Carter R, Sánchez-Corrales YE, Hartley M, Grieneisen VA, Marée AFM** (2017) Pavement cells and the topology puzzle. *Development* **144**: 4386-4397
- Cattaneo P, Hardtke CS** (2017) BIG BROTHER Uncouples Cell Proliferation from Elongation in the Arabidopsis Primary Root. *Plant and Cell Physiology* **58**: 1519-1527
- Cebolla A, María Vinardell J, Kiss E, Oláh B, Roudier F, Kondorosi A, Kondorosi E** (1999) The mitotic inhibitor ccs52 is required for endoreduplication and ploidy-dependent cell enlargement in plants. *The EMBO Journal* **18**: 4476-4484
- Cevik V, Huh S, Cooper A, Furzer O, Fairhead S, Taylor J, Carlier J, Sarris P, Jones JDG, Holub E** (2016) Distinct resistance genes arrest development of the oomycete rust *Albugo candida* in *Arabidopsis thaliana* at different infection stages. *In ISMPMI XVII Congress, Glasgow*
- Chakraborti S, Mandal M, Das S, Mandal A, Chakraborti T** (2003) Regulation of matrix metalloproteinases: An overview. *Molecular and Cellular Biochemistry* **253**: 269-285
- Challa KR, Aggarwal P, Nath U** (2016) Activation of YUCCA5 by the Transcription Factor TCP4 Integrates Developmental and Environmental Signals to Promote Hypocotyl Elongation in Arabidopsis. *The Plant Cell* **28**: 2117-2130
- Chang C, Schaller GE, Patterson SE, Kwok SF, Meyerowitz EM, Bleecker AB** (1992) The TMK1 gene from Arabidopsis codes for a protein with structural and biochemical characteristics of a receptor protein kinase. *The Plant Cell* **4**: 1263-1271
- Cheng Y, Cao L, Wang S, Li Y, Shi X, Liu H, Li L, Zhang Z, Fowke LC, Wang H, Zhou Y** (2013) Downregulation of multiple CDK inhibitor ICK/KRP genes upregulates the E2F pathway and increases cell proliferation, and organ and seed sizes in Arabidopsis. *The Plant Journal* **75**: 642-655
- Cheng Y, Dai X, Zhao Y** (2006) Auxin biosynthesis by the YUCCA flavin monooxygenases controls the formation of floral organs and vascular tissues in Arabidopsis. *Genes and Development* **20**: 1790-1799
- Clark SE, Williams RW, Meyerowitz EM** (1997) The CLAVATA1 Gene Encodes a Putative Receptor Kinase That Controls Shoot and Floral Meristem Size in Arabidopsis. *Cell* **89**: 575-585
- Clough SJ, Bent AF** (1998) Floral dip: a simplified method for Agrobacterium-mediated transformation of Arabidopsis thaliana. *The Plant Journal* **16**: 735-743
- Collier SM, Hamel L-P, Moffett P** (2011) Cell Death Mediated by the N-Terminal Domains of a Unique and Highly Conserved Class of NB-LRR Protein. *Molecular Plant-Microbe Interactions* **24**: 918-931

- Cubas P, Lauter N, Doebley J, Coen E** (1999) The TCP domain: a motif found in proteins regulating plant growth and development. *The Plant Journal* **18**: 215-222
- Czesnick H, Lenhard M** (2015) Size control in plants - lessons from leaves and flowers. *Cold Spring Harbour Perspectives in Biology* **7**: a019190
- Dai N, Wang W, Patterson SE, Bleecker AB** (2013) The TMK subfamily of receptor-like kinases in *Arabidopsis* display an essential role in growth and a reduced sensitivity to auxin. *PLoS One* **8**: e60990
- Danisman S, van Dijk AD, Bimbo A, van der Wal F, Hennig L, de Folter S, Angenent GC, Immink RG** (2013) Analysis of functional redundancies within the *Arabidopsis* TCP transcription factor family. *Journal of Experimental Botany* **64**: 5673-5685
- Davière J-M, Achard P** (2013) Gibberellin signaling in plants. *Development* **140**: 1147-1151
- De Veylder L, Beeckman T, Beechster GTS, Krols L, Terras F, Landrieu I, Van Der Schueren E, Maes S, Naudts M, Inzé D** (2001) Functional Analysis of Cyclin-Dependent Kinase Inhibitors of *Arabidopsis*. *The Plant Cell* **13**: 1653-1668
- De Vylder J, Vandebussche F, Hu Y, Philips W, Van Der Straeten D** (2012) Rosette Tracker: An Open Source Image Analysis Tool for Automatic Quantification of Genotype Effects. *Plant Physiology* **160**: 1149-1159
- Deprost D, Yao L, Sormani R, Moreau M, Leterreux G, Nicolai M, Bedu M, Robaglia C, Meyer C** (2007) The *Arabidopsis* TOR kinase links plant growth, yield, stress resistance and mRNA translation. *EMBO Reports* **8**: 864-870
- Deshaies RJ, Joazeiro CA** (2009) RING domain E3 ubiquitin ligases. *Annual Review of Biochemistry* **78**: 399-434
- Desvoyes B, de Mendoza A, Ruiz-Trillo I, Gutierrez C** (2014) Novel roles of plant RETINOBLASTOMA-RELATED (RBR) protein in cell proliferation and asymmetric cell division. *Journal of Experimental Botany* **65**: 2657-2666
- Desvoyes B, Ramirez-Parra E, Xie Q, Chua N-H, Gutierrez C** (2006) Cell Type-Specific Role of the Retinoblastoma/E2F Pathway during *Arabidopsis* Leaf Development. *Plant Physiology* **140**: 67-80
- Dewitte W, Murray JA** (2003) The plant cell cycle. *Annual Review of Plant Biology* **54**: 235-264
- Dewitte W, Scofield S, Alcasabas AA, Maughan SC, Menges M, Braun N, Collins C, Nieuwland J, Prinsen E, Sundaresan V, Murray JA** (2007) *Arabidopsis* CYCD3 D-time cyclins link cell proliferation and endocycles and are rate-limiting for cytokinin responses. *Proceedings of the National Academy of Sciences* **104**: 14537-14542

- Di Mambro R, De Ruvo M, Pacifici E, Salvi E, Sozzani R, Benfey PN, Busch W, Novak O, Ljung K, Di Paola L, Marée AFM, Costantino P, Grieneisen VA, Sabatini S** (2017) Auxin minimum triggers the developmental switch from cell division to cell differentiation in the Arabidopsis root. *Proceedings of the National Academy of Sciences* **114**: E7641-E7649
- Disch S, Anastasiou E, Sharma VK, Laux T, Fletcher JC, Lenhard M** (2006) The E3 ubiquitin ligase BIG BROTHER controls Arabidopsis organ size in a dosage-dependent manner. *Current Biology* **16**: 272-279
- Dochain D, MacLean H** (2016) Plant Growth Modelling: From Experimental Design to Modelling-The Arabidopsis Experiment. *IFAC-PapersOnLine* **49**: 236-241
- Dong H, Dumenil J, Lu FH, Na L, Vanhaeren H, Naumann C, Klecker M, Prior R, Smith C, McKenzie N, Saalbach G, Chen L, Xia T, Gonzalez N, Seguela M, Inzé D, Dissmeyer N, Li Y, Bevan MW** (2017) Ubiquitylation activates a peptidase that promotes cleavage and destabilization of its activating E3 ligases and diverse growth regulatory proteins to limit cell proliferation in Arabidopsis. *Genes and Development* **31**: 197-208
- Du L, Li N, Chen LL, Xu YX, Li Y, Zhang YY, Li CY, Li YH** (2014) The Ubiquitin Receptor DA1 Regulates Seed and Organ Size by Modulating the Stability of the Ubiquitin-Specific Protease UBP15/SOD2 in Arabidopsis. *Plant Cell* **26**: 665-677
- Duda DM, Borg LA, Scott DC, Hunt HW, Hammel M, Schulman BA** (2008) Structural Insights into NEDD8 Activation of Cullin-RING Ligases: Conformational Control of Conjugation. *Cell* **134**: 995-1006
- Dumenil J** (2013) Investigating the role of DA1 in growth control. University of East Anglia, Norwich
- Easlon HM, Bloom AJ** (2014) Easy Leaf Area: Automated Digital Image Analysis for Rapid and Accurate Measurement of Leaf Area. *Applications in Plant Sciences* **2**: 1400033
- Edgar BA, Sprenger F, Duronio RJ, Leopold P, O'Farrell PH** (1994) Distinct molecular mechanism regulate cell cycle timing at successive stages of Drosophila embryogenesis. *Genes and Development* **8**: 440-452
- Edwards K, Johnstone C, Thompson C** (1991) A simple and rapid method for the preparation of plant genomic DNA for PCR analysis. *Nucleic Acids Research* **19**: 1349
- Eklund DM, Staldal V, Valsecchi I, Cierlik I, Eriksson C, Hiratsu K, Ohme-Takagi M, Sundstrom JF, Thelander M, Ezcurra I, Sundberg E** (2010) The Arabidopsis thaliana

STYLISH1 Protein Acts as a Transcriptional Activator Regulating Auxin Biosynthesis.
The Plant Cell **22**: 349-363

Ellis CM, Nagpal P, Young JC, Hagen G, Guilfoyle TJ, Reed JW (2005) AUXIN RESPONSE FACTOR1 and AUXIN RESPONSE FACTOR2 regulate senescence and floral organ abscission in *Arabidopsis thaliana*. Development **132**: 4563-4574

Enders TA, Oh S, Yang Z, Montgomery BL, Strader LC (2015) Genome Sequencing of *Arabidopsis* *abp1-5* Reveals Second-Site Mutations That May Affect Phenotypes. The Plant Cell: (Commentary)

Endrizzi K, Moussian B, Haecker A, Levin JZ, Laux T (1996) The SHOOT MERISTEMLESS gene is required for maintenance of undifferentiated cells in *Arabidopsis* shoot and floral meristems and acts at a different regulatory level than the meristem genes WUSCHEL and ZWILLE. The Plant Journal **10**: 967-979

Enoksson M, Li J, Ivancic MM, Timmer JC, Wildfang E, Eroshkin A, Salvesen GS, Tao WA (2007) Identification of proteolytic cleavage site by quantitative proteomics. Journal of Proteome Research **6**: 2850-2858

Errera L (1888) Über zellformen und seifenblasen. Bot. Zentralbl. **34**: 395-398

Eshed Y, Izhaki A, Baum SF, Floyd SK, Bowman JL (2004) Asymmetric leaf development and blade expansion in *Arabidopsis* are mediated by KANADI and YABBY activities. Development **131**: 2997-3006

Feldman RMR, Correll CC, Kaplan KB, Deshaies RJ (1997) A Complex of Cdc4p, Skp1p, and Cdc53p/Cullin Catalyzes Ubiquitination of the Phosphorylated CDK Inhibitor Sic1p. Cell **91**: 221-230

Feng G, Qin Z, Yan J, Zhang X, Hu Y (2011) *Arabidopsis* ORGAN SIZE RELATED1 regulates organ growth and final organ size in orchestration with ARGOS and ARL. New Phytologist **191**: 635-646

Ferjani A, Horiguchi G, Yano S, Tsukaya H (2007) Analysis of leaf development in *fugu* mutants of *Arabidopsis* reveals three compensation modes that modulate cell expansion in determinate organs. Plant Physiology **144**: 988-999

Ferreira PC, Hemerly AS, Engler JD, van Montagu M, Engler G, Inzé D (1994) Developmental expression of the *Arabidopsis* cyclin gene *cyc1At*. The Plant Cell **6**: 1763-1774

Fields S, Song O (1989) A novel genetic system to detect protein-protein interactions. Letters to Nature **340**: 245-246

Finn R, Coghill P, Eberhardt R, Eddy S, Mistry J, Mitchell A, Potter S, Punta M, Qureshi M, Sangrador-Vegas A, Salazar G, Tate J, Bateman A (2016) The Pfam protein families

- database: towards a more sustainable future. *In* Nucleic Acids Research, pp D279-D285
- Francis D** (2007) The plant cell cycle – 15 years on. *New Phytologist* **174**: 261-278
- Freemont PS** (1993) The RING Finger. *Annals of the New York Academy of Sciences* **684**: 174-192
- Fridborg I, Kuusk S, Robertson M, Sundberg E** (2001) The Arabidopsis Protein SHI Represses Gibberellin Responses in Arabidopsis and Barley. *Plant Physiology* **127**: 937-948
- Fu Y, Xu L, Xu B, Yang L, Ling Q, Wang H, Huang H** (2007) Genetic Interactions Between Leaf Polarity-Controlling Genes and ASYMMETRIC LEAVES1 and 2 in Arabidopsis Leaf Patterning. *Plant and Cell Physiology* **48**: 724-735
- Fukushima K, Hasebe M** (2014) Adaxial–abaxial polarity: The developmental basis of leaf shape diversity. *Genesis* **52**: 1-18
- Galan J-M, Peter M** (1999) Ubiquitin-dependent degradation of multiple F-box proteins by an autocatalytic mechanism. *Proceedings of the National Academy of Sciences* **96**: 9124-9129
- Gao Y, Zhang Y, Zhang D, Dai X, Estelle M, Zhao Y** (2015) Auxin binding protein 1 (ABP1) is not required for either auxin signaling or Arabidopsis development. *Proceedings of the National Academy of Sciences* **112**: 2275-2280
- Geisler M, Nadeau J, Sack FD** (2000) Oriented Asymmetric Divisions That Generate the Stomatal Spacing Pattern in Arabidopsis Are Disrupted by the too many mouths Mutation. *The Plant Cell* **12**: 2075-2086
- Gendreau E, Traas J, Desnos T, Grandjean O, Caboche M, Hofte H** (1997) Cellular Basis of Hypocotyl Growth in Arabidopsis thaliana. *Plant Physiology* **114**: 295-305
- Gevaert K, Goethals M, Martens L, Van Damme J, Staes A, Thomas GR, Vandekerckhove J** (2003) Exploring proteomes and analyzing protein processing by mass spectrometric identification of sorted N-terminal peptides. *Nature Biotechnology* **21**: 566-569
- Gonzalez N, Pauwels L, Baekelandt A, De Milde L, Van Leene J, Besbrugge N, Heyndrickx KS, Pérez AC, Durand AN, De Clercq R, Van De Slijke E, Vanden Bossche R, Eeckhout D, Gevaert K, Vandepoele K, De Jaeger G, Goossens A, Inzé D** (2015) A Repressor Protein Complex Regulates Leaf Growth in Arabidopsis. *The Plant Cell* **27**: 2273-2287
- Graham JS, Xiong J, Gillikin JW** (1991) Purification and Developmental Analysis of a Metalloendoproteinase from the Leaves of Glycine max. *Plant Physiology* **97**: 786-792
- Gray JE** (2007) Plant Development: Three Steps for Stomata. *Current Biology* **17**: R213-R215

- Gray WM, del Pozo JC, Walker L, Hobbie L, Risseeuw E, Banks T, Crosby WL, Yang M, Ma H, Estelle M** (1999) Identification of an SCF ubiquitin–ligase complex required for auxin response in *Arabidopsis thaliana*. *Genes and Development* **13**: 1678-1691
- Green JM, Appel H, Rehrig EM, Harnsomburana J, Chang J-F, Balint-Kurti P, Shyu C-R** (2012) PhenoPhyte: a flexible affordable method to quantify 2D phenotypes from imagery. *Plant Methods* **8**: 45-57
- Gu X, Jiang D, Wang Y, Bachmair A, He Y** (2009) Repression of the floral transition via histone H2B monoubiquitination. *The Plant Journal* **57**: 522-533
- Guirao B, Bellaïche Y** (2017) Biomechanics of cell rearrangements in *Drosophila*. *Current Opinion in Cell Biology* **48**: 113-124
- Guirao B, Rigaud SU, Bosveld F, Bailles A, López-Gay J, Ishihara S, Sugimura K, Graner F, Bellaïche Y** (2015) Unified quantitative characterization of epithelial tissue development. *eLife* **4**: e08519
- Guo Y, Han L, Hymes M, Denver R, Clark SE** (2010) CLAVATA2 forms a distinct CLE-binding receptor complex regulating *Arabidopsis* stem cell specification. *The Plant Journal* **63**: 889-900
- Hammani K, Gobert A, Small I, Giegé P** (2011) A PPR protein involved in regulating nuclear genes encoding mitochondrial proteins? *Plant Signaling & Behavior* **6**: 748-750
- Hartmann-Petersen R, Seeger M, Gordon C** (2003) Transferring substrates to the 26S proteasome. *Trends in Biochemical Sciences* **28**: 26-31
- Hatfield PM, Gosink MM, Carpenter TB, Vierstra RD** (1997) The ubiquitin-activating enzyme (E1) gene family in *Arabidopsis thaliana*. *The Plant Cell* **11**: 213-226
- Hauvermale AL, Ariizumi T, Steber CM** (2012) Gibberellin Signaling: A Theme and Variations on DELLA Repression. *Plant Physiology* **160**: 83-92
- Hay A, Barkoulas M, Tsiantis M** (2006) ASYMMETRIC LEAVES1 and auxin activities converge to repress BREVIPEDICELLUS expression and promote leaf development in *Arabidopsis*. *Development* **133**: 3955-3961
- Hay A, Tsiantis M** (2010) KNOX genes: versatile regulators of plant development and diversity. *Development* **137**: 3153-3165
- Hendry L, John S** (2004) Regulation of STAT signalling by proteolytic processing. *European Journal of Biochemistry* **271**: 4613-4620
- Hershko A, Ciechanover A** (1998) The Ubiquitin System. *Annual Review of Biochemistry* **67**: 425-479

- Hervé C, Dabos P, Bardet C, Jauneau A, Auriac MC, Ramboer A, Lacout F, Tremousaygue D** (2009) In Vivo Interference with AtTCP20 Function Induces Severe Plant Growth Alterations and Deregulates the Expression of Many Genes Important for Development. *Plant Physiology* **149**: 1462-1477
- Hicke L** (2001) Ubiquitin and proteasomes: protein regulation by monoubiquitin. *Nature Reviews Molecular Cell Biology* **2**: 195-201
- Higuchi M, Pischke MS, Mahonen AP, Miyawaki K, Hashimoto Y, Seki M, Kobayashi M, Shinozaki K, Kato T, Tabata S, Helariutta Y, Sussman MR, Kakimoto T** (2004) In planta functions of the Arabidopsis cytokinin receptor family. *Proceedings of the National Academy of Sciences* **101**: 8821-8826
- Himanen K, Boucheron E, Vanneste S, de Almeida Engler J, Inzé D, Beeckman T** (2002) Auxin-Mediated Cell Cycle Activation during Early Lateral Root Initiation. *The Plant Cell* **14**: 2339-2351
- Hiratsu K, Matsui K, Koyama T, Ohme-Takagi M** (2003) Dominant repression of target genes by chimeric repressors that include the EAR motif, a repression domain, in Arabidopsis. *The Plant Journal* **34**: 733-739
- Hisanaga T, Kawade K, Tsukaya H** (2015) Compensation: a key to clarifying the organ-level regulation of lateral organ size in plants. *Journal of Experimental Botany* **66**: 1055-1063
- Hochstrasser M** (2006) Lingering Mysteries of Ubiquitin-Chain Assembly. *Cell* **124**: 27-34
- Hoeller D, Crosetto N, Blagoev B, Raiborg C, Tikkanen R, Wagner S, Kowanetz K, Breitling R, Mann M, Stenmark H, Dikic I** (2006) Regulation of ubiquitin-binding proteins by monoubiquitination. *Nature Cell Biology* **8**: 163-169
- Hofmeister W** (1863) Zusätze und berichtigungen zu den 1851 veröffentlichten untersuchungen der entwicklung höherer krytogamen. *Jahrb. Wiss. Bot* **3**: 259-293
- Horiguchi G, Kim G-T, Tsukaya H** (2005) The transcription factor AtGRF5 and the transcription coactivator AN3 regulate cell proliferation in leaf primordia of Arabidopsis thaliana. *The Plant Journal* **43**: 68-78
- Hu Y, Poh HM, Chua N-H** (2006) The Arabidopsis ARGOS-LIKE gene regulates cell expansion during organ growth. *The Plant Journal* **47**: 1-9
- Hu Y, Xie Q, Chua N-H** (2003) The Arabidopsis Auxin-Inducible Gene ARGOS Controls Lateral Organ Size. *The Plant Cell* **15**: 1951-1961

- Huibregtse JM, Scheffner M, Beaudenon S, Howley PM** (1995) A family of proteins structurally and functionally related to the E6-AP ubiquitin-protein ligase. *Proceedings of the National Academy of Sciences* **92**: 2563-2567
- Ichihashi Y, Horiguchi G, Gleissberg S, Tsukaya H** (2010) The bHLH Transcription Factor SPATULA Controls Final Leaf Size in *Arabidopsis thaliana*. *Plant and Cell Physiology* **51**: 252-261
- Ikeuchi M, Yamaguchi T, Kazama T, Ito T, Horiguchi G, Tsukaya H** (2011) ROTUNDIFOLIA4 Regulates Cell Proliferation Along the Body Axis in *Arabidopsis* Shoot. *Plant and Cell Physiology* **52**: 59-69
- Imai KK, Ohashi Y, Tsuge T, Yoshizumi T, Matsui M, Oka A, Aoyama T** (2006) The A-Type Cyclin CYCA2;3 Is a Key Regulator of Ploidy Levels in *Arabidopsis* Endoreduplication. *The Plant Cell* **18**: 382-396
- Inzé D, De Veylder L** (2006) Cell Cycle Regulation in Plant Development. *Annual Review of Genetics* **40**: 77-105
- Jackson S, Xiong Y** (2009) CRL4s: the CUL4-RING E3 ubiquitin ligases. *Trends in Biochemical Sciences* **34**: 562-570
- Johnson K, Lenhard M** (2011) Genetic control of plant organ growth. *New Phytologist* **191**: 319-333
- Johnston GC, Pringle JR, Hartwell LH** (1977) Coordination of growth with cell division in the yeast *Saccharomyces cerevisiae*. *Experimental Cell Research* **105**: 79-98
- Jones AR, Forero-Vargas M, Withers SP, Smith RS, Traas J, Dewitte W, Murray JAH** (2017) Cell-size dependent progression of the cell cycle creates homeostasis and flexibility of plant cell size. *Nature Communications* **8**: 15060-15073
- Kadmas JL, Beckerle MC** (2004) The LIM domain: from the cytoskeleton to the nucleus. *Nature Reviews Molecular Cell Biology* **5**: 920-931
- Kawade K, Horiguchi G, Usami T, Hirai Masami Y, Tsukaya H** (2013) ANGUSTIFOLIA3 Signaling Coordinates Proliferation between Clonally Distinct Cells in Leaves. *Current Biology* **23**: 788-792
- Kazama T, Ichihashi Y, Murata S, Tsukaya H** (2010) The mechanism of cell cycle arrest front progression explained by a KLUH/CYP78A5-dependent mobile growth factor in developing leaves of *Arabidopsis thaliana*. *Plant Cell Physiology* **51**: 1046-1054
- Kazama T, Ichihashi Y, Murata S, Tsukaya H** (2010) The Mechanism of Cell Cycle Arrest Front Progression Explained by a KLUH/CYP78A5-dependent Mobile Growth Factor in Developing Leaves of *Arabidopsis thaliana*. *Plant and Cell Physiology* **51**: 1046-1054

- Kellogg DR** (2003) Wee1-dependent mechanisms required for coordination of cell growth and cell division. *Journal of Cell Science* **116**: 4883
- Kerscher O, Felberbaum R, Hochstrasser M** (2006) Modification of proteins by ubiquitin and ubiquitin-like proteins. *Annual Review of Cell and Developmental Biology* **22**: 159-180
- Kieffer M, Master V, Waites R, Davies B** (2011) TCP14 and TCP15 affect internode length and leaf shape in Arabidopsis. *The Plant Journal* **68**: 147-158
- Kim JH, Choi D, Kende H** (2003) The AtGRF family of putative transcription factors is involved in leaf and cotyledon growth in Arabidopsis. *The Plant Journal* **36**: 94-104
- Kim JH, Kende H** (2004) A transcriptional coactivator, AtGIF1, is involved in regulating leaf growth and morphology in Arabidopsis. *Proceedings of the National Academy of Sciences* **101**: 13374-13379
- Kim JH, Tsukaya H** (2015) Regulation of plant growth and development by the GROWTH-REGULATING FACTOR and GRF-INTERACTING FACTOR duo. *Journal of Experimental Botany* **66**: 6093-6107
- Kim MH, Kim Y, Kim JW, Lee HS, Lee WS, Kim SK, Wang ZY, Kim SH** (2013) Identification of Arabidopsis BAK1-Associating Receptor-Like Kinase 1 (BARK1) and Characterization of its Gene Expression and Brassinosteroid-Regulated Root Phenotypes. *Plant and Cell Physiology* **54**: 1620-1634
- Kinoshita T, Cano-Delgado A, Seto H, Hiranuma S, Fujioka S, Yoshida S, Chory J** (2005) Binding of brassinosteroids to the extracellular domain of plant receptor kinase BRI1. *Nature* **433**: 167-171
- Kleefeld O, Doucet A, auf dem Keller U, Prudova A, Schilling O, Kainthan RK, Starr AE, Foster LJ, Kizhakkedathu JN, Overall CM** (2010) Isotopic labeling of terminal amines in complex samples identifies protein N-termini and protease cleavage products. *Nature Biotechnology* **28**: 281
- Knoblich JA** (2010) Asymmetric cell division: recent developments and their implications for tumour biology. *Nature Review Molecular Cell Biology* **11**: 849-860
- Komander D, Rape M** (2012) The ubiquitin code. *Annual Review of Biochemistry* **81**: 203-229
- Kosugi S, Ohashi Y** (2002) DNA binding and dimerization specificity and potential targets for the TCP protein family. *The Plant Journal* **30**: 337-348
- Koyama T, Furutani M, Tasaka M, Ohme-Takagi M** (2007) TCP transcription factors control the morphology of shoot lateral organs via negative regulation of the expression of boundary-specific genes in Arabidopsis. *Plant Cell* **19**: 473-484

- Koyama T, Mitsuda N, Seki M, Shinozaki K, Ohme-Takagi M** (2010) TCP transcription factors regulate the activities of ASYMMETRIC LEAVES1 and miR164, as well as the auxin response, during differentiation of leaves in Arabidopsis. *Plant Cell* **22**: 3574-3588
- Krecek P, Skupa P, Libus J, Naramoto S, Tejos R, Friml J, Zazimalova E** (2009) The PINFORMED (PIN) protein family of auxin transporters. *Genome Biology* **10**: 249-260
- Kuchen EE, Fox S, Barbier de Reuille P, Kennaway R, Bensmihen S, Avondo J, Calder GM, Southam P, Robinson S, Bangham A, Coen E** (2012) Generation of Leaf Shape Through Early Patterns of Growth and Tissue Polarity. *Science* **335**: 1092-1096
- Kumaran MK, Bowman JL, Sundaresan V** (2002) YABBY Polarity Genes Mediate the Repression of KNOX Homeobox Genes in Arabidopsis. *The Plant Cell* **14**: 2761-2770
- Kuusk S, Sohlberg JJ, Long JA, Fridborg I, Sundberg E** (2002) STY1 and STY2 promote the formation of apical tissues during Arabidopsis gynoecium development. *Development* **129**: 4707-4717
- Kuylen E, Beemster GTS, Broeckhove J, De Vos D** (2017) Simulation of regulatory strategies in a morphogen based model of Arabidopsis leaf growth. *Procedia Computer Science* **108**: 139-148
- Kwon SH, Lee BH, Kim EY, Seo YS, Lee S, Kim WT, Song JT, Kim JH** (2009) Overexpression of a Brassica rapa NGATHA gene in Arabidopsis thaliana negatively affects cell proliferation during lateral organ and root growth. *Plant Cell Physiology* **50**: 2162-2173
- Lee BH, Ko J-H, Lee S, Lee Y, Pak J-H, Kim JH** (2009) The Arabidopsis GRF-INTERACTING FACTOR Gene Family Performs an Overlapping Function in Determining Organ Size as Well as Multiple Developmental Properties. *Plant Physiology* **151**: 655-668
- Lee BH, Kwon SH, Lee S-J, Park SK, Song JT, Lee S, Lee MM, Hwang Y-s, Kim JH** (2015) The Arabidopsis thaliana NGATHA transcription factors negatively regulate cell proliferation of lateral organs. *Plant Molecular Biology* **89**: 529-538
- Lee H-S, Chen ZJ** (2001) Protein-coding genes are epigenetically regulated in Arabidopsis polyploids. *Proceedings of the National Academy of Sciences* **98**: 6753-6758
- Lenhard M** (2012) All's Well that Ends Well: Arresting Cell Proliferation in Leaves. *Developmental Cell* **22**: 9-11
- Li C, Potuschak T, Colón-Carmona A, Gutiérrez RA, Doerner P** (2005) Arabidopsis TCP20 links regulation of growth and cell division control pathways. *Proceedings of the National Academy of Sciences* **102**: 12978-12983

- Li HJ, Zhu SS, Zhang MX, Wang T, Liang L, Xue Y, Shi DQ, Liu J, Yang WC** (2015) Arabidopsis CBP1 Is a Novel Regulator of Transcription Initiation in Central Cell-Mediated Pollen Tube Guidance. *Plant Cell* **27**: 2880-2893
- Li J, Wen J, Lease KA, Doke JT, Tax FE, Walker JC** (2002) BAK1, an Arabidopsis LRR Receptor-like Protein Kinase, Interacts with BRI1 and Modulates Brassinosteroid Signaling. *Cell* **110**: 213-222
- Li ST, Zachgo S** (2013) TCP3 interacts with R2R3-MYB proteins, promotes flavonoid biosynthesis and negatively regulates the auxin response in Arabidopsis thaliana. *The Plant Journal* **76**: 901-913
- Li W, Tu D, Brunger AT, Ye Y** (2007) A ubiquitin ligase transfers preformed polyubiquitin chains from a conjugating enzyme to a substrate. *Nature* **446**: 333-337
- Li YH, Zheng LY, Corke F, Smith C, Bevan MW** (2008) Control of final seed and organ size by the DA1 gene family in Arabidopsis thaliana. *Genes and Development* **22**: 1331-1336
- Li ZY, Li B, Dong AW** (2012) The Arabidopsis transcription factor AtTCP15 regulates endoreduplication by modulating expression of key cell-cycle genes. *Molecular Plant* **5**: 270-280
- Liu J, Furukawa M, Matsumoto T, Xiong Y** (2002) NEDD8 Modification of CUL1 Dissociates p120 CAND1, an Inhibitor of CUL1-SKP1 Binding and SCF Ligases. *Molecular Cell* **10**: 1511-1518
- Liu YF, Wang F, Zhang HY, He H, Ma LG, Deng XW** (2008) Functional characterization of the Arabidopsis ubiquitin-specific protease gene family reveals specific role and redundancy of individual members in development. *The Plant Journal* **55**: 844-856
- Lobet G, Draye X, Périlleux C** (2013) An online database for plant image analysis software tools. *Plant Methods* **9**: 38
- Lovering R, Hanson IM, Borden KL, Martin S, O'Reilly NJ, Evan GI, Rahman D, Pappin DJC, Trowsdale J, Freemont PS** (1993) Identification and preliminary characterization of a protein motif related to the zinc finger. *Proceedings of the National Academy of Sciences* **90**: 2112-2116
- MacAlister CA, Ohashi-Ito K, Bergmann DC** (2007) Transcription factor control of asymmetric cell divisions that establish the stomatal lineage. *Nature* **445**: 537-540
- Makkena S, Lamb RS** (2013) The bHLH transcription factor SPATULA regulates root growth by controlling the size of the root meristem. *BMC Plant Biology* **13**: 1

- Mallory AC, Reinhart BJ, Jones - Rhoades MW, Tang G, Zamore PD, Barton MK, Bartel DP** (2004) MicroRNA control of PHABULOSA in leaf development: importance of pairing to the microRNA 5' region. *The EMBO Journal* **23**: 3356-3364
- Marangos P, Carroll J** (2008) Securin regulates entry into M-phase by modulating the stability of cyclin B. *Nature Cell Biology* **10**: 445
- Mariconti L, Pellegrini B, Cantoni R, Stevens R, Bergounioux C, Cella R, Albani D** (2002) The E2F Family of Transcription Factors from *Arabidopsis thaliana*: novel and conserved components of the RETINOBLASTOMA/E2F pathway in plants. *Journal of Biological Chemistry* **277**: 9911-9919
- Martin-Trillo M, Cubas P** (2010) TCP genes: a family snapshot ten years later. *Trends in Plant Science* **15**: 31-39
- Martin SG, Berthelot-Grosjean M** (2009) Polar gradients of the DYRK-family kinase Pom1 couple cell length with the cell cycle. *Nature* **459**: 852
- Martínez-Fernández I, Sanchís S, Marini N, Balanzá V, Ballester P, Navarrete-Gómez M, Oliveira AC, Colombo L, Ferrándiz C** (2014) The effect of NGATHA altered activity on auxin signaling pathways within the *Arabidopsis* gynoecium. *Frontiers in Plant Science* **5**: 210-222
- Masuda HP, Cabral LM, De Veylder L, Tanurdzic M, de Almeida Engler J, Geelen D, Inzé D, Martienssen RA, Ferreira PCG, Hemerly AS** (2008) ABAP1 is a novel plant Armadillo BTB protein involved in DNA replication and transcription. *The EMBO Journal* **27**: 2746-2756
- Mayer KFX, Schoof H, Haecker A, Lenhard M, Jürgens G, Laux T** (1998) Role of WUSCHEL in Regulating Stem Cell Fate in the *Arabidopsis* Shoot Meristem. *Cell* **95**: 805-815
- McGinnis KM, Thomas SG, Soule JD, Strader LC, Zale JM, Sun T-p, Steber CM** (2003) The *Arabidopsis* SLEEPY1 Gene Encodes a Putative F-Box Subunit of an SCF E3 Ubiquitin Ligase. *The Plant Cell* **15**: 1120-1130
- Melaragno JE, Mehrotra B, Coleman AW** (1993) Relationship between Endopolyploidy and Cell Size in Epidermal Tissue of *Arabidopsis*. *The Plant Cell* **5**: 1661-1668
- Michelsen JW, Sewell AK, Louis HA, Olsen JI, Davis DR, Winge DR, Beckerle MC** (1994) Mutational analysis of the metal sites in an LIM domain. *Journal of Biological Chemistry* **269**: 11108-11113
- Miyashima S, Honda M, Hashimoto K, Tatematsu K, Hashimoto T, Sato-Nara K, Okada K, Nakajima K** (2013) A Comprehensive Expression Analysis of the *Arabidopsis* MICRORNA165/6 Gene Family during Embryogenesis Reveals a Conserved Role in

Meristem Specification and a Non-Cell-Autonomous Function. *Plant and Cell Physiology* **54**: 375-384

Mizukami Y, Fischer RL (2000) Plant organ size control: AINTEGUMENTA regulates growth and cell numbers during organogenesis. *Proceedings of the National Academy of Sciences* **97**: 942-947

Möller B, Poeschl Y, Plötner R, Bürstenbinder K (2017) PaCeQuant: A Tool for High-Throughput Quantification of Pavement Cell Shape Characteristics. *Plant Physiology* **175**: 998-1017

Montagne J, Stewart MJ, Stocker H, Hafen E, Kozma SC, Thomas G (1999) Drosophila S6 Kinase: A Regulator of Cell Size. *Science* **285**: 2126-2129

Moon J, Hake S (2011) How a leaf gets its shape. *Current Opinion in Plant Biology* **14**: 24-30

Moseley JB, Mayeux A, Paoletti A, Nurse P (2009) A spatial gradient coordinates cell size and mitotic entry in fission yeast. *Nature* **459**: 857-860

Müller R, Bleckmann A, Simon R (2008) The Receptor Kinase CORYNE of Arabidopsis Transmits the Stem Cell-Limiting Signal CLAVATA3 Independently of CLAVATA1. *The Plant Cell* **20**: 934-946

Mündermann L, Erasmus Y, Lane B, Coen E, Prusinkiewicz P (2005) Quantitative Modeling of Arabidopsis Development. *Plant Physiology* **139**: 960-968

Nakata M, Matsumoto N, Tsugeki R, Rikirsch E, Laux T, Okada K (2012) Roles of the Middle Domain-Specific WUSCHEL-RELATED HOMEBOX Genes in Early Development of Leaves in Arabidopsis. *The Plant Cell* **24**: 519-535

Narita NN, Moore S, Horiguchi G, Kubo M, Demura T, Fukuda H, Goodrich J, Tsukaya H (2004) Overexpression of a novel small peptide ROTUNDIFOLIA4 decreases cell proliferation and alters leaf shape in Arabidopsis thaliana. *The Plant Journal* **38**: 699-713

Natesh R, Schwager SLU, Sturrock ED, Acharya KR (2003) Crystal structure of the human angiotensin-converting enzyme-lisinopril complex. *Nature* **421**: 551-554

Nath U, Crawford BCW, Carpenter R, Coen E (2003) Genetic Control of Surface Curvature. *Science* **299**: 1404-1407

Ng A, Xavier RJ (2011) Leucine-rich repeat (LRR) proteins: Integrators of pattern recognition and signaling in immunity. *Autophagy* **7**: 1082-1084

Nijman SMB, Luna-Vargas MPA, Velds A, Brummelkamp TR, Dirac AMG, Sixma TK, Bernards R (2005) A Genomic and Functional Inventory of Deubiquitinating Enzymes. *Cell* **123**: 773-786

- Nishimura C, Ohashi Y, Sato S, Kato T, Tabata S, Ueguchi C** (2004) Histidine Kinase Homologs That Act as Cytokinin Receptors Possess Overlapping Functions in the Regulation of Shoot and Root Growth in Arabidopsis. *The Plant Cell* **16**: 1365-1377
- Norberg M, Holmlund M, Nilsson O** (2005) The BLADE ON PETIOLE genes act redundantly to control the growth and development of lateral organs. *Development* **132**: 2203-2213
- Ohashi-Ito K, Bergmann DC** (2006) FAMA Controls the Final Proliferation/Differentiation Switch during Stomatal Development. *The Plant Cell* **18**: 2493
- Ori N, Eshed Y, Chuck G, Bowman JL, Hake S** (2000) Mechanisms that control knox gene expression in the Arabidopsis shoot. *Development* **127**: 5523-5532
- Ostapenko D, Burton JL, Solomon MJ** (2015) The Ubp15 deubiquitinase promotes timely entry into S phase in *Saccharomyces cerevisiae*. *Molecular Biology of the Cell* **26**: 2205-2216
- Pagnussat GC, Yu HJ, Ngo QA, Rajani S, Mayalagu S, Johnson CS, Capron A, Xie LF, Ye D, Sundaresan V** (2005) Genetic and molecular identification of genes required for female gametophyte development and function in Arabidopsis. *Development* **132**: 603-614
- Palatnik JF, Allen E, Wu X, Schommer C, Schwab R, Carrington JC, Weigel D** (2003) Control of leaf morphogenesis by microRNAs. *Nature* **425**: 257-263
- Peng YC, Chen LL, Lu YR, Wu YB, Dumenil J, Zhu ZG, Bevan MW, Li YH** (2015) The Ubiquitin Receptors DA1, DAR1, and DAR2 Redundantly Regulate Endoreduplication by Modulating the Stability of TCP14/15 in Arabidopsis. *The Plant Cell* **27**: 649-662
- Perrot-Rechenmann C** (2010) Cellular Responses to Auxin: Division versus Expansion. *Cold Spring Harbor Perspectives in Biology* **2**: a001446
- Peterson KM, Rychel AL, Torii KU** (2010) Out of the Mouths of Plants: The Molecular Basis of the Evolution and Diversity of Stomatal Development. *The Plant Cell* **22**: 296-306
- Pillitteri LJ, Guo X, Dong J** (2016) Asymmetric cell division in plants: mechanisms of symmetry breaking and cell fate determination. *Cellular and Molecular Life Sciences* **73**: 4213-4229
- Pillitteri LJ, Sloan DB, Bogenschutz NL, Torii KU** (2007) Termination of asymmetric cell division and differentiation of stomata. *Nature* **445**: 501-505
- Polymenis M, Schmidt EV** (1997) Coupling of cell division to cell growth by translational control of the G1 cyclin CLN3 in yeast. *Genes and Development* **11**: 2522-2531
- Potter CJ, Xu T** (2001) Mechanisms of size control. *Current Opinion in Genetics and Development* **11**: 279-286

- Potuschak T, Lechner E, Parmentier Y, Yanagisawa S, Grava S, Koncz C, Genschik P** (2003) EIN3-Dependent Regulation of Plant Ethylene Hormone Signaling by Two Arabidopsis F Box Proteins: EBF1 and EBF2. *Cell* **115**: 679-689
- Potuschak T, Stary S, Schlogelhofer P, Becker F, Nejnskaia V, Bachmair A** (1998) PRT1 of Arabidopsis thaliana encodes a component of the plant N-end rule pathway. *Proceedings of the National Academy of Sciences of the United States of America* **95**: 7904–7908
- Potuschak T, Stary S, Schlögelhofer P, Becker F, Nejnskaia V, Bachmair A** (1998) PRT1 of Arabidopsis thaliana encodes a component of the plant N-end rule pathway. *Proceedings of the National Academy of Sciences* **95**: 7904-7908
- Prigge MJ, Otsuga D, Alonso JM, Ecker JR, Drews GN, Clark SE** (2005) Class III Homeodomain-Leucine Zipper Gene Family Members Have Overlapping, Antagonistic, and Distinct Roles in Arabidopsis Development. *The Plant Cell* **17**: 61-76
- Prunet N, Jack TP, Meyerowitz EM** (2016) Live confocal imaging of Arabidopsis flower buds. *Developmental Biology* **419**: 114-120
- Rasband WS** (1997-2016) ImageJ. *In*. Bethesda, Maryland, USA, US National Institutes of Health
- Rawlings ND** (2016) Peptidase specificity from the substrate cleavage collection in the MEROPS database and a tool to measure cleavage site conservation. *Biochimie* **122**: 5-30
- Rawlings ND, Barrett AJ** (1996) MEROPS: The Peptidase Database. *In*, Ed 11.0 Vol 2017
- Rawlings ND, Barrett AJ, Finn R** (2016) Twenty years of the MEROPS database of proteolytic enzymes, their substrates and inhibitors. *Nucleic Acids Research* **44**: D343-350
- Ray DK, Mueller ND, West PC, Foley JA** (2013) Yield Trends Are Insufficient to Double Global Crop Production by 2050. *PLOS ONE* **8**: e66428
- Rayle DL, Cleland RE** (1992) The Acid Growth Theory of auxin-induced cell elongation is alive and well. *Plant Physiology* **99**: 1271-1274
- Reddy GV, Heisler MG, Ehrhardt DW, Meyerowitz EM** (2004) Real-time lineage analysis reveals oriented cell divisions associated with morphogenesis at the shoot apex of Arabidopsis thaliana. *Development* **131**: 4225-4237
- Reinhardt D, Mandel T, Kuhlemeier C** (2000) Auxin regulates the initiation and radial position of plant lateral organs. *The Plant Cell* **12**: 5017-5518

- Reinhardt D, Pesce E, Stieger P, Mandel T, Baltenspürger K, Bennett M, Traas J, Friml J, Kuhlemeier C** (2003) Regulation of phyllotaxis by polar auxin transport. *Nature* **426**: 255-260
- Rhoades MW, Reinhart BJ, Lim LP, Burge CB, Bartel B, Bartel DP** (2002) Prediction of Plant MicroRNA Targets. *Cell* **110**: 513-520
- Richard C, Granier C, Inzé D, De Veylder L** (2001) Analysis of cell division parameters and cell cycle gene expression during the cultivation of *Arabidopsis thaliana* cell suspensions. *Journal of Experimental Botany* **52**: 1625-1633
- Robertson SC, Tynan JA, Donoghue DJ** (2000) RTK mutations and human syndromes: when good receptors turn bad. *Trends in Genetics* **16**: 265-271
- Rodriguez RE, Mecchia MA, Debernardi JM, Schommer C, Weigel D, Palatnik JF** (2010) Control of cell proliferation in *Arabidopsis thaliana* by microRNA miR396. *Development* **137**: 103-112
- Roeder AHK, Chickarmane V, Cunha A, Obara B, Manjunath BS, Meyerowitz EM** (2010) Variability in the Control of Cell Division Underlies Sepal Epidermal Patterning in *Arabidopsis thaliana*. *PLoS Biology* **8**: e1000367
- Sablowski R** (2016) Coordination of plant cell growth and division: collective control or mutual agreement. *Current Opinion in Plant Biology* **34**: 54-60
- Sablowski R, Carnier Dornelas M** (2014) Interplay between cell growth and cell cycle in plants. *Journal of Experimental Botany* **65**: 2703-2714
- Sachs J** (1878) Über die anordnung der zellen in jüngsten pflanzenteilen. *Arb. Bot. Inst. Würzburg* **2**: 46-104
- Sadanandom A, Bailey M, Ewan R, Lee J, Nelis S** (2012) The ubiquitin-proteasome system: central modifier of plant signalling. *New Phytologist* **196**: 13-28
- Sarojam R, Sappl PG, Goldshmidt A, Efroni I, Floyd SK, Eshed Y, Bowman JL** (2010) Differentiating *Arabidopsis* Shoots from Leaves by Combined YABBY Activities. *The Plant Cell* **22**: 2113-2130
- Savaldi-Goldstein S, Peto C, Chory J** (2007) The epidermis both drives and restricts plant shoot growth. *Nature* **446**: 199-202
- Saveliev S, Bratz M, Zubarev R, Szapacs M, Budamgunta H, Urh M** (2013) Trypsin/Lys-C protease mix for enhanced protein mass spectrometry analysis. *Nature Methods* **10**
- Schaller A** (2004) A cut above the rest: the regulatory function of plant proteases. *Planta* **220**: 183-197

- Schimke RT** (2006) Control of Enzyme Levels in Mammalian Tissues. *In* Advances in Enzymology and Related Areas of Molecular Biology. John Wiley & Sons, Inc., pp 135-187
- Schmeichel KA, Beckerle MC** (1997) Molecular Dissection of a LIM Domain. *Molecular Biology of the Cell* **8**: 219-230
- Schmeichel KL, Beckerle MC** (1994) The LIM domain is a modular protein-binding interface. *Cell* **79**: 211-219
- Schommer C, Debernardi JM, Bresso EG, Rodriguez RE, Palatnik JF** (2014) Repression of Cell Proliferation by miR319-Regulated TCP4. *Molecular Plant* **7**: 1533-1544
- Schommer C, Palatnik JF, Aggarwal P, Chetelat A, Cubas P, Farmer EE, Nath U, Weigel D** (2008) Control of jasmonate biosynthesis and senescence by miR319 targets. *PLoS Biology* **6**: e230
- Schruff MC, Spielman M, Tiwari S, Adams S, Fenby N, Scott RJ** (2006) The AUXIN RESPONSE FACTOR 2 gene of Arabidopsis links auxin signalling, cell division, and the size of seeds and other organs. *Development* **133**: 251-261
- Scofield S, Dewitte W, Murray JAH** (2014) STM sustains stem cell function in the Arabidopsis shoot apical meristem and controls KNOX gene expression independently of the transcriptional repressor AS1. *Plant Signaling & Behavior* **9**: e28934
- Scofield S, Dewitte W, Nieuwland J, Murray JAH** (2013) The Arabidopsis homeobox gene SHOOT MERISTEMLESS has cellular and meristem-organisational roles with differential requirements for cytokinin and CYCD3 activity. *The Plant Journal* **75**: 53-66
- Serna L** (2013) Antagonistic regulation of the meristemoid-to-guard mother-cell-transition. *Frontiers in Plant Science* **4**: 401
- Shamloul M, Trusa J, Mett V, Yusibov V** (2014) Optimization and Utilization of Agrobacterium-mediated Transient Protein Production in Nicotiana. *Journal of Visualized Experiments* **86**: e51204
- Shapiro BE, Tobin C, Mjolsness E, Meyerowitz EM** (2015) Analysis of cell division patterns in the Arabidopsis shoot apical meristem. *Proceedings of the National Academy of Sciences* **112**: 4815-4820
- Sheen J** (2001) Signal Transduction in Maize and Arabidopsis Mesophyll Protoplasts. *Plant Physiology* **127**: 1466-1475

- Shimotohno A, Ohno R, Bisova K, Sakaguchi N, Huang J, Koncz C, Uchimiya H, Umeda M** (2006) Diverse phosphoregulatory mechanisms controlling cyclin-dependent kinase-activating kinases in Arabidopsis. *The Plant Journal* **47**: 701-710
- Siegfried KR, Eshed Y, Baum SF, Otsuga D, Drews GN, Bowman JL** (1999) Members of the YABBY gene family specify abaxial cell fate in Arabidopsis. *Development* **126**: 4117-4128
- Sigrist CJA, de Castro E, Cerutti L, Cucho BA, Hulo N, Bridge A, Bougueleret L, Xenarios I** (2013) New and continuing developments at PROSITE. *Nucleic Acids Research* **41**: D344-D347
- Simmonds J, Scott P, Brinton J, Mestre TC, Bush M, del Blanco A, Dubcovsky J, Uauy C** (2016) A splice acceptor site mutation in TaGW2-A1 increases thousand grain weight in tetraploid and hexaploid wheat through wider and longer grains. *Theoretical and Applied Genetics* **129**: 1099-1112
- Skowyra D, Craig KL, Tyers M, Elledge SJ, Harper JW** (1997) F-Box Proteins Are Receptors that Recruit Phosphorylated Substrates to the SCF Ubiquitin-Ligase Complex. *Cell* **91**: 209-219
- Sohlberg JJ, Myrenas M, Kuusk S, Lagercrantz U, Kowalczyk M, Sandberg G, Sundberg E** (2006) STY1 regulates auxin homeostasis and affects apical-basal patterning of the Arabidopsis gynoecium. *The Plant Journal* **47**: 112-123
- Somssich M, Je BI, Simon R, Jackson D** (2016) CLAVATA-WUSCHEL signaling in the shoot meristem. *Development* **143**: 3238-3248
- Song S-K, Lee MM, Clark SE** (2006) POL and PLL1 phosphatases are CLAVATA1 signaling intermediates required for Arabidopsis shoot and floral stem cells. *Development* **133**: 4691-4698
- Song XJ, Huang W, Shi M, Zhu MZ, Lin HX** (2007) A QTL for rice grain width and weight encodes a previously unknown RING-type E3 ubiquitin ligase. *Nature Genetics* **39**: 623-630
- Spartz AK, Gray WM** (2008) Plant hormone receptors: new perceptions. *Genes and Development* **22**: 2139-2148
- Staldal V, Cierlik I, Chen S, Landberg K, Baylis T, Myrenas M, Sundstrom JF, Eklund DM, Ljung K, Sundberg E** (2012) The Arabidopsis thaliana transcriptional activator STYLISH1 regulates genes affecting stamen development, cell expansion and timing of flowering. *Plant Molecular Biology* **78**: 545-559
- Stals H, Inzé D** (2001) When plant cells decide to divide. *Trends in Plant Science* **6**: 359-364

- Stary S, Yin XJ, Potuschak T, Schlogelhofer P, Nizhynska V, Bachmair A** (2003) PRT1 of Arabidopsis is a ubiquitin protein ligase of the plant N-end rule pathway with specificity for aromatic amino-terminal residues. *Plant Physiology* **133**: 1360-1366
- Steeves TA, Sussex IM** (1989) *Patterns in Plant Development*, Ed 2. Cambridge University Press, Cambridge
- Stone SL, Hauksdottir H, Troy A, Herschleb J, Kraft E, Callis J** (2005) Functional analysis of the RING-type ubiquitin ligase family of Arabidopsis. *Plant Physiology* **137**: 13-30
- Sugimoto-Shirasu K, Roberts K** (2003) "Big it up": endoreduplication and cell-size control in plants. *Current Opinion in Plant Biology* **6**: 544-553
- Suzuki T, Sakurai K, Ueguchi C, Mizuno T** (2001) Two Types of Putative Nuclear Factors that Physically Interact with Histidine-Containing Phosphotransfer (Hpt) Domains, Signaling Mediators in His-to-Asp Phosphorelay, in Arabidopsis thaliana. *Plant & Cell Physiology* **42**: 37-45
- Swain SM, Tseng TS, Thornton TM, Gopalraj M, Olszewski N** (2002) SPINDLY is a nuclear-localised repressor of gibberellin signal transduction expressed throughout the plant. *Plant Physiol* **129**: 605-615
- Tabata R, Ikezaki M, Fujibe T, Aida M, Tian C-e, Ueno Y, Yamamoto KT, Machida Y, Nakamura K, Ishiguro S** (2010) Arabidopsis AUXIN RESPONSE FACTOR6 and 8 Regulate Jasmonic Acid Biosynthesis and Floral Organ Development via Repression of Class 1 KNOX Genes. *Plant and Cell Physiology* **51**: 164-175
- Tan X, Calderon-Villalobos LIA, Sharon M, Zheng C, Robinson CV, Estelle M, Zheng N** (2007) Mechanism of auxin perception by the TIR1 ubiquitin ligase. *Nature* **446**: 640-645
- Telfer A, Bollman KM, Poethig RS** (1997) Phase change and the regulation of trichome distribution in Arabidopsis thaliana. *Development* **124**: 645-654
- Thrower JS, Hoffman L, Rechsteiner M, Pickart CM** (2000) Recognition of the polyubiquitin proteolytic signal. *The EMBO Journal* **19**: 94-102
- Tomé F, Jansseune K, Saey B, Grundy J, Vandebroucke K, Hannah MA, Redestig H** (2017) rosetR: protocol and software for seedling area and growth analysis. *Plant Methods* **13**: 13-23
- Tréhin C, Planchais S, Glab N, Perennes C, Tregear J, Bergounioux C** (1998) Cell cycle regulation by plant growth regulators: involvement of auxin and cytokinin in the re-entry of Petunia protoplasts into the cell cycle. *Planta* **206**: 215-224

- Trigueros M, Navarrete-Gómez M, Sato S, Christensen SK, Pelaz S, Weigel D, Yanofsky MF, Ferrándiz C** (2009) The NGATHA Genes Direct Style Development in the Arabidopsis Gynoecium. *The Plant Cell* **21**: 1394-1409
- Uberti-Manassero NG, Lucero LE, Viola IL, Vegetti AC, Gonzalez DH** (2012) The class I protein AtTCP15 modulates plant development through a pathway that overlaps with the one affected by CIN-like TCP proteins. *Journal of Experimental Botany* **63**: 809-823
- Umeda M, Bhalerao RP, Schell J, Uchimiya H, Koncz C** (1998) A distinct cyclin-dependent kinase-activating kinase of Arabidopsis thaliana. *Proceedings of the National Academy of Sciences* **95**: 5021-5026
- Van den Heuvel S** (2005) Cell-cycle regulation. *In* M Chalfie, ed, *WormBook: The Online Review of C. elegans Biology*, Pasadena
- van der Geer P, Hunter T, Lindberg RA** (1994) Receptor protein-tyrosine kinases and their signal transduction pathways. *Annual Review of Cell Biology* **10**: 251-337
- van der Graaff E, Dulk-Ras AD, Hooykaas PJ, Keller B** (2000) Activation tagging of the LEAFY PETIOLE gene affects leaf petiole development in Arabidopsis thaliana. *Development* **127**: 4971-4980
- van der Walt S, Smith N** (2015) Viridis. *In* MPL Colormaps,
- van Ooijen G, Mayr G, Kasiem MMA, Albrecht M, Cornelissen BJC, Takken FLW** (2008) Structure–function analysis of the NB-ARC domain of plant disease resistance proteins. *Journal of Experimental Botany* **59**: 1383-1397
- Van Wart HE, Birkedal-Hansen H** (1990) The cysteine switch: A principle of regulation of metalloproteinase activity with potential applicability to the entire matrix metalloproteinase gene family. *Proceedings of the National Academy of Sciences* **87**: 5578-5582
- Vanhaeren H, Nam YJ, De Milde L, Chae E, Storme V, Weigel D, Gonzalez N, Inzé D** (2017) Forever Young: The Role of Ubiquitin Receptor DA1 and E3 Ligase BIG BROTHER in Controlling Leaf Growth and Development. *Plant Physiology* **173**: 1269-1282
- Varshavsky A** (2011) The N-end rule pathway and regulation by proteolysis. *Protein Science* **20**: 1298-1345
- Ve T, Williams SJ, Kobe B** (2015) Structure and function of Toll/interleukin-1 receptor/resistance protein (TIR) domains. *Apoptosis* **20**: 250-261
- Venne AS, Vögtle FN, Meisinger C, Sickmann A, Zahedi RP** (2013) Novel Highly Sensitive, Specific, and Straightforward Strategy for Comprehensive N-Terminal Proteomics

- Reveals Unknown Substrates of the Mitochondrial Peptidase Icp55. *Journal of Proteome Research* **12**: 3823-3830
- Verma R, Annan RS, Huddleston MJ, Carr SA, Reynard G, Deshaies RJ** (1997) Phosphorylation of Sic1p by G1 Cdk Required for Its Degradation and Entry into S Phase. *Science* **278**: 455-460
- Vierstra RD** (1996) Proteolysis in plants: mechanisms and functions. *Plant Molecular Biology* **32**: 275-302
- Vierstra RD** (2009) The ubiquitin–26S proteasome system at the nexus of plant biology. *Nature Reviews Molecular Cell Biology* **10**: 385-397
- Von Wangenheim D, Hauschild R, Fendrych M, Barone V, Benkova E, Friml J** (2017) Live tracking of moving samples in confocal microscopy for vertically grown roots. *Elife* **6**: e26792
- Wang H, Fowke LC, Crosby WL** (1997) A plant cyclin-dependent kinase inhibitor gene. *Nature* **386**: 451-452
- Wang JL, Tang MQ, Chen S, Zheng XF, Mo HX, Li SJ, Wang Z, Zhu KM, Ding LN, Liu SY, Li YH, Tan XL** (2017) Down-regulation of BnDA1, whose gene locus is associated with the seeds weight, improves the seeds weight and organ size in *Brassica napus*. *Plant Biotechnology Journal* **15**: 1024-1033
- Wang X, Kota U, He K, Blackburn K, Li J, Goshe MB, Huber SC, Clouse SD** (2008) Sequential Transphosphorylation of the BRI1/BAK1 Receptor Kinase Complex Impacts Early Events in Brassinosteroid Signaling. *Developmental Cell* **15**: 220-235
- Wang X, Taplick J, Geva N, Oren M** (2004) Inhibition of p53 degradation by Mdm2 acetylation. *FEBS Letters* **561**: 195-201
- Wang Z-Y, Seto H, Fujioka S, Yoshida S, Chory J** (2001) BRI1 is a critical component of a plasma-membrane receptor for plant steroids. *Nature* **410**: 380-383
- Weight C, Parnham D, Waites R** (2008) TECHNICAL ADVANCE: LeafAnalyser: a computational method for rapid and large-scale analyses of leaf shape variation. *The Plant Journal* **53**: 578-586
- Werner T, Motyka V, Strnad M, Schmülling T** (2001) Regulation of plant growth by cytokinin. *Proceedings of the National Academy of Sciences* **98**: 10487-10492
- White DWR** (2006) PEAPOD regulates lamina size and curvature in *Arabidopsis*. *Proceedings of the National Academy of Sciences* **103**: 13238-13243

- Wildwater M, Campilho A, Perez-Perez JM, Heidstra R, Blilou I, Korthout H, Chatterjee J, Mariconti L, Gruitsem W, Scheres B** (2005) The RETINOBLASTOMA-RELATED Gene Regulates Stem Cell Maintenance in Arabidopsis Roots. *Cell* **123**: 1337-1349
- Williams TA, Corvol P, Soubrier F** (1994) Identification of Two Active Site Residues in Human Angiotensin I-converting Enzyme. *The Journal of Biological Chemistry* **269**: 29430-29434
- Willis L, Refahi Y, Wightman R, Landrein B, Teles J, Huang KC, Meyerowitz EM, Jönsson H** (2016) Cell size and growth regulation in the Arabidopsis thaliana apical stem cell niche. *Proceedings of the National Academy of Sciences* **113**: E8238-E8246
- Wolf DH, Hilt W** (2004) The proteasome: a proteolytic nanomachine of cell regulation and waste disposal. *Biochim Biophys Acta* **1695**: 19-31
- Wolf S, Hematy K, Hofte H** (2012) Growth Control and Cell Wall Signalling in Plants. *Annual Review of Plant Biology* **63**: 381-407
- Wu FH, Shen SC, Lee LY, Lee SH, Chan MT, Lin CS** (2009) Tape-Arabidopsis Sandwich - a simpler Arabidopsis protoplast isolation method. *Plant Methods* **5**
- Wu G, Lin W-c, Huang T, Poethig RS, Springer PS, Kerstetter RA** (2008) KANADI1 regulates adaxial-abaxial polarity in Arabidopsis by directly repressing the transcription of ASYMMETRIC LEAVES2. *Proceedings of the National Academy of Sciences* **105**: 16392-16397
- Xia T, Li N, Dumenil J, Li J, Kamenski A, Bevan MW, Gao F, Li YH** (2013) The Ubiquitin Receptor DA1 Interacts with the E3 Ubiquitin Ligase DA2 to Regulate Seed and Organ Size in Arabidopsis. *Plant Cell* **25**: 3347-3359
- Xie G, Li Z, Ran Q, Wang H, Zhang J** (2017) Over-expression of mutated ZmDA1 or ZmDAR1 gene improves maize kernel yield by enhancing starch synthesis. *Plant Biotechnology Journal*: n/a-n/a
- Xu D, Woodfield SE, Lee TV, Fan Y, Antonio C, Bergmann A** (2009) Genetic control of programmed cell death (apoptosis) in Drosophila. *Fly* **3**: 78-90
- Xu L** (2002) The SCFCO11 Ubiquitin-Ligase Complexes Are Required for Jasmonate Response in Arabidopsis. *The Plant Cell Online* **14**: 1919-1935
- Xu L, Ménard R, Berr A, Fuchs J, Cognat V, Meyer D, Shen W-H** (2009) The E2 ubiquitin-conjugating enzymes, AtUBC1 and AtUBC2, play redundant roles and are involved in activation of FLC expression and repression of flowering in Arabidopsis thaliana. *The Plant Journal* **57**: 279-288

- Xu TD, Dai N, Chen J, Nagawa S, Cao M, Li H, Zhou Z, Chen X, De Rycke R, Rakusova H, Wang W, Jones AM, Friml J, Patterson SE, Bleecker AB, Yang Z** (2014) Cell surface ABP1-TMK auxin-sensing complex activates ROP GTPase signalling. *Science* **343**: 1025-1028
- Yang H, Shi Y, Liu J, Guo L, Zhang X, Yang S** (2010) A mutant CHS3 protein with TIR-NB-LRR-LIM domains modulates growth, cell death and freezing tolerance in a temperature-dependent manner in Arabidopsis. *The Plant Journal* **63**: 283-296
- Yang M, Gao X, Dong J, Gandhi N, Cai H, von Wettstein DH, Rustgi S, Wen S** (2017) Pattern of Protein Expression in Developing Wheat Grains Identified through Proteomic Analysis. *Front Plant Sci* **8**: 962
- Yoo S-D, Cho Y-H, Sheen J** (2007) Arabidopsis mesophyll protoplasts: a versatile cell system for transient gene expression analysis. *Nat. Protocols* **2**: 1565-1572
- Yoshida S, Barbier de Reuille P, Lane B, Bassel George W, Prusinkiewicz P, Smith Richard S, Weijers D** (2014) Genetic Control of Plant Development by Overriding a Geometric Division Rule. *Developmental Cell* **29**: 75-87
- Yu H, Yao X** (2008) Cyclin B1: conductor of mitotic symphony orchestra. *Cell Research* **18**: 218-220
- Zeng D, Tian Z, Rao Y, Dong G, Yang Y, Huang L, Leng Y, Xu J, Sun C, Zhang G, Hu J, Zhu L, Gao Z, Hu X, Guo L, Xiong G, Wang Y, Li J, Qian Q** (2017) Rational design of high-yield and superior-quality rice. *Nature Plants* **3**: 17031
- Zhang HY, Lei G, Zhou HW, He C, Liao JL, Huang YJ** (2017) Quantitative iTRAQ-based proteomic analysis of rice grains to assess high night temperature stress. *Proteomics* **17**
- Zhang J, Wei B, Yuan R, Wang J, Ding M, Chen Z, Yu H, Qin G** (2017) The Arabidopsis RING-type E3 ligase TEAR1 controls leaf development by targeting the TIE transcriptional repressor for degradation. *The Plant Cell* **29**: 243-259
- Zheng J, Yang X, Harrell JM, Ryzhikov S, Shim E-H, Lykke-Andersen K, Wei N, Sun H, Kobayashi R, Zhang H** (2002) CAND1 Binds to Unneddylated CUL1 and Regulates the Formation of SCF Ubiquitin E3 Ligase Complex. *Molecular Cell* **10**: 1519-1526
- Zheng N, Schulman BA, Song L, Miller JJ, Jeffrey PD, Wang P, Chu C, Koeppe DM, Elledge SJ, Pagano M, Conaway RC, Conaway JW, Harper JW, Pavletich NP** (2002) Structure of the Cul1-Rbx1-Skp1-F boxSkp2 SCF ubiquitin ligase complex. *Nature* **416**: 703
- Zheng N, Wang P, Jeffrey PD, Pavletich NP** (2000) Structure of a c-Cbl-UbcH7 Complex: RING Domain Function in Ubiquitin-Protein Ligases. *Cell* **102**: 533-539

Zhou P, Howley PM (1998) Ubiquitination and Degradation of the Substrate Recognition Subunits of SCF Ubiquitin-Protein Ligases. *Molecular Cell* **2**: 571-580

APPENDIX 1 - SUPPLEMENTARY FIGURES

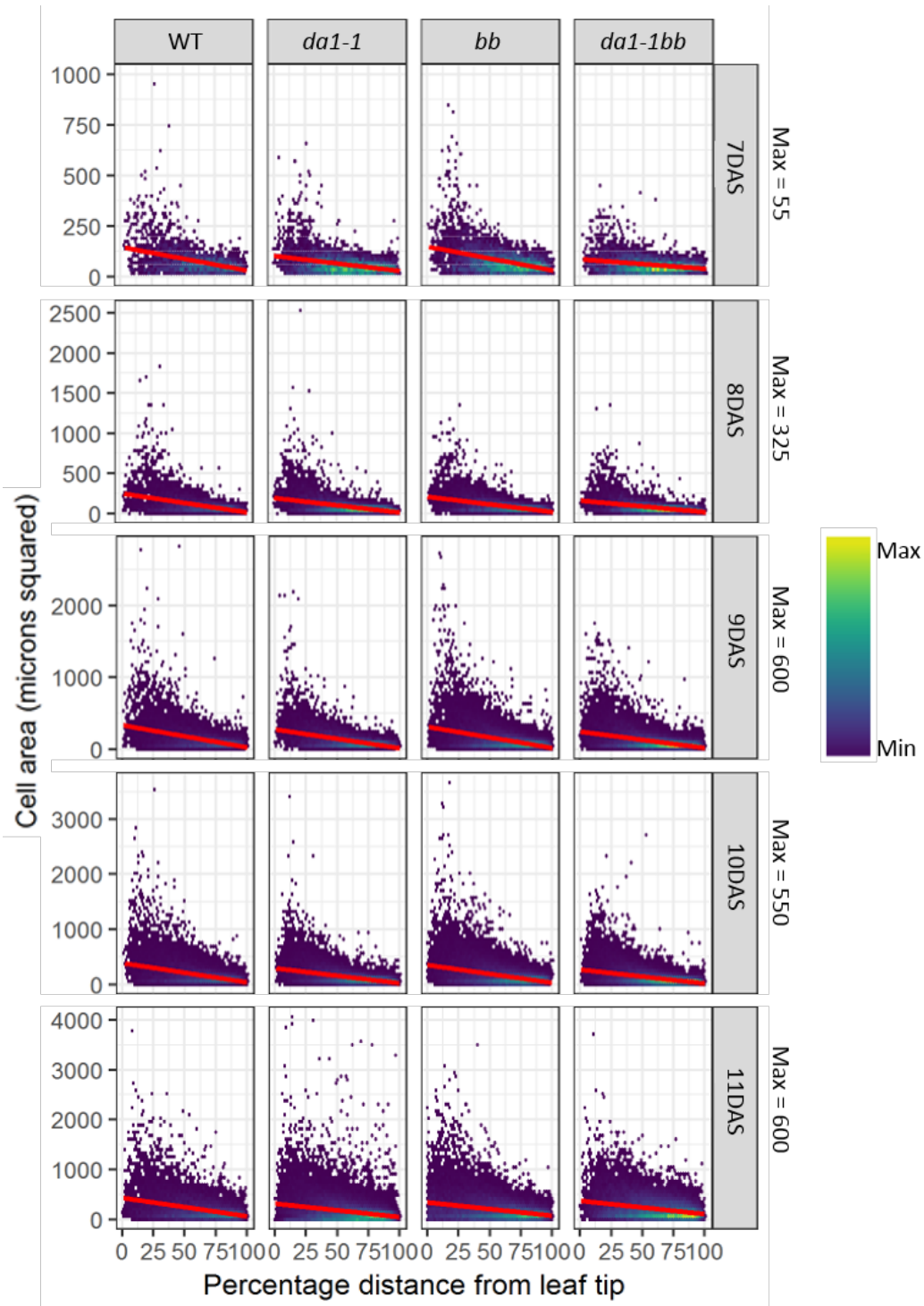


Figure S1 Cell area distributions within wild type, *da1-1*, *bb*, and *da1-1bb* leaves

Binned hex-plots of cell areas by relative distance from the leaf tip in wild type *pAR169*, *da1-1 pAR169*, *bb pAR169*, and *da1-1bb pAR169* leaves from 7 to 11 days after stratification. Each heatmap represents three pooled independent samples. Red lines indicate linear regressions. Cells in the midvein and the leaf margin are excluded from these data. Total cells analysed > 370,000. This figure represents the data from Figure 3.12 without the removal of data beyond three standard deviations of the mean of each pooled sample.

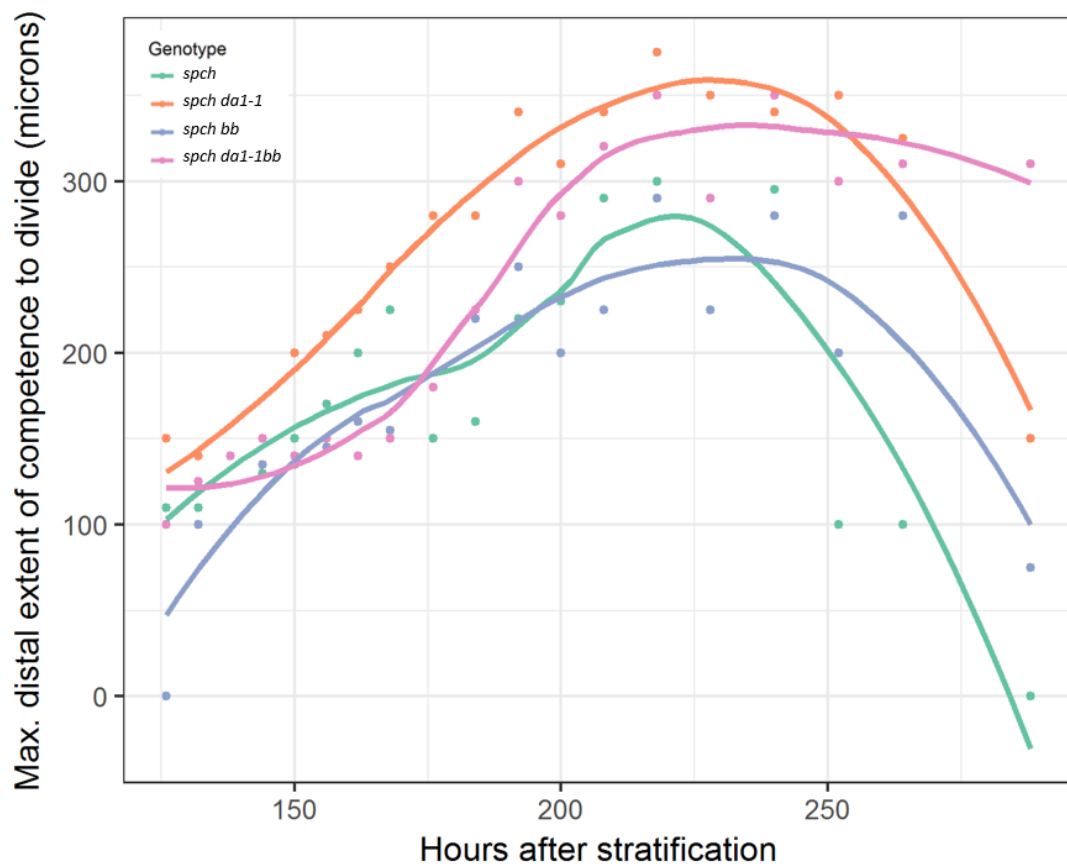


Figure S2 Maximum distal extent of zone of competency to divide in *spch*, *da1-1*, *bb*, and *da1-1bb* leaves

Distance from the petiole-lamina boundary of the most distal cell with competency to divide of the first leaf of *spch pAR169*, *spch da1-1 pAR169*, *spch bb pAR169*, and *spch da1-1bb pAR169* plants from 120 to 288 hours after stratification.

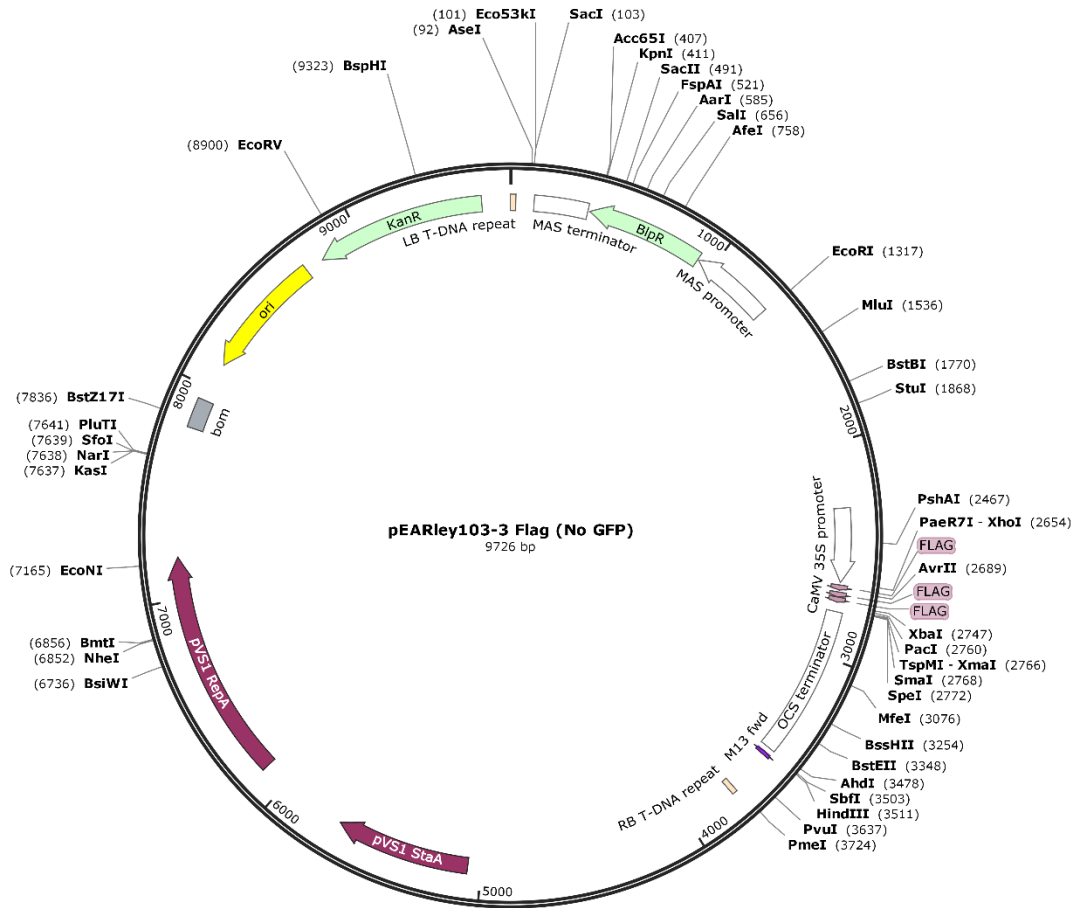


Figure S3 Vector map of modified pEarleyGate 103

Vector modified by Dr Hui Dong. Map produced in Snapgene 4.1.2.

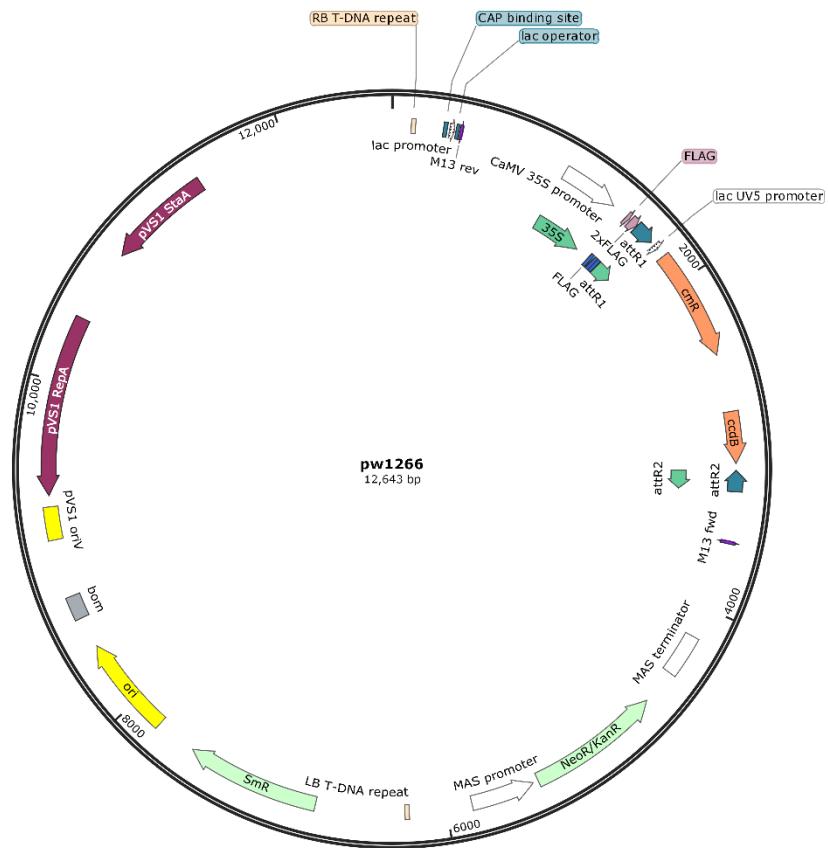


Figure S4 Vector map of pw1266

Map produced in Snapgene 4.1.2.

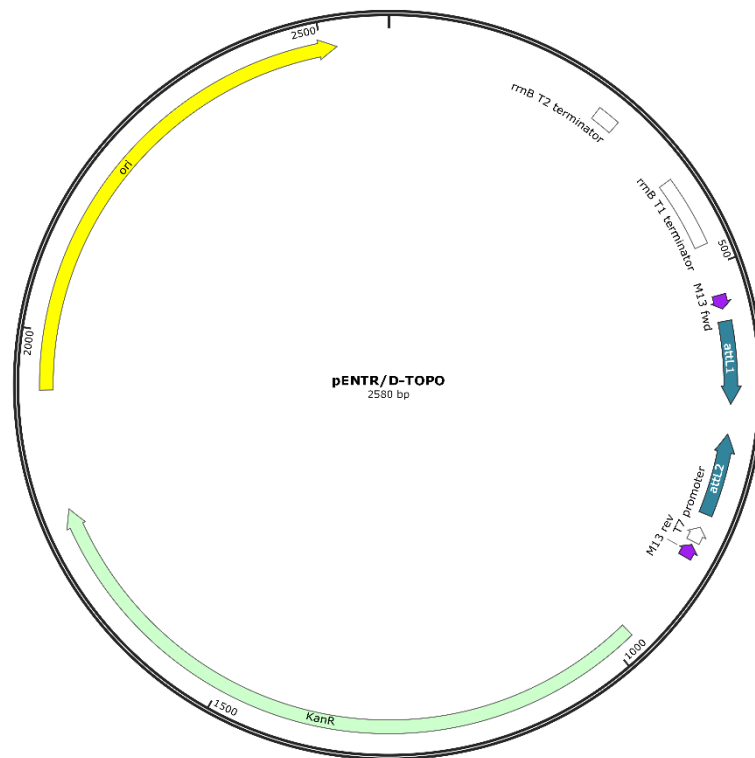


Figure S5 Vector map of pENTR/D-TOPO

Map produced in Snapgene 4.1.2.

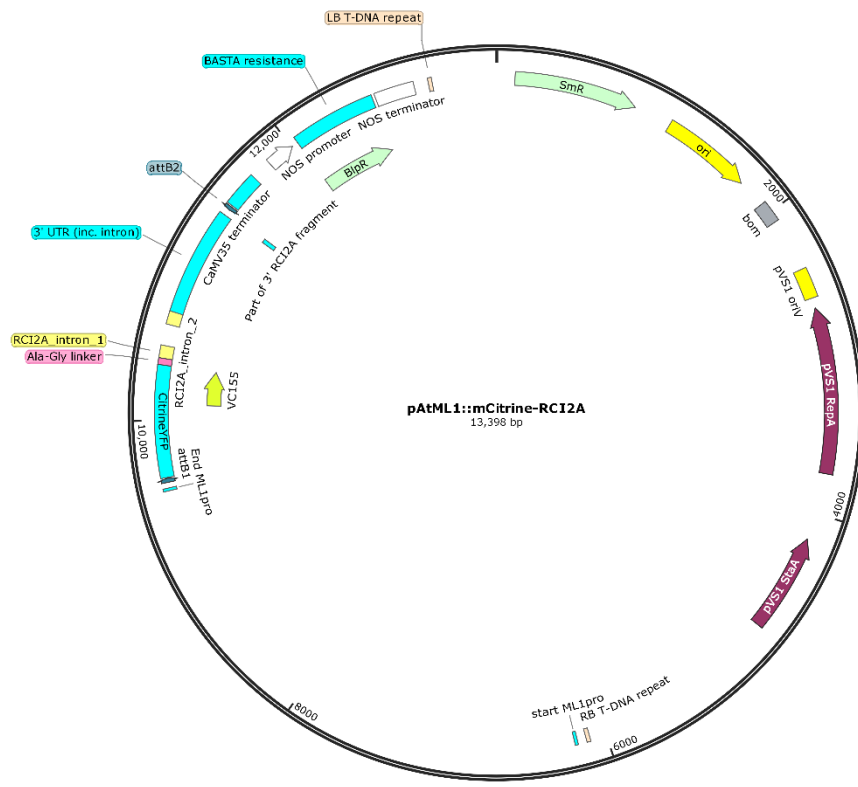


Figure S6 Vector map of pAtML1::mCitrine-RCI2A

Map produced in Snapgene 4.1.2.

APPENDIX 2 - DONG ET AL., 2017

Ubiquitylation activates a peptidase that promotes cleavage and destabilization of its activating E3 ligases and diverse growth regulatory proteins to limit cell proliferation in *Arabidopsis*

Hui Dong,^{1,6} Jack Dumenil,^{1,6} Fu-Hao Lu,^{1,6} Li Na,^{2,6} Hannes Vanhaeren,³ Christin Naumann,⁴ Maria Klecker,⁴ Rachel Prior,¹ Caroline Smith,¹ Neil McKenzie,¹ Gerhard Saalbach,¹ Liangliang Chen,² Tian Xia,² Nathalie Gonzalez,³ Mathilde Seguela,^{1,5} Dirk Inzé,³ Nico Dissmeyer,⁴ Yunhai Li,² and Michael W. Bevan¹

¹John Innes Centre, Norwich NR4 7QA, United Kingdom; ²State Key Laboratory of Plant Cell and Chromosome Engineering, CAS Centre of Excellence in Molecular Plant Biology, Institute of Genetics and Developmental Biology, Chinese Academy of Sciences, Beijing 100101, China; ³VIB-UGent Centre for Plant Systems Biology, Ghent University, 9052 Gent, Belgium; ⁴Leibniz Institute of Plant Biochemistry (IPB), D-06120 Halle, Germany

The characteristic shapes and sizes of organs are established by cell proliferation patterns and final cell sizes, but the underlying molecular mechanisms coordinating these are poorly understood. Here we characterize a ubiquitin-activated peptidase called DA1 that limits the duration of cell proliferation during organ growth in *Arabidopsis thaliana*. The peptidase is activated by two RING E3 ligases, Big Brother (BB) and DA2, which are subsequently cleaved by the activated peptidase and destabilized. In the case of BB, cleavage leads to destabilization by the RING E3 ligase PROTEOLYSIS 1 (PRT1) of the N-end rule pathway. DA1 peptidase activity also cleaves the deubiquitylase UBP15, which promotes cell proliferation, and the transcription factors TEOSINTE BRANCHED 1/CYCLOIDEA/PCF 15 (TCP15) and TCP22, which promote cell proliferation and repress endoreduplication. We propose that DA1 peptidase activity regulates the duration of cell proliferation and the transition to endoreduplication and differentiation during organ formation in plants by coordinating the destabilization of regulatory proteins.

[*Keywords:* ubiquitylation; organ size; *Arabidopsis*; ubiquitin-activated peptidase; N-end rule-mediated degradation]

Supplemental material is available for this article.

Received October 17, 2016; revised version accepted January 11, 2017.

The shapes and sizes of organs are established by mechanisms that orient cell proliferation and determine the final numbers and sizes of cells forming the organ. Transplantation experiments showed that some animal organs have an intrinsic mechanism that determines their final size by controlling the duration of cell proliferation (Barry and Camargo 2013), which is controlled in part by the HIPPO/YAP pathway that limits cell proliferation and promotes apoptosis (Pan 2010). However, the mechanisms coordinating cell proliferation and cell size during organ growth remain poorly understood (Johnston and

Gallant 2002). Due to the simpler planar structures of their organs, such as leaves and petals, and the absence of cell movement due to rigid cell walls, plants have some experimental advantages for studying organ growth (Green et al. 2010).

Leaf growth in plants is initiated at shoot meristems (for review, see Sluis and Hake 2015). After specification of boundaries and growth axes, the leaf lamina grows in an initial period of cell division in which cell size is relatively constant, followed by a transition to endoreduplication associated with cell expansion and differentiation (Breuer et al. 2010; De Veylder et al. 2011). The transition from cell proliferation to cell expansion is spatially and temporarily regulated during leaf growth and appears to progress from the tip to the base of the leaf as a cell division arrest

⁵Present address: UMR1318, Institut Jean-Pierre Bourgin, 78000 Versailles, France.

⁶These authors contributed equally to this work.

Corresponding authors: michael.bevan@jic.ac.uk, yhli@genetics.ac.cn
Article Published online ahead of print. Article and publication date are online at <http://www.genesdev.org/cgi/doi/10.1101/gad.292235.116>. Freely available online through the *Genes & Development* Open Access option.

© 2017 Dong et al. This article, published in *Genes & Development*, is available under a Creative Commons License (Attribution 4.0 International), as described at <http://creativecommons.org/licenses/by/4.0/>.

front (Kazama et al. 2010) accompanied by shifts in gene expression patterns (Efroni et al. 2008; Andriankaja et al. 2012). A key question is how the transition from cell proliferation to cell expansion and differentiation is coordinated to generate a correctly sized organ.

The RING E3 ligases Big Brother (BB) (Disch et al. 2006) and DA2 (Xia et al. 2013) limit the duration of cell proliferation during organ growth. Members of the *DA1* family also limit cell proliferation (Li et al. 2008), and loss-of-function mutations in *BB* and *DA2* interact synergistically with the *da1-1* allele of *DA1* to increase organ and seed size in *Arabidopsis* (Li et al. 2008; Xia et al. 2013), suggesting that one of their growth-limiting activities is mediated by enhancing the growth-repressive activity of DA1 family members. Genetic analyses showed that DA1 reduced the stability of both UBP15 (Du et al. 2014), a deubiquitylation enzyme promoting cell proliferation (Liu et al. 2008), and TEOSINTE BRANCHED 1/CYCLOIDEA/PCF 14 (TCP14) and TCP15 proteins (Peng et al. 2015), which repress endoreduplication by transcriptional control of *RETINOBLASTOMA-RELATED1* (*RBR1*) and *CYCLIN A2;3* (*CYCA2;3*) gene expression (Li et al. 2012).

Here we show that DA1 is an endopeptidase activated by multiple ubiquitylations mediated by the E3 ligases BB and DA2. In a feedback mechanism, DA1 then cleaves BB and DA2, leading to their destabilization. DA1-mediated cleavage of BB exposed a destabilizing N-terminal that was substrate for the N-end rule E3 ligase PROTEOLYSIS 1 (PRT1). This mechanism is predicted to transiently activate DA1 peptidase, which also cleaves UBP15, TCP15, and the related TCP22, leading to their predicted inactivation and destabilization. DA1 peptidase may therefore contribute to the concerted transition from cell proliferation to endoreduplication and differentiation, limiting organ size.

Results

Genetic and physical interactions of DA1, BB, and DA2

We previously identified genetic interactions between the *da1-1* allele of *DA1* and genes encoding the RING E3 ligases BB (Li et al. 2008) and DA2 (Xia et al. 2013) that led to synergistic increases in seed and organ sizes. In this study, we used the *da1-1*-enhancing allele of *BB* called *eod1-2* (Li et al. 2008) and refer to the mutant version as *bb-eod1-2* and the wild-type version as *BB*. The *da1-1* allele, an R358K change in a highly conserved region, had a negative influence on the functions of *DA1* and the close family member *DAR1*, but the basis of this was not known, which complicated interpretation of DA1 function. We therefore assessed phenotypes of a loss-of-function T-DNA allele of *DA1* (*da1-ko1*).

Measurements of petal and seed sizes using high-resolution scanning showed that the *da1-ko1* T-DNA allele led to increased petal (Fig. 1A,B) and seed (Fig. 1C,D) sizes and that it also interacted genetically with the loss-of-function allele *bb-eod1-2* and *da2-1* in both petal size and seed area. This showed that *DA1* can be studied independently of other *DA1* family members. Both the *da1-1*

and *bb-eod1-2* mutations increased the maximum growth rate, while the double mutant *da1-1 bb-eod1-2* showed a further increased maximum growth rate and continued to grow for ~5 d longer than either single mutant (Fig. 1E). The time at maximum growth rates was slightly earlier in *bb-eod1-2* than in Columbia (Col-0), in contrast to *da1-1* and *da1-1 bb-eod1-2*, which showed a 3-d retardation of the time of maximum growth rate, and final leaf sizes showed a more than additive increase in the double mutant, as observed previously (Li et al. 2008). These data indicated that *BB* may influence leaf final size at earlier stages of growth than *DA1*. We demonstrated previously that DA1 and DA2 physically interact (Xia et al. 2013). Pull-down experiments showed that GST-tagged DA1 also interacted with HIS-tagged BB but not with HIS-tagged BBR (BB-related; At3g19910), a close homolog of BB (Fig. 1F; Breuninger and Lenhard 2012). These in vitro interactions were verified by *Agrobacterium*-mediated coexpression of BB-GFP and Myc-tagged DA1 in *Nicotiana benthamiana* leaves. Myc-DA1 was detected only in a complex with BB-GFP and not GFP (Fig. 1G).

DA1 is multiply ubiquitylated by BB and DA2

The interactions of DA1 with BB and DA2 suggested that DA1 might be a substrate of these RING E3 ligases, so we conducted in vitro ubiquitylation reactions using BB, DA2, and BBR E3 ligases. Figure 2A shows that BB ubiquitylated DA1 in an E1- and E2-dependent reaction, as did DA2 (Fig. 2B), while BBR did not (Fig. 2C). Supplemental Figure S1 shows that DA2 also ubiquitylated DAR1 and DAR2 but not DAR3. The extent of DA1 ubiquitylation suggested that DA2 was more efficient at ubiquitylation than BB, and the sizes of ubiquitylated DA1 indicated that between four and seven ubiquitin molecules may be conjugated to DA1. Mass spectrometric analyses of ubiquitylated DA1 prepared in vitro were used to identify peptides containing the characteristic diglycine ubiquitylation signature of a lysine residue (KGG). Analysis of DA1 ubiquitylated by DA2 or BB identified seven ubiquitylated lysine residues in DA1, with four lysines in the C-terminal domain of DA1 (K381, K391, K475, and K591) consistently conjugated with ubiquitin (Supplemental Fig. S2). This number of ubiquitylation sites concurred with the patterns of ubiquitylation observed in Figure 2, A and B, suggesting that DA1 molecules are multiply ubiquitylated (Haglund et al. 2003; Komander and Rape 2012). Mutation of the consistently ubiquitylated lysines to arginine in DA1 [termed DA1(4K-4R)] did not reduce ubiquitylation by DA2 in vitro (Fig. 2D), and mass spectrometric analyses showed ectopic ubiquitylation of other lysines across DA1 (Supplemental Fig. S2B). Therefore, the DA1 ubiquitylation mechanism has a preference, but not specificity, for certain lysines. These patterns of ubiquitylation are shown in Figure 2D.

DA1 and four other family members have multiple ubiquitin interaction motifs (UIMs) that interact with ubiquitin (Li et al. 2008; Peng et al. 2015). UIMs are part of a larger class of ubiquitin-binding domains (UBDs) formed from a single α helix that is often found in multiple

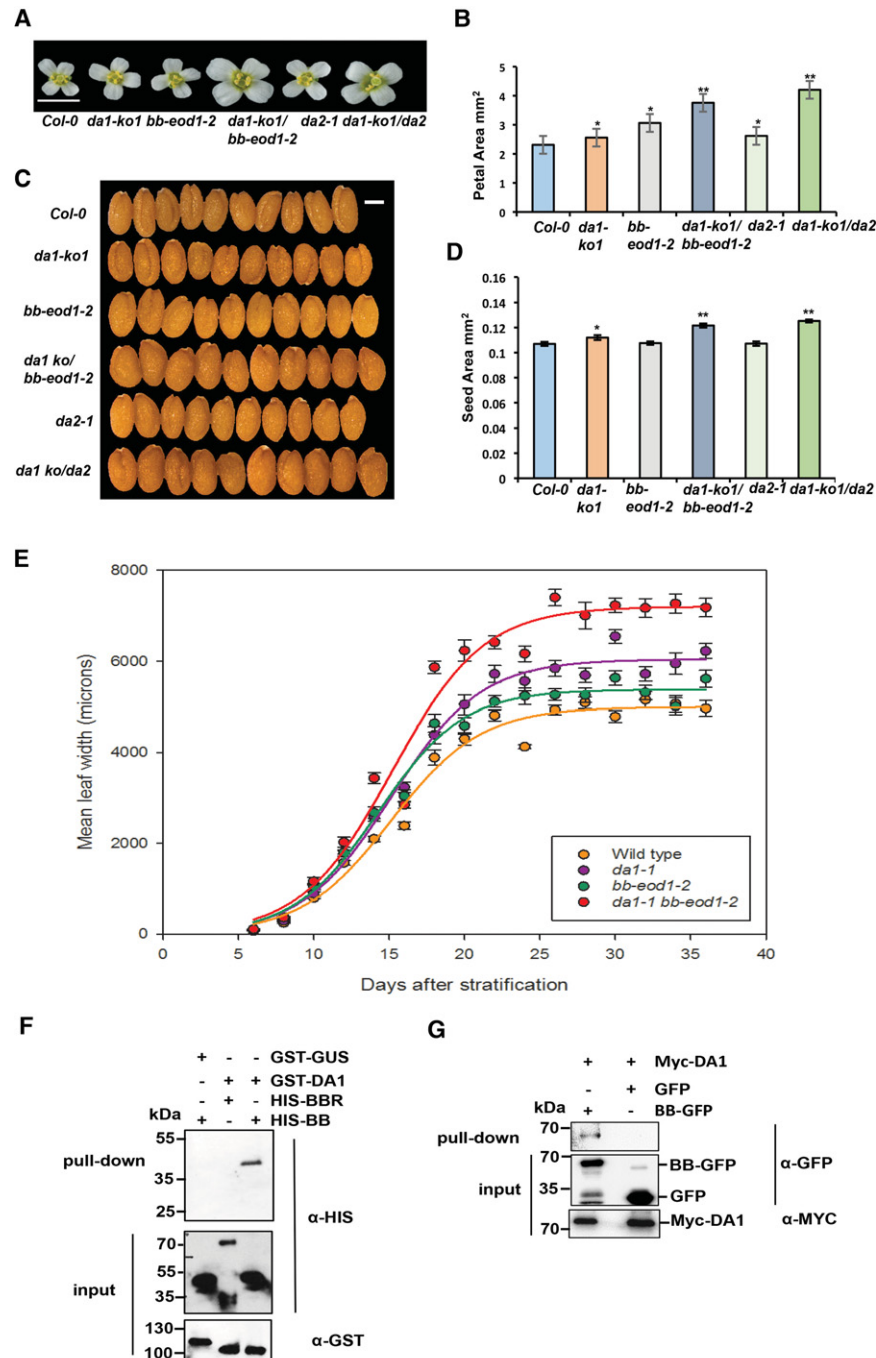


Figure 1. Genetic and physical interactions of DA1, BB, and DA2. (A,B) The single loss-of-function *da1-ko1* allele interacts with *bb-eod1-2* and *da2-1* to increase petal area. (A) An image of flower heads showing the sizes of petals. Bar, 5 mm. (B) Petal areas. The values given are means ($n = 36$) \pm SE. (*) $P < 0.05$; (**) $P < 0.01$ (Student's *t*-test) compared with wild-type Col-0. (C,D) The single loss-of-function *da1-ko1* allele interacts with *bb-eod1-2* and *da2-1* to increase seed area. (C) Ten seeds aligned to reveal size differences. Bar, 2 mm. (D) Seed areas. The values given are means ($n = 50$) \pm SE. (*) $P < 0.05$; (**) $P < 0.01$ (Student's *t*-test) compared with wild-type Col-0. (E) Dynamic growth measurements of leaf 1 width in Col-0, *da1-1*, and *da1-1 bb-eod1-2*. Lines were fitted to data points using the sigmoidal function of Sigmaplot 13. (F) DA1 interacts with BB in vitro. GST-DA1 interacted with HIS-BB. GST-DA1 did not interact with HIS-BBR, an E3 ligase closely related to BB. GST-GUS (β -glucuronidase) was used as a negative control. (G) Myc-tagged DA1 interacted with BB-GFP after transient coexpression in *N. benthamiana* leaves. BB-GFP and GFP were coexpressed with Myc-DA1 using *Agrobacterium*-mediated transient expression in *N. benthamiana* leaves. Expressed proteins were purified using GFP trap and immunoblotted.

arrays (Hicke et al. 2005; Husnjak and Dikic 2012). Tandem UIMs have been shown to bind K63-linked ubiquitin chains in the mammalian DNA repair protein RAP80 (Sato et al. 2009). To assess their function in DA1, the N-terminal region of DA1 containing mutated UIM1 and UIM2 was fused to GST and expressed in *Escherichia coli*, and conserved Ala and Ser residues, predicted to be in the α -helical domain of the UIMs (Supplemental Fig. S3; Kim et al. 2007), were mutated to Gly in both UIMs of GST-UIM1+2 and in DA1. GST-UIM1+2 bound ubiquitin, and mutation of UIM1 alone did not reduce binding of

ubiquitin, while mutation of UIM2 abolished ubiquitin binding, confirming that the GST-UIM1+2 protein bound ubiquitin via its UIM motifs (Supplemental Fig. S3). Figure 2E shows that UIM1+2 conferred BB- and DA2-dependent ubiquitylation on GST in vitro, with DA2 again facilitating higher levels of ubiquitylation. Figure 2F shows that mutation of both UIM1 and UIM2 in GST-UIM1+2 strongly reduced in vitro ubiquitylation of GST-UIM1+2 by BB and DA2. The UIM1 and UIM2 mutations in DA1 also reduced its ubiquitylation in vitro (Fig. 2G), and DA1 with mutated UIMs did not

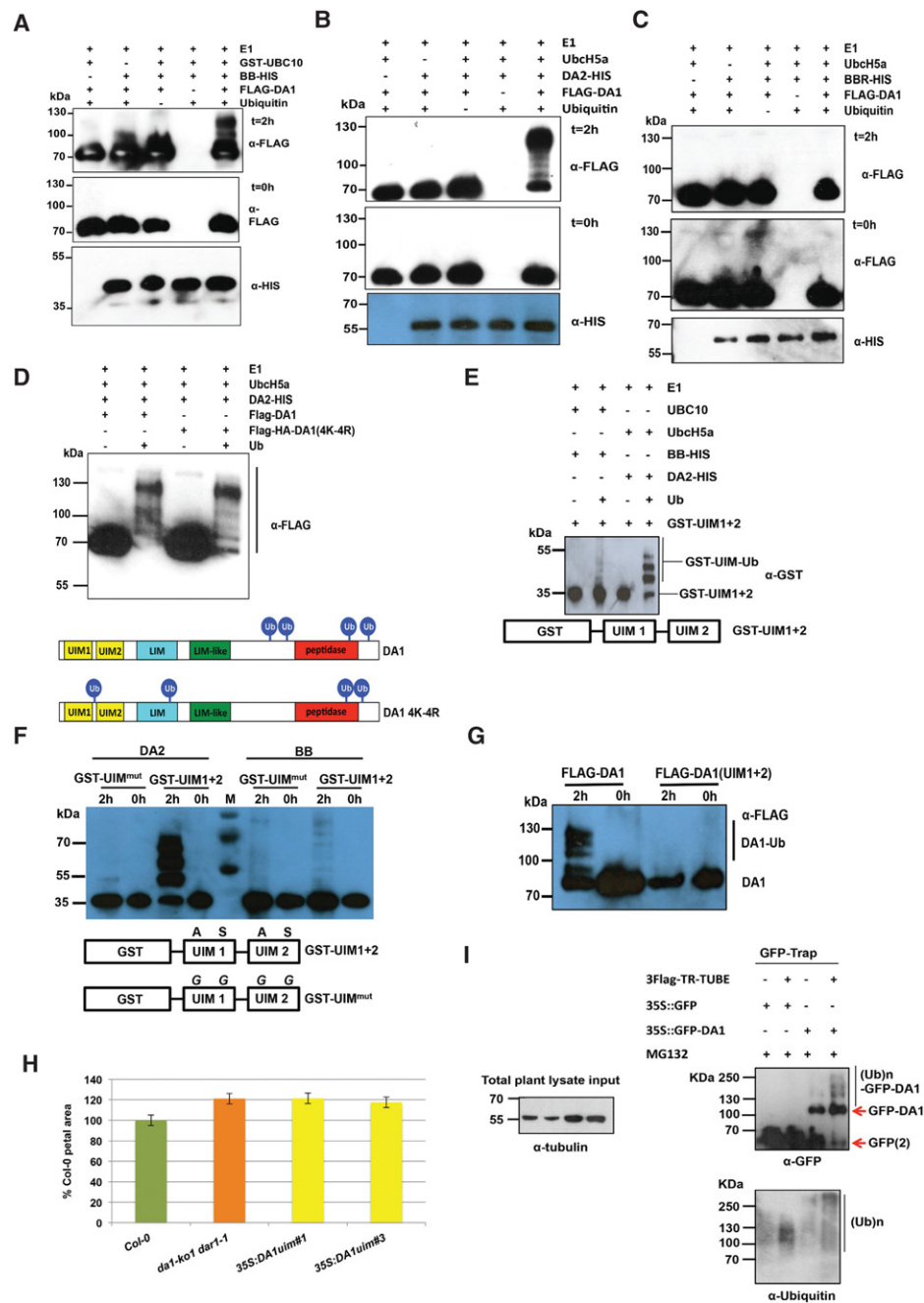


Figure 2. DA1 is multiply ubiquitylated by BB and DA2 in a ubiquitin interaction motif (UIM)-dependent reaction. (A–C) In vitro ubiquitylation of DA1 by the RING E3 ligases BB (A) and DA2 (B), but not BBR (C), in an E1-, E2-, and ubiquitin-dependent reaction. Anti-Flag antibodies detected Flag-ubiquitylated forms of Flag-DA1 ranging from >70 kDa to ~130 kDa. Anti-HIS antibodies detected BB-HIS, DA2-HIS, or BBR-HIS fusion proteins. (D) Both Flag-DA1 and Flag-DA1(4K-4R) are ubiquitylated by DA2 in similar patterns in an in vitro ubiquitylation reaction. In the *bottom* panel, Ub represents a ubiquitin moiety conjugated to a lysine at the approximate location in DA1 and DA1(4K-4R). Regions of protein similarity with known domains are shown: UIM1 and UIM2 are similar to UIMs, LIM is similar to canonical LIM domains, LIM-like is a related motif found in DA1 family members, and peptidase contains a predicted peptidase active site. (E) An in vitro ubiquitylation reaction with DA2 and BB as E3 ligases and GST-UIM1+2 is ubiquitylated in a pattern similar to that of DA1 by both DA2 and BB, with DA2 conferring higher levels of ubiquitylation than BB. (F) An in vitro ubiquitylation reaction with DA2 and BB as E3 ligases and GST-UIM1+2 with mutations that reduce ubiquitin binding. Mutated versions of UIM1 and UIM2 strongly reduced DA2- and BB-mediated ubiquitylation of GST-UIM1+2. (G) A time course of Flag-DA1 and Flag-DA1(UIM1+2) with mutations in the UIMs as in E. These strongly reduced DA1 ubiquitylation. (H) DA1(UIM1+2) is not functional in vivo, as it does not complement the large petal phenotype of the *da1-kol1 dar1-1* double mutant. Two independent homozygous T-DNA insertion lines were scored for petal size and compared with wild-type Col-0 and *da1-kol1 dar1-1*. The values given are means ($n = 120$) \pm SE, expressed as the percentage of wild-type Col-0 petal areas. Student's *t*-test showed no significant differences between the transformants and the parental *da1-kol1 dar1-1* line. (I) Transgenic *Arabidopsis* plants expressing a GFP-DA1 fusion protein under the control of the 35S promoter were used to detect DA1 ubiquitylation in vivo. GFP ran as a dimer on the gel due to high protein concentrations. Protein extract input levels are shown using anti-tubulin antibody.

complement the large petal size in the double mutant *da1-ko dar1-1* (Fig. 2H). To detect ubiquitylation *in vivo*, DA1 was expressed from the constitutive 35S promoter as an N-terminal GFP fusion protein and purified from seedling tissues using a GFP trap. Characteristic patterns of DA1 ubiquitylation were detected on purified GFP-DA1 (Fig. 2I, right panel). Therefore, DA1 is ubiquitylated by the E3 ligases BB and DA2 *in vitro* by a UIM1- and UIM2-dependent mechanism, DA1 is ubiquitylated *in vivo*, and UIMs are required for DA1 function.

DA1 cleaves BB and DA2 with a ubiquitin-dependent peptidase activity

A time course of BB-HIS incubated with purified Flag-DA1 that had been ubiquitylated by BB or incubated with non-ubiquitylated Flag-DA1 showed that, in the presence of ubiquitylated DA1, a HIS-tagged BB fragment of ~35 kDa was produced after 4 h of incubation (Fig. 3A, arrows). When ubiquitylated Flag-DA1 was incubated with DA2-HIS, a 25-kDa HIS-tagged DA2 cleavage product was also detected after 4 h of incubation (Fig. 3A, arrows). Similar experiments using Flag-DA1 ubiquitylated by DA2 showed identical patterns of BB-HIS and DA2-HIS cleavage (Fig. 3B). BBR-HIS did not show a cleavage product in these conditions. Thus, DA1 ubiquitylated by either BB or DA2 generated cleavage products from both BB and DA2 *in vitro*.

Examination of the conserved C-terminal region of DA1 revealed an extended sequence motif, HEMMHX₁₅EE (Supplemental Fig. S4), which is a zinc aminopeptidase active site found in clan MA endopeptidases (Rawlings et al. 2012). The HEMMH motif was mutated to AEMMA, removing the putative zinc-coordinating histidine residues, to form DA1(pep). Figure 3C shows that DA1(pep) and DA1 were ubiquitylated *in vitro* to an equal extent by both BB and DA2. In an *in vitro* time-course reaction, ubiquitylated DA1(pep) did not generate the 25-kDa HIS-tagged DA2 band seen after incubation with ubiquitylated DA1 (Fig. 3D). Coexpression of BB-Flag, DA2-Flag, or BBR-Flag with HA-DA1 or HA-DA1(pep) in *da1-ko1 dar1-1* mutant leaf protoplasts showed that HA-DA1, but not HA-DA1(pep), generated a similar-sized 35-kDa BB-Flag cleavage product (Fig. 3E, top panel, arrow) as seen in *in vitro* reactions (Fig. 3A,B). Longer exposure of the same Western blot (Fig. 3E, bottom panel) was required to identify the 25-kDa DA2-Flag cleavage product, which was not generated by coexpression with DA1(pep). Figure 3F shows that the mutation in DA1 abolishing DA1 peptidase activity did not complement the *da1-ko1 dar1-1* large petal phenotype, establishing that DA1 peptidase activity is required for *in vivo* function. To detect DA1 peptidase activity *in vivo*, transgenic plants expressing *BB::gsGreen-BB* gene fusion and a RING domain mutant version that was predicted to be more stable *in vivo* due to reduced autopolyubiquitylation (Disch et al. 2006) were generated. Analysis of GFP trap-purified proteins (Fig. 3G, left panel) showed a cleavage product of the expected size generated from RING mutant *gsGreen* protein in two independent transformants. Full-length

wild-type *gsGreen-BB* was not detected, although low levels of an expected cleavage product were identified. For comparison, the same constructs, together with a noncleavable form (AY-GG) (see Fig. 5B, below), were expressed using the 35S promoter in protoplasts with DA1 (Fig. 3G, right panel). This showed the predicted DA1-mediated BB cleavage product, which was not generated in the AY-GG version of BB.

A Förster resonance energy transfer (FRET) DA1 peptidase sensor was constructed using eGFP donor and mCherry acceptor pairs (van der Krogt et al. 2008) connected by BB to provide another measure of DA1 peptidase activity *in vivo*. Cleavage of the fluorophore pair by DA1 would increase the fluorescence lifetime toward that of eGFP-BB compared with that of the intact sensor protein by impairing energy transfer between the fluorophores. The peptidase sensor and a control donor sensor were transfected into *da1-ko1 dar1-1* root protoplasts, and fluorescence lifetime imaging (FLIM) was performed. Figure 4A shows that the fluorescence lifetime (τ) of the GFP-BB donor control was ~2.48 nsec, while that of an intact donor-acceptor pair was ~2.25 nsec, demonstrating efficient FRET. When cotransfected with DA1, the fluorescent lifetime of the donor-acceptor pair increased to ~2.38 nsec. Lifetime imaging of typical transfected protoplasts showed a generalized cellular localization of DA1-mediated cleavage. Figure 4B shows that the eGFP-BB-mCherry donor-acceptor pair was cleaved by DA1 peptidase at the expected site in transfected root protoplasts. Therefore, DA1 has a latent peptidase activity that is activated by multiple ubiquitylation mediated by its UIM1+2 domain and the RING E3 ligases BB and DA2, and activated DA1 peptidase then specifically cleaves these two E3 ligases.

Identification of a DA1 peptidase cleavage site in BB

To define the potential functions of DA1-mediated cleavage, the DA1 cleavage site in BB was identified using Edman sequencing of purified cleaved BB-HIS. Supplemental Figure S5 shows neo-N-terminal amino acid sequences that had a unique match to six amino acids in BB (Fig. 5A). This indicated a potential DA1 cleavage site within BB between A₆₀ and Y₆₁, consistent with the sizes of BB and its ~35-kDa cleaved form (Fig. 3A). Two mutant forms of BB were made to assess this potential DA1 cleavage site: a four-amino-acid deletion surrounding the site (Δ NAYK) and AY changed to GG (AY-GG) (Fig. 5B). These proteins were coexpressed in *Arabidopsis da1-ko1 dar1-1* mesophyll protoplasts as C-terminal Flag fusion proteins with HA-DA1 and HA-DA1(pep). Figure 5B shows that the mutant BB-Flag proteins were not cleaved by DA1, establishing that DA1 peptidase activity cleaved BB between A₆₀ and Y₆₁. A cleaved form of BB, called MY61-BB, was also made with an initiator Met followed by Y₆₁ (Fig. 5B). MY61-BB was expressed using the 35S promoter in *da1-ko1 bb-eod1-2* mutant *Arabidopsis*. Its lack of complementation of *bb-eod1-2* (Fig. 5C) showed that DA1 peptidase-mediated cleavage reduced BB activity.

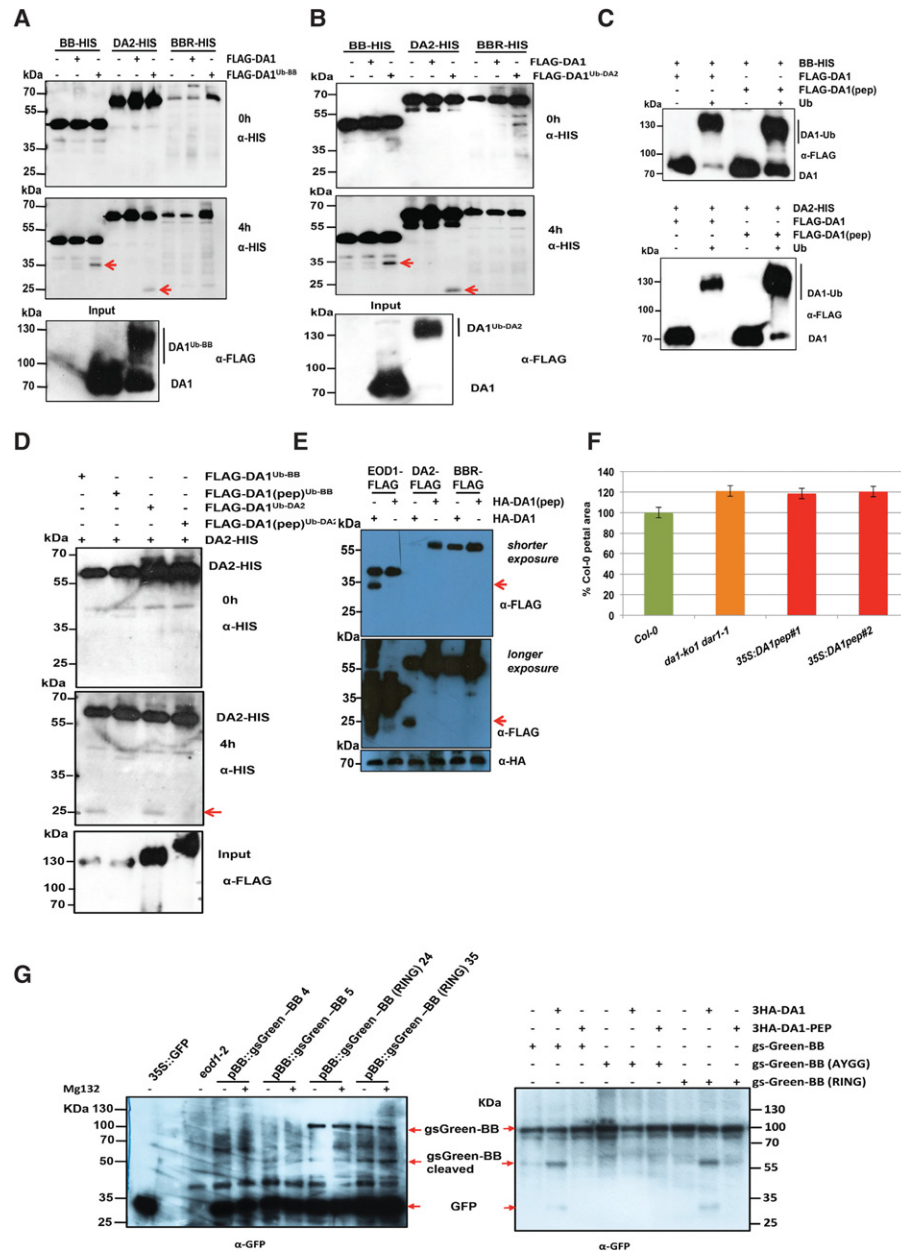


Figure 3. DA1 is an endopeptidase activated by multiple ubiquitylations and cleaves the E3 ligases BB and DA2 that ubiquitylate it. (A,B) Time course of an in vitro reaction of Flag-DA1 or Flag-DA1 ubiquitylated by BB (A) or DA2 (B) with BB-HIS, DA2-HIS, and BBR-HIS. The bottom panels show loading of Flag-DA1 and Flag-DA1^{Ub-BB}. After 4 h, cleavage products (shown by red arrows) of BB and DA2 had been produced by ubiquitylated Flag-DA1 but not Flag-DA1. BBR was not cleaved under these conditions. (C) An in vitro ubiquitylation reaction of DA1 and DA1(pep) using BB-HIS (top panel) and DA2-HIS (bottom panel) as E3 ligases. Ubiquitin-dependent multiple monoubiquitylations of Flag-DA1 and Flag-DA1(pep) by both BB and DA2 were detected. (D) A time course of an in vitro cleavage reaction using DA2-HIS as a substrate (left panels) and Flag-DA1 or Flag-DA1(pep) ubiquitylated by either BB or DA2 (loading shown in the bottom panel). The red arrow in the bottom left panel indicates the DA2 cleavage product at 4 h that was produced only by Flag-DA1^{Ub} and not Flag-DA1(pep)^{Ub}. (E) *Arabidopsis da1-ko1 dar1-1* mesophyll protoplasts were cotransfected with plasmids expressing BB-Flag, DA2-Flag, BBR-Flag, HA-DA1, and HA-DA1(pep). The same-sized cleavage products (red arrows) from BB-Flag and DA2-Flag were detected as seen in A and B above. (Middle panel) Longer exposure of the top immunoblot showed cleaved DA2. The bottom panel shows loading of HA-DA1 and HA-DA1(pep). (F) DA1(pep) is not functional in vivo, as it does not complement the large petal phenotype of the *da1-ko1 dar1-1* double mutant. Transformants expressing 35S::DA1(pep) were scored for petal size and compared with wild-type Col-0 and *da1-ko1 dar1-1*. The values given are means ($n = 150$) \pm SE, expressed as percentage of wild-type Col-0 petal areas. Student's *t*-test showed no significant differences between the transformants and the parental *da1-kodar1-1* line. (G) Cleavage of gsGreen-BB is shown in planta in the left panel and in transiently expressed protoplasts in the right panel for comparison. Large-scale protein extracts from transgenic 8-d-old seedlings expressing BB::gsGreen-BB and BB::gsGreen-BB (RING) were purified on a GFP trap. Loading controls used levels of free GFP. The expected size cleavage products (arrows) were observed in plant extracts and protoplasts for comparison.

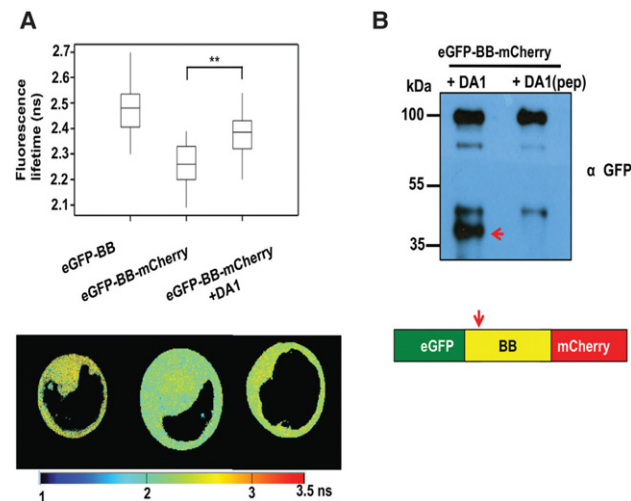


Figure 4. Detection of DA1-mediated cleavage of BB in vivo using FRET. (A) Root protoplasts of *da1-ko1 dar1-1* plants were transfected with the FRET construct eGFP-BB or a control eGFP-BB-mCherry construct together with DA1 to detect DA1-mediated cleavage of BB. Transfected 2protoplasts were imaged using multiphoton microscopy, and fluorescence half-times of protoplasts ($n = 13$) were captured. The heat map shows fluorescent lifetime values, and typical protoplasts are shown to illustrate fluorescent half-lives imaged over the cell. The box plots show significantly increased fluorescence lifetime after DA1 transfection. (***) $P \leq 0.001$, Student's *t*-test. (B) Cleavage of eGFP-BB-mCherry by DA1 in the imaged protoplasts shown in A. The arrow shows the major cleavage product of ~40 kDa expected from DA1 cleavage near the N terminus of BB.

BB stability is dependent on its N terminus and N-end rule function

DA1 cleavage products of DA2 were unstable, indicating that one function of DA1-mediated cleavage may be to destabilize proteins (Fig. 3E). This was also observed for BB in cell-free degradation assays, in which MY61-BB was unstable compared with wild-type BB (Supplemental Fig. S6). To test the role of the neo-N terminus of BB on protein stability, 61BB proteins with different N termini (Y, G, and MY) were expressed using the ubiquitin fusion technique (UFT) (Bachmair et al. 1986). HA-tagged constructs were translationally coexpressed in a cell-free rabbit reticulocyte system with or without MG132 proteasome inhibitor, and translation was stopped by the addition of cycloheximide. Y61-BB was highly unstable, whereas G61-BB was stable (Fig. 5D). Interestingly, the artificial MY61-BB was also highly unstable in a proteasome-independent mechanism. The neo-N-terminal sequence of DA1-cleaved BB starts with YK, a potentially destabilizing sequence of a type II N-end rule degron (Varshavsky 2011). The N-end rule E3 ligase PRT1 mediates the stability of model N-end rule substrates with such aromatic N-terminal residues (Potuschak et al. 1998). To assess the potential role of PRT1 in N-end rule-mediated degradation of BB, we tested the binding of PRT1 to 17-mer peptides representing variants of the neo-N termini

of BB on a backbone sequence of an N-end rule test substrate in SPOT (synthetic peptide arrays on membrane support technique) assays. Purified recombinant HIS-MBP-PRT1 protein was incubated with the SPOT array, and binding was visualized by Western blotting. Recombinant PRT1 had a preference for binding to the large aromatic acids tyrosine and phenylalanine, consistent with previously suggested specificity (Fig. 5E; Potuschak et al. 1998; Stary 2003; Faden et al. 2016). To assess whether PRT1 had a role in DA1-mediated BB degradation, BB was expressed with an N-terminal ubiquitin fusion and a C-terminal luciferase fusion to reveal neo-N termini in Col-0 or *prr1* mutant mesophyll protoplasts. BB-LUC activity was reduced in wild-type protoplasts with a neo-N-terminal tyrosine, which was not seen in *prr1* mutant protoplasts (Fig. 5F). Neo-N-terminal glycine BB-LUC levels were not altered in either Col-0 or *prr1* mutant protoplasts. This indicated a strong dependence of Tyr-61BB stability on PRT1 activity. In planta evidence supporting the role of DA1 in reducing the growth inhibitory role of BB via N-end rule-mediated degradation was shown by the suppression of growth reduction in a transgenic 35S::RFP-BB overexpression line by overexpression of DA1 (Fig. 5G). Western blots (Fig. 5H) confirmed that 35S::DA1 reduced levels of RFP-BB.

Functional analyses of DA1

We showed previously that the *da1-1* allele of DA1 has a negative interfering phenotype with respect to the closely related family member DAR1 (Li et al. 2008). The peptidase activity of the protein encoded by the *da1-1* allele, called DA1(R358K), which has an arginine to a lysine residue altered in a highly conserved C-terminal region, (Supplemental Fig. S4) was assessed. This mutation did not influence ubiquitylation of Flag-DA1(R358K) (Fig. 6A) or create a site for ectopic ubiquitylation of Flag-DA1(R358K), as determined by mass spectrometric analysis (Supplemental Fig. S2C). The peptidase activity of ubiquitylated Flag-DA1(R358K) was qualitatively assessed in vitro and in vivo [using HA-DA1(R358K)] by comparison with wild-type DA1 peptidase activity (Fig. 6A,B). Both assays showed that DA1(R358K) had lower peptidase activity compared with DA1, suggesting that regions of the conserved C-terminal region are required for peptidase activity and that the *da1-1* phenotype may be due to reduced peptidase activity. Figure 6B also shows that DA1(4K-4R), which is ubiquitylated (Fig. 2E), had peptidase activity toward BB. This suggested that precise patterns of ubiquitylation are not required for activating DA1 latent peptidase activity.

DAR4, another DA1 family member (Li et al. 2008), encodes a protein with an N-terminal TIR-NB-LRR and has a gain-of-function *chs3-2d* allele in the conserved C-terminal region (Supplemental Fig. S3) that activated constitutive defense responses (Xu et al. 2015). Alignments revealed high similarity to predicted protein sequences from the photosynthetic bacteria *Roseiflexus* sp (Supplemental Fig. S7; Burroughs et al. 2011) that included four pairs of CxxC/H motifs with the potential to bind

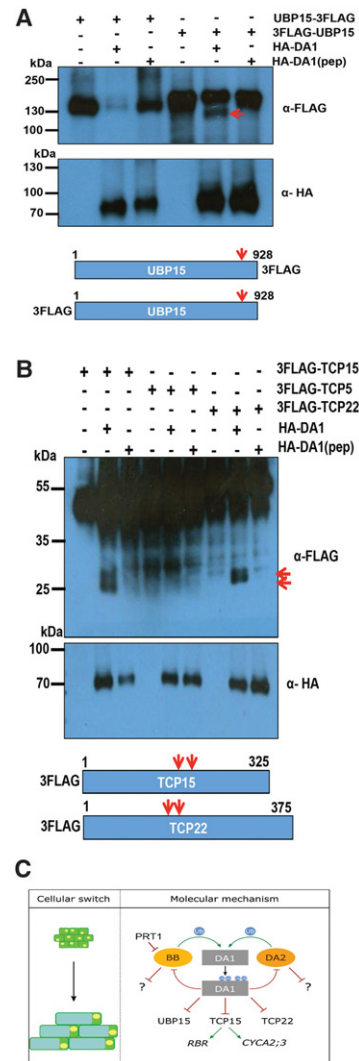


Figure 7. DA1 cleaves UBP15, TCP15, and TCP22 in vivo. (A,B) In vivo cleavage reactions of UBP15-3Flag and 3Flag-UBP15 (A) as well as 3-Flag-TCP15, 3-Flag-TCP22, and 3-Flag TCP5 (a non-cleaved control) (B) using HA-DA1 and HA-DA1(pep). Constructs expressed from the 35S promoter were cotransfected into *da1-ko1 dar1-1* mesophyll protoplasts. UBP15, TCP14, TCP15, and TCP22 cleavage products are shown in the *top* immunoblots. The *bottom* immunoblots show HA-DA1 and HA-DA1(pep) protein levels. The approximate locations of DA1 cleavage sites (arrows) are shown in UBP15, TCP15, and TCP22. (C) A model of the proposed transient mechanism of DA1 peptidase activation and the consequences of DA1-mediated cleavage of growth regulators during organ growth. PRT1 activity is shown as degrading BB.

establishing a biochemical foundation for their joint activities in growth control. Zinc metallopeptidases are maintained in an inactive form by a “cysteine switch” (Van Wart and Birkedal-Hansen 1990) that coordinates a cysteine residue with the zinc atom at the active site to block it. Conformational changes release this and activate the peptidase.

Ubiquitylation of DA1 has the potential to trigger a conformational change that may release inhibition of pep-

tidase activity. Hoeller et al. (2006) showed that UBD- and UIM-mediated monoubiquitylation of endocytotic proteins, including epsin, led to a conformational change mediated by intramolecular interactions between UBDs/UIMs and *cis*-ubiquitin, which regulated endocytosis. The binding of ubiquitin to DA1 UIMs was required for DA1 function in vivo (Fig. 2H), and the UIMs conferred patterns of ubiquitylation on the heterologous protein GST similar to that seen for DA1 (Fig. 2G [for DA1], E,F [for GST-UIM1+2]). Related observations were seen in the monoubiquitylation of epsin (Oldham et al. 2002) through coupled monoubiquitylation (Woelk et al. 2006), where UIMs recruit the UIM-containing protein to the ubiquitylation machinery by direct interaction with ubiquitin coupled to ubiquitin donor proteins (Haglund and Stenmark 2006). Mutation of Cys274 in the C-terminal zinc finger loop of the LIM-like domain of DA1 abrogated both ubiquitylation and peptidase activity (Fig. 6A,B), suggesting a functional role for this ancient conserved LIM-like domain (Supplemental Fig. S7; Burroughs et al. 2011) in peptidase activation. Analyses of conformational changes caused by DA1 ubiquitylation and their influence on peptidase activity are required to establish this potential mechanism.

DA1 cleavage destabilizes its activating E3 ligases (BB and DA2), and cleavage of BB leads to targeting by the N-recognin PRT1

The RING E3 ligases BB and DA2 activate DA1 peptidase by ubiquitylation and are also cleaved by DA1 peptidase (Figs. 3A,B,E,G, 4). Once cleaved, DA2 appeared to be destabilized in transiently expressed protoplasts (Fig. 3E). Identification of the DA1 cleavage site in BB (Fig. 5A,B) revealed Y61-BB at the neo-N terminus of cleaved BB. This neo-N terminus conferred proteasome-mediated degradation in a cell-free system (Fig. 5D). This degradation depended on recognition of the neo-N terminus by the *Arabidopsis* E3 ligase PRT1 (Fig. 5E,F; Potuschak et al. 1998; Stary 2003), an N-recognin catalyzing N-end rule-mediated degradation (Varshavsky 2011) with a suggested preference for aromatic amino acid N termini. Interestingly, the neo-N-terminal MY61-BB, which was used to express a cleaved version of BB in planta, conferred strong proteasome-independent instability (Fig. 5D) in a mechanism that is not yet clear. The lack of MY61-BB function in vivo (Fig. 5C) supported the observation that DA1-mediated cleavage of BB leads to its loss of function in vivo. Overexpression of BB strongly reduced growth, as expected from its inhibitory role in growth (Disch et al. 2006). The reversal of this inhibition by overexpression of DA1, which reversed growth inhibition (Fig. 5G) and reduced RFP-BB levels (Fig. 5H), is consistent with a mechanism involving DA1-mediated reduction of BB activity via peptidase-mediated cleavage and subsequent degradation by the N-end rule pathway. Such an activation–destruction mechanism mediated by BB, DA2, and DA1 may provide a way of tightly controlling peptidase activity. The physiological role of these

mechanisms, which often involve ubiquitylation and proteolytic degradation, is to drive unidirectional cellular processes; for example, in cell cycle progression (Reed 2003). The factors that trigger DA1 ubiquitylation by BB and coordinate the activities of BB and DA2 remain unknown.

DA1 peptidase activity also cleaves diverse growth regulators

We showed previously that *TCP14* and *TCP15* function downstream from DA1 and other family members in controlling organ size in *Arabidopsis*, and reduced function of DA1 family members led to increased *TCP14* and *TCP15* protein levels (Peng et al. 2015). Similarly, levels of UBP15 protein, which promotes cell proliferation (Liu et al. 2008) and also functions downstream from DA1, were increased in the *da1-1* reduced-function mutant (Du et al. 2014). We showed that *TCP15* and the related *TCP22* as well as UBP15 were cleaved by DA1 peptidase activity (Fig. 7A,B) but could not reliably detect *TCP14* cleavage by DA1 or DAR1. DA1-mediated cleavage of *TCP15* and UBP15 is a plausible mechanism that accounts for these observed reduced protein levels, similar to DA1-mediated inactivation and destabilization of BB by peptidase cleavage. Taken together, these observations suggest a mechanism (Fig. 7C) in which DA1 peptidase, activated transiently by BB or DA2, coordinates a “one-way” cessation of cell proliferation and the initiation of endoreduplication through the cleavage and potential inactivation of proteins that promote cell proliferation and inhibit endoreduplication.

Materials and methods

Plant materials, growth conditions, and organ size measurements

A. thaliana Col-0 was the wild-type plant used. Plants were grown in growth rooms at 20°C with 16-h day/8-h dark cycles using either soil or MS medium supplemented with 0.5% glucose. Petal and seed areas were imaged by high-resolution scanning (3600 dpi; Hewlett Packard Scanjet 4370) and analyzed using ImageJ software (<http://rsbweb.nih.gov/ij>).

In vitro DA1-mediated cleavage assays

Flag-DA1 was ubiquitylated in vitro using either DA2-HIS or BB-HIS as E3 ligases, purified using Flag magnetic beads, and quantified, and 100 ng was added to 100 ng of BB-HIS, DA2-HIS, or BBR-HIS in a 30- μ L reaction in 50 mM Tris HCl (pH 7.4) and 5 mM MgCl₂. Reactions were carried out for 4 h at 30°C and terminated by the addition of SDS sample buffer.

Mass spectrometry analysis

DA1 ubiquitylation patterns were determined from trypsinized proteins purified on SDS-PAGE gels. For liquid chromatography-tandem mass spectrometry analysis, peptides were applied to an LTQ-Orbitrap (Thermo-Fischer) using a nanoAcquity ultraperformance liquid chromatography system (Waters Ltd.). Further details are in the Supplemental Material.

Acknowledgments

We thank Dr. Paul Thomas (Henry Wellcome Laboratory for Cell Imaging, University of East Anglia) for advice and operating the multiphoton microscope, and Dr. Cristoph Bücherl (The Sainsbury Laboratory, Norwich) for advice on FRET. We thank Shimadzu Europa GMBH for carrying out Edman sequencing. We thank Andreas Bachmair for the *prt1* EMS allele, and Yukiko Yoshida for the TR-TUBE construct. This work was supported by Biological and Biotechnological Sciences Research Council (BBSRC) grant BB/K017225 and Strategic Programme grant BB/J004588 to M.W.B., and European Commission contract 037704 (AGRONomics) to M.W.B. and D.I. J.D. was supported by a Biotechnology and Biological Sciences Research Council (BBSRC) CASE Studentship, C.N. was supported by a PhD Fellowship from the Landesgraduiertenförderung Sachsen-Anhalt, and N.D. was supported by an Independent Junior Research Group grant from the ScienceCampus Halle-Plant-based Bioeconomy, the Deutsche Forschungsgemeinschaft (DFG; grant DI 1794/3-1), the DFG Graduate Training Centre (GRK1026), and the Leibniz Institute of Plant Biochemistry. Y.L. was supported by the National Natural Science Foundation of China (grants 91417304, 31425004, 91017014, 31221063, and 31100865), the National Basic Research Program of China (grant 2009CB941503), and the Ministry of Agriculture of China (grant 2016ZX08009-003). M. W.B. and Y.L. are in the Chinese Academy of Sciences (CAS)-John Innes Centre (JIC) Centre of Excellence in Plant and Microbial Sciences (CEPAMS). M.W.B., J.D., H.D., F.-H.L., H.V., N.D., Y.L., and D.I. designed the research; H.D., F.-H.L., J.D., R.P., H. V., C.N., M.K., C.S., N.M., L.N., H.V., T.X., L.C., G.S., N.G., and M.S. performed the research and analyzed the data; and M. W.B. wrote the paper.

References

- Andriankaja M, Dhondt S, De Bodt S, Vanhaeren H, Coppens F, De Milde L, Mühlenbock P, Skirycz A, Gonzalez N, Beemster GTS, et al. 2012. Exit from proliferation during leaf development in *Arabidopsis thaliana*: a not-so-gradual process. *Dev Cell* **22**: 64–78.
- Bachmair A, Finley D, Varshavsky A. 1986. In vivo half-life of a protein is a function of its amino-terminal residue. *Science* **234**: 179–186.
- Barry ER, Camargo FD. 2013. The Hippo superhighway: signaling crossroads converging on the Hippo/Yap pathway in stem cells and development. *Curr Opin Cell Biol* **25**: 247–253.
- Breuer C, Ishida T, Sugimoto K. 2010. Developmental control of endocycles and cell growth in plants. *Curr Opin Plant Biol* **13**: 654–660.
- Breuninger H, Lenhard M. 2012. Expression of the central growth regulator BIG BROTHER is regulated by multiple *cis*-elements. *BMC Plant Biol* **12**: 41.
- Burroughs AM, Iyer LM, Aravind L. 2011. Functional diversification of the RING finger and other binuclear treble clef domains in prokaryotes and the early evolution of the ubiquitin system. *Mol Biosyst* **7**: 2261.
- De Veylder L, Larkin JC, Schnittger A. 2011. Molecular control and function of endoreplication in development and physiology. *Trends Plant Sci* **16**: 624–634.
- Disch S, Anastasiou E, Sharma VK, Laux T, Fletcher JC, Lenhard M. 2006. The E3 ubiquitin ligase BIG BROTHER controls *Arabidopsis* organ size in a dosage-dependent manner. *Curr Biol* **16**: 272–279.
- Du L, Li N, Chen L, Xu Y, Li Y, Zhang Y, Li C, Li Y. 2014. The ubiquitin receptor DA1 regulates seed and organ size by

- modulating the stability of the ubiquitin-specific protease UBP15/SOD2 in *Arabidopsis*. *Plant Cell* **26**: 665–677.
- Efroni I, Blum E, Goldshmidt A, Eshed Y. 2008. A protracted and dynamic maturation schedule underlies *Arabidopsis* leaf development. *Plant Cell* **20**: 2293–2306.
- Faden F, Ramezani T, Mielke S, Almudi I, Nairz K, Froehlich MS, Höckendorff J, Brandt W, Hoehenwarter W, Dohmen RJ, et al. 2016. Phenotypes on demand via switchable target protein degradation in multicellular organisms. *Nat Commun* **7**: 12202.
- Green AA, Kennaway JR, Hanna AI, Bangham JA, Coen E. 2010. Genetic control of organ shape and tissue polarity. *PLoS Biol* **8**: e1000537.
- Haglund K, Stenmark H. 2006. Working out coupled monoubiquitination. *Nat Cell Biol* **8**: 1218–1219.
- Haglund K, Di Fiore PP, Dikic I. 2003. Distinct monoubiquitin signals in receptor endocytosis. *Trends Biochem Sci* **28**: 598–603.
- Hicke L, Schubert HL, Hill CP. 2005. Ubiquitin-binding domains. *Nat Rev Mol Cell Biol* **6**: 610–621.
- Hoeller D, Dikic I. 2010. Regulation of ubiquitin receptors by coupled monoubiquitination. *Subcell Biochem* **54**: 31–40.
- Hoeller D, Crosetto N, Blagoev B, Raiborg C, Tikkanen R, Wagner S, Kowanetz K, Breitling R, Mann M, Stenmark H, et al. 2006. Regulation of ubiquitin-binding proteins by monoubiquitination. *Nat Cell Biol* **8**: 163–169.
- Husnjak K, Dikic I. 2012. Ubiquitin-binding proteins: decoders of ubiquitin-mediated cellular functions. *Annu Rev Biochem* **81**: 291–322.
- Johnston LA, Gallant P. 2002. Control of growth and organ size in *Drosophila*. *Bioessays* **24**: 54–64.
- Kadmas JL, Beckerle MC. 2004. The LIM domain: from the cytoskeleton to the nucleus. *Nat Rev Mol Cell Biol* **5**: 920–931.
- Kazama T, Ichihashi Y, Murata S, Tsukaya H. 2010. The mechanism of cell cycle arrest front progression explained by a KLUH/CYP78A5-dependent mobile growth factor in developing leaves of *Arabidopsis thaliana*. *Plant Cell Physiol* **51**: 1046–1054.
- Kim H, Chen J, Yu X. 2007. Ubiquitin-binding protein RAP80 mediates BRCA1-dependent DNA damage response. *Science* **316**: 1202–1205.
- Komander D, Rape M. 2012. The ubiquitin code. *Annu Rev Biochem* **81**: 203–229.
- Li Y, Zheng L, Corke F, Smith C, Bevan MW. 2008. Control of final seed and organ size by the DA1 gene family in *Arabidopsis thaliana*. *Genes Dev* **22**: 1331–1336.
- Li Z-Y, Li B, Dong A-W. 2012. The *Arabidopsis* transcription factor AtTCP15 regulates endoreduplication by modulating expression of key cell-cycle genes. *Mol Plant* **5**: 270–280.
- Liu Y, Wang F, Zhang H, He H, Ma L, Deng XW. 2008. Functional characterization of the *Arabidopsis* ubiquitin-specific protease gene family reveals specific role and redundancy of individual members in development. *Plant J* **55**: 844–856.
- Oldham CE, Mohny RP, Miller SLH, Hanes RN, O'Bryan JP. 2002. The ubiquitin-interacting motifs target the endocytic adaptor protein epsin for ubiquitination. *Curr Biol* **12**: 1112–1116.
- Pan D. 2010. The hippo signaling pathway in development and cancer. *Dev Cell* **19**: 491–505.
- Peng Y, Chen L, Lu Y, Wu Y, Dumenil J, Zhu Z, Bevan MW, Li Y. 2015. The ubiquitin receptors DA1, DAR1, and DAR2 redundantly regulate endoreduplication by modulating the stability of TCP14/15 in *Arabidopsis*. *Plant Cell* **27**: 649–662.
- Potuschak T, Stary S, Schlögelhofer P, Becker F, Nejjinskaia V, Bachmair A. 1998. PRT1 of *Arabidopsis thaliana* encodes a component of the plant N-end rule pathway. *Proc Natl Acad Sci* **95**: 7904–7908.
- Rawlings ND, Barrett AJ, Bateman A. 2012. MEROPS: the database of proteolytic enzymes, their substrates and inhibitors. *Nucleic Acids Res* **40**: D343–D350.
- Reed SI. 2003. Ratchets and clocks: the cell cycle, ubiquitylation and protein turnover. *Nat Rev Mol Cell Biol* **4**: 855–864.
- Sato Y, Yoshikawa A, Mimura H, Yamashita M, Yamagata A, Fukai S. 2009. Structural basis for specific recognition of Lys 63-linked polyubiquitin chains by tandem UIMs of RAP80. *EMBO J* **28**: 2461–2468.
- Sluis A, Hake S. 2015. Organogenesis in plants: initiation and elaboration of leaves. *Trends Genet* **31**: 300–306.
- Stary S. 2003. PRT1 of *Arabidopsis* is a ubiquitin protein ligase of the plant N-end rule pathway with specificity for aromatic amino-terminal residues. *Plant Physiol* **133**: 1360–1366.
- Tholander F, Roques B-P, Fournié-Zaluski M-C, Thunnissen MMGM, Haeggström JZ. 2010. Crystal structure of leukotriene A4 hydrolase in complex with ketolorphan, implications for design of zinc metallopeptidase inhibitors. *FEBS Lett* **584**: 3446–3451.
- van der Krogt GNM, Ogink J, Ponsioen B, Jalink K. 2008. A comparison of donor-acceptor pairs for genetically encoded FRET sensors: application to the Epac cAMP sensor as an example. *PLoS* **3**: e1916.
- Van Wart HE, Birkedal-Hansen H. 1990. The cysteine switch: a principle of regulation of metalloproteinase activity with potential applicability to the entire matrix metalloproteinase gene family. *Proc Natl Acad Sci* **87**: 5578–5582.
- Varshavsky A. 2011. The N-end rule pathway and regulation by proteolysis. *Protein Sci* **20**: 1298–1345.
- Woelk T, Oldrini B, Maspero E, Confalonieri S, Cavallaro E, Di Fiore PP, Polo S. 2006. Molecular mechanisms of coupled monoubiquitination. *Nat Cell Biol* **8**: 1246–1254.
- Xia T, Li N, Dumenil J, Li J, Kamenski A, Bevan MW, Gao F, Li Y. 2013. The ubiquitin receptor DA1 interacts with the E3 ubiquitin ligase DA2 to regulate seed and organ size in *Arabidopsis*. *Plant Cell* **25**: 3347–3359.
- Xu F, Zhu C, Çevik V, Johnson K, Liu Y, Sohn K, Jones JD, Holub EB, Li X. 2015. Autoimmunity conferred by chs3-2D relies on CSA1, its adjacent TNL-encoding neighbour. *Sci Rep* **5**: 8792.